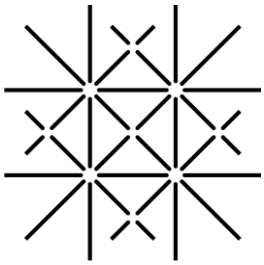

Engineering Artificial Metalloenzymes Based on Biotin-Streptavidin Technology for DNA Recognition and Asymmetric Transfer Hydrogenation Catalysis

Inauguraldissertation

zur

Erlangung der Würde eines

Doktors der Philosophie

vorgelegt der

Philosophisch-Naturwissenschaftlichen Fakultät

der Universität Basel

von

Malcolm Jeremy ZIMBRON

aus Toluca, MEXICO

Basel, 2012

Genehmigt von der Philosophisch-Naturwissenschaftlichen Fakultät der Universität Basel auf Antrag von Prof. Dr. Thomas R. Ward und Prof. Dr. Karl Gademann

Basel, den 21 Februar 2012

Prof. Dr. Martin Spiess

Dekan

Acknowledgements

When I look back on these four years of my life I am really surprised and proud by the work accomplished during my thesis. It would not have been possible without the help and support of different people to whom I would like to give a particular mention here.

Firstly I would like to thank Professor Thomas Ward for his patience, motivation, enthusiasm, and knowledge. His guidance helped me in all the time of research and writing of this thesis. He provided an insightful view of my work. He has shaped me as a scientist and has certainly led me where I am now.

It would not have been possible to cross this thesis adventure without the help and support of the people around me in the AMEL lab. They contributed to make this thesis journey more enjoyable with the moments shared in and outside the lab: Alessia Sardo, Cheikh Lo, Didier Hamels, Elisa Nogueira, Fabien Monnard, Gregory Upert, Marc Creus, Ruben Cal, Sabina Burazerovic, Thibaud Rossel, Anca Pordea, Annette Mutschler, Johannes Steinreiber, Julien Pierron, Julietta Gradinaru, Jincheng Mao, Karoline Kersten, Livia Knörr, Marc Dürrenberger, Marc Ringenberg, Maurus Schmid, Narasimha Rao, Thérèse Wohlschlager, Tillmann Heinisch, Tommaso Quinto, Valentin Köhler, Yves Casta, Yvonne Wilson. Special thanks to the Neuchâtel team, Alessia Sardo (for the really pleasant Italian time), Cheikh (for his philosophy and football discussions), Marc (for his indestructible cheerfulness and positivity), Sabina (for her joy of living and frankness), Thibaud (for his friendship and his scientific passion); a special thank to the French connection, Fabien (my scientific, bassoonist lab partner: a great support in the lab during the last years), Elisa (the best social network person, the kindest person in the world and the one who revealed me the existence of E.T.), Greg (the nicest person among all angry people) Didier (for being a Jedi).

I would also like to thank all the colleagues and administrative staff in the institute of Chemistry in Neuchatel and in Basel.

Thanks also go out to those who helped me, supported me, and shared my life before and during my PhD thesis, my friends: Oliv and Cédric, Leaticia, Marc, Toto, Julien, O'drey, Antoine, Guillaume, Audrey, Greg, Will, Hugues, Bonny, and the others…

The most important, I would like to thank my family, especially my Mother Florence and my Father Gustavo for the support they provided me through my entire life and in particular during my thesis. I do not forget Simone, Jacques, Ana Maria, Isabelle, Melina, Roger, Joelle, and all my family in Mexico.

Finally, it is impossible to finish without addressing my deep love and gratitude to Stéphanie. With your love, encouragement and patience you guided me and helped me during through the most difficult and the best days of my life.

à Florence

La volonté c'est la matérialisation des idées en actes

Gustavo

Abstract

Engineering Artificial Metalloenzymes Based on Biotin-Streptavidin Technology for DNA Recognition and Asymmetric Transfer Hydrogenation Catalysis

Malcolm Jeremy ZIMBRON

Metalloproteins occupy a central place among all proteins since they represent nearly half of all proteins in nature. Metalloenzymes catalyze important biological processes (photosynthesis, respiration, water oxidation) and other chemical reactions (oxidoreduction reactions). Artificial metalloenzymes, which can be created from insertion of a metal-containing moiety within a protein scaffold, combine the attractive properties of organometallic chemistry (activity provided by accurate chemical cofactor design) and enzymatic mean (fine-tuning of second coordination sphere to afford high substrate specificity, activity and selectivity) to provide a powerful tool with a great optimization potential.

The biotin-streptavidin technology represents a versatile tool to create artificial metalloenzymes and other supramolecular assemblies, due to i) the exceptionally strong and precise anchoring ability; ii) the range of possibilities of chemical derivatization of the biotinylated compounds and iii) genetic optimization of the host protein.

In the spirit of surface borrowing, i.e. modulating ligand-affinity by harnessing existing protein surfaces, the biotin-streptavidin assembly was exploited to create a metallodrug-presenter protein assembly. With the aim of investigating the mechanisms by which such assembly could deliver small molecules to preferred macromolecular targets *in vitro*, a biotinylated piano stool ruthenium complex was synthesized and incorporated into streptavidin. The metallodrug-protein assembly was constructed to provide non-covalent interactions that modulated binding of the organometallic moiety to specific DNA targets. Guided by the X-ray

structure of the drug embedded within the Sav protein, we explored the formation of metallodrug-mediated ternary complexes between the presenter protein and DNA. The study suggests that rational targeting of metallodrugs *via* presenter proteins could be exploited to improve selectivity of small molecules for G-quadruplex DNA over double-stranded DNA.

In addition to target-selectivity for binding, we also investigated catalytically-active supramolecular complexes. With the aim of improving the screening efficiency of metalloenzymes in catalytic reactions, a new synthetic platform for fast chemical optimization of biotinylated catalysts was implemented. Incorporation of various d^6-transition metal (rhodium and iridium) piano stool complexes, containing a tetramethylcyclopentadienyl (C_5Me_4) tethered to biotin into streptavidin provided a fast and convenient means of screening and optimizing of hybrid catalysts that affords new catalytically active artificial metalloenzymes in ATH of cyclic imines (production of salsolidine). Furthermore, *in silico* investigations allowed the use of the new synthetic platform in the design of a novel type of metal catalyst/protein assembly. Combination of rational ligand design and genetic optimization of the biomolecular host resulted in the creation of the first biotin/streptavidin-based metalloenzyme using a dually anchored (supramolecular and dative anchoring) metal capable of performing enantioselective transfer hydrogenation reactions. Finally, the two strategies developed above were transposed to the less explored reductive amination of α-keto acids. These studies provide the first example of synthetic enantioselective reductive amination for the preparation of a range of unprotected chiral α-amino acids in water, thus demonstrating the great potential of artificial metalloenzyme technology.

Keywords: Artificial metalloenzymes, asymmetric catalysis, DNA recognition, chemo-genetic optimization, biotin-streptavidin, metallodrug, transfer hydrogenation, imine reduction, reductive amination.

Table of contents

1. General Introduction

1.1. Preamble

This thesis describes the potential of hybrid supramolecular systems consisting of streptavidin and biotinylated piano stool complexes either as anticancer drugs or as well as transfer hydrogenation catalysts. For that purpose, a brief overview of piano stool complexes i) as anticancer metallodrugs, ii) as valuable catalysts in asymmetric transfer hydrogenation reactions and iii) as suitable scaffolds for the creation of novel artificial metalloproteins is presented below.

i) The organometallic ruthenium half-sandwich complexes are described as promising anticancer drugs and their potential to preferentially interact with DNA is highlighted. In addition, telomeric DNA is also presented as new target for such metal-based drugs.

ii) Piano stool complexes are further described as efficient transfer-hydrogenation catalysts, with a focus on ketone and imine reduction.

iii) Finally, different strategies to design new artificial metalloenzymes are described with a focus on the biotin-streptavidin technology.

1.2. Organometallic Half-Sandwich Complexes

1.2.1. Piano Stool Complexes: Structure and Activity

Organometallic chemistry has received increased attention in the last decades and provided great potential for the development of innovative complexes that find application in a wide range of domains.[1] Chiral-at-metal half-sandwich compounds, which are important representatives of the field, have been the subject of extensive research since the very early stage of transition metal chemistry.[2] Brunner and Ganter were very active in this chemistry and meticulously described the strategies to prepare chiral-at-metal compounds and their configurational stability.[3] After initial theoretical research, chiral metal complexes received a

growing interest that culminated with the Nobel prize awarded jointly to Knowles, Noyori and Sharpless in 2001 for their outstanding contributions in this field.[4] The half-sandwich complexes of d^6-transition metals (see Figure 1a) have found a privileged place in organometallic chemistry. Piano stool ruthenium, rhodium and iridium complexes display interesting features such as air- and water-stability that explain their central role in the development of green chemistry.[5] They have found wide applications in catalysis and, more recently, in inorganic medicinal chemistry for their properties as anticancer agents.[6]

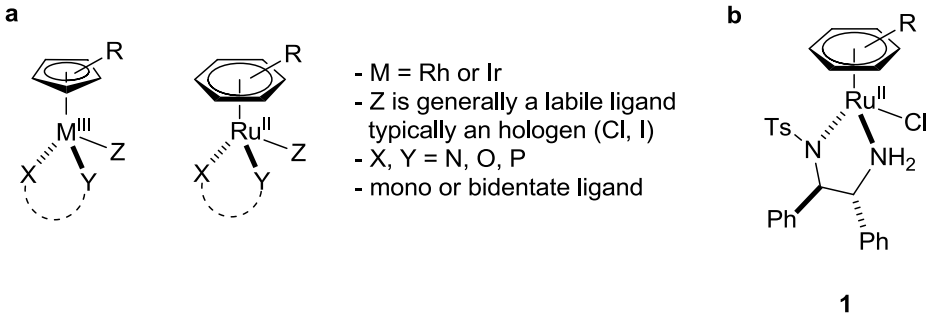

Figure 1 a) Typical organometallic half-sandwich ruthenium, rhodium and iridium d^6-complexes, b) Noyori's Ru^{II}-TsDPEN **1**.

The discovery by Noyori and coworkers of the highly active Ru^{II}-*N*-(*p*-toluenesulfonyl)-1,2-diphenylethylenediamine complex **1** (see Figure 1b) as catalyst for the asymmetric transfer hydrogenation (ATH) brought to light the organometallic chemistry involving half-sandwich complexes.[7] Since then, η^6-arene ruthenium complexes have been the subject of numerous studies in ATH.[8] Chiral piano stool scaffolds containing rhodium and iridium metals have been less investigated than the ruthenium counterpart. However, half-sandwich complexes bearing rhodium and iridium have found important applications in asymmetric reduction reactions.[9] Although the Cp*-rhodium complexes have been primarily described in the context of transfer hydrogenation, the Cp*-iridium catalysts have also been employed in a wide variety of different reactions, including numerous reports on amine alkylation with alcohols,[10] water oxidation[11] and oxidation of alcohol.[12]

It is interesting to note that many of the typical classes of organometallics, such as metallocenes, half-sandwich complexes, carbene-, CO-, or π-ligands containing complexes that have been widely used in catalysis or biosensing, have now also found applications in medicinal chemistry.[6] In this context, the efforts of Sadler and Dyson have provided significant advances in the area of bioorganometallic chemistry. They developed half-sandwich ruthenium metallodrugs that exhibit promising anticancer activity.[13] In parallel to this, monofunctional organometallic half-sandwich Ir^{III}-complexes bearing pentamethylcyclopentadienyl ligands have also recently emerged as promising anticancer compounds.[14]

The attractive features of piano stool complexes have also been extended to create new classes of catalysts: artificial metalloenzymes. The latter metal cofactor/protein assemblies have been shown to catalyze challenging processes in water.[15]

1.2.2. Metallodrugs in Anticancer Therapy

1.2.2.1. Organometallic Ruthenium Half-Sandwich Complexes

Ruthenium metallodrugs have attracted considerable attention since the successful completion of phase I clinical trials of the compounds NAMI-A and KP1019 (see Figure 2).[16]

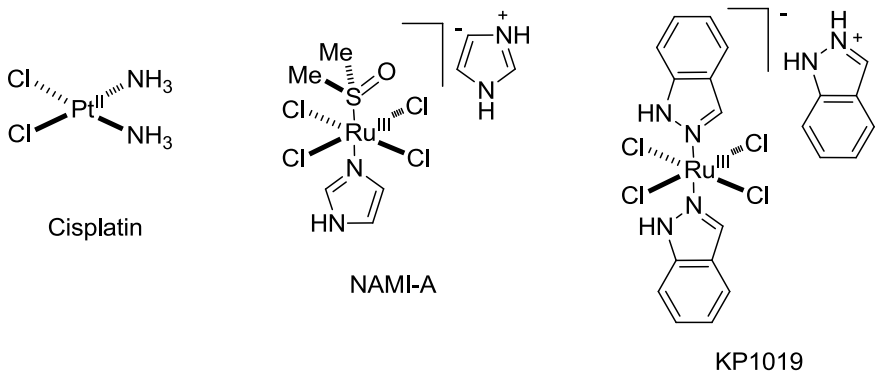

Figure 2 Structures of widely-researched metal-based anticancer compounds.

Anticancer drugs containing this metal represent an interesting alternative to the widely-used metallodrug cisplatin (see Figure 2) with possible different modes of action and with a supposed reduced potential to develop tumor resistance.[17] Consequently, the last three decades have seen the development of an important number of ruthenium compounds that have been investigated for potential anticancer activity.[18]

The idea of using ruthenium-containing organometallics as anticancer agents was first developed by Tochter and coworkers[19] before being intensively investigated in the groups of Sadler and Dyson.[20] They based their research on ruthenium piano stool complexes inspired by the "activation by reduction" hypothesis.[21] Indeed, it was expected that active Ru^{II} species may be formed *in vivo* from Ru^{III} precursors such as NAMI-A or KP1019. To date, these novel piano stool complexes represent the most numerous group of cytotoxic ruthenium-based agents with promising anticancer activity *in vitro* and *in vivo*.[20] Representative examples of such organometallic Ru^{II}-arene compounds are RAPTA-C[22] and RM175 (see Figure 3).[23] A rapid glance at the Sadler and Dyson anticancer complexes might suggest that such similar structures would result in comparable mechanism of action. However, it appears that they exhibit different anticancer activity.

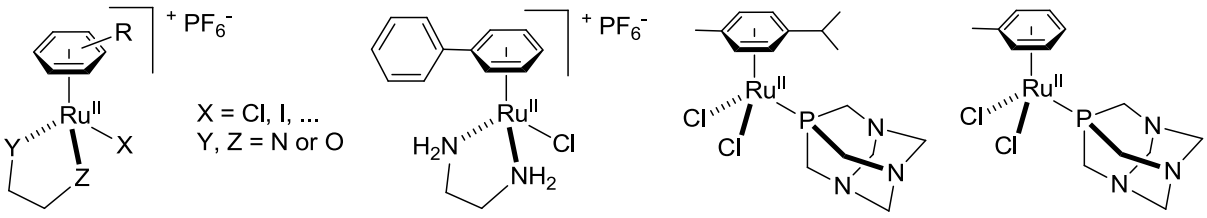

[(η^6-arene)Ru(en)Cl]PF_6 RM175 RAPTA-C RAPTA-T

Figure 3 Representative examples of ruthenium half-sandwich complexes developed by Sadler and Dyson.

Sadler and coworkers have extensively investigated ruthenium half-sandwich compounds of the type [(η^6-arene)Ru(chel)X], where chel is a neutral or mono-anionic N,N-, N,O-, or O,O-chelating ligand (e.g., ethylenediamine, bipyridine, picolinate, 8-hydroxyquinolate, acetylacetonate, maltolate) and X is typically a halide (see Figure 3).[20b] These half-sandwich

compounds are either neutral or positively charged (typically isolated as PF_6 salts), depending on the nature of the chelating ligand.

Among the different organometallic half-sandwich complexes that displayed interesting anticancer activity *in vitro* and *in vivo*,[21a, 23-24] extensive structure-activity relationship investigations demonstrated that the ruthenium compounds containing ethylenediamine (en, Y and Z = N, see Figure 3) and extended polycyclic arenes were the most active toward A2780 human ovarian cancer cells.[25] The mechanism of action of such metallodrugs has many of analogies to that of cisplatin. Like for cisplatin, rapid hydrolysis of the Ru-Cl bond occurs, thereby generating an active monofunctional $Ru\text{-}OH_2$ metabolite. The chloride ligands are believed to be stable at extracellular chloride concentration (about 0.1 M) enabling cell penetration but rapidly hydrolyzed where the chloride concentration is much lower (4-25 mM, corresponding to intracellular conditions). The kinetics of aquation and cellular uptake of such complexes can be fine-tuned by the nature of the metal center, the arene or the chelating ligands.[24c, 25-26] It was proposed that the cytotoxicity of such ruthenium organometallic compounds is related to the ability of aquated products to bind to nuclear DNA.[20b] It was also demonstrated that ruthenium-arene complexes preferentially form monofunctional adducts *via* the N^7 atom of guanine residues.[23, 27] Such strong preference for G bases may allow ruthenium complexes to selectively target G-rich regions of DNA. In this context, telomeres which are guanine-rich DNA sequence overhanging at the ends of eukaryotic chromosomes could represent and interesting target.[28] Furthermore, interactions between aromatic arenes (like the biphenyl RM175, see Figure 3) of the ruthenium complexes and nucleobase can be stabilized by π-π stacking.[23] Different studies carried out with human ovarian cancer cells A2780 revealed that cytotoxicity increases with the hydrophobicity of the arene ligands: ruthenium compounds bearing arene of the type biphenyl (RM175, see Figure 3) display similar activity than the antitumor drug carboplatin, whereas compounds with bulkier tetrahydronaphthalene arene are equipotent with cisplatin.[29]

Studies on the interactions between ruthenium arene complexes and several biologically relevant molecules such as cytochrome c, histidine, cysteine, methionine and glutathione were conducted.[20b, 21a, 24b, 30] Overall, they reveal that the ruthenium complexes exhibit higher reactivity towards DNA than with amino acids and proteins, thus explaining the low toxic side effects exhibited by these metallodrugs.[29] Moreover, the relatively weak binding of amino acids and proteins is suspected to help the transport and delivery to cancer cells. Similarly to cisplatin, some amino acids, peptides and proteins could serve as drug reservoirs for DNA ruthenation.[31] Although DNA is believed to be the main target of these metal-based drugs,[24a] the exact mechanism of action is still matter of debate.

Sadler and coworkers have recently moved towards new metals as possible anticancer compounds (Os and Ir).[14] Furthermore, new bifunctional neutral half-sandwich *cis*-dichlorido Ru^{II}-amine complexes ([(η^6-arene)$Ru(NH_3)Cl_2$], where arene is biphenyl or *p*-cymene) are also under investigation.[32]

The RAPTA piano-stool-derivatives developed by Dyson and coworkers are typically characterized by a monodentate 1,3,5-triaza-7-phosphatricyclo-[3.3.1.1]decane (pta) ligand that were originally designed to improve the metallodrug aqueous solubility (see Figure 3). Similarly to cisplatin and Sadler's complexes, RAPTA compounds have chloride ligands that are kinetically labile and may undergo rapid hydrolysis. It was then first anticipated that RAPTA complexes had DNA as primary target.[33] However, *in vitro* studies demonstrated that generally RAPTA complexes only exhibit modest cytotoxicities.[26b] In contrast, the RAPTA complexes exhibit high affinity for extracellular targets without prior aquation. Such interactions seem to be favored over DNA binding due to the presence of the hydrophobic arene moiety. These extracellular targets are strongly implicated in the ability of RAPTA metallodrugs to prevent metastasis: RAPTA-C and RAPTA-T (see Figure 3) demonstrated interesting antimetastatic activity.[26b, 34] For example, protein-RAPTA-C adducts were characterized by ESI-MS: reaction of RAPTA-C with horse heart cytochrome c and with hen egg white lysozyme revealed stable metalloadducts.[35] RAPTA compounds were also found

to be potent inhibitors of cathepsin B and weak inhibitors of thioredoxin reductase.[36] It was also demonstrated that RAPTA-C induces apoptosis and slows down cell division in cancer cells.[37]

Beyond the conventional approach of drug discovery and with the aim to improve drug efficiency targeted drug design strategy has become a field of increasing interest. In this context, RAPTA derivatives and analogues were designed to have multiple modes of action and functionalized to achieve specific outcomes.[6, 38] This tailoring of functionality is well exemplified by the tethered RAPTA-human serum albumin (RAPTA-HSA), which was found to cause a twenty-fold increase of the cytoxicity compared to RAPTA-C.[39] The RAPTA complexes were the subject of detailed structure-activity investigations, where the arene cap, pta and the anionic ligands were systematically derivatized or substituted.[38] For example, Dyson and coworkers recently prepared RAPTA carboxylato derivatives.[40] This work was inspired by the structures of carboplatin and oxaliplatin. It was assumed that the carboxylato ligands may hydrolyze more slowly and in a more controllable way than the chloride ligands in the original RAPTA-C compound.

It is clear that RAPTA compounds have multiple modes of action and that a target validation has yet to be achieved. However, RAPTA complexes exhibit promising antitumor properties and represent ideal templates for the design and development of tailored therapeutic drug. Surprisingly, given their structural similarities, Sadler and Dyson anticancer compounds displayed different modes of actions on tumor cells.

1.2.2.2. DNA-Targeting Strategies for Metal-Based Therapeutics

1.2.2.2.1. Targeting Double-Stranded DNA with Metallointercalators

An increasing number of therapeutic agents designed to target nucleic acids has recently emerged.[41] The most effective metallodrug in anticancer therapy, cisplatin and its derivatives is thought to have DNA as a main target: DNA-metallodrug adducts generate

lesions which ultimately trigger cell death. However, platinum-based drugs often suffer from high systemic toxicity, inherent or acquired resistance, which is a main problem that limits their clinical use. Consequently, much effort was devoted in designing more selective drug delivery systems and/or activation of cisplatin-related prodrugs.[24a] The specific recognition of DNA by therapeutic agents has received increasing interest and metal-based drugs are viewed as playing an important role in the field. Metal complexes traditionally interact with DNA in one of the three ways, leading to the following classification: metallointercalators,[42] groove binders[43] and the more novel metalloinserters.[44] Perhaps the most commonly encountered type, the metallointercalators are made of organic intercalators covalently attached to transition metal complexes that offer new DNA interactions opportunities, which can ultimately influence the biological activity. Intercalative binding refers to the non-covalent stacking interaction between a planar heterocyclic aromatic ring belonging to the metal-based molecule and the base pairs of the DNA double helix. Metallointercalators can bind specifically to sequences in the major groove of the DNA double helix. Such intercalations can stabilize, lengthen, stiffen or unwind DNA by acting as a kind of “new base pair”. Modulation of the aromatic side chain of the metal complex opens the way to fine-tune the DNA binding and allows the introduction of new modes of metallodrug-biomolecule interaction.

This strategy has been investigated by Sadler and coworkers with the Ru^{II}-piano stool complexes bearing polycyclic arene ligands such as RM175 (see Figure 3). Such complexes were found to be more potent toward cancer cells than their non-intercalating analogs (e.g., ruthenium bearing η^6-*p*-cymene or η^6-benzene).[23] This design concept can be applied to structure activity relationships for other organometallic anticancer complexes, including cyclopentadienyl complexes.[14] In this context, Liu *et al.* reported that the hydrophobicity and intercalative ability of Ir^{III}-half-sandwich complexes make a major contribution to the anticancer potency.

1.2.2.2.2. Targeting Telomeric DNA

As mentioned above, ruthenium complexes preferentially interact with guanine bases and, consequently, bind mostly to guanine-rich DNA sequences. Telomeres, which are structures found at the ends of eukaryotic chromosomes,[45] consist of highly conserved and repeated G-rich sequences and can be considered as a privileged target. Telomeric DNA consisting of (TTAGGG)*n* repeats in humans, protects the very end of linear chromosomes and thus preserves the stability and the structural integrity of chromosomes[46] particularly during mitotic cell division.[47] Telomeres are also important because they preserve the genome integrity by protecting chromosomes from a loss of genetic information. However, in normal cells the chromosomes are progressively shortened over rounds of cell replication until a length-limit (Hayflick limit) that induces a signal in the cell, leading to senescence.[48] The telomere dysfunction can lead to chromosome instability and abnormalities, senescence or apoptosis, and represents potentially the most widespread cause of genome instability in cancer.[49] The enzyme telomerase, which counteracts this shortening by adding base pair repeats to the 3' end of DNA strands, is largely absent in healthy cells, but is expressed in 85-90% of tumor cells.[50] A particularity of cancer cells is their unlimited proliferative capacity, which is at least in part sustained by the activation of a telomere maintenance mechanism (TMM). Disruption of the TMM, facilitates rapid and infinite proliferation of the tumor cells.

The 3′-G-overhang of the telomere, (TTAGGG)*n* is able to fold in a G-quadruplex structure that consists of a planar arrangement of tetrads of guanine bases associated by Hoogsteen-type hydrogen bonds. The G-quadruplex structures can be classified depending on the orientation of the DNA:[51] parallel,[52] antiparallel[53] and two mixed-hybrid structures (see Figure 4).[54] In most cases, the structures are determined in the presence of a monovalent cation (mostly Na^+ or K^+)[55] which plays an important role in the stabilization of tetrad structure due to electrostatic interactions engaged with the guanine carbonyl groups of two adjacent G-quartets (see Figure 4).[56]

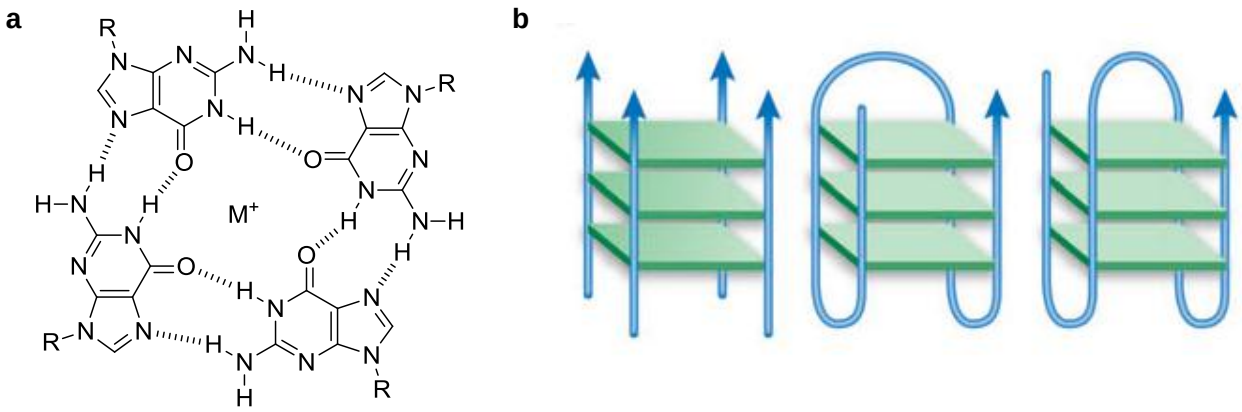

Figure 4 G-quartets and G4 DNA. a) G-quadruplex, a planar ring of four guanines, with a monovalent central metal cation. b) G4 DNA. Strands may be parallel (left), antiparallel (center) or mixed (right). The latter stabilization was found to be of major interest.

Telomerase exclusively recognizes the extremity of the 3'-G-overhang of telomeric DNA. Consequently, the formation of G-quadruplex structures may hinder telomeric recognition by telomerase and may interfere with telomere elongation.[57] Therefore, the stabilization of G-quadruplex DNA structures by chemotherapeutics has been proposed as a new anticancer strategy.[58]

1.2.3. Piano-Stool Complexes in Transfer Hydrogenation Reactions

1.2.3.1. Asymmetric Transfer Hydrogenation of Ketones

The catalytic asymmetric transfer hydrogenation (ATH) has emerged as a practical alternative to hydrogenation processes (no use of hazardous H_2). ATH has demonstrated to be particularly suitable for the preparation of optically active secondary alcohols which are important intermediates in the synthesis of various high value-added chemicals.[59]

Discovered in 1925, the Meerwein-Ponndorf-Verley (MPV) reduction was the first example of transfer hydrogenation of carbonyl groups.[60] Since then, the majority of the research carried out in this area has relied on piano stool complexes involving Ru^{II}-arene or Ir^{III}/Rh^{III}-cyclopentadienyl moieties and bearing optically active phosphine and amino/sulfonamide

ligands.[61] Perhaps the most important advance in such catalytic systems employed in ATH of ketones was the discovery by Noyori and coworkers of the Ru^{II}-TsDPEN catalyst **1** (see Figure 1),[7a] which displays broad substrate scope and provides optically active alcohols at high enantiomeric purity and yield.

The most common sources of hydrogen for ATH of ketones are isopropanol, azeotropic mixtures of isopronapol with triethylamine, formic acid or formate salts. However, mixtures of formate salts or formic acid and triethylamine are increasingly used since the irreversible formation of CO_2 (g) with generation of the metal hydride favors an irreversible reaction.[7a] One limitation of the process is the decomposition of the catalyst in contact with high concentrations of formic acid.[61b]

The advantage of using transition metal catalysts for asymmetric transformations is the possibility of catalyst improvement by easy modification of the ligands. Most of the metal complexes bear bi-, tri-, or tetradentate ligands containing nitrogen, oxygen or phosphorus as coordinating atoms.[61b, 61e, 62] Water-soluble ligands and addition of surfactants have contributed to the development aqueous transfer hydrogenation reactions.[62-63] Finally, the reduction rates were considerably faster using HCOONa than the $HCOOH/Et_3N$ azeotrope or *i*PrOH.[64] In this context, Xiao has shown that both the reaction rate and the enantioselectivity of aqueous transfer hydrogenation reactions critically depend on the pH.[65]

The mechanisms by which hydrogen is transferred from a donor to an acceptor can proceed in different manners depending on the metal, ligand and hydrogen donor used (see Figure 5).

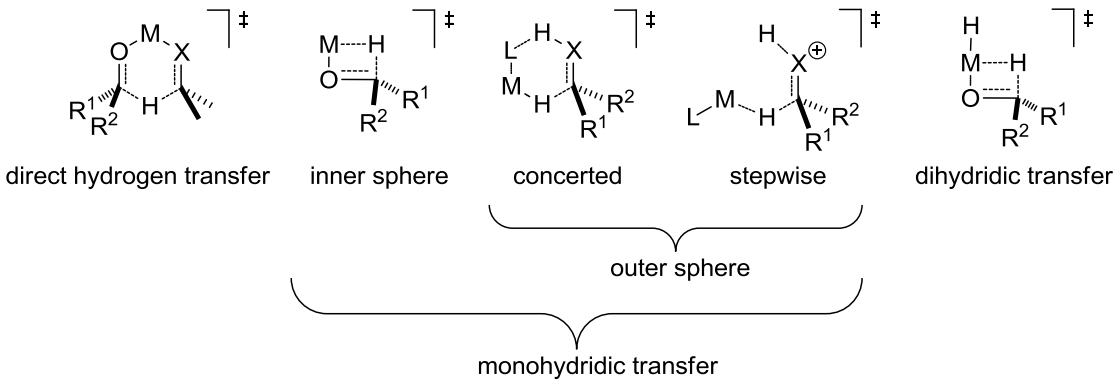

Figure 5 Postulated transition states for the mechanism of hydrogen transfer to a ketone.

The “direct hydrogen transfer” usually occurs with main group metals, while transition metal catalysts follow the “hydridic route”, in which a mono- or a dihydride metal species is involved.[61c, 66] The monohydridic transfer can either occur *via* ketone coordination to the metal, or *via* an outer sphere mechanism. Finally, when no substrate-metal interaction is involved, the mechanism can be concerted or stepwise.[61c]The currently accepted mechanism for the Noyori-type transfer hydrogenation catalyzed by Ru-, Rh- or Ir-complexes proceeds *via* an outer sphere concerted hydride transfer and relies on metal-ligand cooperation.[66b, 67] Both the metal and the ligand participate to the bond-breaking and forming process and the transition state does not involve direct coordination of the substrate to the metal (see Figure 5). Ligands possessing acidic protons (*i.e.* metal-coordinated primary or secondary amines), facilitate the hydride delivery to the carbonyl (see Scheme 1).

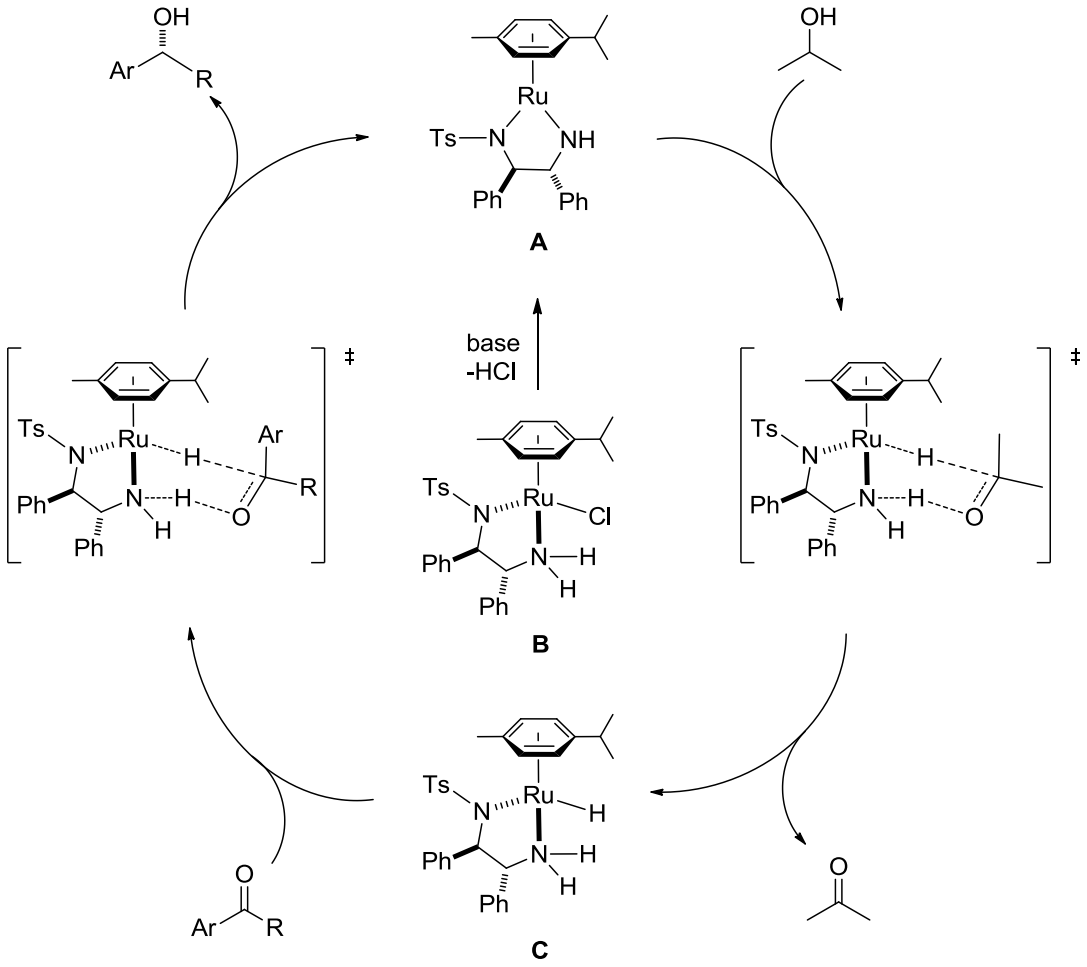

Scheme 1 Postulated catalytic cycle for the transfer hydrogenation of an aromatic ketone using [Ru(*p*-cymene)(*R*,*R*-TsDPEN)Cl] and *i*PrOH as hydrogen donor.

The true catalytic species is the 16 e^- Ru-complex **A** formed from the catalyst precursor **B** by elimination of HCl in the presence of a base. The protonation of the amide leads to the 18 e^- Ru-hydride complex **C**. The hydride and the axial NH proton are transferred simultaneously from the 18 e^- Ru-complex to the substrate *via* a six membered ring transition state, to regenerate the 16 e^- complex **A**.[68]

1.2.3.2. Asymmetric Transfer Hydrogenation of Imines

Optically active amines are highly valuable products in industry[69] and intermediates of great importance in chemical synthesis as chiral ligands, auxiliaries or catalysts.[70] In 1981, Grigg and coworkers reported the first example of transfer hydrogenation of imines.[71] In this work, Wilkinson's catalyst, $[RhCl(Ph_3P)_3]$ was used for the reduction of aldimines by isopropanol in the presence of sodium carbonate. Later on, Brune *et al.* attempted to elucidate the mechanism of proton and hydride transfer from 2-propanol to imines in the presence of Wilkinson's catalyst.[72] Since the pioneering use of the Wilkinson's catalyst, an increasing number of catalytic systems, including chiral variants, have been developed. Among them, the most studied and most successful ones are those employing half-sandwich complexes as catalysts. In 2001, Casey studied one of the most famous catalysts for the stoichiometric TH of imines: the bifunctional Shvo catalyst **2** (see Figure 6).[73] Bäckvall and coworkers subsequently reported the catalytic reduction of imines with the Shvo catalyst using 2-propanol as the hydrogen source with benzene as a co-solvent.[74] In solution, the Shvo pre-catalyst dissociates into species **3** and **4**; the 18 e^- catalyst **3** effects the hydrogenation, turning into complex **4** which dehydrogenates isopropanol to regenerate the specie **3** (see Figure 6).

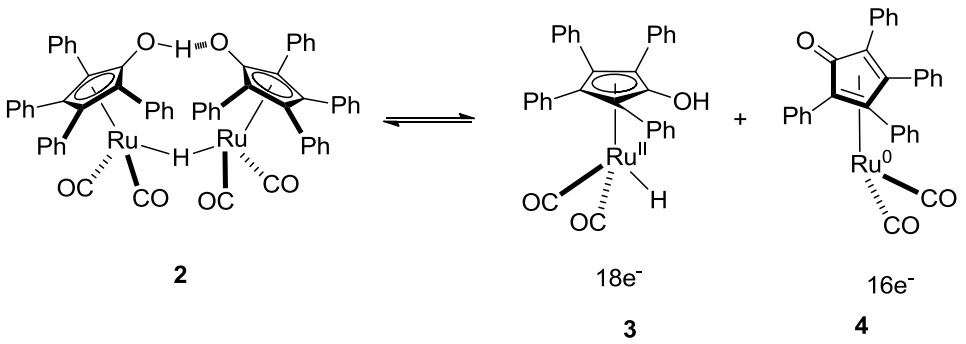

Figure 6 Reduction of imines with Shvo's catalyst **2**.

In 1996, Noyori and coworkers described the first chiral Ru^{II}-TsDPEN **1** complex that efficiently catalyzed the ATH of cyclic and acylic imines under mild conditions using formic acid-triethylamine as the hydrogen source (see Scheme 2).[75] Since these pioneering studies, ATH has become a powerful tool for the reduction of imines.[76] Moreover, these studies on cyclic imines led to consider tetrahydroisoquinoline-based scaffolds as substrates of choice for the implementation of new reactions. The synthesis of salsolidine **5** was considered to be a model reaction in ATH.

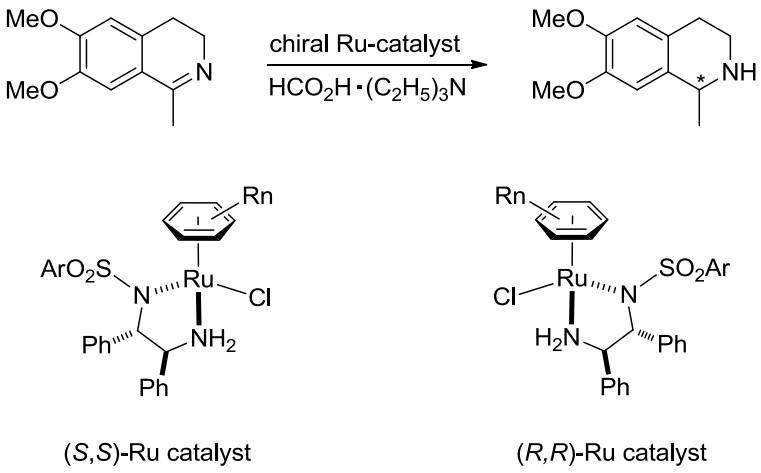

Scheme 2 Noyori's chiral Ru-precatalyst for ATH of cyclic imines: preparation of salsolidine.

The increasing demand for efficient and environmentally friendly chemistry resulted in the development of catalysts that are water-compatible with particular emphasis on the development of water-soluble catalysts. In such media Ru^{II}, Rh^{III} and Ir^{III} are quite effective metal cations in ATH reactions. In 2006, Wu *et al.* reported the first ATH of cyclic imines and

iminiums using a water soluble catalyst.[77] Deng and coworkers reported yield up to 99% and enantioselectivities up to 99% when enantiopure *o,o'*-disulfonated *N*-tosyl-1,2-diphenylethylene diamine was combined with $[Ru(p\text{-cymene})Cl_2]_2$ using HCOONa as the hydrogen source and CTAB (cetyltrimethylammonium bromide) as a surfactant (see Scheme 3).

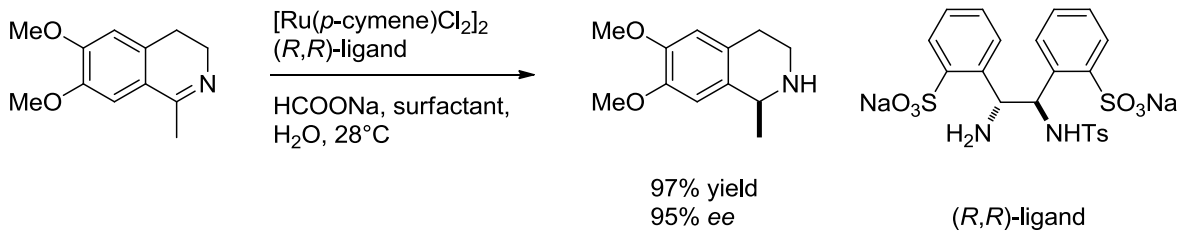

Scheme 3 Asymmetric transfer hydrogenation of cyclic imine in water.

Later, Süss-Fink and coworkers reported cationic arene ruthenium aquo complexes containing enantiopure chiral monosulfonated diamine ligands that performed ATH of aromatic ketones and imines in aqueous solution using sodium formate without any additional surfactant.[78] The investigations conducted by Xiao and coworkers on ATH reactions in water highlighted the determinant role of pH in the reaction rate.[9a, 65, 79]

Compared to the extensively studied mechanism for the transfer hydrogenation of ketones, the mechanism by which imines are hydrogenated is still matter of debate.[80] The first mechanistic studies conducted by Bäckvall and coworkers proposed an inner sphere mechanism in which the addition of acid is necessary to pre-activate the substrate by protonation prior to hydrogen transfer.[80a] In contrast, based on DFT calculations using Shvo's catalyst, Casey found the transition state to be a concerted outer sphere mechanism, comparable to the ketone reduction mechanism.[80b] Since then, various lines of evidence appear to favor an ionic mechanism[66a, 81] where the metal-hydride transfers to a protonated and hence activated imine, involving no coordination of the imine to the metal centre during the hydride transfer. This is in contrast to the well-established metal-ligand bifunctional pathway for ketone reductions.[67, 82] Further evidence for the ionic pathway is found in the TH of quinolines, where acidic conditions are required.[79] In addition, Xiao and coworkers

developed cyclometalated iridium catalyst with no free NH allowing metal-ligand bifunctional action that would also follow the same ionic mechanism.[83]

Practical studies on the ATH of cyclic imines revealed that the mechanism of ketone reduction cannot be transposed to isoquinoline-type imines since the opposite enantiomer is observed compared to the enantiomer produced in ATH of ketones with the same catalyst. With the aim to better understand the system, Martins *et al.* proposed two alternative mechanisms (see Figure 7).[84] The first mechanism depicted the reduction of imine *via* a six-membered transition state (see Figure 7b). The orientation of the alkyl and the aryl groups are inverted thus avoiding the CH/π interaction proposed in Noyori's mechanism (see Figure 7a). The second proposed mechanism is an ionic mechanism in which Wills proposed the formation of an iminium cation that would be oriented away from the NH of the ligand amine (see Figure 7c). The latter mechanism proceeds without the formation of a concerted six-membered transition state but would allow the CH/π interaction to afford the right enantiomer.

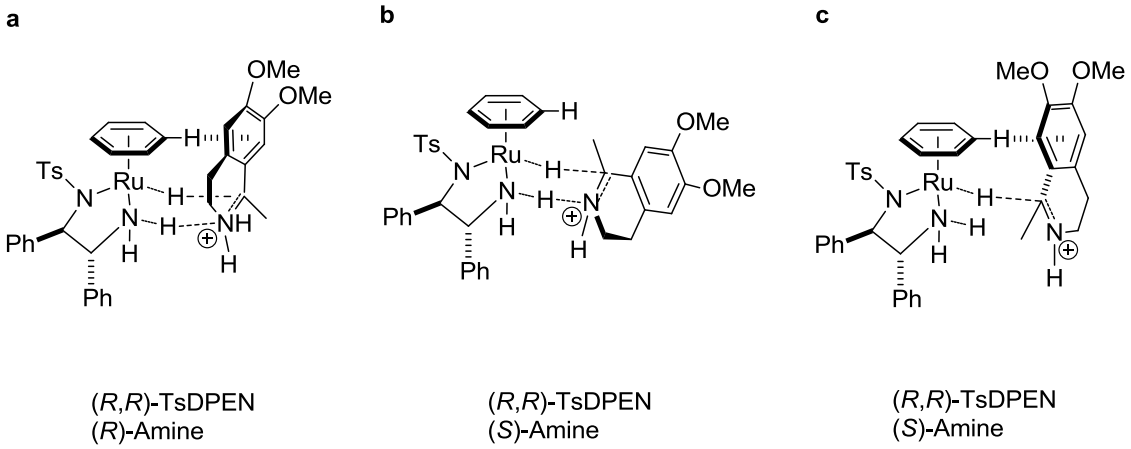

Figure 7 Possible mode of reduction in ATH of cyclic isoquinoline-type imines with Noyori's (*R,R*)-TsDPEN catalyst **1**.[84]

Although the investigations of Bäckvall and Wills tend to support an ionic mechanism, the pathway of the transfer hydrogenation of imines is not yet completely understood and the possibility of a substrate-specific mechanism cannot be excluded.

1.2.3.3. Asymmetric Reductive Amination to Prepare Optically Pure Amino Acids

Optically pure amino acids are important chiral building blocks[85] that are widely present in many natural bio-active molecules,[86] chiral synthons for the manufacturing of fine chemicals,[87] the design of chiral ligands and in total synthesis.[88] The synthesis of α-amino acids is an area of research that has gained a lot of attention in recent years.[89] However, no single methodology has yet emerged for the asymmetric synthesis of all natural and unnatural amino acids.[69a] The different approaches to obtain α-amino acids are summarized in Scheme 4. These methods can also be applied for the synthesis of unnatural α-amino acids which are now finding widespread application in the pharmaceutical, agrochemical, food additives and cosmetic industry.[90] Among the different methodologies to synthesize proteinogenic and non-proteinogenic α-amino acids, one of the most interesting is the asymmetric reductive amination of α-keto acids.[91]

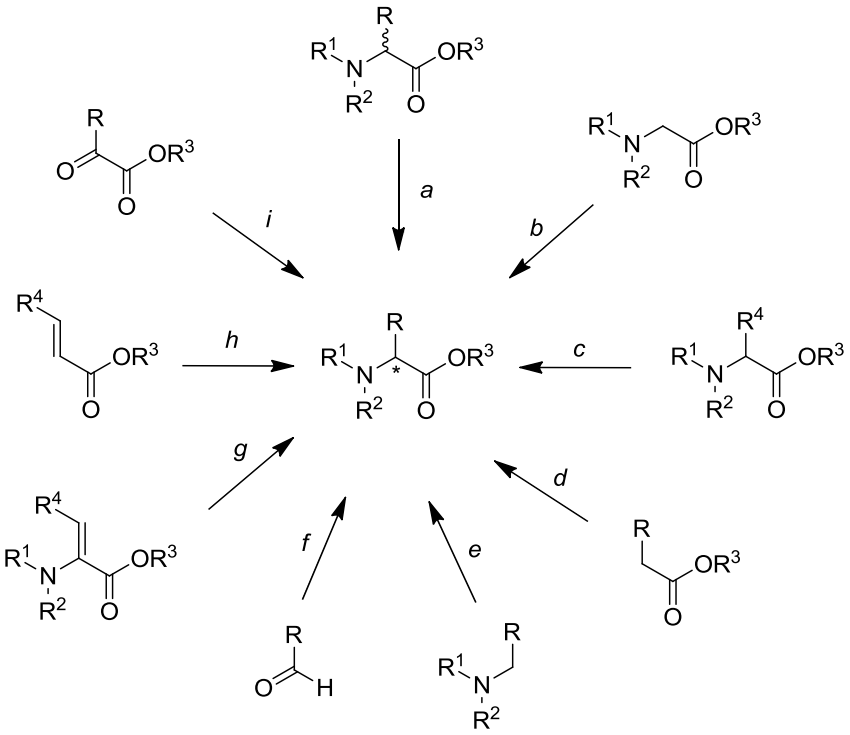

Scheme 4 Different approaches for the synthesis of natural and unnatural amino acids.[89]

The resolution approach is depicted in method *a*. This method includes the separation of racemic mixture into single enantiomers or dynamic resolutions where the undesired

enantiomer is isomerized to allow a single product enantiomer to be formed. The second approach (*b*) involves the introduction of the side-chain for example through alkylation reaction using benzyl halides. Method *c* involves the chemical modifications of the side-chain to prepare the desired product. For example the synthesis of (*L*)-homoserine from methionine.[92] Amino acids can be obtained by introduction of either the nitrogen moiety (see method *d*) or the carboxylic acid group (see method *e*). In the first method the electrophilic introduction of azide with chiral imide enolates was used to prepare α-amino acids with high diastereoselection (the azide is further reduced to an amine)[93] Most of the methods involving the introduction of carboxylic acid group use the Strecker reaction where a nitrile is used as a masked carboxylic acid. Indeed, the Strecker reaction combines these last two approaches (method *f*).[94] In the classical Strecker reaction an aldehyde is condensed with ammonium chloride in the presence of potassium cyanide. The resulting α-aminonitrile is subsequently hydrolyzed to give the desired α-amino acid. Hydrogenation is depicted in method *g*: an example is the asymmetric reduction of the enamide with chiral rhodium catalysts.[4c]. Method *h* introduces the nitrogen group to unsaturation and this can be performed by an enzyme. Method *i* describes either a transamination or reductive amination approach, usually achieved by enzymes.

The explosive growth of synthesis of α-AAs has been achieved as a result of the enormous effort in creating asymmetric catalysts.[95] Most enantioselective catalysts are either metal complexes with chiral organic ligands or chiral organic molecules, so-called organocatalysts.[96] However, asymmetric synthesis of pure α-amino acids often suffers from a lack of environmental awareness, since some of the most widely employed methods use organic solvents and highly toxic agents such as cyanides.[97] Moving towards a greener synthesis, the direct reductive amination (DRA) of α-keto acids may offer an attractive alternative. DRA transforms prochiral carbonyls into amines through the *in situ* generation of imine in the presence of a reducing agent.[98] Despite its long history and common use of the term reductive amination[99] only a few studies on the homogeneous direct reductive amination of carbonyls have been reported.[76d] Perhaps the best known example of

enantioselective reductive amination is that reported by Blaser and co-workers for the synthesis of the herbicide (*S*)-metolachlor® (see Scheme 5).[61e, 100]

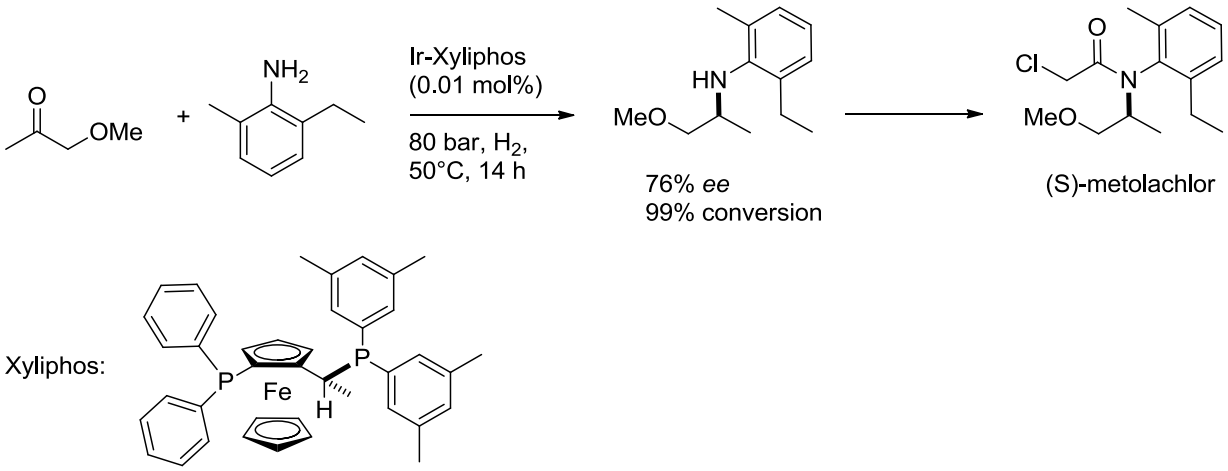

Scheme 5 Enantioselective synthesis of Metolachlor by reductive amination of a prochiral ketone.[101]

In 2003, Zhang studied the reductive amination of aryl alkyl ketones with *p*-anisidine using an Ir-f-Binaphane complex as the catalyst.[102] Full conversions (TON of 100) and high enantioselectivies (up to 96% *ee*) were achieved in asymmetric reductive amination in the presence of $Ti(O^iPr)_4$ and I_2. The combined efforts of Kadyrov and Börner led to important advances in the field of chiral amine synthesis.[103] In 2009, Xiao exploited different Cp^*Ir^{III}-TsDPEN complexes in combination with a BINOL-based chiral phosphate counter-anion (TRIP anion) to perform reductive amination of 46 ketones derivatives (see Scheme 6).[104]

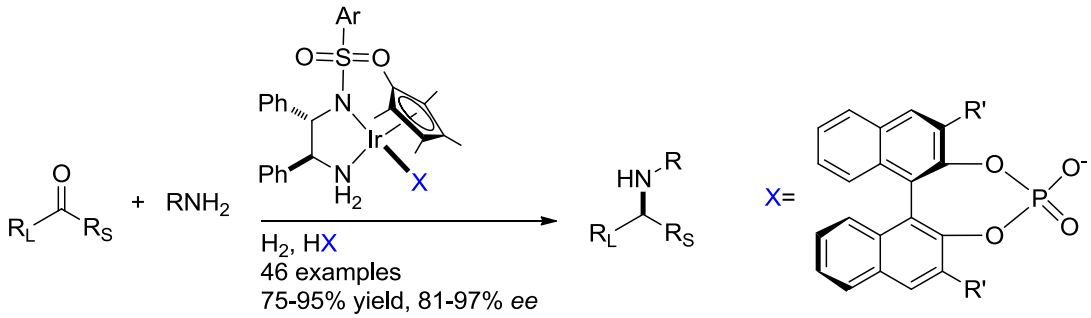

Scheme 6 DRA of a wide range of ketones by the cooperative catalysis of an Ir^{III}-aminosulfonamide complex and an enantiopure phosphoric acid or its conjugate base.[104]

Direct reductive amination has been less investigated for the synthesis of α-AAs from α-keto acids.[105] The first catalytic enantioselective reductive amination using rhodium was reported by Tararov *et al.* (see Scheme 7).[106]

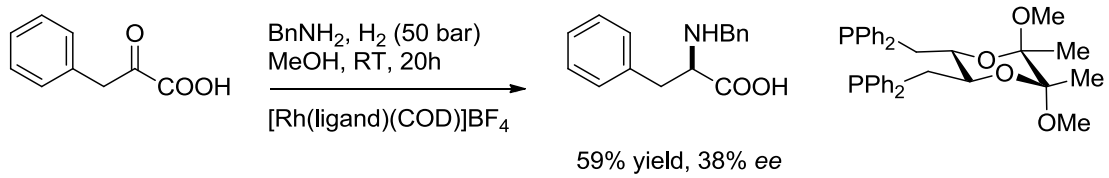

Scheme 7 First catalytic enantioselective reductive amination of α-keto acids.[106]

Fukuzumi and co-workers reported the first non-enzymatic highly chemoselective synthesis of α-amino acids by the reductive amination α-keto acids using $HCOONH_4$ in water.[107] They employed an acid-stable mononuclear iridium hydride complex and succeeded in the synthesis of all major types of α-AAs by controlling pH (see Scheme 8). The major advance of this work was the simplicity of performing reductive amination while using ammonium as a nitrogen source to produce α-AAs in water and formate as hydride source.

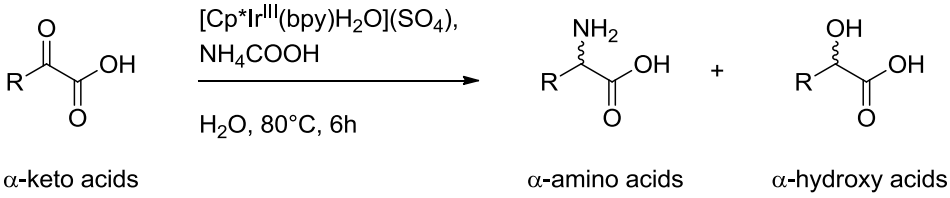

Scheme 8 Synthesis of α-amino acids by reductive amination of α-keto acids with ammonia in water.[107]

Selective reduction of the imine is critical because reduction of the carbonyl compounds results in undesired alcohol formation. Rhodium-, iridium- and ruthenium-based catalysts are useful in this respect because they are known to be more efficient at hydrogenating C=N bonds over carbonyls.[61b, 75] Several important factors contribute to the efficiency of catalytic direct reductive amination, including possible interactions between the resulting amine, which could readily coordinate to the unsaturated metal complex; and interactions between the transition metal catalyst and the starting material or the hydroxy acid, which could lead to

reaction inhibition. The DRA approach is useful in the cases where unstable intermediates are encountered during the reductive amination of α-keto acids.

1.3. Artificial Metalloenzymes

1.3.1. Designing Artificial Metalloenzymes

Artificial metalloenzymes attempt to take advantage of the best of both homogeneous and enzymatic catalysts. Indeed, artificial metalloenzymes are created by incorporating a catalytically active transition metal complex within a biomacromolecule, typically a protein[108] or DNA.[109] The resulting hybrid can thus potentially give access to the best features from the mentioned fields of catalysis. In transition metal-mediated catalysis the first coordination sphere is provided by a ligand, thus influencing both activity and selectivity. In contrast, enzymes are able to provide, through hydrogen bonding and hydrophobic interactions, both first and second coordination sphere interactions responsible for the high activity, selectivity and efficiency. Inspired by these features, artificial metalloenzymes aim at harnessing second coordination sphere interactions to create transition metal-biomolecular assemblies that display enzyme-like activities and selectivities. For that purpose, different approaches make use of ligand-functionalized peptide chains, DNA, RNA and proteins.[110] One of the most challenging approaches is the *de novo* design of enzymes. This *de novo* strategy involves constructing a polypeptide sequence that is not directly related to any natural protein and that folds precisely into a defined three dimensional structure, providing the required second coordination sphere to the metal ion.[111] Designing metalloproteins using *de novo*-designed scaffolds is extremely challenging since the protein's structure and metal-binding properties must be designed. Unfortunately, the limited knowledge of the precise rules of protein folding limits the growth of the field. Only a few *de novo*-designed scaffolds have emerged, such as the α-helical bundles.[111] For this reason, the design of metalloproteins has focused on the creation of active sites within existing, native, biomolecular scaffolds,

such as proteins and DNA. The design of active sites into native scaffolds encounters some advantages, such as abundant scaffold choices from the Protein Database (PDB) and the finding that most of the natural protein scaffolds are thermodynamically stable and tolerate mutagenesis.[112] When designing an artificial metalloenzyme, it is also important to ensure that the catalytic moiety is localized within or close to the biomolecular scaffold, because only close contact to the second coordination sphere can eventually lead to selectivity for a given transformation. With this aim in mind, three different anchoring strategies have been pursued: supramolecular anchoring, dative anchoring and covalent anchoring.

1.3.1.1. Supramolecular anchoring

Supramolecular anchoring is based on strong and highly specific non-covalent interactions between the biomolecular scaffold and a specific moiety acting as an anchor. A perfect example of supramolecular anchoring is represented by biotin-streptavidin technology. Indeed, the strength of biotin/streptavidin interaction is so strong that it ensures precise biotinylated catalyst localization, which can be characterized structurally.[113]

1.3.1.2. Dative anchoring

Dative anchoring allows localization of the catalytically active metal through coordination to the biomolecular scaffold *via* dative bonds. Such coordinative bonds are created between the catalytic metal ion and functionalities presented by the biomolecular scaffold. Examples include artificial metalloenzymes made by incorporation of Mn-salen complexes in apo-myoglobin and Fe and Mn corroles in serum albumins which have been used in catalytic enantioselective sulfoxidation reactions.[114] Another interesting example involves the metal-substitution in carbonic anhydrase exploited independently by Kazlauskas and Soumillon.[115]

1.3.1.3. Covalent anchoring

In covalent anchoring, a covalent bond is formed between the transition metal complex and the biomolecular scaffold. The covalent anchoring approach is based on the pioneering work of Kaiser.[116] Most often, a cysteine residue is used as the anchoring site which allows for site-selective anchoring of the catalytic moiety. Although the covalent strategy guarantees control over the structure and geometry of the catalytic site, this anchoring method involves chemical modifications and non-trivial purification steps, which limit the number of mutants which can easily be studied.

1.3.1.4. Combining Different Anchoring Strategies

Particular attention has to be devoted to the "dual" anchoring strategies. For example, Lu *et al*. used a "dual" covalent anchoring strategy to introduce an achiral manganese salen complex, into apo-sperm whale myoglobin.[117] This dual anchoring approach was shown to affect the catalytic sulfoxidation of thioanisole providing higher *ee* and rate than either non-covalent or single-point covalent attachment strategies. In the same spirit, Watanabe and coworkers also exploited the exceptional properties of myoglobin in a "dual" anchoring approach to build artificial peroxidases: combination of supramolecular (hydrophobic interactions between the ligand [salen, salophen and porphycene] and the protein) and dative (metal-proximal histidine) interactions.[114a, 118]

1.3.2. The Biotin-Streptavidin Technology

1.3.2.1. Structural Considerations

Designing new artificial metalloenzymes using supramolecular anchoring strategy relies on the accurate choice of the guest/host couple. As mentioned before, the supramolecular anchoring strategy takes advantage of the strong specific interactions between a biomolecule

and its substrate. For that purpose, the biotin-streptavidin system appears to be a perfect system to build artificial metalloenzymes.[119] Many reasons can explain the success of the biotin-streptavidin couple:

i) The affinity of biotin for (strept)avidin is among the strongest known for a cofactor-protein assembly ($K_a \approx 10^{13}$ M^{-1}).[120] The affinity is so strong that the position of the metal complex in the protein is unambiguous, which allows improving the catalytic performances of metalloenzymes. Furthermore, derivatization of the valeric chain of biotin by introduction of linkers or modulation of the chelators does not cause dramatic changes in affinity.[120-121]

ii) Streptavidin has an exceptional stability towards environment changes which allows the creation of a large repertoire of reactions: a fully biotin loaded streptavidin is stable at 110°C for several minutes, the protein is not fully denatured under extreme pH conditions (6 M guanidinium chloride at pH 1.5), streptavidin tolerates high concentrations of organic solvent (50% EtOH) and the presence of surfactants (such as sodium dodecyl sulphate, SDS).[122]

iii) The biotin-(strept)avidin technology allows for a modular approach of optimization: protein and cofactor can be modified separately, by genetic and by chemical means, respectively. In addition, no chemical modification is needed after the incorporation of the catalyst precursor, ensuring the integrity of the catalytic moiety.

iv) The easy access to a biomolecular host is an important parameter in the creation of metalloenzymes. From this point of view, streptavidin which is secreted by *Streptomyces* bacteria,[120] can be expressed from *E. coli* culture and produced as recombinant protein with high yields (about 200 mg per liter of *E.coli* culture).[123] In addition, streptavidin is easy to purify by affinity chromatography using immobilized iminobiotin.

1.3.2.2. Optimization of the Catalytic Activity of Artificial Metalloenzymes

In addition to traditional synthetic tools for optimization of the cofactor (ligand, spacer, counterion for example), the structure of the protein scaffold can be optimized. This strategy was coined by Distefano and Häring the “chemogenetic approach”.[124] In principle this

approach allows fine-tuning of the first and second coordination sphere, leading to hybrid catalyst library that can be screened for a specific reaction. For that purpose, the studies of Ward and Reetz on the biotin-strep(avidin) system highlighted the potential of evolving systems by the combinatorial screening of large numbers of mutant proteins.[125] Reetz and coworkers reported a "directed evolution" strategy.[126] This Darwinian approach, which involves repeated cycles of random mutagenesis coupled with an efficient high throughput screening (HTS) system for evaluating enantioselectivity, allows the generation of a large library of different enzymes.[127] Although direct evolution is a powerful tool to improve enzyme and protein performance,[128] the screening of large mutant libraries is time-consuming and labor-intensive. To reduce the screening effort, a new methodology coined "Combinatorial Active-Site Saturation Test" (CAST),[129] was introduced by Reetz *et al.*[130] In contrast to directed evolution, Ward and coworkers implemented a strategy coined "designed evolution",[131] where chemogenetic optimization is guided by rational decisions on sites of mutation. Structural information obtained either by crystallographic[113] or computational[132] means leads to site-directed mutagenesis of selected amino acids to tune the second coordination sphere around the metal catalyst.

1.3. Aim of Thesis

Engineered artificial metalloenzymes attempt to take advantage of the attractive properties both of homogeneous catalysis and biocatalysis, for example to perform important catalytic processes such as transfer hydrogenations. However, two of the main challenges in the field are i) the development of artificial enzymes for novel reactions and ii) increased mechanistic understanding, so that new features can be engineered "bottom-up". This thesis contributes toward solving these challenges, by setting up synthetic tools and methodologies to expand the biotin-avidin technology for new applications, in particular for specific DNA targeting for improved delivery of anticancer metallodrugs and for new reactions, including reductive amination.

Throughout the thesis, the methods rely on synthesis and incorporation of biotinylated piano stool complexes into host streptavidin protein. In the first part of the thesis, the aim is to rationally design a metallodrug-presenter protein to improve selectivity of a ruthenium-based drug for G-quadruplex DNA over double-stranded DNA.

The second part of this thesis deals with the development of artificial metalloenzymes by two different approaches:

i) Setting up a new synthetic platform for accelerated chemical optimization of biotinylated catalysts; using d^6-piano stool rhodium and iridium complexes with a tethered-tetramethylcyclopentadienyl moitey directly attached to biotin.

ii) Exploiting the versatility of the biotin-streptavidin technology to create new artificial metalloenzymes consisting of rational ligand design combined with genetic optimization of the biomolecular host.

The two implemented strategies were investigated in asymmetric transfer hydrogenation reactions: the well established reduction of cyclic imines and the less explored reductive amination.

In summary, this thesis describes studies of hybrid supramolecular constructs of streptavidin and biotinylated piano stools, with a focus on developing new methods and novel applications, leading to increased mechanistic understanding of this technology.

2. Chemo-Genetic Optimization of DNA Recognition by Metallodrugs Using a Presenter Protein Strategy

2.1. Introduction

In this chapter, I describe mechanisms by which a presenter protein could be exploited to deliver small molecules like metallodrugs to preferred macromolecular targets *in vitro*. A ruthenium metallodrug-protein assembly based on the biotin-streptavidin technology was constructed to provide non-covalent interactions that modulate binding of the organometallic moiety to specific DNA targets. Guided by the X-ray structure of the drug embedded within the Sav protein, we explored the formation of metallodrug-mediated ternary complexes between the presenter protein and DNA.

The assemblies bound more strongly to telomere G-quadruplexes than to double-stranded DNA; chemo-genetic modifications (varying the complex or mutating the protein) modulated binding to these targets. We suggest that rational targeting of metallodrugs *via* presenter proteins could be exploited to improve selectivity of small molecules to preferred macromolecular targets.

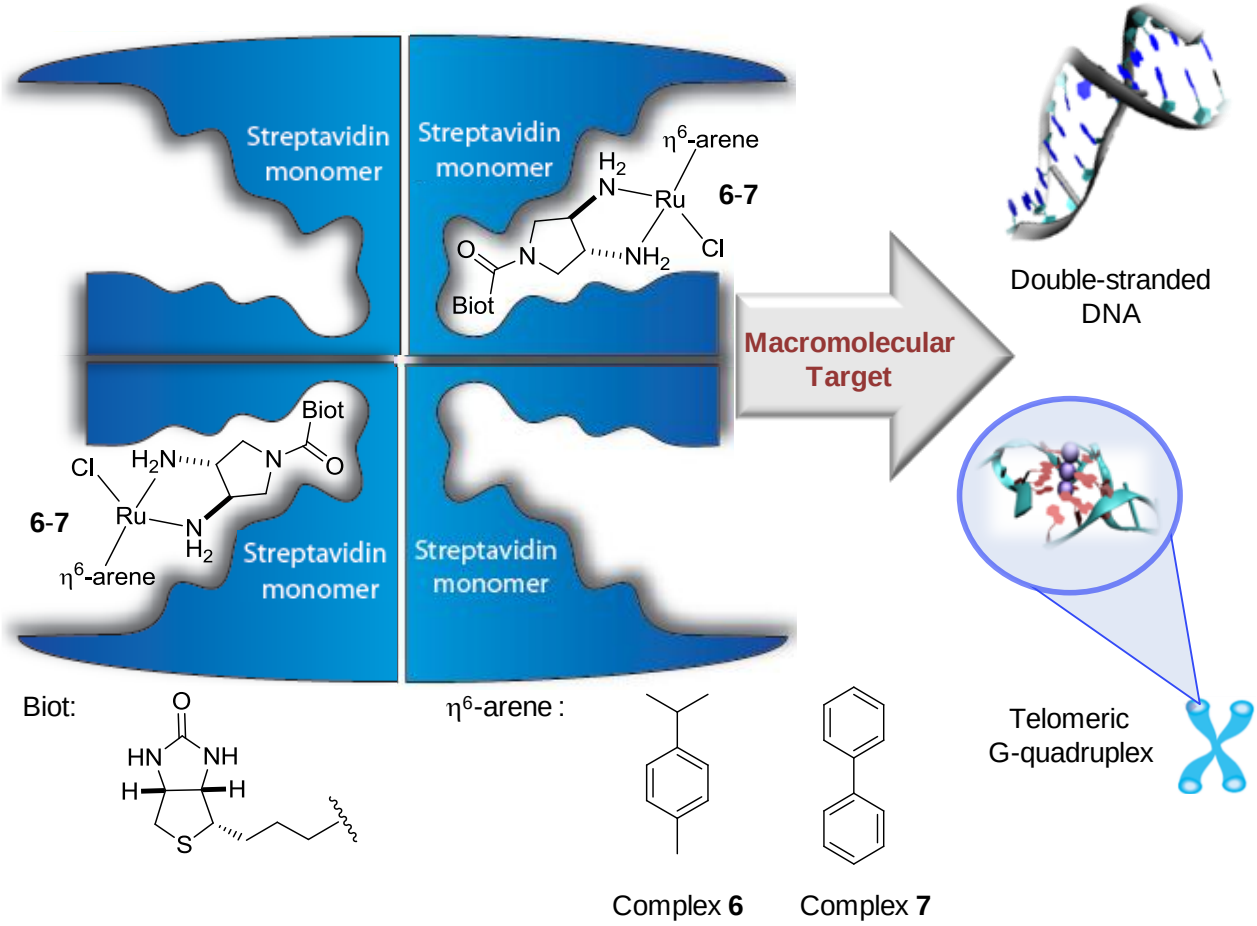

Figure 8 Presenter protein strategy for targeting DNA with ruthenium metallodrugs. The ruthenium drug embedded into tetrameric WT Sav in a 2 : 1 molar ratio forms a supramolecular complex that may allow extensive interactions with DNA. Chemo-genetic optimization, i.e. mutations of defined Sav residues (e.g. K121 and S112) or modifying the arene cap of the biotinylated ruthenium piano stool complex can modulate the affinity of the assembly for the DNA target. Compound **6** = [(η^6-*p*-cymene)Ru(Biot-L)Cl]CF_3SO_3 and **7** = [(η^6-biphenyl)Ru(Biot-L)Cl]CF_3SO_3; Biot-L = Biotin-*N*-(*R*,*R*)-3,4-diaminopyrrolidine.

2.2. Construction of the Presenter Protein and Metallodrug-Assembly: 6 ⊂ WT Sav

2.2.1. Choice of the Organometallic Drug

Organometallic drugs have received increasing attention spurred by their non cross-resistance with Pt-based drugs. In specific, the study of ruthenium piano stool complexes as potential anti-tumor drugs has begun to establish structure-activity relationships.[133]

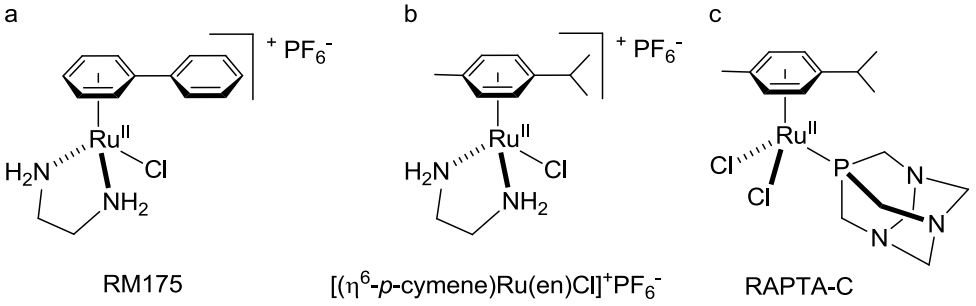

Figure 9 Ruthenium piano stool metallodrug complexes developed by a) and b) Sadler[133a] and by c) Dyson.[133b]

These studies also highlighted the importance of non-covalent interactions in the second coordination sphere, such as hydrophobic interactions:

i) The arene cap stabilizes Ru^{II} and provides also a hydrophobic face for the complex, which might improve biomolecular recognition processes.[24c, 134]

ii) The transport of ruthenium through cell membranes can also be enhanced by such hydrophobic ligands.

ii) Intercalation of the phenyl moiety of the biphenyl arene cap involving π stacking and DNA bases provides also further interaction that help to improve selectivity between the metallodrug and the target (see Figure 9a).

Recently, the nature of the second coordination sphere has also been shown to influence both kinetic- and thermodynamic properties of binding to proteins, which constitute alternative macromolecular targets of anticancer drugs.[135]

2.2.2. Ruthenium Piano Stool Complexes as a Model for Metallodrugs

Inspired by promising anticancer Ru^{II}-piano stool complexes developed by Sadler *et al.*[24a, 133a] (see Figure 9a and b), we set-off to modify the second coordination sphere around the metal by embedding the piano stool inside a protein scaffold. Such metallodrug presenter protein will be chemogenetically engineered to target DNA. With the hope of increasing the specificity of metallodrugs towards DNA and as proof-of-concept that target selectivity can be engineered into a supramolecular assembly of drug and presenter protein, biotinylated ruthenium piano stool complexes [(η^6-*p*-cymene)Ru(Biot-L)Cl]CF_3SO_3 **6** and [(η^6-biphenyl)Ru(Biot-L)Cl]CF_3SO_3 **7** where Biot-L = Biotin-*N*-(*R,R*)-3,4-diaminopyrrolidine were synthesized (see Figure 10). These complexes were designed to be incorporated into a streptavidin host protein to build the supramolecular assembly.

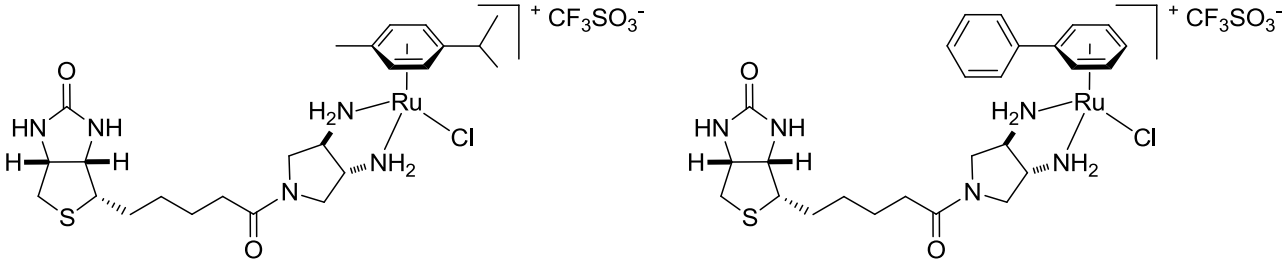

6 **7**

Figure 10 Biotinylated ruthenium piano stool complexes [(η^6-*p*-cymene)Ru(Biot-L)Cl]CF_3SO_3 **6** and [(η^6-biphenyl)Ru(Biot-L)Cl]CF_3SO_3 **7** where Biot-L = Biotin-*N*-(*R,R*)-3,4-diaminopyrrolidine.

2.2.3. Synthesis of Biotinylated Metallodrugs

In order to connect the ethylenediamine-type ligand to biotin, a pyrrolidine moiety was selected. The synthesis of the diaminopyrrolidine scaffold was achieved by using the protocol of Löwik *et al.*,[136] who used (*L*)-tartric acid as a starting material for the preparation of (*R*,*R*)-3,4-diaminopyrrolidine (see Scheme 9).

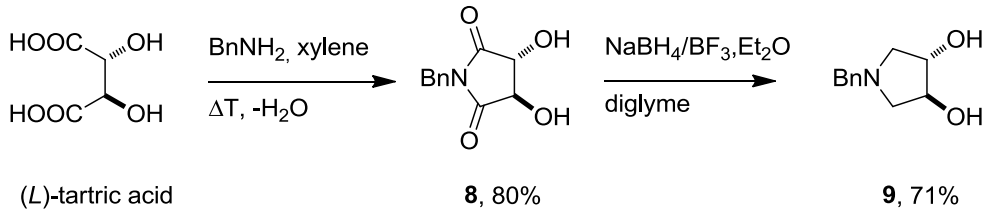

Scheme 9 Synthesis of (*S*,*S*)-*N*-benzyl-3,4-dihydropyrrolidine **9**.

Benzylamine and (*L*)-tartaric acid were azeotropically dehydrated with boiling xylene in a Dean-Stark trap. After cooling, the crystalline product (with a yellowish color) was filtered, washed with acetone and recrystallized in EtOH. Compound **8** was obtained as a white solid (80% yield). Subsequently, reduction of the carbonyl group was performed by treating **8** with $NaBH_4/BF_3$ in dimethylester diglycol (diglyme) to yield **9** (71% yield). The resulting dihydroxy compound was reacted with methanesulfonylchloride to yield **10**. The resulting crude product was directly used for the next step without additional purification. Addition of NaN_3 to **10**, through nucleophilic attack, yielded the diazide **11** in almost quantitative amounts (93% yield, see Scheme 10). The latter reaction step allowed to obtain the (*R*,*R*)-diaminopyrrolidine moiety.

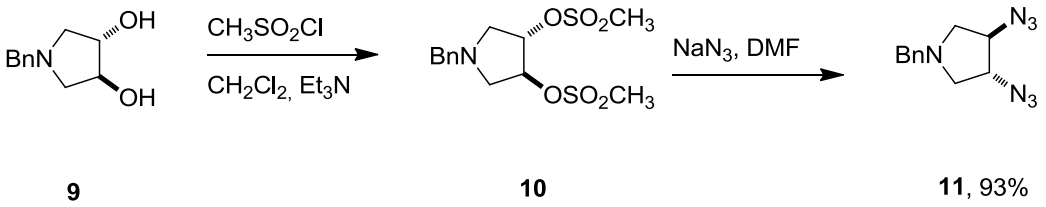

Scheme 10 Synthesis of (3*R*,4*R*)-*N*-benzyl-pyrrolidine-3,4-diazide **11**.

Compound **11** was then reduced with Pd/C to yield (3*R*,4*R*)-*N*-benzyl-3,4-diaminopyrrolidine **12** (74% yield). The resulting amino groups were protected with *tert*-butyloxycarbonyl protective groups. Compound **13** was obtained in quantitative yield (see Scheme 11).

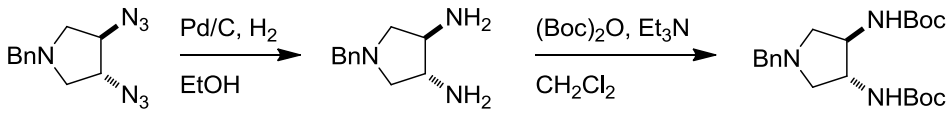

11 **12**, 74% **13**, 98%

Scheme 11 Synthesis of (3*R*,4*R*)-*N*-benzyl-3,4-di(*N,N-tert*-butyloxycarbonyl)aminopyrrolidine **13**.

Subsequent hydrogenolysis of the benzyl group on $Pd(OH)_2/C$ afforded (3*R*,4*R*)-3,4-di(*N,N-tert*-butyloxycarbonyl)aminopyrrolidine **14** in quantitative yield (see Scheme 12).

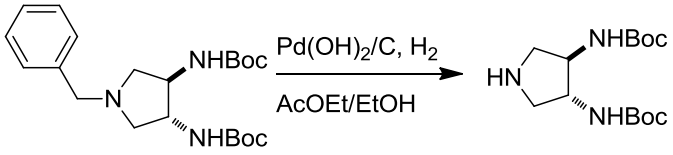

13 **14**, 97%

Scheme 12 Synthesis of (3*R*,4*R*)-3,4-di(*N,N-tert*-butyloxycarbonyl)aminopyrrolidine **14**.

The next reaction consisted of coupling **14** with biotin. For that purpose, an activated biotin was used. One common activated form of biotin used in the Ward group is the *N*-hydroxysuccinimide ester of biotin (BNHS).[137] Compound **14** was mixed with BNHS in the presence of Et_3N as a base in DMF (see Scheme 13). The reaction was stirred overnight to afford **15**. The reaction necessitated a further step of purification because of the presence of free biotin in the crude reaction mixture.

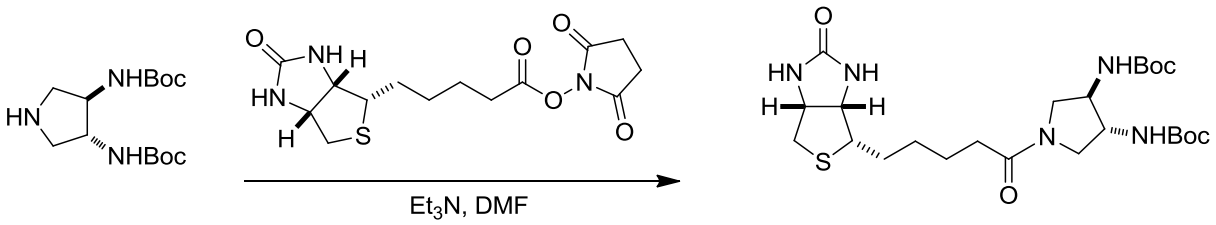

14 **15**, 95%

Scheme 13 Synthesis of biotinylated (3*R*,4*R*)-3,4-di(*N,N-tert*-butyloxycarbonyl)aminopyrrolidine **15**.

The presence of free biotin may be due to the degradation of the activated biotin during the reaction. The resulting product was purified by column chromatography on silica gel yielding

15 as a white solid in excellent yield (95%). In order to cleave the Boc protective groups, acidic conditions (trifuoroacetic acid, TFA) were used: Compound **15** was dissolved in CH_2Cl_2 and TFA was added to the solution. The reaction was stirred at RT until completion of the reaction as revealed by thin layer chromatography. The crude product was purified by column chromatography to afford **16** as a white solid (57% yield, see Scheme 14).

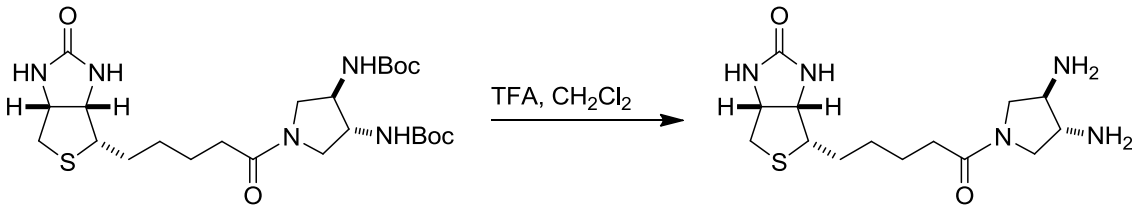

15 **16**, 57%

Scheme 14 Synthesis of biotinylated (3*R*,4*R*)-3,4-diaminopyrrolidine **16**.

With the biotinylated diaminopyrrolidine ligand in hand, complexation with ruthenium was performed. Two different ruthenium complexes were envisaged: the first complex bears a *p*-cymene arene cap (complex **6**) while the second one possesses a biphenyl cap (complex **7**, see Figure 10). To synthesize complex **6**, the commercially available dimer $[(\eta^6\text{-}p\text{-cymene})RuCl_2]_2$ was used as a precursor (see Scheme 15).

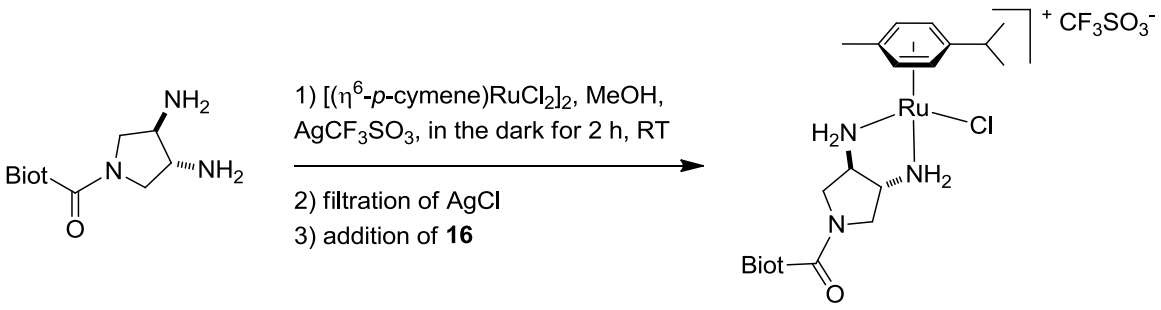

16 **6**, 95%

Scheme 15 Synthesis of $[(\eta^6\text{-}p\text{-cymene})Ru(\text{Biotin-}N\text{-}(3R,4R)\text{-3,4-diaminopyrrolidine-}N,N)Cl]CF_3SO_3$ **6**.

The dimer $[(\eta^6\text{-}p\text{-cymene})RuCl_2]_2$ was dissolved in MeOH and treated with 2 equivalents of $AgCF_3SO_3$ in order to precipitate the chlorides. The reaction mixture was then stirred in the dark for 2 h at RT. The resulting AgCl salts were filtered off and biotinylated ligand **16** was

added to the solution. The mixture was stirred for another 2 h. The solvent was evaporated and the residue was washed with $CHCl_3$, precipitated and filtered to afford complex **6** as a yellow solid (95% yield, see Scheme 15). The same protocol was applied to afford biotinylated piano stool complex **7**. However, since the dimeric biphenyl ruthenium complex precursor $[(\eta^6\text{-biphenyl})RuCl_2]_2$ was not commercially available, its synthesis was performed according to the protocol of Bennett *et al*.[138] For that purpose, biphenyl was first subjected to a Birch reduction (see Scheme 16).[139] This reaction allows the transformation of aromatic cyclic compounds into 1,4-cyclohexadiene products. The Birch reduction of aromatic rings generally proceeds in liquid ammonia with sodium, lithium or potassium solid and an alcohol, such as EtOH or *tert*-butanol. In our case we used EtOH and sodium in liquid ammonia. (see Scheme 16). The crude material was used directly in the next step without further purification.

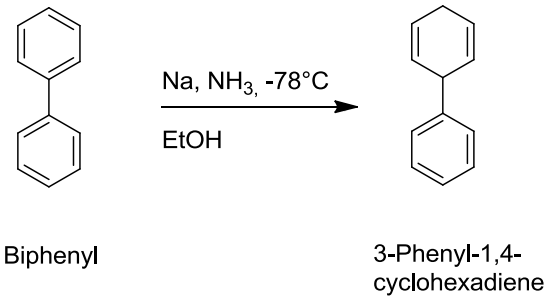

Scheme 16 Birch reduction for the synthesis of 3-phenyl-1,4-cyclohexadiene.[139]

With the 3-phenyl-1,4-cyclohexadiene in hand, dimeric biphenyl ruthenium complex was prepared applying the protocol of Bennett *et al.*[138] Reaction of 3-phenyl-1,4-cyclohexadiene with ethanolic Ru^{III}-trichloride provided $[(\eta^6\text{-biphenyl})RuCl_2]_2$ in 44% yield (see Scheme 17).

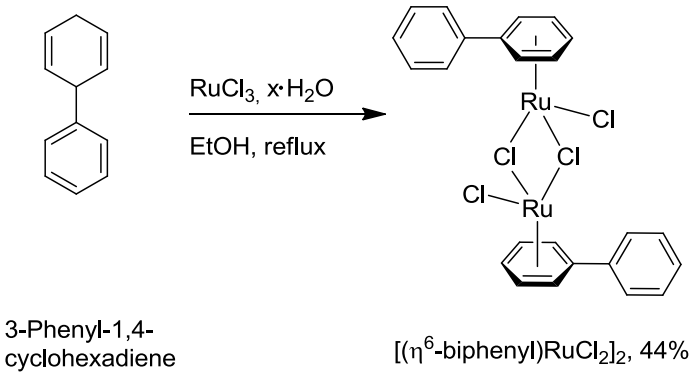

Scheme 17 Synthesis of $[(\eta^6\text{-biphenyl})RuCl_2]_2$.[138]

Having obtained the dimeric biphenyl ruthenium complex, the synthesis of biotinylated piano stool complex **7** was carried out using the same protocol as for the synthesis of complex **6**. Thus, biotinylated piano stool complex **7** was obtained in 55% yield (see Scheme 18).

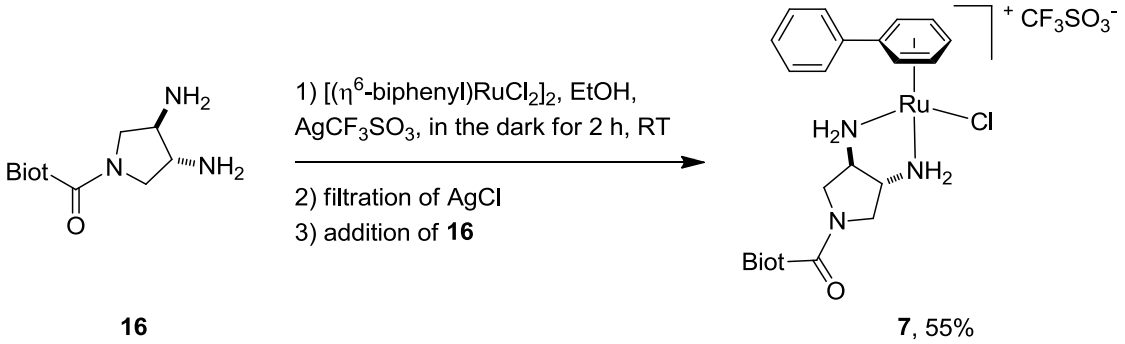

Scheme 18 Synthesis of $[(\eta^6\text{-biphenyl})Ru(\text{Biotin-}N\text{-}(3R,4R)\text{-3,4-diaminopyrrolidine-}N,N)Cl]CF_3SO_3$ **7**.

2.3. Presenter Protein and Metallodrug-Assembly: 6 ⊂ WT Sav

2.3.1. Isothermal Titration Calorimetry Titrations

Telomeric DNA recognition by **6** ⊂ WT Sav was first investigated. For that purpose incorporation of biotinylated piano stool complex **6** into WT Sav was primarily studied by isothermal titration calorimetry (ITC). These ITC experiments demonstrated the strong binding affinity of biotinylated piano stool complex **6** for WT Sav with a calculated K_d < 60 nM (see Figure 11).

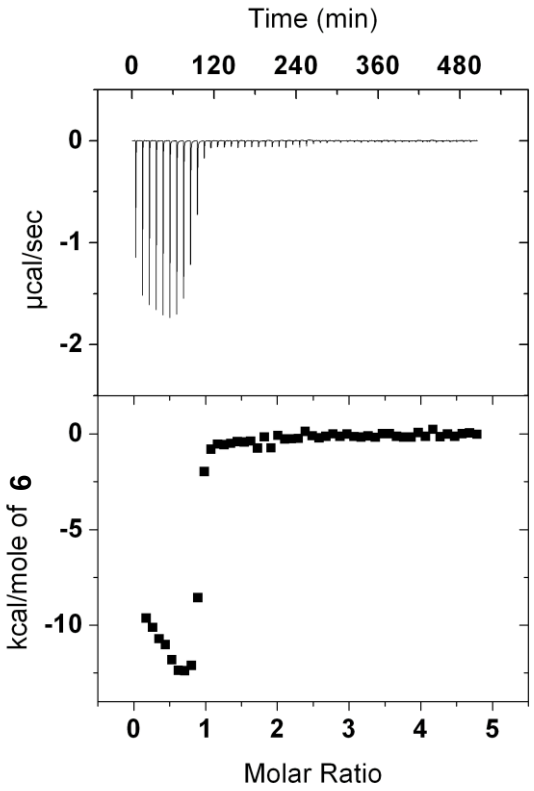

Figure 11 ITC profile for the binding of **6** to WT Sav. Titration was carried out at 25°C in MOPS buffer (75 mM) at pH 6.5 with 10 mM of KOH. The upper panel displays the raw titration data plotted as heat versus time. The lower panel displays the integrated heat measurements plotted as a function of **6** to WT Sav molar ratio. The heat values are plotted as a function of **6** to WT Sav molar ratio, to give the corresponding binding isotherms. The resulting isotherms were then fitted to a two set binding sites model.

2.3.2. X-ray Crystal Structure of 6 ⊂ WT Sav

The crystal structure of the metallodrug-presenter protein assembly **6** ⊂ WT Sav was obtained by soaking crystals of WT Sav with an aqueous solution of complex **6** (see Figure 12). The structure was solved at 2.0 Å resolution by Tillmann Heinisch. The X-ray data demonstrates that the four biotin-binding sites are fully occupied with the metallodrug.

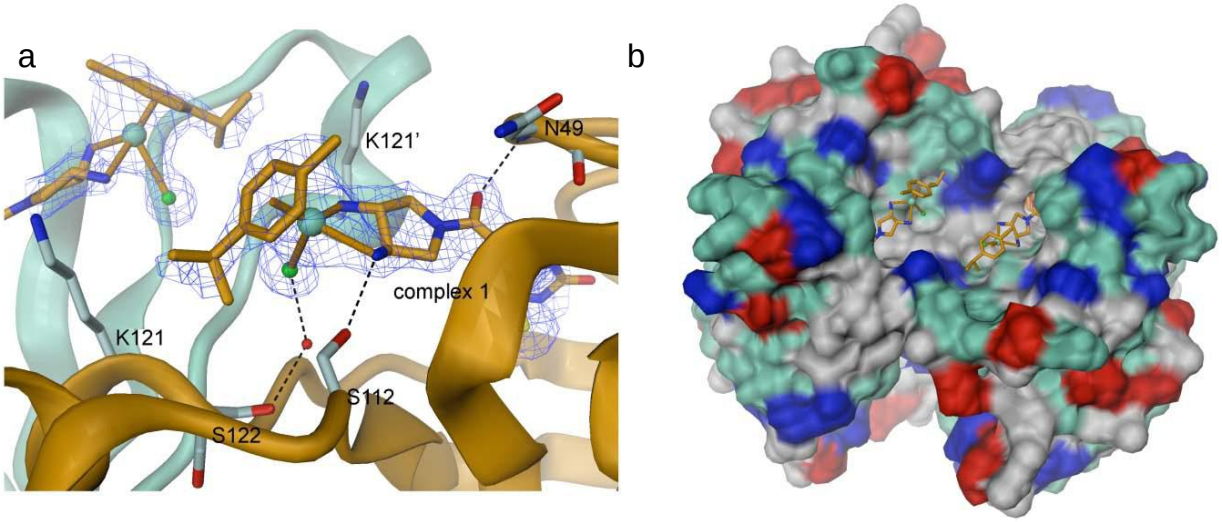

Figure 12 Crystal structure of biotinylated piano stool complex **6** embedded into the WT Sav presenter protein (**6** ⊂ WT Sav). a) Close-up view of **6** bound to a WT Sav monomer (orange) also showing the *cis*-related ruthenium moiety (upper-left corner) that is bound to the symmetry-related WT Sav monomer (aquamarine). Selected Sav residues are shown in full and are labeled. Primed residues belong to the symmetry-related monomer. The 2 Fo-Fc electron density map of **6** is contoured at 1.0 σ. The ruthenium atom is tetrahedrally coordinated by two amino groups of the diaminopyrrolidine, the *p*-cymene and a putative chloride ion (shown in green). b) Molecular surface representation of the WT Sav tetramer showing two *cis*-related ruthenium moieties. The WT Sav surface is colored according to amino acid, with blue = basic residues, red = acidic residues, green = polar residues, grey = hydrophobic residues.

Ruthenium is coordinated by four ligands, two amino groups of the (3*R*,4*R*)-diaminopyrrolidine, a chloride molecule and the aromatic ring of the *p*-cymene (see Figure 12). The metal complex has a distorted-tetrahedral “piano stool”-like conformation. In addition to the well documented biotin-Sav interactions,[140] other interactions between **6** and WT Sav found in the crystal structure enforce the localization of the piano stool moiety within the biotin binding pocket (see Figure 12):

i) H-bonding of diaminopyrrolidine nitrogen to the side-chain of S112.

ii) Apolar interactions of *p*-cymene with T114 (see Figure 13)

iii) Indirect binding of the labile chloride (or water) ligand to the backbone carbonyl of S122 *via* a well-ordered water molecule.

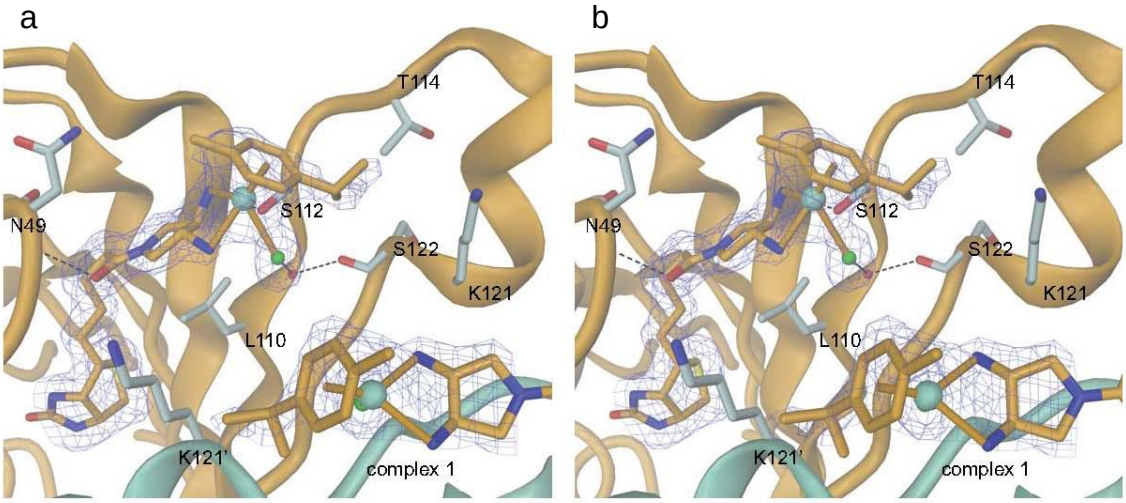

Figure 13 Stereoview on the binding site between WT Sav and the head group of biotinylated piano stool complex **6**.

The diaminopyrrolidine S112H-bond is reminiscent of a critical interaction between a Pt ligand N-H group and the phosphate backbone of dsDNA identified by Lippard *et al.* in both cisplatin and oxaliplatin X-ray structures.[141] In the latter work they reported the 2.4-Å resolution X-ray crystal structure of the major adduct between a platinum complex $[Pt(ammine)(cyclohexylamine)]^{2+}$ and a DNA dodecamer. They concluded that hydrogen bonding, hydrophobic, and other major groove interactions between protein, DNA, and the ligands on the platinum may affect drug activity.

In the crystal structure, symmetry related *cis*-Ru atoms are 10.4 Å apart. In the absence of a neighboring biotinylated piano stool complex **6** in *cis* (see Figure 14), the size and charge of the pocket would allow multiple interactions with an incoming DNA molecule (see Figure 15). The orientation of the labile Ru-Cl bond is compatible with coordination to electron-rich N^7 atoms of purines[134] in an *endo*-base of single-stranded DNA (ssDNA).

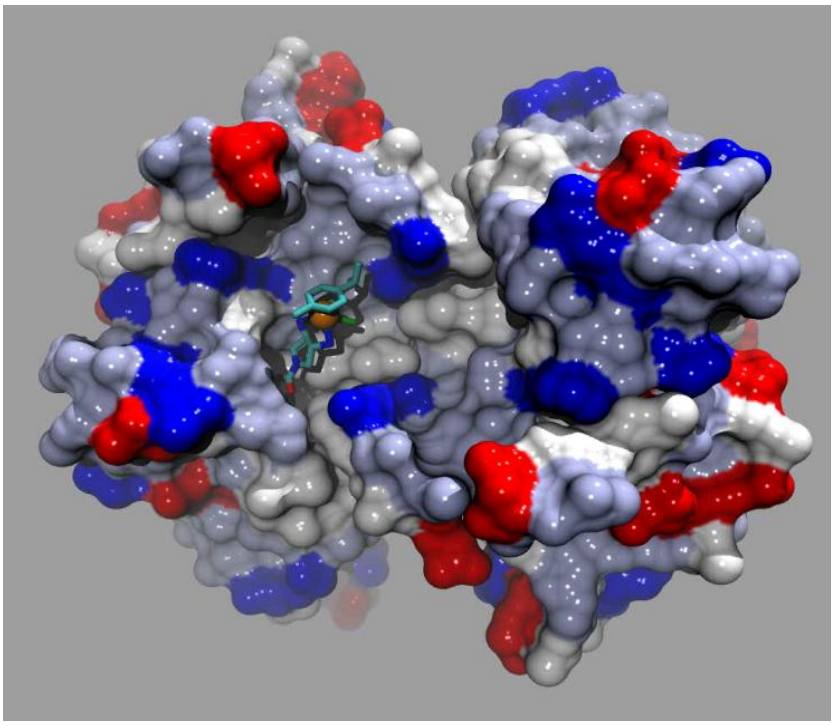

Figure 14 Model of the metallodrug-presenter protein assembly from crystal structure with vacated neighboring biotin-binding site in *cis*.

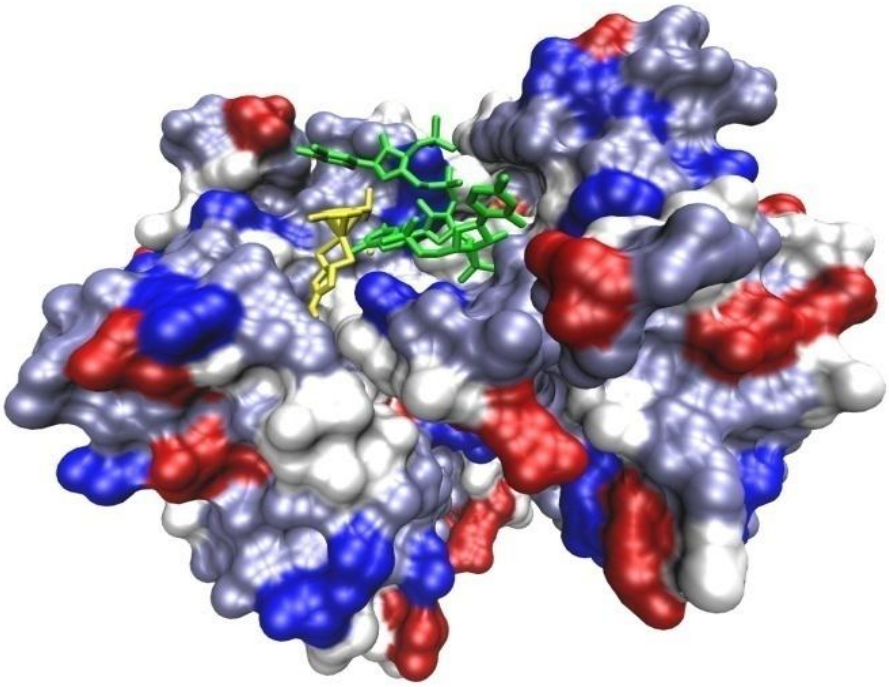

Figure 15 Assembly of biotinylated piano stool complex **6** ⊂ WT Sav with modeled incoming DNA. The biotinylated piano stool complex **6** (yellow) is shown for illustration purposes in only one of the two *cis* biotin-binding sites, reflecting experimental conditions The vacated biotin-binding site is large enough to accommodate a trinucleotide sequence AGT (shown in green).

2.4. DNA Recognition by the Presenter Protein: 6 ⊂ WT

2.4.1. Investigation on Telomeric G-quadruplex DNA Binding by 6 ⊂ WT

Having established the structure of the metallodrug-presenter protein assembly, we next investigated the binding of **6** ⊂ WT Sav to a model G-quadruplex telomeric DNA consisting of 39 bases (G4A).[142] The assembly was constructed by mixing two equivalents of biotinylated piano stool complex **6** with one equivalent of tetrameric WT Sav. The ability of **6** ⊂ WT Sav to bind G-quadruplex was first investigated by ITC (see Figure 16).

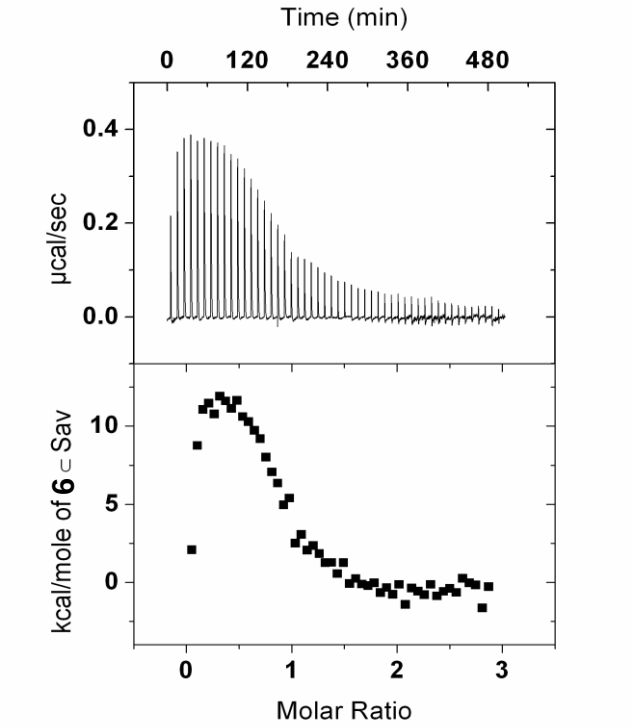

Figure 16 Binding of biotinylated piano stool drug-presenter protein assembly **6** ⊂ WT Sav to G4A monitored by ITC. Titration was carried out at 25°C in MOPS buffer (75 mM) at pH 6.5 with 10 mM of KOH. The upper panel displays the raw titration data plotted as heat versus time. The lower panel displays the integrated heat measurements plotted as a function of **6** ⊂ WT Sav to G4A molar ratio, to give the corresponding binding isotherms: A single set of identical sites model provided a dissociation constant of $(0.74 \pm 0.28)\cdot10^{-6}$ M, enthalpy of $(1.23 \pm 0.355)\cdot10^{4}$ kcal/mol, and stoichiometry of 0.90 ± 0.02.

ITC titration presented in Figure 16 suggested the formation of a ternary complex between the drug-presenter protein assembly **6** ⊂ WT Sav and G4A, with sub-micromolar affinity (K_d = 0.74 µM). The integrated heat measurements were fitted as a single-binding model providing a stoichiometry approaching one quadruplex bound per WT Sav tetramer (molar ratio = 0.90). The enthalpy of binding at 25°C was endothermic ($\Delta H = 1.23 \cdot 10^4$ kcal/mol), and therefore the strong affinity implies a favorable entropic component upon binding **6** ⊂ WT Sav to G4A. Binding capacity of **6** ⊂ WT Sav for G4A was also determined by electrophoretic mobility-shift assays (EMSA, see Figure 17).

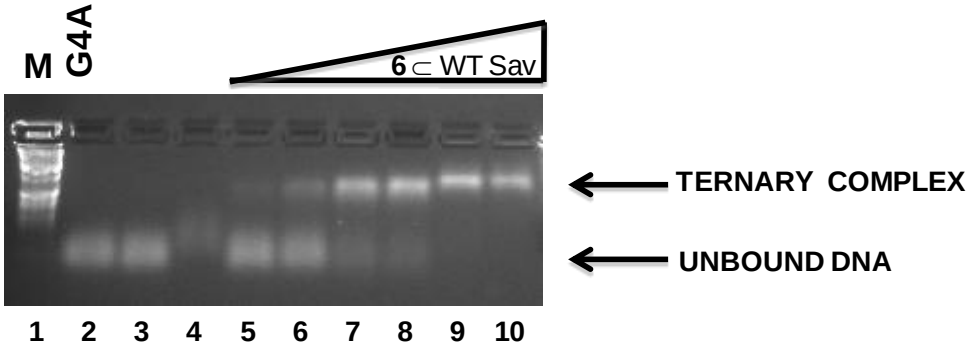

Figure 17 Binding of assembly of metallodrug and presenter protein (**6** ⊂ WT Sav) to G4A monitored by EMSA on agarose-gels. Lane 1: DNA Marker. Lane 2: G4A. Lane 3: G4A (3.3 µM) + WT Sav (39.6 µM); Lane 4: G4A (3.3 µM) + **6** (85.7 µM). Lanes 5-10: G4A (3.3 µM) + **6** ⊂ WT WT Sav at increasing concentrations: 0.8 µM, 1.6 µM, 3.9 µM, 7.9 µM, 19.8 µM, 39.6 µM, representing a **6** ⊂ WT Sav : G4A ratio from 0.2 to 12. In all cases 500 ng of DNA was loaded onto the gel.

The supramolecular assembly of WT Sav with the biotinylated ruthenium drug produced a concentration-dependent change in migration of G4A DNA in EMSA, leading to a single slow migrating species that was also consistent with the formation of a ternary complex with a defined 1 : 1 stoichiometry (DNA : **6** ⊂ WT Sav, see Figure 17). This ternary complex **6** ⊂ WT Sav-G4A DNA displayed a $K_d \approx 2$ µM as extrapolated from EMSA analyses, a value in agreement with the affinity data found by ITC (K_d = 0.74 µM). Thus, whether measured accurately in solution by ITC or more conservatively in EMSA, both these studies supported

the conclusion that the presenter protein contributed to the binding and to the formation of a defined ternary complex with quadruplex DNA.

The affinity of WT Sav alone for DNA was also investigated. In comparison, the binding of the protein alone with quadruplex DNA was markedly weaker (K_d = 15.2 µM) in the absence of biotinylated piano stool complex **6** (see Figure 18).

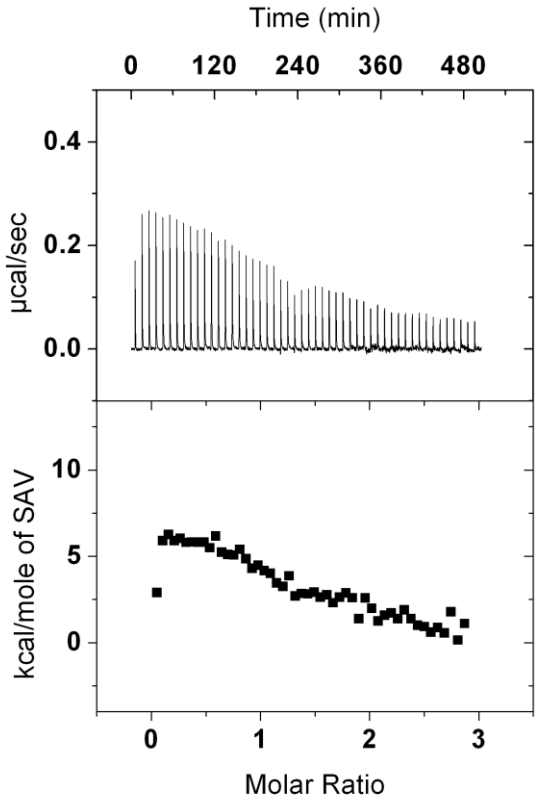

Figure 18 Binding of WT Sav to G4A monitored by ITC. Titration was carried out at 25°C in MOPS buffer (75 mM) at pH 6.5 with 10 mM of KOH. The upper panel displays the raw titration data plotted as heat versus time. The lower panel displays the integrated heat measurements plotted as a function of Sav to G4A molar ratio, to give the corresponding binding isotherms: A single set of identical sites model give a dissociation constant of $(15.20 \pm 2.35)\cdot10^{-3}$ M, enthalpy of $(1.055 \pm 0.124)\cdot10^{3}$ kcal/mol, and stoichiometry of 1.81 ± 0.09.

The weak affinity of WT Sav for DNA (theoretical WT Sav pI ≈ 7) was one of the reasons for using Sav for biotechnology applications involving biotinylated DNA (rather than the related, but very basic protein avidin, pI ≈ 10.4).[143] The binding affinity of the protein alone was more than ten times weaker than in the presence of biotinylated piano stool complex **6**. Lack of detectable binding of WT Sav in the absence of biotinylated piano stool complex **6** for DNA was also confirmed by EMSA gels (see Figure 17, Lane 3)

EMSA gels and ITC using G4A as target were also carried out with biotinylated piano stool complex **6** alone (in absence of Sav). These data revealed the formation of a mixture of fast migrating species that cannot be resolved by EMSA (see Figure 17, Lane 4). ITC analysis revealed multiple binding equilibria with a large enthalpic contribution (see Figure 19).

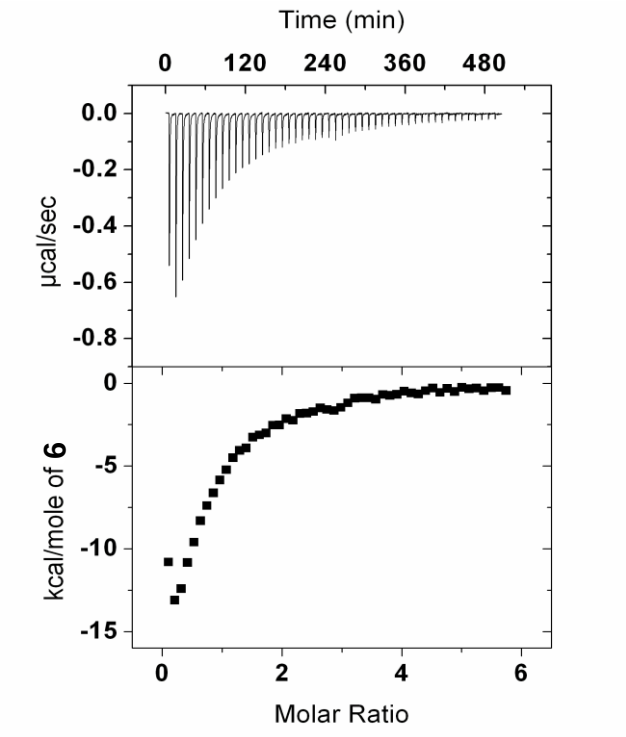

Figure 19 Binding of biotinylated piano stool complex **6** to G-quadruplex DNA monitored by ITC. Titration was carried out at 25°C in 75 mM MOPS (pH 6.5) with 10 mM KOH. The upper panel displays the raw titration data plotted as heat versus time. The lower panel displays the integrated heat measurements plotted as kcal/mol of drug injected into telomeric DNA. The resulting isotherms could not be fitted to a one-site binding model.

These experiments supported the expected multiple strong binding events to the DNA. Similar multiple binding events of piano stool complexes to oligonucleotides have been described before and support the notion that metallodrugs exhibit little DNA-sequence selectivity.[144] There is ample experimental evidence for related ruthenium piano stool complexes that display preferential binding to N^7 guanine in DNA;[134] a QM-MM calculation predicts a K_d of 0.1 μM for a related Ru piano stool.[145]

Both ITC and EMSA analyses demonstrated that binding of biotinylated piano stool complex **6** to DNA in the absence or presence of the presenter protein assembly is very different, indicating that the protein influenced the mode of binding of biotinylated piano stool complex **6** and helped to form a defined ternary complex with quadruplex DNA. The binding of a single drug-protein to a G4A DNA containing 39 nucleotides intimated the existence of an extended contact between both macromolecules. This large contact between WT Sav and G4A DNA, both of comparable size, would suggest that such drug-presenter protein can be engineered to display selectivity towards the DNA sequence.

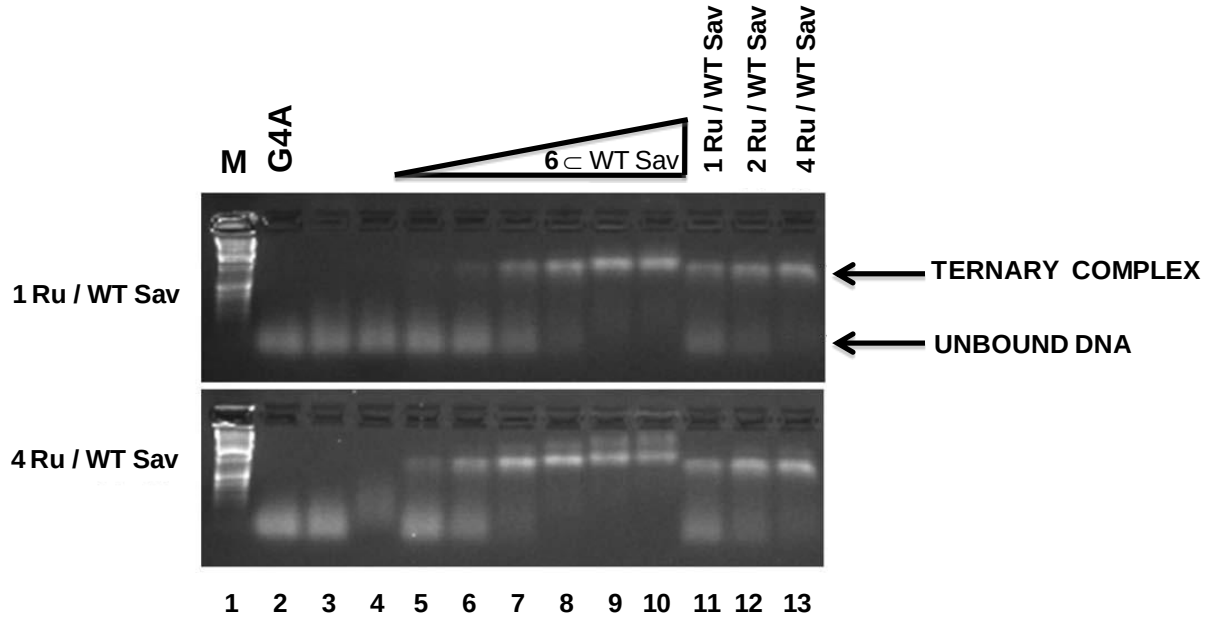

Figure 20 Binding of assembly of metallodrug and presenter protein (**6** ⊂ Sav), at 1 or 4 equivalents of Ru metallodrug per tetramer, to G4A DNA monitored by EMSA on agarose-gels. Lane 1: Marker (M). Lane 2: G4A, Lane 3: G4A (3.3 μM) + Sav (39.6 μM). Lane 4: G4A (3.3 μM) + complex **6** (43 μM for 1 Ru/Sav and 160 μM for 4 Ru/Sav, respectively). Lane 5-10: G4A (3.3 μM) + **6** ⊂ Sav at increasing

concentrations: 0.8 µM, 1.6 µM, 3.9 µM, 7.9 µM, 19.8 µM, 39.6 µM, representing a **6** ⊂ Sav : G4A ratio from 0.2 to 12. In all cases 500 ng of DNA was loaded onto the gel. Lane 11: 1 ⊂ Sav : G4A ratio of 1.2, with 1 equivalent of ruthenium per tetramer. Lane 12: 1 ⊂ Sav : G4A ratio of 1.2, with 2 equivalents of ruthenium per tetramer. Lane 13: 1 ⊂ Sav : G4A ratio of 1.2, with 4 equivalent of ruthenium per tetramer.

Affinities obtained by varying the ratio of **6** : Sav from 1 : 1 to 4 : 1 are comparable (see Figure 20). The 2 : 1 ratio was selected for all subsequent studies as it yielded a well defined 1 : 1 stoichiometry (**6** ⊂ Sav : G4A) by ITC (see Figure 16) and EMSA (see Figure 17).

2.4.2. Selectivity for Single Stranded DNA (ssDNA)

2.4.2.1. Binding of 6 ⊂ Sav to Unstructured G-quadruplex DNA

We also investigated the selectivity of interaction of **6** ⊂ Sav for different DNA targets. DNA quadruplexes are known to be greatly stabilized by potassium ions. Accordingly, by carrying out binding assays in Li^+ salts instead of K^+, the formation of quadruplex DNA by G4A can be prevented.[146] Affinity binding between **6** ⊂ Sav and unstructured DNA (G4A in presence of LiOH) were investigated (see Figure 21).

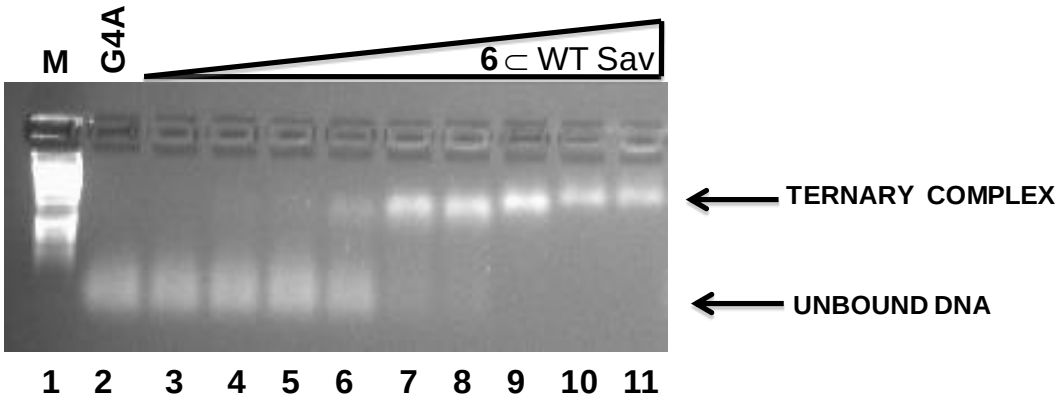

Figure 21 EMSA gel for the titration of **6** ⊂ Sav into G4A in MOPS (75mM) with LiOH (140mM). Lane 1: Marker, Lane 2: G4A, Lane 3-11: concentration increase of **6** ⊂ Sav: 1.8 µM, 2.65 µM, 3.5 5µM, 7 µM, 14.5 µM, 18 µM, 35.5 µM, 89 µM, 178.5 µM with a **6** ⊂ Sav:G4A ratio from 0.1 to 12.5.

The experiment monitored in EMSA gels with **6** ⊂ Sav and "lithiated" G4A DNA demonstrated that under these conditions, the resulting presumably unstructured ssDNA oligonucleotide bound to the metallodrug-protein assembly with a similar apparent affinity to that of its more structured G-quadruplex form (estimated K_d < 1.6 μM, see Figure 21).

ITC titrations of **6** ⊂ Sav with this unstructured lithiated G4A were also performed. These experiments support the notion that **6** ⊂ Sav displays comparable affinities for both unstructured ssDNA and folded G4A, albeit with different forms of binding (see Figure 22).

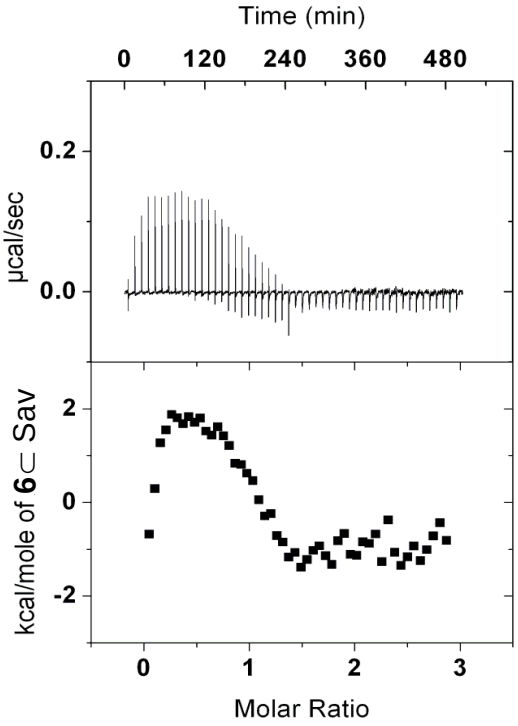

Figure 22 Binding of **6** ⊂ Sav to G-quadruplex DNA with LiOH monitored by ITC. Titration was carried out at 25°C in 75 mM MOPS (pH 6.5) with 140 mM LiOH. The upper panel displays the raw titration data plotted as heat versus time. The lower panel displays the integrated heat measurements plotted as kcal/mol of **6** ⊂ Sav injected into G4A DNA. The data could not be fitted to a one-site binding model.

Comparison of the ITC experiment displayed in Figure 16 and 22 suggests that the binding-modes of **6** ⊂ Sav folded G-quadruplex and its unstructured form are different. Although EMSA gels established comparable apparent affinities, ITC data did not yield unambiguous

and interpretable binding isotherms. Consequently this titration suggests that a complicated binding mechanism occurs when **6** ⊂ Sav and unstructured G4A are mixed together.

2.4.2.2. Binding of 6 ⊂ Sav to Scrambled Telomeric DNA

To test whether **6** ⊂ Sav recognized structural features of G4A or simply its nucleotide content, we used a "scrambled" telomeric sequence (scG4A) that could not form a G-quadruplex structure (see Figure 23).

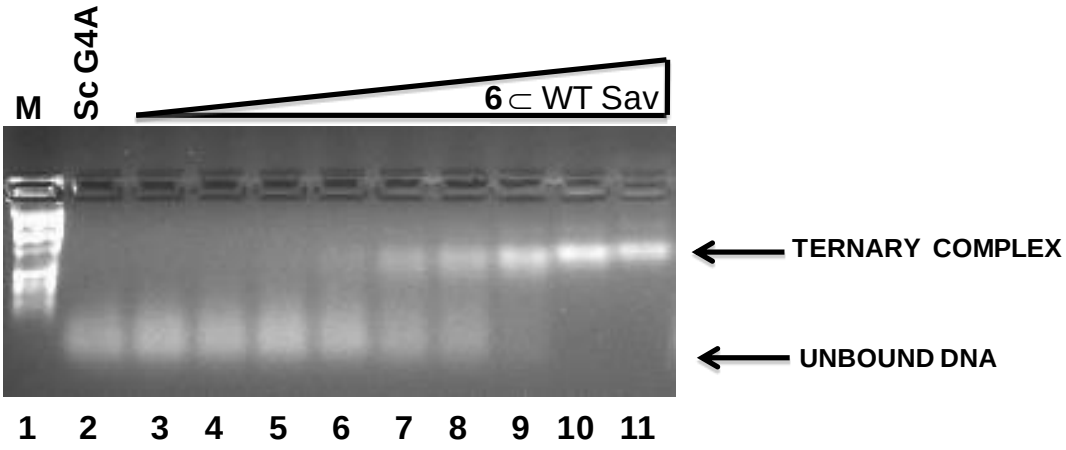

Figure 23 EMSA gel for the titration of **6** ⊂ Sav into scG4A in MOPS (75mM) with KOH (135 mM). Lane 1: Marker, Lane 2: scrambled G4A, Lane 3-11: concentration increase of 1 ⊂ Sav: 1.8 µM, 2.65 µM, 3.55 µM, 7 µM, 14.5 µM, 18 µM, 35.5 µM, 89 µM, 178.5 µM with a 1 ⊂ Sav : ScG4A ratio from 0.1 to 12.5.

As displayed in Figure 23 the binding of **6** ⊂ Sav to this control oligonucleotide (scG4A) was measurably weaker than for G4A (K_d = 2.3 µM, see Figure 23), which was bound stoichiometrically in our EMSA assay (K_d < 1.6 µM, see Figure 17). Scrambled G4A had the same sequence than G4A and was designed to be unable to form quadruplexes even in the presence of K^+. The metalloprotein **6** ⊂ Sav formed a ternary complex in the presence of scG4A as determined by EMSA, suggesting that the metallodrug-presenter protein could

also interact with other ssDNA, with little sequence selectivity. Titration experiments of scG4A with **6** ⊂ Sav were carried out (see Figure 24).

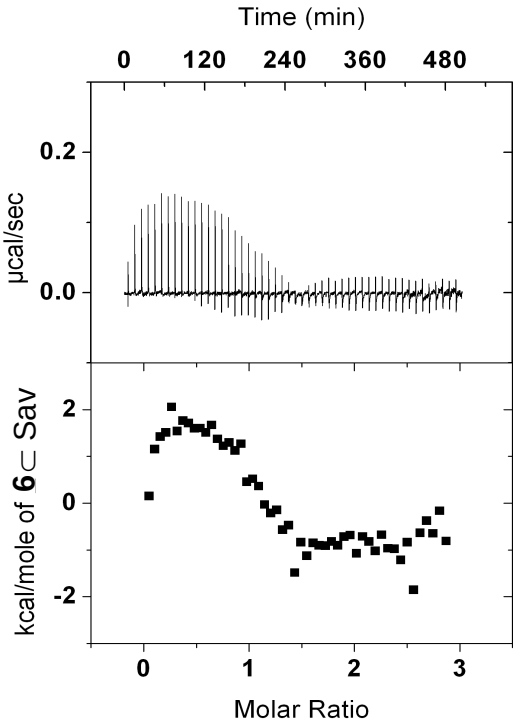

Figure 24 Binding of **6** ⊂ Sav to a "scrambled" telomeric DNA (scG4A) monitored by ITC. Titration was carried out at 25°C in 75 mM MOPS (pH 6.5) with 10 mM KOH. The upper panel displays the raw titration data plotted as heat versus time. The lower panel displays the integrated heat measurements plotted as kcal/mol of **6** ⊂ Sav injected into scG4A DNA. The resulting isotherms gave markedly different and more complicated than the one-site-model binding to G-quadruplex G4A, but is very reminiscent of binding of **6** ⊂ Sav to unstructured G4A with LiOH (see Figure 22).

The binding of **6** ⊂ Sav to this control oligonucleotide gave a similar ITC titration curve to that of unstructured G4A (Figure 22), which could not be fitted to a one-site binding model. Therefore, under these conditions, **6** ⊂ Sav binds strongly to the G-quadruplex in a defined 1 : 1 stoichiometry that fits a single-binding site mechanism and also binds to other ssDNA, whether scrambled ssDNA or unstructured G4A with LiOH, with marginally less affinity and in a more complicated manner. Similar binding flexibility has been observed in nucleotide shuffling experiments of natural ssDNA binding proteins.[147] It is noteworthy that, although many ssDNA binding-proteins are unable to recognize G-quadruplexes,[146] the

bioengineered **6** ⊂ Sav assembly described here can bind to both unstructured ssDNA and to a G4A telomeric quadruplex with similar affinity.

2.4.3. Competitive Binding

2.4.3.1. Glutathione

To test the selectivity of a ternary complex with DNA, experiments in the presence of potentially interfering molecules were carried out. The first competition studies were performed with glutathione (GSH). Glutathione has been shown to coordinate anticancer Ru complexes *in vitro*[24b, 148] and has also been implicated in metallodrug inactivation *in vivo.*[149]. It has also been demonstrated that GSH plays a key role in the regulation of cisplatin resistance in cancer chemotherapy.[150] Interactions between biotinylated piano stool complex **6** and GSH were investigated by mixing both species in water at 25°C. Mass spectrometry measurements demonstrated that biotinylated piano stool complex **6** reacted rapidly with glutathione presumably through the thiol group, which is a highly abundant intracellular form, giving rise to GSH adducts (see Figure 25).

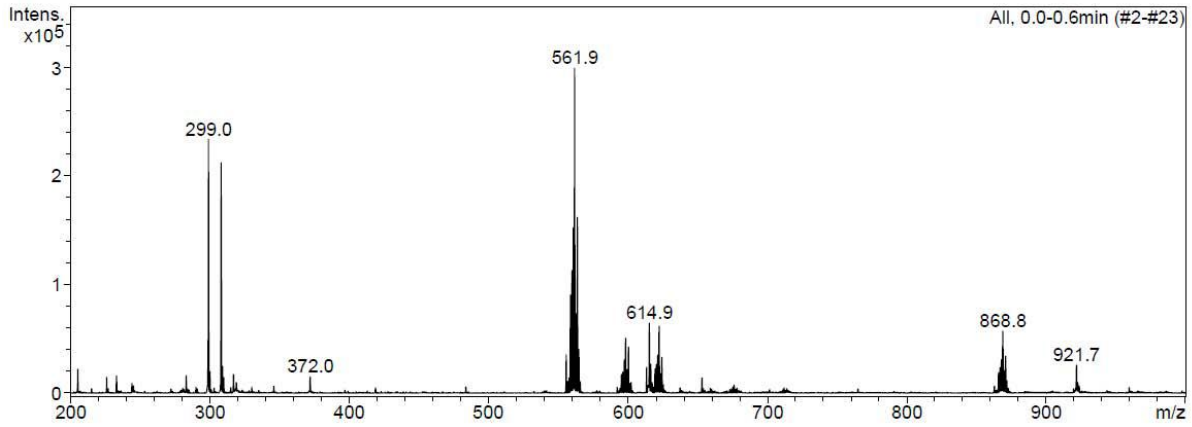

Figure 25 Mass spectrum of biotinylated piano stool complex **6**-GSH adduct, prepared by adding an excess of GSH (83 µM) compared to the biotinylated piano stool complex **6** (12 µM) in H_2O. The mass spectrum was recorded after only 5 min at 25°C.

Table 1 Main peaks identified in the mass spectrum of biotinylated piano stool complex **6** with GSH in H_2O at 25°C.

Entry	Reaction and observed ions	m/z (measured)	m/z (theoretica)
1	$[Glutathione + H]^+$	308.0	307.1
2	$[\mathbf{6} - Cl]^+$	561.9	562.7
3	$[\mathbf{6}]^+$	597.9	598.2
4	$[GSSG]^+$	614.9	612.6
5	$[\mathbf{6} + Na]^+$	621.9	621.1
6	$[\mathbf{6}\text{-}(GS)]^+$	868.8	869.1

Mass spectrometry experiments displayed in Figure 25 suggest the presence of GSH (Table 1, entry 1), biotinylated piano stool complex **6** alone (Table 1, entries 2 and 3) and GSH dimer (Table 1,entry 4). The mass of 868.8 corresponding to the biotinylated piano stool complex **6**-GSH adduct was visible with the expected isotopic distribution (see Figure 25 and Table 1).

These experiments confirmed that biotinylated ruthenium piano stool complex **6** can easily bind to GSH. Binding affinities between our metallodrug-presenter protein and G4A DNA in the presence of interfering GSH was investigated by EMSA gels (see Figure 26).

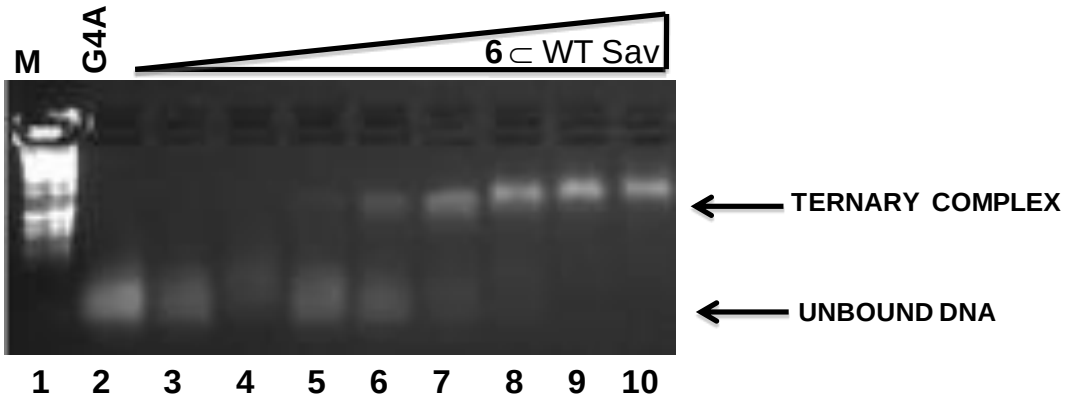

Figure 26 Binding of assembly of **6** ⊂ WT Sav to G4A monitored by EMSA on agarose-gels in the presence of 1 mM GSH. Lane 1: DNA Marker. Lane 2: G4A. Lane 3: G4A (3.3 μM) + WT Sav (39.6

μM); Lane 4: G4A (3.3 μM) + **6** (85.7 μM). Lanes 5-10: G4A (3.3 μM) + **6** ⊂ Sav at increasing concentrations: 0.8 μM, 1.6 μM, 3.9 μM, 7.9 μM, 19.8 μM, 39.6 μM, representing a **6** ⊂ WT Sav : G4A ratio from 0.2 to 12. In all cases 500 ng of DNA was loaded onto the gel.

These experiments were carried out in the presence of 300-fold excess GSH compared to G4A (final concentration of glutathione = 1 mM; *i.e.* within the physiological range). The presence of such high concentration of GSH did not appreciably affect the formation of the complex with G4A as evidenced by EMSA (estimated K_d < 1.6 μM, see Figure 26). In analogy, the anticancer-drug picoplatin was rationally designed to provide steric bulk around the metal centre, reducing its inactivation by species like GSH.[149a, 151] We hypothesize that the protein also offers steric and electronic shielding from competing species, such as GSH or other macromolecules.

2.4.3.2. Competing ssDNA

Interactions of our assembly with single stranded DNA were investigated by EMSA gels (see Figure 27). A 12mer ssDNA and a trinucleotide GGG were selected for the study.

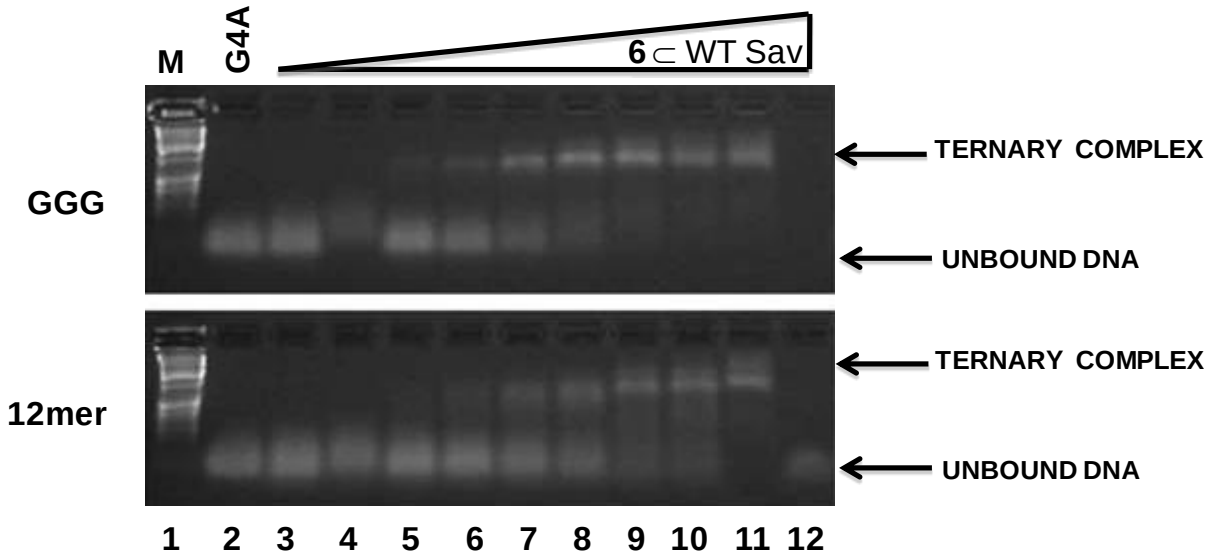

Figure 27 Binding of **6** ⊂ WT Sav to G-quadruplex DNA in the presence of competing DNA substrates, monitored by EMSA on agarose-gels. Lane 1: Marker (M). Lane 2: G4A. Lane 3: G4A (3 μM) + GGG

trinucleotide (206.5 μM) or 12mer ssDNA (462 μM) respectively. Lane 4: G4A (3 μM) + GGG (206.5 μM) or 12mer (462 μM) respectively + complex **6** (76.5 μM). Lane 5-10: GGG (206.5 μM) or 12mer (462 μM) were co-incubated with G4A (3 μM) and the **6** ⊂ WT Sav assembly at increasing concentrations: 0.7 μM, 1.4 μM, 3.5 μM, 7 μM, 17.7 μM, 35.3 μM; under these conditions, the molar ratio **6** ⊂ WT Sav : G4A ranges from 0.2 to 12, while GGG : G4A and 12mer : G4A ratio is 69 and 154, respectively. Lane 11: G4A (3 μM) and **6** ⊂ WT Sav assembly (35.3 μM). Lane 12: GGG (206.5 μM) or 12mer (462 μM) in the presence of **6** ⊂ WT Sav assembly (35.3 μM); GGG or 12mer are barely visible by ethidium bromide staining due to lack of intercalation of the dye in ssDNA.

An excess of competing ssDNA co-incubated with G4A (up to 157 equivalents of competing ssDNA compared to G4A) lowered binding of the metallodrug-protein assembly as determined by EMSA, but only marginally. The 12mer ssDNA was better at inhibiting G4A-binding (estimated K_d = 5.4 μM) than GGG (estimated K_d = 2 μM), which may intimate the existence of a more extended interaction with the **6** ⊂ WT Sav assembly compared with the smaller GGG-trinucleotide. These results supported the notion that G4A is a privileged target for the **6** ⊂ WT Sav assembly.

2.4.4. Genetic Control of the 2nd Coordination Sphere

Next, we investigated the influence of the second-coordination sphere on G4A binding through site-directed mutagenesis. The crystal structure revealed two lysines (K121 of the two adjacent monomers) within 10 Å of the ruthenium, at the entrance of the largely hydrophobic biotin-binding pocket (see Figure 12). Binding affinities of **6** ⊂ K121A for G4A DNA were investigated by EMSA gels (see Figure 28).

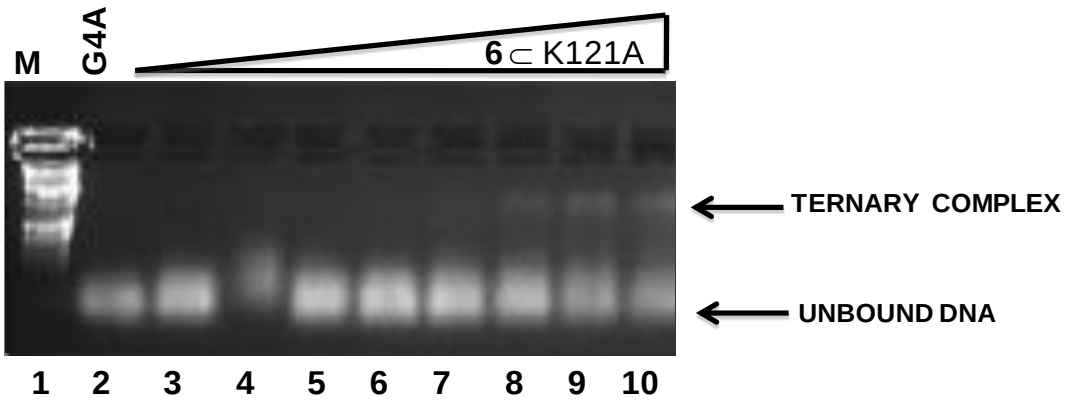

Figure 28 Binding of assembly of metallodrug and presenter protein (**6** ⊂ K121A) to G4A monitored by EMSA on agarose-gels. Lane 1: DNA Marker. Lane 2: G4A. Lane 3: G4A (3.3 μM) + K121A (39.6 μM); Lane 4: G4A (3.3 μM) + **6** (85.7 μM). Lanes 5-10: G4A (3.3 μM) + **6** ⊂ K121A at increasing concentrations: 0.8 μM, 1.6 μM, 3.9 μM, 7.9 μM, 19.8 μM, 39.6 μM, representing a **6** ⊂ K121A : G4A ratio from 0.2 to 12. In all cases 500 ng of DNA was loaded onto the gel.

These experiments demonstrated that mutation of this positively-charged residue (K121A) decreased affinity greatly (estimated K_d = 28.8 μM), such as also seen in other nucleic acid-binding proteins.[146, 152] These experiments suggested that the lysines might form a salt-bridge with the phosphate backbone. Similarly, the introduction of a negative charge in the vicinity of the ruthenium (S112D) also reduced binding-affinity (see Figure 29). This is probably caused by charge-repulsion between the overall negatively charged DNA and the deprotonated aspartic acid in position 112 (estimated K_d = 12.2 μM).

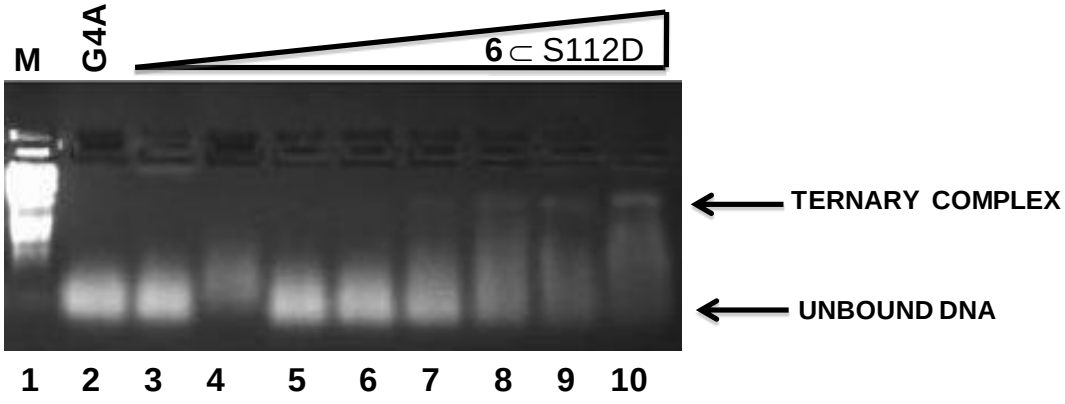

Figure 29 Binding of assembly of metallodrug and presenter protein (**6** ⊂ S112D) to G4A monitored by EMSA on agarose-gels. Lane 1: DNA Marker. Lane 2: G4A. Lane 3: G4A (3.3 μM) + S112D (39.6

μM); Lane 4: G4A (3.3 μM) + **6** (85.7 μM). Lanes 5-10: G4A (3.3 μM) + **6** ⊂ S112D at increasing concentrations: 0.8 μM, 1.6 μM, 3.9 μM, 7.9 μM, 19.8 μM, 39.6 μM, representing a **6** ⊂ S112D : G4A ratio from 0.2 to 12. In all cases 500 ng of DNA was loaded onto the gel.

The influence of a bulky hydrophobic residue on DNA binding was also investigated. EMSA on agarose-gels were carried out with a mutated presenter protein bearing a phenylalanine in position 112 (S112F, see Figure 30).

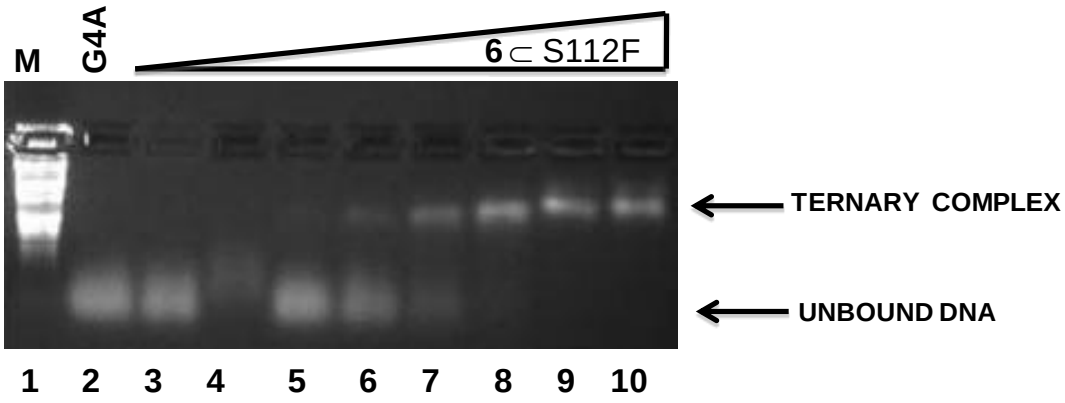

Figure 30 Binding of assembly of metallodrug and presenter protein (**6** ⊂ S112F) to G4A monitored by EMSA on agarose-gels. Lane 1: DNA Marker. Lane 2: G4A. Lane 3: G4A (3.3 μM) + S112F (39.6 μM); Lane 4: G4A (3.3 μM) + **6** (85.7 μM). Lanes 5-10: G4A (3.3 μM) + **6** ⊂ S112D at increasing concentrations: 0.8 μM, 1.6 μM, 3.9 μM, 7.9 μM, 19.8 μM, 39.6 μM, representing a **6** ⊂ S112F : G4A ratio from 0.2 to 12. In all cases 500 ng of DNA was loaded onto the gel.

Compared to the other two mutated Sav tested (K121A and S112D), introduction of an aromatic residue in position 112 did not appreciably change the affinity for G4A (estimated K_d < 1.6 μM). These results demonstrated that DNA binding of the cationic Ru complex **6** is influenced by the second coordination sphere provided by the presenter protein, particularly by charged residues in the vicinity of Ru. These data support the notion that optimized genetic screening could be carried out to improve the affinity of binding of a ternary complex.

2.4.5. Chemo-Genetic Optimization for Improved Binding to dsDNA

We also explored whether Sav could present the metallodrug **6** to dsDNA. For this purpose, we used an 18 base pair dsDNA that includes the sequence of the common Braf V599E oncogenic mutation (dsOnc).[153] It has been argued that recognition of ssDNA and dsDNA by proteins are fundamentally different. For example, Theobald *et al.* explored the mechanisms of sequence-specific ssDNA recognition.[147] They determined the crystal structures of 10 different non-cognate ssDNAs complexed with the Oxytricha nova telomere end-binding protein and evaluated their corresponding binding affinities. Their investigations highlighted a fundamental difference between protein recognition of ssDNA versus dsDNA. Consequently, we decided to extend our EMSA experiments to investigate the binding ability of **6** ⊂ WT Sav for dsOnc DNA (see Figure 31).

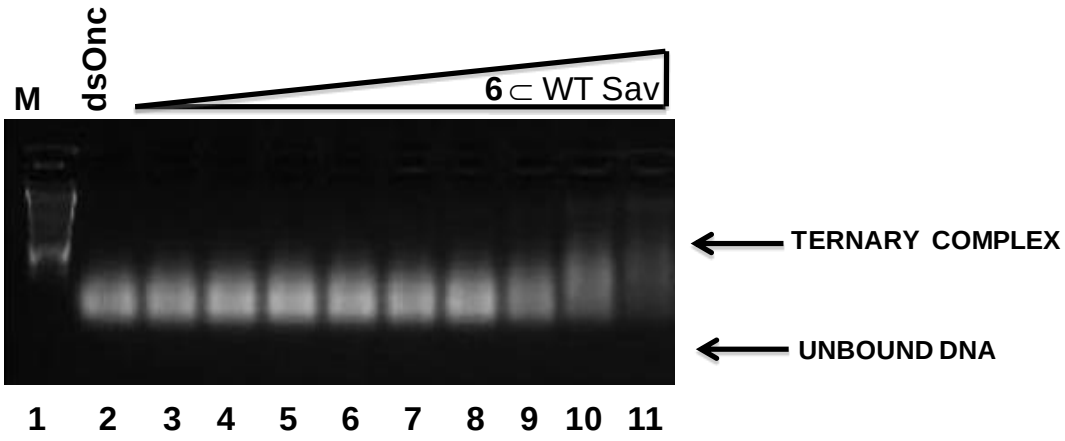

Figure 31 Binding of assembly of metallodrug and presenter protein (**6** ⊂ WT Sav) to dsOnc monitored by EMSA on agarose-gels. Lane 1: Marker (M). Lane 2: dsOnc. Lanes 3-11: dsOnc (3.12 µM) + concentration increase of **6** ⊂ WT Sav: 0.4 µM, 0.6 µM, 0.8 µM, 1.6 µM, 3.2 µM, 3.9 µM, 7.9 µM, 19.8 µM, 39.6 µM with a **6** ⊂ WT Sav : dsOnc ratio from about 0.1 to 13. In all cases 500 ng of DNA was loaded onto the gel.

Compared to the affinity for G4A (K_d < 1.6 µM as estimated by EMSA; Figure 17), the affinity for dsOnc was significantly lower, with K_d ≈ 37.9 µM (see Figure 31). We hypothesize that a different organization of functional groups as well as the reduced flexibility of dsDNA

hampered efficient interaction between the ruthenium and nucleophilic sites on the bases. With the aim of improving binding to dsDNA, chemical optimization by modifying the 2nd coordination sphere of the complex was investigated. It has been reported that η^6-biphenyl piano stool complexes can improve binding between ruthenium and dsDNA through intercalation.[153] In analogy, we synthesized the biphenyl derivative [(η^6-biphenyl)Ru(Biot-L)Cl]CF_3SO_3 **7** (see Figure 10). Combination of WT Sav with this chemical variation was investigated in DNA binding (see Figure 32).

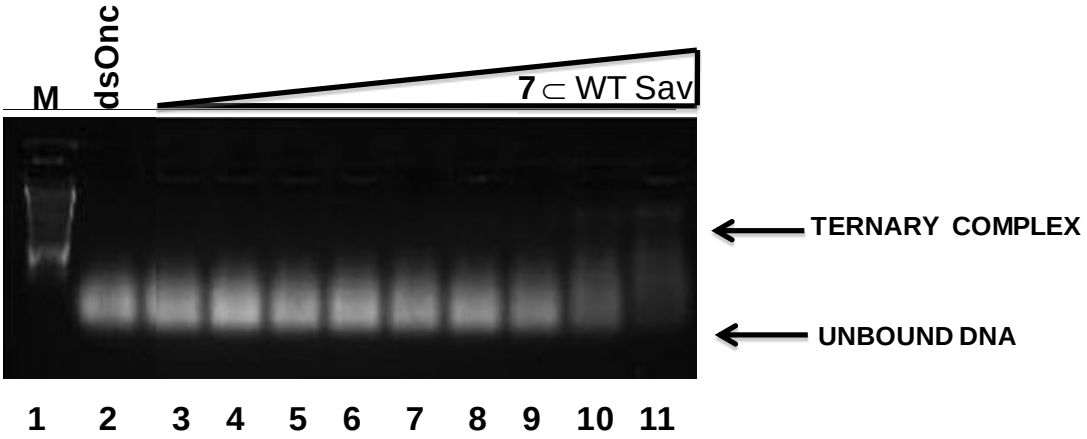

Figure 32 Binding of assembly of metallodrug and presenter protein (**7** ⊂ WT Sav) to dsOnc monitored by EMSA on agarose-gels. Lane 1: Marker (M). Lane 2: dsOnc. Lanes 3-11: dsOnc (3.12 µM) + concentration increase of **7** ⊂ WT Sav: 0.4 µM, 0.6 µM, 0.8 µM, 1.6 µM, 3.2 µM, 3.9 µM, 7.9 µM, 19.8 µM, 39.6 µM with a **7** ⊂ WT Sav : dsOnc ratio from about 0.1 to 13. In all cases 500 ng of DNA was loaded onto the gel.

Experiments presented in Figure 32 demonstrated that the introduction of an intercalator such as biphenyl did not improve the binding affinity when such complex was combined with WT Sav. The assembly **7** ⊂ WT Sav was found to bind to dsOnc with an estimated K_d of 37.9 µM, which is the same affinity displayed by **6** ⊂ WT Sav (estimated by EMSA, see Figure 31).

To further demonstrate that DNA binding can be fine-tuned using an assembly of drug and presenter protein, we thought to improve binding to dsDNA chemo-genetically by using the complex **7** combined with a genetic mutated protein. For example by introducing an aromatic

residue in the position closest to Ru metal (S112). Subsequently, binding of **7** ⊂ S112F to dsOnc was investigated and monitored by EMSA gels (see Figure 33).

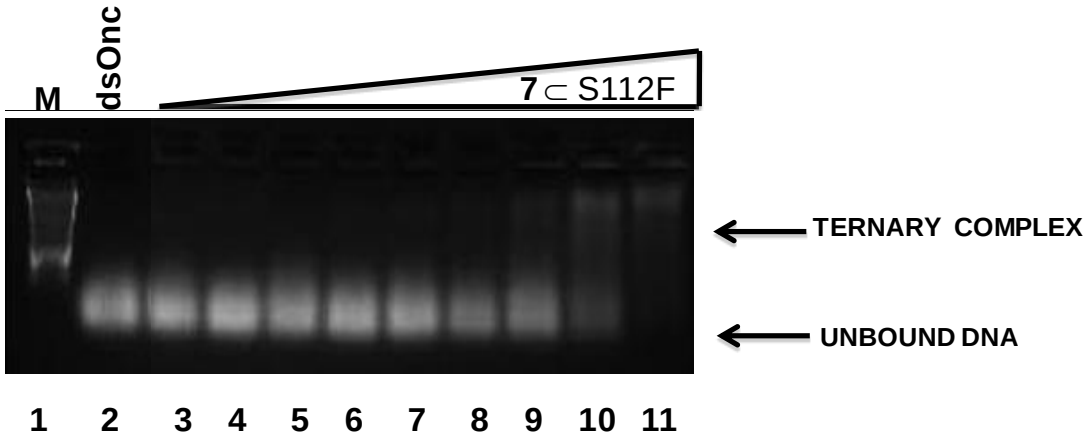

Figure 33 Binding of assembly of metallodrug and presenter protein (**7** ⊂ S112F) to dsOnc monitored by EMSA on agarose-gels. Lane 1: Marker (M). Lane 2: dsOnc. Lanes 3-11: dsOnc (3.12 μM) + concentration increase of **7** ⊂ S112F: 0.4 μM, 0.6 μM, 0.8 μM, 1.6 μM, 3.2 μM, 3.9 μM, 7.9 μM, 19.8 μM, 39.6 μM with a **7** ⊂ S112F: dsOnc ratio from about 0.1 to 13. In all cases 500 ng of DNA was loaded onto the gel.

Experiments presented in Figure 33 demonstrated that the biphenyl-containing S112F variant (**7** ⊂ S112F) increased the affinity to dsOnc (K_d = 18.2 μM as estimated by EMSA). Indeed, the latter metallodrug-presenter protein was found to bind to dsOnc with an improvement of at least a factor of 2 when compared with **6** ⊂ WT Sav, **6** ⊂ S112F or **7** ⊂ WT Sav (K_d = 37.9 μM for every assembly). Both the molecular weight and the estimated size of G-quadruplex-forming G4A (39 bases) and of this dsDNA (18 base pair) are similar and in both cases a single slow-mobility species was found. Moreover, the value of 18bp in a 1 : 1 stoichiometry with Sav is consistent with the experimentally-derived spacing of avidin onto plasmid DNA.[143] Importantly, the finding that the metalloprotein **7** ⊂ S112F improved the affinity for dsDNA suggested that modulation of non-covalent interactions in complexes of metallodrugs and presenter proteins can be engineered chemo-genetically to afford more specialized binders, with increased target-selectivity.

2.4.6. Summary

Table 2 Summary of dissociation constants (K_d) of Ru ⊂ Sav assemblies for various DNA targets, as estimated from EMSA.

Entry	DNA Target	Metal complex	Ratio Ru/Sav	Sav	K_d (μM)
1	G4A	**none**	-	WT	> 145[a]
2	G4A	**6**	2	WT	< 1.6[b], [c]
3	G4A	**6**	2	S112F	< 1.6[c]
4	G4A	**6**	2	S112D	12.2
5	G4A	**6**	2	K121A	28.8
6	G4A (GSH)[d]	**6**	2	WT	< 1.6[c]
7	dsOnc	**6**	2	WT	37.9
8	dsOnc	**6**	2	S112F	37.9
9	dsOnc	**7**	2	WT	37.9
10	dsOnc	**7**	2	S112F	18.2
11	scG4A[e]	**6**	2	WT	2.3
12	G4A (LiOH)[f]	**6**	2	WT	< 1.6[c]
13	G4A (GGG)[d]	**6**	2	WT	2
14	G4A (12mer)[d]	**6**	2	WT	5.4
15	G4A	**6**	1	WT	2.3
16	G4A	**6**	4	WT	< 1.6[c]

[a] K_d determined by ITC: 15.2 μM (from K_d determined in Figure 18); [b] K_d determined by ITC: 0.74 mM; [c] Binding was stoichiometric and probably beyond the sensitivity of these EMSA; [d] In brackets competing species: glutathione (GSH), trinucleotide GGG (GGG) and ssDNA 12mer (12mer); [e] "Scrambled" G4A has identical nucleotide content to G4A but with a different sequence and structure. [f] Experiment performed with LiOH instead of KOH: similar to unstructured G4A.

Our investigations are a proof-of-concept for a possible rational drug-design: binding a drug to a host presenter protein can be used both to protect a drug from unwanted interactions and to provide additional surface contacts ("surface borrowing")[154] for a more specific recognition of the desired macromolecular target. The importance of the extended second coordination sphere that is provided by the presenter protein for selective binding of a small molecule to a macromolecular target is shown by:

i) The different modes of binding of cationic biotinylated ruthenium piano stool complex **6** to G4A in presence or absence of Sav.

ii) The influence of chemogenetic modifications on DNA binding: for example decreasing binding to G4A using a K121A mutant or by increasing the affinity for dsDNA by a judicious combination of genetic variant (S112F) and biotinylated piano stool complex **7** (containing a biphenyl arene-cap).

In contrast, selective DNA binding is difficult to achieve with small metallodrugs, such as cationic biotinylated ruthenium piano stool complex **6** alone, because there are only limited interactions available for recognition of the target.

2.5. Conclusion

In this chapter we demonstrated that a supramolecular assembly consisting of a metallodrug (i.e., biotinylated ruthenium piano stool) combined with a presenter protein (i.e., streptavidin) modulated the recognition profile *in vitro* through the provision of additional non-covalent interactions. Such extended contacts, which are not typically available to small molecule drugs, allowed modulation of affinity and selectivity towards DNA telomeres, even in the presence of competing targets (such as glutathione and dsDNA).

In the present form such assemblies cannot be delivered easily into cells, thus hampering *in vivo* studies. To overcome this challenge, our current alternative efforts include the following:

i) Appending cell penetrating peptide sequences to the presenter protein.

ii) Exploring non-DNA,[135a] extracellular targets, which circumvents the need for intracellular delivery.

ii) Exploiting endogenous species as presenter proteins, such as those overexpressed in cancer cells. The latter would thus only require cell penetration of the metallo-prodrug.

The ultimate aim of these experiments is to use such tethered or cross-linking drugs[155] in which an initial kinetic binder[31, 156] does not merely act as a "carrier"[157] or "reservoir"[158] but also chaperones the drug selectively to a macromolecular target *in vivo*, contributing ultimately to the inhibitory (bioactive) species.

3. Streptavidin as Host Protein for Asymmetric Transfer Hydrogenation of Imines

3.1. Introduction

Within this chapter I present the synthesis and reactivity of a new generation of biotinylated half-sandwich complexes that potentially give access to high chemo-diversity and thus faster chemical screening of artificial metalloenzymes. The new scaffold involves d^6-transition metal (rhodium and iridium) piano stool complexes that contain a pentamethylcyclopentadienyl moiety (Cp*) tethered to biotin for incorporation into a host protein, streptavidin. Two different strategies were pursued:

i) The functionalized piano stool complexes were associated with a variety of bidentate ligands (N-N, N-O…) potentially giving rise to high chemical diversity of biotinylated catalysts.

ii) The biotinylated piano stool moiety was found to fit into the host protein containing a histidine residue and could act as a ligand, thereby creating a supramolecular (biotin-streptavidin) and dative (metal-histidine) anchoring to the host protein. This approach constituted a novel metalloprotein design in which the host protein provided simultaneously the first and the second coordination sphere.

The reduction of cyclic imines by ATH was selected as the model reaction to screen the potential of these metalloenzymes in enantioselective catalysis.

3.2. New Generation of Biotinylated Complexes Displaying High Chemo-Diversity

3.2.1. First Generation of Biotinylated Complexes Developed for ATH Reactions

Since the development, by Letondor *et al.* of highly active and selective biotinylated catalysts [η^6-(arene)Ru(Biot–*q*–L)Cl], all the complexes that have been used for asymmetric transfer hydrogenation in the Ward group shared this scaffold (Figure 34).[159]

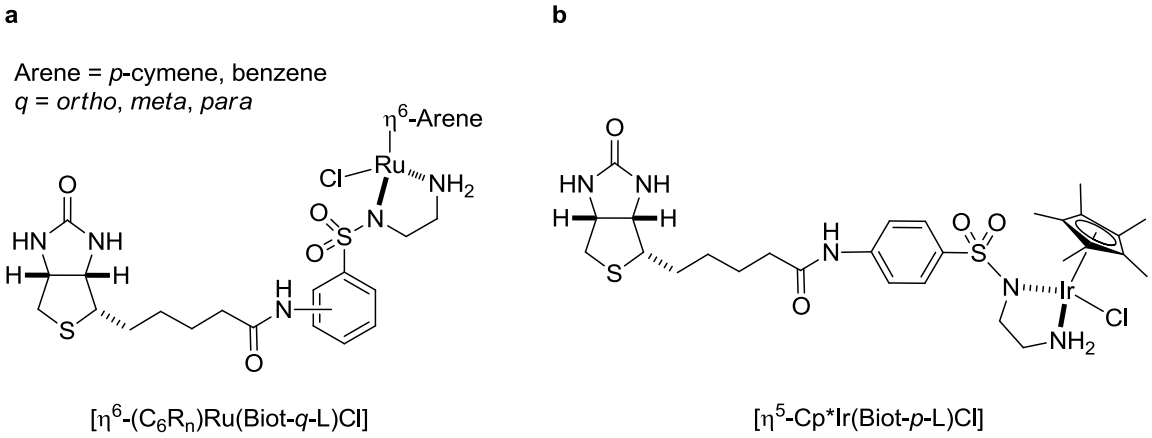

Figure 34 Biotinylated complexes designed by Ward and coworkers for ATH of ketones and imines.[159-160]

During the development of the first generation of Cp* iridium catalysts, I supervised a Master student, Annette Mutschler for the synthesis of [Cp*Ir(Biot–*p*–L)Cl]. Although this ligand approach has been successively applied in enantioselective reduction of both ketones and cyclic imines,[160] this method offered relatively limited chemical diversity. Diversification of the bidentate ligand and/or the spacer was time consuming.

3.2.2. Second Generation of Biotinylated Complexes Offering High Chemo-Diversity

To create organometallic complexes with high chemo-diversity potential, direct attachment of biotin to the arene cap was envisioned (see Figure 35).

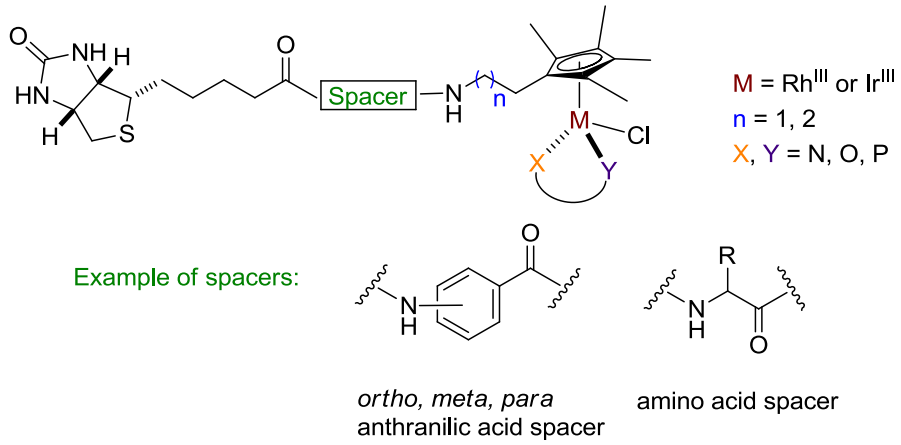

Figure 35 Design principle of a new generation of biotinylated piano stool complexes affording high chemo-diversity.

This strategy gave a straightforward access to a new generation of biotinylated Cp* moiety and allowed the introduction of potentially high chemo-diversity through variation of the bidentate ligand bound to the metal (N-N, N-O, P-N, P-P): **X**, **Y**. Furthermore, chemical diversity can also be achieved in a similar fashion to the first generation of biotinylated piano stool complexes (see Figure 34):

i) Introduction of a spacer between the biotin anchor and the Cp* moiety: **Spacer**.

ii) Variation of the metal Ir^{III}, Rh^{III} and Ru^{II}: **M**.

iii) Modification of the length of the arm on the functionalized tethered Cp* (n = 1 or 2): $(\,)_n$.

These biotinylated complexes can subsequently be incorporated into streptavidin as host protein for the construction of a variety of chemogenetically engineered metalloenzymes. Based on the work of Reiner *et al.*[161] and van Leusen *et al.*,[162] we synthesized tethered complexes with an ethylene spacer (n = 1, see Figure 35).[162] The biotinylated dimeric complexes $[(\eta^5\text{-}Me_4Cp\text{-}(CH_2)_2\text{-}N\text{-Biot})MCl_2]_2$ (where M = Rh or Ir, see Figure 36) were selected for the creation of artificial metalloenzymes:

i) The dimers were used as staring material for the synthesis of diverse mononuclear biotinylated piano stool complexes bearing an additional bidentate ligand.

ii) Combination of the dimers with Sav mutants bearing a suitably positioned histidine residue allowed the creation of dually anchored artificial metalloenzymes.

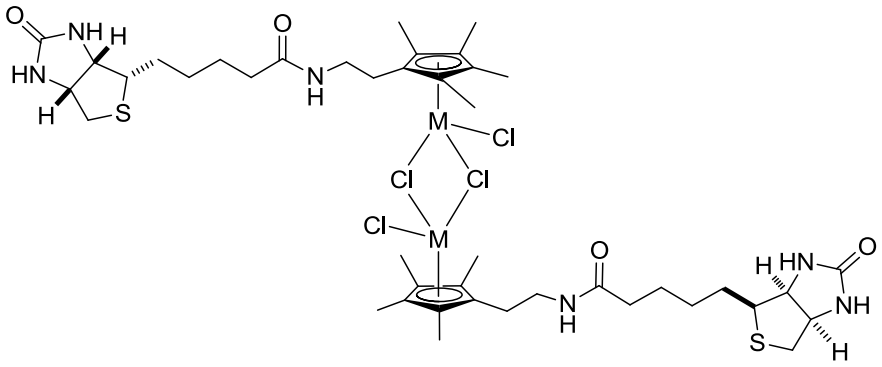

$[\eta^5\text{-}Me_4Cp(CH_2)_2\text{-}N\text{-Biot})MCl_2]_2$
M = Rh, **17** and M = Ir, **18**

Figure 36 Biotinylated dimeric rhodium **17** and iridium **18** complexes.

3.2.3. Synthesis of Biotinylated Complexes 17 and 18

For the synthesis of the dimeric complexes **17** and **18**, the procedure by van Leusen *et al.* was slightly modified.[162] To accomplish the synthesis of various ethylene-bridged tetramethylcyclopentadienylamines, van Leusen *et al.* used the commercially available 2,3,4,5-tetramethylcyclopent-2-enone **19** as starting material (see Scheme 19).

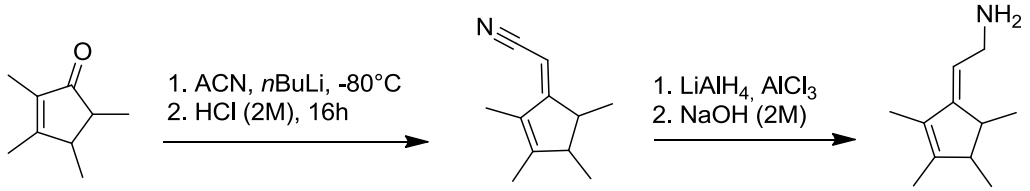

19 **20**: 90% **21**

Scheme 19 Synthesis of ethylaminocyclopentene precursor **21**.[162]

Treatment of 2,3,4,5-tetramethylcyclopent-2-enone **19** with deprotonated acetonitrile in THF at -80°C afforded the hydroxy intermediate which, upon acidic treatment, underwent dehydration to yield the corresponding nitrile **20** (90% yield). The resulting nitrile **20** could not be reduced using the van Leusen protocol. Instead, the procedure published by McCalmont *et al.*[163] using activated $(AlCl_3)\bullet LiAlH_4$ in dry THF was employed and yielded the

corresponding amine **21** as a mixture of isomers. The crude amine was directly used as a starting material for the next step as it was found to be unstable. The dimeric rhodium complex **22** was prepared from **21** following the protocol of Reiner *et al.* (see Scheme 20).[161] While Reiner *et al.* performed the reaction in EtOH to afford **22** in 72% yield, MeOH proved to be a better solvent in our hands: the dimer **22** was obtained in higher yield (85%).

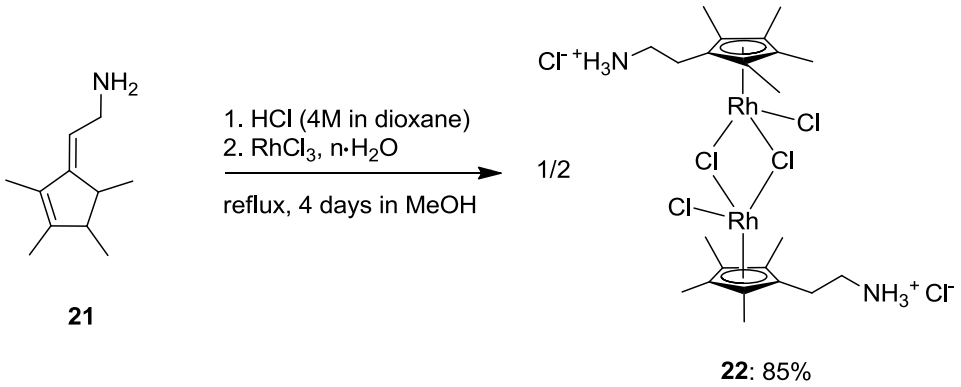

21

22: 85%

Scheme 20 Synthesis of the dimeric rhodium complex $[(\eta^5\text{-}Me_4Cp\text{-}(CH_2)_2NH_3)RhCl_2]_2(Cl)_2$ **22**.[161]

The coupling of biotin to **22** proved challenging. One common activated form of biotin used in the Ward group is the *N*-hydroxysuccinimide ester of biotin (BNHS).[137] The dimeric rhodium complex was mixed with BNHS in the presence of Et_3N as a base in DMF. The reaction was stirred overnight to afford the biotinylated rhodium dimer **17** (80% yield, see Scheme 21). However, ^1H NMR spectrum revealed the presence of biotin impurities. The reaction with BNHS was incomplete due to biotin *N*-hydroxysuccinimide degradation during the reaction which liberated biotin. To overcome this problem, biotin pentafluorophenyl ester was used (see Scheme 21).[164]

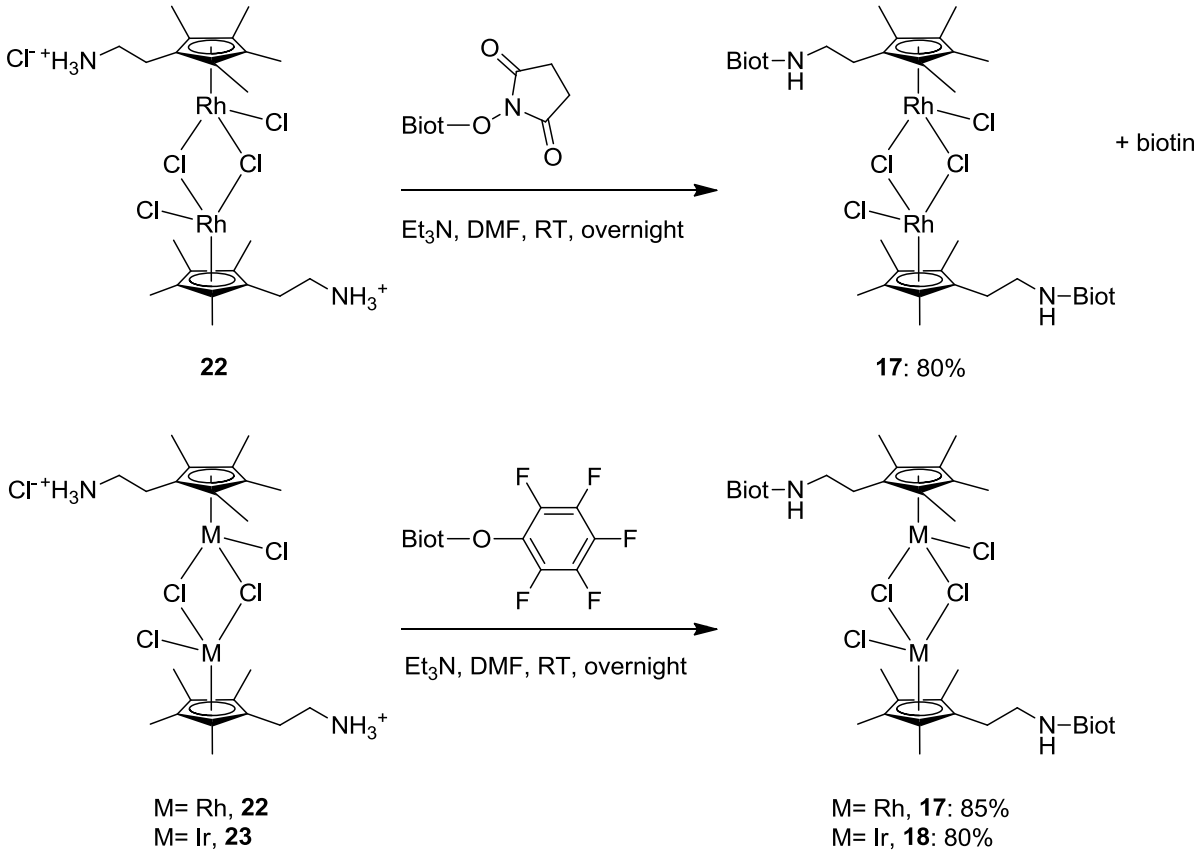

Scheme 21 Synthesis of $[(\eta^5\text{-}Me_4Cp\text{-}(CH_2)_2\text{-}N\text{-Biot})MCl_2]_2$ (M = Rh, **17** and M = Ir, **18**).

The complex **17** was obtained as a pure solid in good yield (85%). It was found to be particularly stable and could be stored under air without significant degradation. The successful synthesis of **17** through this route was applied to the synthesis of the biotinylated iridium dimer $[(\eta^5\text{-}Me_4Cp\text{-}(CH_2)_2\text{-}N\text{-Biot})IrCl_2]_2$ **18** (see Scheme 21). Unfortunately, synthesis of the analog dimeric iridium complex **18** displayed distinct differences. Reiner *et al.* described the reaction affording the μ-chloro bridged η^5-cyclopentadienyl iridium homolog complex in poor yield (16 %, see Scheme 22).[161] They found the iridium dimer **23** had increased solubility in EtOH compared to the rhodium dimer **22** analog. Consequently the dimer **22** remained dissolved, leading to limited product recovery.

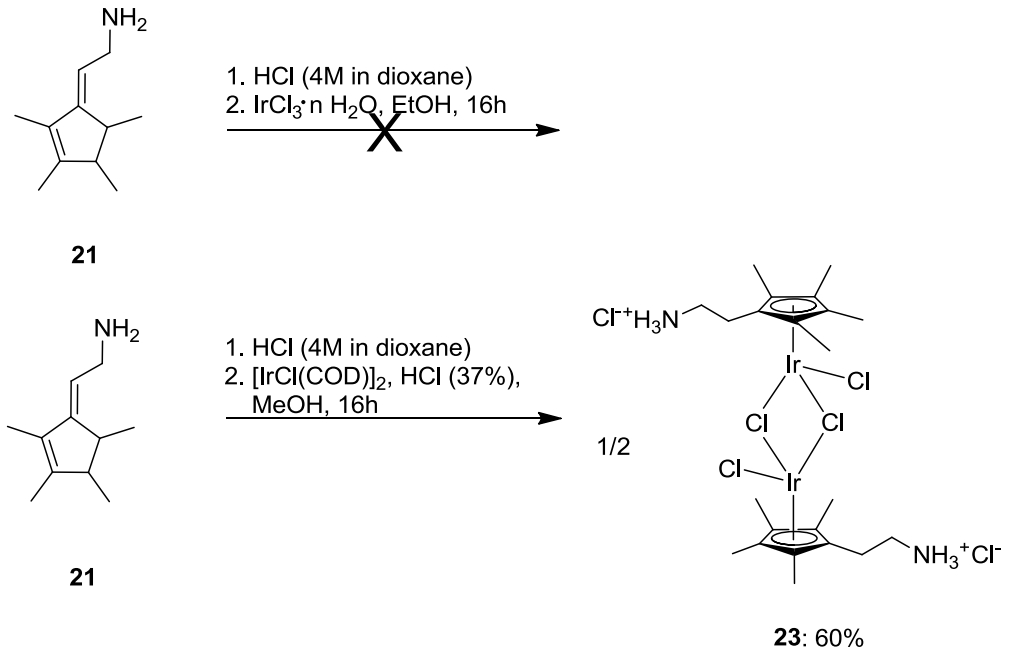

Scheme 22 Alternative synthesis for the preparation of $[(\eta^5\text{-}Me_4Cp\text{-}(CH_2)_2NH_3)IrCl_2]_2(Cl)_2$ **23**.

An alternative synthesis to yield dimeric iridium complex **23** was developed, based on the work of Jaouen *et al*.[165] They described an efficient synthesis of $[Cp^*MCl_2]_2$ complexes (M = Rh or Ir) in high yield (90%) involving the oxidation of M^I to M^{III} with concentrated HCl. This method allowed the transformation of dimeric complex $[IrCl(COD)]_2$ (COD = 1,5-cyclooctadiene) in to $[Cp^*IrCl_2]_2$. The protocol of Jaouen *et al.* was then adapted to perform the synthesis of dimer **23**. To prevent coordination of the amine to the metal, the cyclopentadienyl precursor **21** was first protonated. Then $[IrCl(COD)]_2$ was used instead of $IrCl_3 \bullet nH_2O$, in the presence of concentrated HCl. The presence of HCl was essential because the oxidation of the starting Ir^I proceeded by oxidative addition to give the intermediate $[Ir^{III}HCl_2(COD)]_2$. The iridium hydride generated *in situ* was allowed to react with the protonated amine derived from **21** to produce the iridium dimer **23** as a yellowish solid in 60% yield (see Scheme 22). The dimeric iridium **23** was subjected to the same biotinylation protocol as the rhodium analog **22**. The coupling reaction between the dimer **23** and BPFP yielded biotinylated iridium dimer **18** as a yellowish powder in 80% yield (see Scheme 21). The biotinylated complex was found to be highly stable against air.

3.3. Designing New Metalloenzymes

3.3.1. Incorporation of Biotinylated Bidentate Catalysts into Streptavidin for the ATH of Imines

3.3.1.1. Chemical Optimization

With the dimeric biotinylated tethered-Cp* rhodium and iridium complexes **17** and **18** in hand, various bidentate chelating ligands were added to generate a small library of catalysts for further incorporation into Sav (see Figure 37). This new synthetic platform allowed fast chemical optimization to design artificial metalloenzymes that were tested in the transfer hydrogenation reaction.

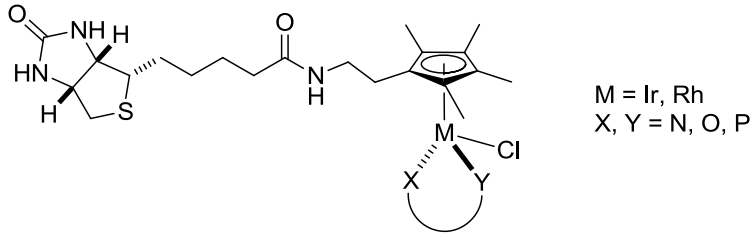

Figure 37 Biotinylated tethered-Cp* catalyst: a new synthetic platform for the generation of chemical diversity.

Inspired by the work of Ogo *et al.* on the transfer hydrogenation using piano stool complexes bearing 2,2'-bipyridine bidentate ligands,[166] the biotinylated rhodium and iridium dimers **17** and **18** were tested as precursors for the preparation of piano stool complexes bearing diimine ligands (see Scheme 23).[167]

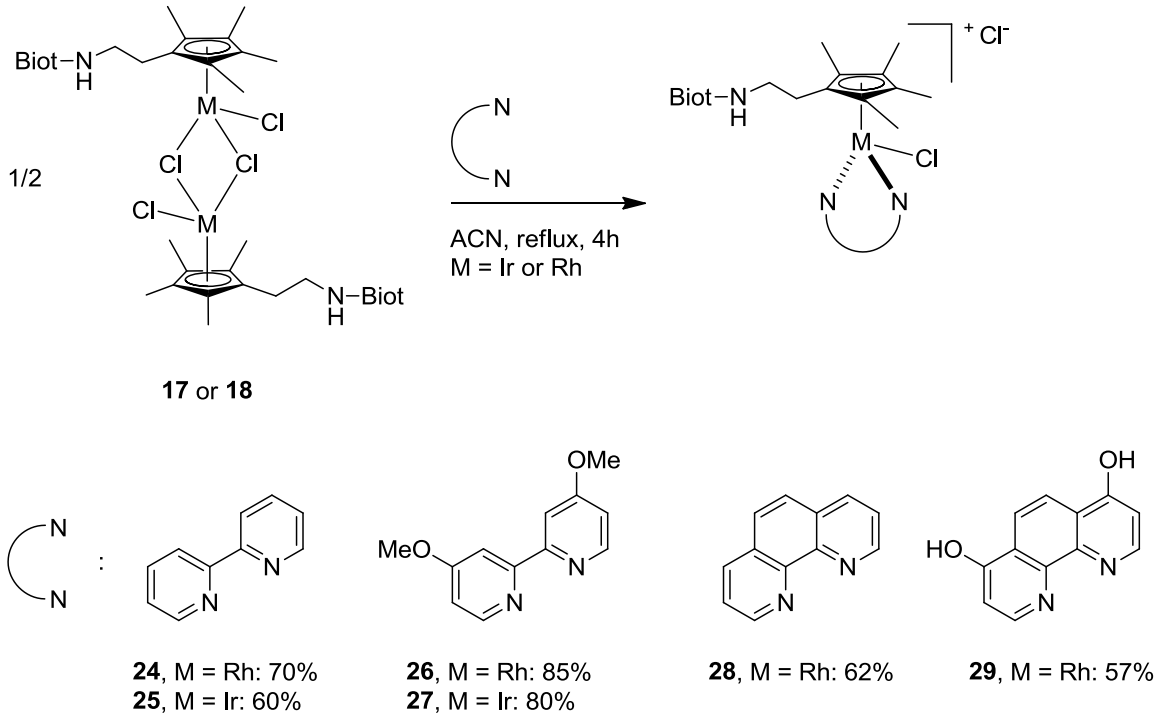

Scheme 23 Synthesis of diverse biotinylated *N,N*-bidentate rhodium and iridium complexes **24**-**29**.

The biotinylated piano stool complexes **24**-**29** bearing diimine ligands were synthesized, isolated and characterized. The resulting biotinylated catalysts were incorporated into WT Sav and tested in the ATH of imines using the catalytic conditions described by Ogo *et al.* (see Scheme 24 and Table 3).[166] The reduction of 6,7-dimethoxy-1-methyl-3,4-dihydroisoquinoline, the precursor of salsolidine **5**, was selected as a model system (Scheme 24).

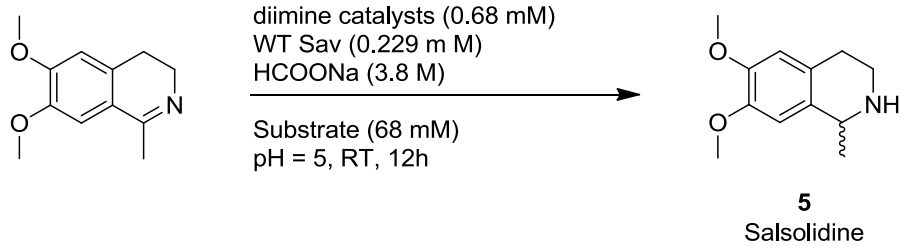

Scheme 24 Asymmetric transfer hydrogenation of imines for the production of salsolidine **5**.

Table 3 Results for the production of salsolidine **5** using biotinylated piano stool complexes bearing diimine ligands.[a]

Entry	Complex	Protein	Conversion (%)	*ee* (%)
1	**24**	no	quant.	rac.
2	**25**	no	quant.	rac.
3	**26**	no	quant.	rac.
4	**27**	no	quant.	rac.
5	**28**	no	quant.	rac.
6	**29**	no	52	rac.
7	**17**	no	32	rac.
8	**18**	no	43	rac.
9	**24**	WT Sav	-[b]	n.d.
10	**25**	WT Sav	-[b]	n.d.
11	**26**	WT Sav	74	rac.
12	**27**	WT Sav	-[b]	n.d.
13	**28**	WT Sav	35	rac.
14	**29**	WT Sav	23	rac.
15	**17**	WT Sav	-[b]	n.d.
16	**18**	WT Sav	-[b]	n.d.

[a] Reactions were carried out at 25°C for 12 h using 1 mol% complex *vs.* substrate (680 µM final metal concentration, 68 mM substrate) and 0.33 mol% tetrameric WT Sav (corresponding to 916 µM biotin binding sites) at pH 5.0 containing 3.88 M of HCOONa in a total reaction volume of 200 µL. [b] Peaks were too small to determine conversion.

The results demonstrated the high activity of the bipyridine-type complexes in the absence of protein: full conversion was observed after 12 h at 25°C. Interestingly, some catalysis experiments were inhibited in the presence of WT Sav (see Table 3, entries 9, 10, 12, 15 and 16). Only the bulkier diimine catalysts exhibited promising activity when combined with WT

Sav (see Table 3, entries 11, 13 and 14). The best candidate was found to be the rhodium-based catalyst **26** which bears 4,4'-dimethoxybipyridine ligand (74% yield, see Table 3, entry 11). However, only racemic product was obtained in the presence of WT Sav.

Encouraged by these results, we screened different complexes. For that purpose, the *in situ* preparation of biotinylated catalysts was tested. This method was exploited by Parekh *et al.* in ATH of quinolines using tethered Ru^{II} catalysts.[168] In order to verify the reliability of the method, parallel reactions were performed with biotinylated complex **26** and the *in situ* prepared catalyst **26-*is*** (***is*** = *in situ* formed, see Scheme 25 and Table 4). In parallel, a complex bearing *N*-tosylethylenediamine ligand (TsEN, catalyst **30**, see Scheme 25 and Table 4) was also tested. Indeed, this ligand on the rhodium scaffold exhibits high conversion and *ee* for the enantioselective preparation of salsolidine by ATH.[160] The *in situ* method of preparation was the following: the precatalyst was generated *in situ* by reacting the bidentate ligand (from a stock solution in DMSO) with rhodium dimer **17** (from a stock solution in DMSO) at RT for 30 minutes. This *in situ* prepared catalyst was added to the protein, which was previously dissolved in a solution containing the hydride source, and stirred for 15 min. The ATH was initiated by adding the substrate.

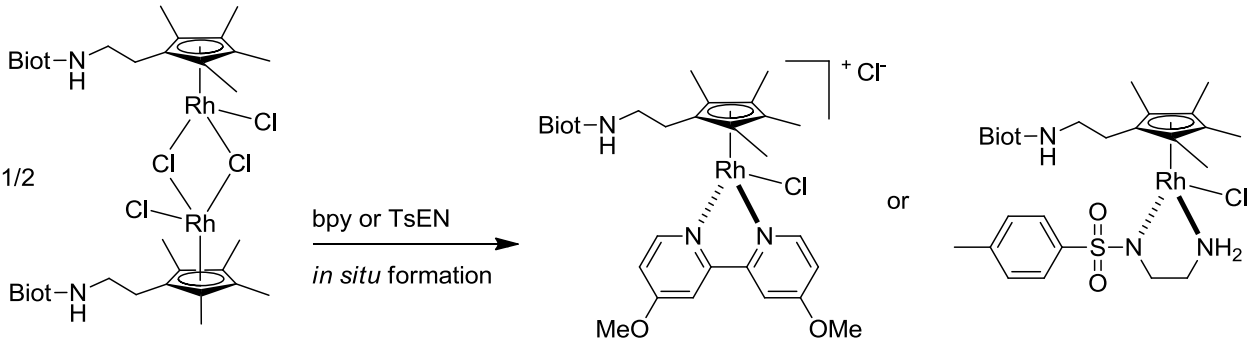

17 **26-*is*** **30**

Scheme 25 *In situ* preparation of [(η^5-Me_4Cp-$(CH_2)_2$-*N*-Biot)Rh(4,4'-diMeObpy)Cl]Cl **26-*is*** and [(η^5-Me_4Cp-$(CH_2)_2$-*N*-Biot)Rh(TsEN)Cl] **30**.

Table 4 Results for the production of salsolidine **5** using preformed and *in situ* prepared biotinylated piano stool complexes.[a]

Entry	Complex	Protein	Conversion (%)	*ee* (%)
1	**26**	no	quant.	rac.
2	**26-*is***	no	quant.	rac.
3	**30**[c]	no	65	rac.
4	**17**	no	32	rac.
5	**26**	WT Sav	74	rac.
6	**26-*is***	WT Sav	68	rac.
7	**30**[c]	WT Sav	70	rac.
8	**17**	WT Sav	-[b]	n.d.

[a] Reactions were carried out at 25°C for 12 h using 1 mol% complex *vs.* substrate (680 µM final metal concentration, 68 mM substrate) and 0.33 mol% tetrameric WT Sav (corresponding to 916 µM biotin binding sites) at pH 5.0 containing 3.88 M of HCOONa in a total reaction volume of 200 µL. [b] Peaks were too small to determine conversion. [c] pH 6.5 with MOPS buffer (3.1 M) and 3.88 M HCOONa were used for catalysis carried out with complex **30**.[160]

As expected, both preformed **26** and *in situ* prepared **26-*is*** provided similar results (see Table 4, entries 1, 2, 5 and 6). These results constituted a first proof of principle: bidentate complexes formed *in situ* display comparable activity to that of pure isolated analogues. The metalloenzyme **30** ⊂ WT Sav exhibited good activity but no enantioselectivity (70% yield, see Table 4, entry 7). The dimer **17** displayed modest activity alone (32% yield) and was inactive in the presence of WT Sav (see Table 4, entries 4 and 8).

3.3.1.2. Genetic Optimization

Encouraged by the results obtained with the catalysts prepared *in situ*, a genetic optimization was carried out. The complex **30** was selected as catalyst (see Table 5).

Table 5 Results for the production of salsolidine **5** using Sav-incorporated biotinylated piano stool complex **30**.[a]

Entry	Complex	Protein	Conversion (%)	*ee* (%)
1	**30**	S112G	75	rac.
2	**30**	S112A	28	rac.
3	**30**	S112F	94	rac.
4	**30**	S112K	70	rac.
5	**30**	S112E	26	rac.
6	**30**	S112R	42	rac.
7	**30**	S112Y	95	rac.
8	**30**	S112W	quant.	rac.
9	**30**	S112H	quant.	48 (*S*)
10	**30**	P64G	quant.	rac.
11	**30**	L124Y	quant.	rac.
12	**30**	L124G	quant.	rac.
13	**30**	L124H	quant.	rac.
14	**30**	K121H	quant.	65 (*R*)
15	**30**	K121G	66	rac.
16	**30**	K121N	quant.	rac.
17	**30**	H87A	58	rac.
18	**30**	H127A	54	rac.
19	**30**	no	95	rac.
20	**17**	no	18	rac.
21	**17**	S112H	95	41 (*S*)
22	**17**	K121H	95	60 (*R*)

[a] Reactions were carried out at 55°C for 12 h using 1 mol% complex *vs.* substrate (680 µM final metal concentration, 68 mM substrate) and 0.33 mol% tetrameric Sav isoforms (corresponding to 916 µM biotin binding sites) at pH 6.5 (MOPS buffer 3.1 M) containing 3.88 M HCOONa in a total reaction volume of 200 µL.

Having identified a catalytically active hybrid catalyst **30** ⊂ WT Sav (see Table 4, entry 7), we proceeded to optimize its performance by screening various Sav single point mutants. Aminosulfonamide-piano stool complex **30** was screened for the synthesis of salsolidine **5**. In previous studies, positions S112, K121, P64 and L124 were identified as residues lying close to the organometallic moiety.[159, 169]

We initially screened a focused library of Sav mutants S112X (X = A, G, F, K, E, R, Y, H and W, see Table 5, entries 1-9). In most cases, the conversions were good. Concerning enantioselectivity, salsolidine **5** was obtained in racemic form except for the S112H mutant that yielded (*S*)-salsolidine in 48% *ee* (see Table 5, entry 9). This fascinating result suggests that histidine at this position plays a critical role in enantioselection. Next, mutants at positions P64, K121 and L124 were tested in the presence of complex **30**. Of all this second round of screening with Sav mutants, only K121H yielded significant levels of enantioselectivity (65% *ee* for the (*R*)-enantiomer of salsolidine **5**, see Table 5, entry 14). To our delight **30** ⊂ S112H and **30** ⊂ K121H yielded opposite enantiomers. In contrast, introduction of a histidine residue at position 124 (L124H) afforded racemic material (see Table 4, entry 13). WT Sav possesses two solvent exposed histidine residues: H87 and H127. To test their potential influence on catalysis, both single point mutants H127A and H87A were tested in catalysis. These mutants produced racemic material but with a reduced conversion (see Table 5, entries 17 and 18). This result may suggest that these residues may bind to complex **30** albeit with a dangling biotin anchor. The Lewis basic properties of these His residues have been illustrated in the group in various X-ray characterizations: anomalous X-ray scattering, diagnostic of the presence of precious metals has been detected with Os,[170] Ir[160] as well as with Ru (unpublished). To test their involvement, it would be interesting to produce triple mutants Sav H87A-S112H-H127A and Sav H87A-K121H-H127A. This would ensure that none of the biotinylated complex **30** is interacting with these surface exposed residues. Due to the difficulty of refolding the single point mutant H87A, these experiments remain to be performed.

As amply demonstrated, imine reduction by piano stool complexes proceeds without coordination of the substrate to the d^6-transition metal: A single free coordination site at the metal is required for hydride generation (from formate) and delivery to one prochiral face of the imine. Considering that, the three-legged piano stool complex **30** bears a bidentate ligand, we speculated that, upon coordination of a histidine side-chain to the metal would create a catalytically inactive, coordinatively saturated, piano stool complex. To rationalize the observed results, we envisaged two possible mechanisms:

i) The histidine does not bind to the piano stool complex, instead it interacts with the substrate, thus leaving a free coordination site available for catalysis.

ii) Alternatively, the proximity of the histidine residue to the Rh center leads to a very high effective molarity of the Lewis basic residue, eventually displacing the bidentate aminosulfonamide ligand.

To distinguish between these two alternative mechanisms, the dinuclear rhodium catalyst precursor **17** was tested in the presence of both histidine containing mutants Sav S112H and Sav K121H (see Table 5, entries 21 and 22). The results obtained with the catalyst derived from dinuclear complex **17** (which is expected to break down in solution to yield the corresponding solvated mononuclear complex) were very similar to those obtained with complex **30**: Compare 65 % *ee* (*R*) and 48 % *ee* (*S*) for **30** $\subset$ K121H and **30** $\subset$ S112H with 60 % *ee* (*R*) and 41 % *ee* (*S*) for **17** $\subset$ K121H and **17** $\subset$ S112H respectively. These results suggest that the bidentate ligand may indeed be displaced by the close-lying histidine residue.

Overall, the mutants S112H and K121H provided a suitable chiral environment to rhodium catalysts which lead to enantioselective reduction of the salsolidine precursor. Next, the metalloenzymes consisting of the incorporation of biotinylated Rh-complexes with bidentate ligands into Sav isoforms were screened against more challenging enantioselective reactions, such as reductive amination for the preparation of unprotected chiral α-amino acids (see Chapter 4).

3.3.2. Towards New Artificial Transfer Hydrogenases: Dual Anchoring Strategy

3.3.2.1. Incorporation of the Rhodium Dimer 17 into S112H and K121H: Docking Studies

We have highlighted that combination of dimer **17** and proteins bearing histidine mutants at position 112 and 121 may form active artificial metalloenzymes in ATH. In order to obtain a qualitative model of these hybrid catalysts, *in silico* studies were carried out. The combination of dimer **17** with selected host proteins and its capacity to form dually-anchored (dative and supramolecular) artificial metalloenzymes was then tested. Docking experiments were carried out by Maurus Schmid using the VMD program: the biotinylated rhodium monomer [η^5-Me_4Cp-$(CH_2)_2$-*N*-Biot)$RhCl_2(H_2O)$] **17'** embedded into S112H (see Scheme 26 and Figure 38) and K121H (see Scheme 26 and Figure 39).

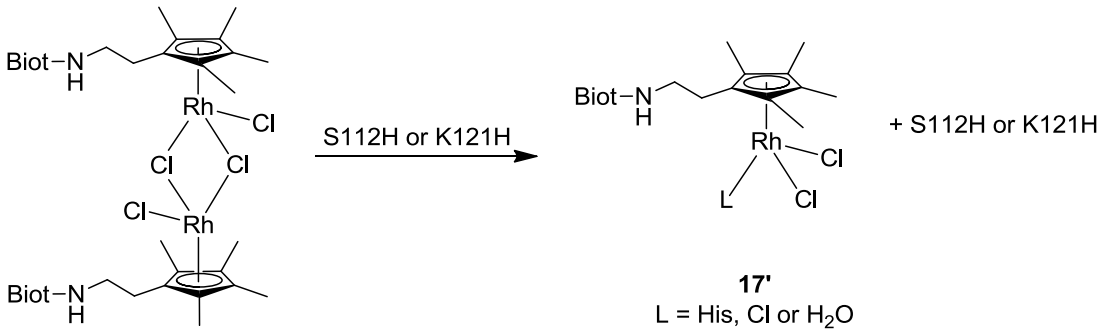

Scheme 26 Anticipated biotinylated rhodium monomer (**17'** derived from **17**) embedded into S112H or K121H host proteins.

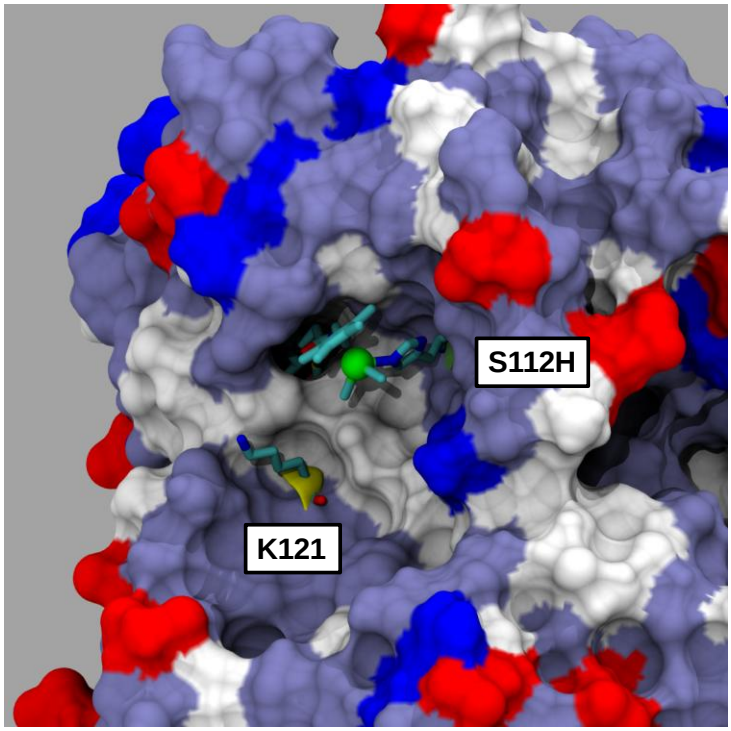

Figure 38 Docking simulation of biotinylated complex **17'** in S112H host protein.

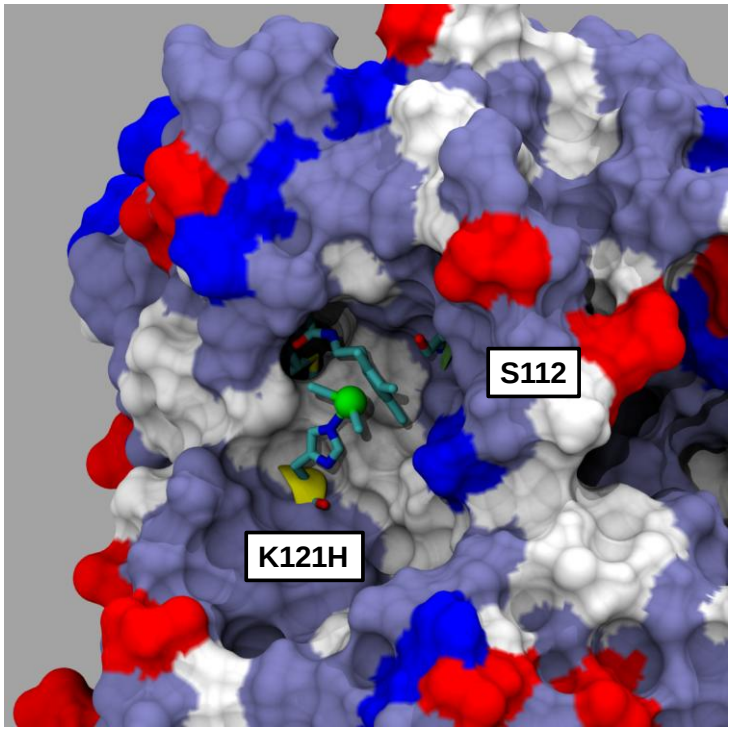

Figure 39 Docking simulation of biotinylated complex **17'** in K121H host protein.

Docking experiments suggested an ideal spacer length for the incorporation of biotinylated complex **17'** into S112H and K121H Sav mutants. The ethylene spacer between the biotin

anchor and the Cp*, places the metal in close proximity to histidines either at position 112 or 121 in mutants S112H or K121H respectively.

3.3.2.2. Artificial Metalloenzymes 17' ⊂ S112H and 17' ⊂ K121H for ATH of Imines

3.3.2.2.1 Chemo-Genetic Optimization

In order to confirm the importance of histidines residues at position 112 and 121 in the formation of metalloenzymes, **17'** ⊂ S112H and **17'** ⊂ K121H, catalysis experiments were performed using proteins bearing a possible dative anchoring site (Lewis basic residues, see Table 6).

Table 6 Results for the production of salsolidine **5** using biotinylated piano stool rhodium complex **17'** and proteins with a possible dative anchor.[a]

Entry	Complex	Protein	Conversion (%)	*ee* (%)
1	**17**	no	31	rac.
2	**17'**	WT Sav	15	rac.
3	**17'**	S112H	95	41 (*S*)
4	**17'**	K121H	95	60 (*R*)
5	**17'**	L124H	67	rac.
6	**17'**	S112C	12	rac.

[a] Reactions were carried out at 55°C for 12 h using 2 mol% complex *vs.* substrate (680 µM final metal concentration, 34 mM substrate) and 0.66 mol% tetrameric Sav isoforms (corresponding to 916 µM biotin binding sites) at pH 6.5 (MOPS buffer 3.1 M) with 3.88 M HCOONa in a total reaction volume of 200 µL.

The catalysis experiments carried out with WT Sav, L124H and S112C as hosts exhibited modest activity and no enantioselectivity (see Table 6, entries 2, 5 and 6). As expected, the catalysis experiments carried out with rhodium dimer **17** in the absence of protein provided

racemic product, in low yield (see Table 6, entry 1). The latter result highlighted the importance of metal/imidazole coordination in the activation of the catalyst. The study corroborated the docking experiments and supported the crucial role of bound histidines in ATH of imines: the protein scaffold simultaneously provided the first and second coordination sphere contacts to the catalyst affording new active and enantioselective artificial metalloenzymes.

3.3.2.2.1.1. pH Optimization

The influence of pH was tested using hybrid catalysts **17'** ⊂ S112H and **17'** ⊂ K121H; reactions were performed with HCOONa in non-buffered solutions (see Figure 40).

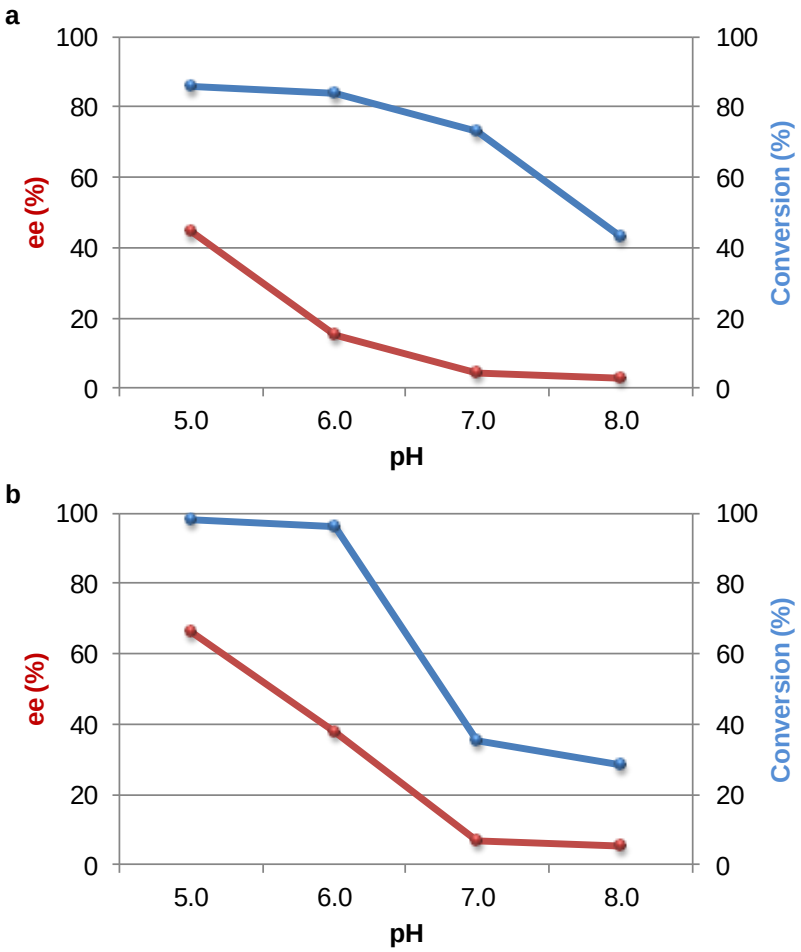

Figure 40 Influence of pH on *ee* and conversion using hybrid catalysts a) **17'** ⊂ S112H and b) **17'** ⊂ K121H. For experimental details, see experimental part on Table 6.

As expected, the pH influenced the reaction outcome: increasing the pH from 5.0 to 8.0 resulted in a decrease of both the conversion and the enantioselectivity. The best results in terms of activity and enantioselectivity were obtained when catalysis experiments were carried out at pH 5.0, in unbuffered solutions: the metalloenzyme **17'** ⊂ S112H yielded (*S*)-salsolidine in 86% yield with 45% *ee* (see Figure 40a) and **17'** ⊂ K121H afforded (*R*)-salsolidine in 98% yield with 66% *ee* (see Figure 40b).

3.3.2.2.1.2. Buffer Optimization

In order to further examine the pH influence during the reaction, different buffers were tested at pH 5.0 and 5.5 (acetate, citric acid, MES, MOPS, see Table 7).

Table 7 Influence of buffer composition on *ee* and conversion using hybrid catalysts **17'** ⊂ S112H and **17'** ⊂ K121H at pH 5.0 and 5.5.[a]

Entry	Complexes	Buffer	pH	Protein	Conversion (%)	*ee* (%)
1	**17'**	acetate	5.0	S112H	36	32 (*S*)
2	**17'**	acetate	5.5	S112H	32	28 (*S*)
3	**17'**	citric acid	5.0	S112H	60	40 (*S*)
4	**17'**	citric acid	5.5	S112H	60	38 (*S*)
5	**17'**	MES	5.0	S112H	83	38 (*S*)
6	**17'**	MES	5.5	S112H	86	40 (*S*)
7	**17'**	MOPS	5.0	S112H	quant.	55 (*S*)
8	**17'**	MOPS	5.5	S112H	quant.	53 (*S*)
9	**17'**	acetate	5.0	K121H	37	50 (*R*)
10	**17'**	acetate	5.5	K121H	37	50 (*R*)
11	**17'**	citric acid	5.0	K121H	quant.	65 (*R*)
12	**17'**	citric acid	5.5	K121H	quant.	64 (*R*)

13	**17'**	MES	5.0	K121H	quant.	69 (*R*)
14	**17'**	MES	5.5	K121H	quant.	67 (*R*)
15	**17'**	MOPS	5.0	K121H	quant.	72 (*R*)
16	**17'**	MOPS	5.5	K121H	quant.	70 (*R*)

[a] Reactions were carried out at 55°C for 12 h using 2 mol% complex *vs.* substrate (680 µM final metal concentration, 34 mM substrate) and 0.66 mol % tetrameric Sav (corresponding to 916 µM biotin binding sites) with 3.88 M HCOONa in a total reaction volume of 200 µL. Reactions were carried out with acetate, citric acid, MES and MOPS (2 M).

The catalysis experiments carried out with MOPS as a buffer provided the best results regarding conversion and enantioselectivity: (*S*)-salsolidine was produced quantitatively in 55% *ee* with **17'** ⊂ S112H while **17'** ⊂ K121H quantitatively yielded the (*R*)-enantiomer in 72% *ee* (see Table 7, entries 7 and 15). The results suggested that MOPS played an important role in determining the enantioselectivity. Recently, Chan *et al.* reported the participation of the sulfonic group of TfO^- *via* a possible 10-membered transition state during the enantioselective hydrogenation of quinolines.[171] In a similar fashion, the sulfonic group of MOPS could be involved in the transition state of the proton transfer to the amine of salsolidine: MOPS could provide the proton to the amine and form the iminium intermediate prior to transfer hydrogenation (see the mechanism proposed by Wills on Figure 7c).[84]

In order to further study the influence of MOPS, catalysis experiments with varying concentrations of buffer were run at pH 5.0. For that purpose, the concentration of formate was kept constant while MOPS concentration was varied from 0.36 M to 2.9 M (see Figure 41).

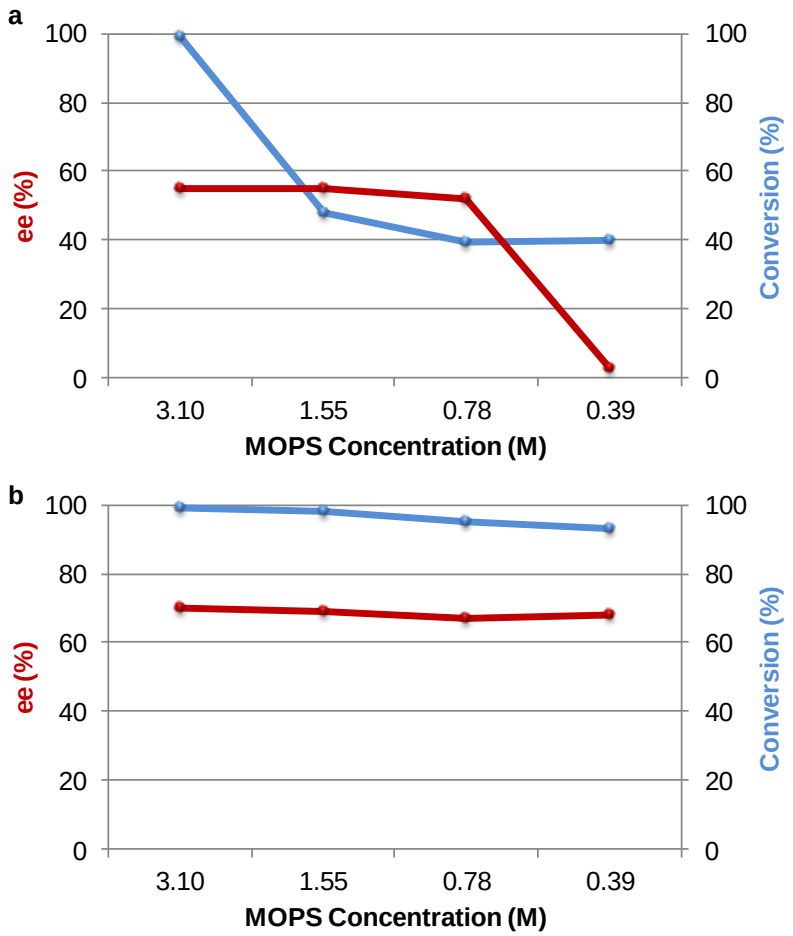

Figure 41 Influence of MOPS-concentration at pH 5.0 on *ee* and conversion using hybrid catalysts a) **17'** ⊂ S112H and b) **17'** ⊂ K121H. For experimental details, see experimental part on Table 7.

The variation in buffer concentration experiments demonstrated that MOPS has a greater influence on hybrid catalyst **17'** ⊂ S112H than on metalloenzyme **17'** ⊂ K121H. The hybrid catalyst **17'** ⊂ S112H displayed a dramatic decrease in activity and selectivity at MOPS concentrations lower than 1.55 M and 0.78 M respectively (see Figure 41a). In contrast the metalloenzyme **17'** ⊂ K121H exhibited high activity and constant enantioselectivity in all reactions performed (see Figure 41b). In order to avoid any deleterious influence of MOPS during catalysis experiments, reactions were carried out with a concentrated MOPS solution (3.10 M).

3.3.2.2.1.3. Temperature Optimization

The influence of temperature on catalytic performance of the artificial metalloenzymes was tested. Reactions were carried out at different temperatures (5°C, 25°C, 37°C and 55°C) for a period of 12 h using the previously optimized catalytic conditions (see Table 8).

Table 8 Temperature optimization using hybrid catalysts **17'** ⊂ S112H and **17'** ⊂ K121H.[a]

Entry	Complexes	Temperature (°C)	Protein	Conversion (%)	*ee* (%)
1	**17'**	5	S112H	5	45 (*S*)
2	**17'**	25	S112H	85	52 (*S*)
3	**17'**	37	S112H	90	53 (*S*)
4	**17'**	55	S112H	quant.	55 (*S*)
5	**17'**	5	K121H	5	50 (*R*)
6	**17'**	25	K121H	25	50 (*R*)
7	**17'**	37	K121H	50	48 (*R*)
8	**17'**	55	K121H	quant.	67 (*R*)

[a] Reactions were carried out for 12 h at pH 5.0 using 2 mol% complex *vs.* substrate (680 µM final metal concentration, 34 mM substrate) and 0.66 mol % tetrameric Sav (corresponding to 916 µM biotin binding sites) with 3.88 M HCOONa and 3.1 M MOPS in a total reaction volume of 200 µL.

Temperature is known to play a major role in the reaction outcome and particularly in the enantioselectivity. Previous work in the Ward group confirmed that selectivity could be increased in imine reduction by lowering the temperature from 55°C to 5°C.[160] Unexpectedly, a drop in *ee* was observed at lower temperatures, accompanied by a decrease in catalytic capacity (see Table 8, entries 1 and 5). These unexpected results suggested that there is a pre-equilibrium between the substrate and the catalyst (second coordination sphere provided by the protein), also called "Curtin-Hammet conditions". In our case decreasing the temperature would mean that the equilibrium will be pushed further

towards the less stable diastereomer which reacts faster with the hydridic metal. After 12 hours, both metalloenzymes **17'** ⊂ S112H and **17'** ⊂ K121H displayed the best results for reactions carried out at 55°C (see Table 8, entries 4 and 8). Consequently, 55°C was selected in subsequent investigations.

3.3.2.2.1.4. Metal/Active Site Ratio Investigations

Previous investigations demonstrated that histidine was able to activate the catalyst presumably *via* dative anchoring of the biotinylated complex. In order to confirm this trend, increasing amounts of biotinylated catalyst **17'** were added to the host protein (see Figure 42).

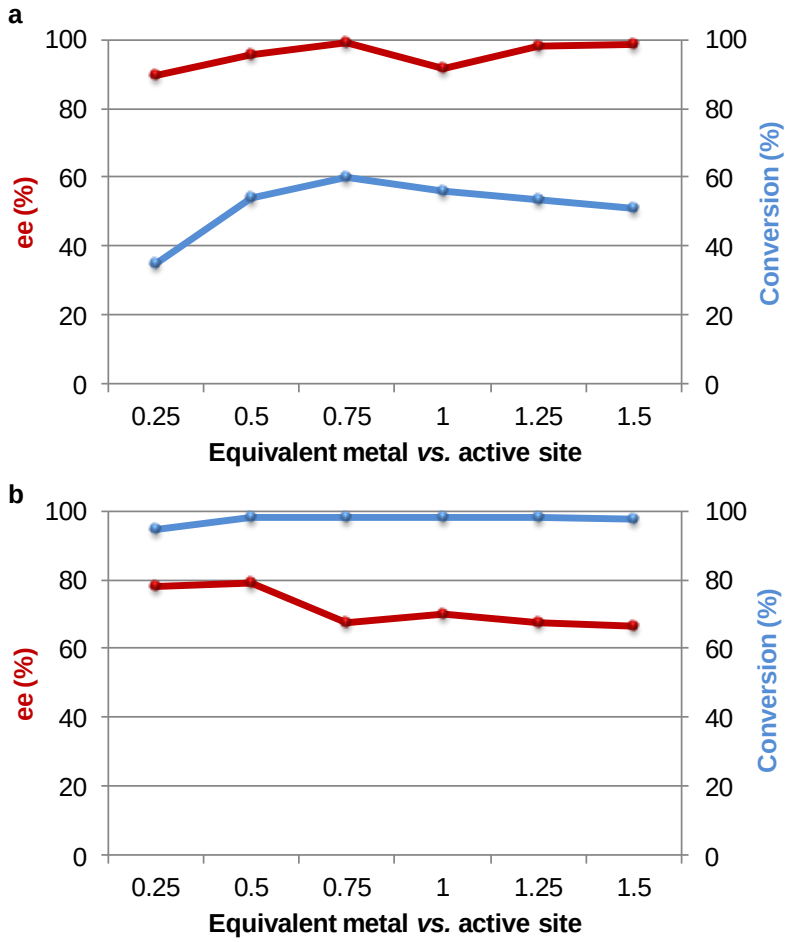

Figure 42 Metal/active site ratio using hybrid catalysts a) **17'** ⊂ S112H and b) **17'** ⊂ K121H. For experimental details see experimental part on Table 8.

The best metal/active site ratio for the hybrid catalyst **17'** ⊂ S112H was observed at 0.75: quantitative production of (*S*)-salsolidine with 60% *ee*. On the other hand, the metalloenzyme **17'** ⊂ K121H exhibited the highest conversions and enantioselectivities when the metal/active site ratio was at 0.50 equivalent: full conversion and 79% *ee* in favor of the (*R*)-enantiomer were obtained. Previous work conducted in the Ward group concerning metal/active site ratios demonstrated that an excess of metal *vs.* biotin binding site led to a decrease in enantioselectivity.[160] Interestingly, the experiments performed with the new artificial metalloenzymes did not exhibit such a trend. The fact that the rhodium dimer **17** displayed remarkably low activity in ATH of imine (see Table 6, entry 1) may account for this result. This study reinforced the hypothesis that the catalyst is activated by the protein (dative anchoring with histidine residues) to successfully perform imine reduction. The same trend was observed by Roelfes *et al.* in the DNA-based catalytic enantioselective Michael addition and Friedel-Crafts alkylation reaction.[172]

These results augur well for the implementation of direct evolution protocols with artificial metalloenzymes. Indeed, the phenomenon of protein accelerated catalysis highlighted herein may allow a more straightforward screening, as the amount of protein will not have to be determined precisely.

3.3.2.2.1.5. Loading Optimization

In order to study the catalyst performance of both metalloenzymes **17'** ⊂ S112H and **17'** ⊂ K121H, loading of the metal complex was varied by keeping the concentration of salsolidine precursor constant. Reactions were carried out with the best metal/active site ratios of each protein (see Table 9).

Table 9 Loading optimization using hybrid catalysts **17'** ⊂ S112H and **17'** ⊂ K121H keeping the substrate concentration constant[a]

Entry	Complexes	Loading (%)	Complex concentration (mM)	Protein	Conversion (%)	*ee* (%)
1	**17'**	1	0.68	S112H	quant.	59 (*S*)
2	**17'**	0.1	0.068	S112H	17	56 (*S*)
3	**17'**	0.01	0.0068	S112H	2	42 (*S*)
4	**17'**	1	0.458	K121H	quant.	79 (*R*)
5	**17'**	0.1	0.0458	K121H	24	77 (*R*)
6	**17'**	0.01	0.00458	K121H	4	56 (*R*)

[a] Reactions were carried out at 55°C for 12 h at pH 5.0 using a fixed salsolidine precursor concentration (68 mM with **17'** ⊂ S112H and 45.8 mM with **17'** ⊂ K121H) with MOPS buffer (3.1 M) containing 3.88 M HCOONa in a total reaction volume of 200 µL.

The study allowed to determine the TON and TOF of artificial metalloenzymes. The hybrid catalyst **17'** ⊂ S112H yielded (*S*)-enantiomer with up to 170 TONs and 56% *ee* while the metalloenzyme **17'** ⊂ K121H provided the (*R*)-enantiomer with up to 240 TONs and 77% *ee*. However, low TOFs were observed: the catalyst **17'** ⊂ K121H exhibited TOFs of 20 h^{-1} and the metalloenzyme **17'** ⊂ S112H demonstrated TOFs of 14 h^{-1}.

3.4. Conclusion

In summary, a new synthetic platform for fast chemical optimization of biotinylated catalysts was implemented. Embedding of such metal cofactors within streptavidin mutants led to the creation of new active artificial metalloenzymes for the ATH of cyclic imines (production of salsolidine **5**). Furthermore, *in silico* investigations allowed the design of a novel type of metal catalyst/protein assembly in which both supramolecular and dative anchoring are involved. Both (*S*)- and (*R*)-enantiomers could be obtained with the same metal complex

depending on the host protein employed. Indeed, the metalloenzyme consisting of the incorporation of dimer **17** into K121H provided (*R*)-salsolidine with up to 240 TONs and remarkable enantioselectivity (77% *ee*). The complementary metalloenzyme, **17'** ⊂ S112H yielded (*S*)-product with up to 170 TONs, and promising enantioselectivity (56% *ee*). The importance of MOPS in ATH reactions was highlighted (see Table 7 and Figure 41).[171] A crystal structure of hybrid catalysts **17'** ⊂ S112H and **17'** ⊂ K121H would allow to rationalize the catalytic results and to provide clues for further sites of mutations to improve the performance of these artificial metalloenzymes.

4. Non-enzymatic Reductive Amination of α-Keto Acids for the Enantioselective Synthesis of Unprotected α-Amino Acids in Water

4.1. Introduction

The aim of this chapter is to test the two different approaches to create new artificial metalloenzymes in the challenging reductive amination of α-keto acids. Reductive amination has recently emerged as an interesting water compatible process for the straightforward synthesis of unprotected α-amino acids. Indeed, in 2004 Fukuzumi and coworkers reported on the synthesis of α-amino acids catalyzed by bipyridine iridium complexes using NH_4COOH as an amine and hydrogen source (see Scheme 27). This pioneering work forms the basis of this project.[173]

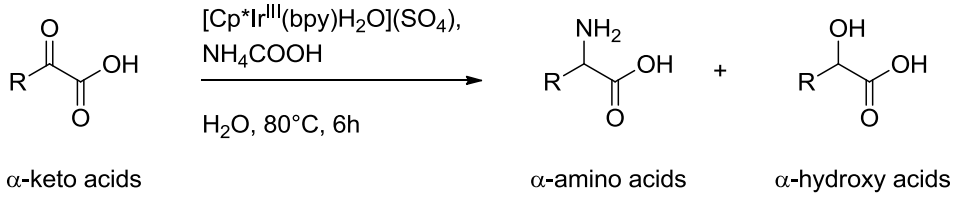

Scheme 27 Reductive amination of α-keto acids for the synthesis of racemic α-amino acids.

The two promising artificial metalloenzymes consisting of i) combination of functionalized piano stool complexes associated with bidentate ligands (see Figure 43a) or ii) hybrid catalysts **17'** ⊂ Sav S112H and **17'** ⊂ Sav K121H (see Figure 43b) were investigated as catalysts for the synthesis of natural (phenylalanine) and unnatural (phenylglycine) α-amino acids.

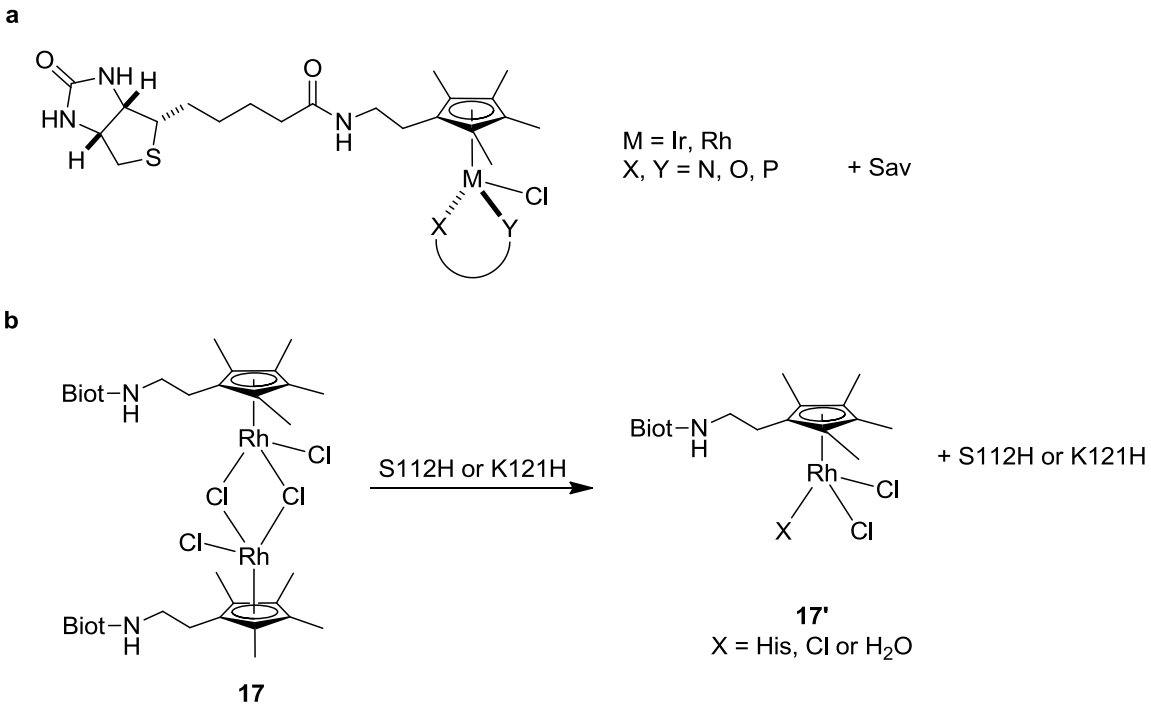

Figure 43 Artificial Metalloenzymes used for the reductive amination of α-keto acids.

4.2. New Artificial Metalloenzymes for the Enantioselective Synthesis of α-Amino Acids in Water

4.2.1. Dually-Anchored Rhodium Complex 17' into Streptavidin for the Production of α-Amino Acids

The metalloenzymes resulting from the incorporation of dimer **17** either into S112H or K121H were investigated as catalysts in reductive amination reaction. For that purpose, the formation of phenylalanine **34** was selected as model (see Scheme 28).

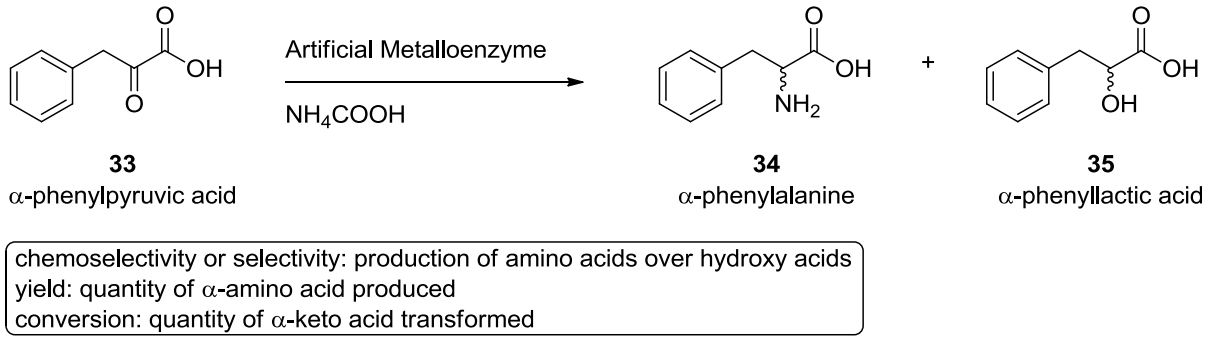

Scheme 28 Enantioselective synthesis of α-phenylalanine **34** *via* reductive amination.

Fukuzumi and coworkers developed acid-stable bipyridyl iridium complexes for the chemoselective preparation of α-AAs and reported that pH had a strong influence on the chemoselectivity of catalyst (see Scheme 27).[173] Therefore, the influence of pH on the metalloenzyme was investigated by performing the catalysis experiments with increasing pH (from 5.0 to 9.0). In this initial study, only chemoselectivity was investigated (see Figure 44).

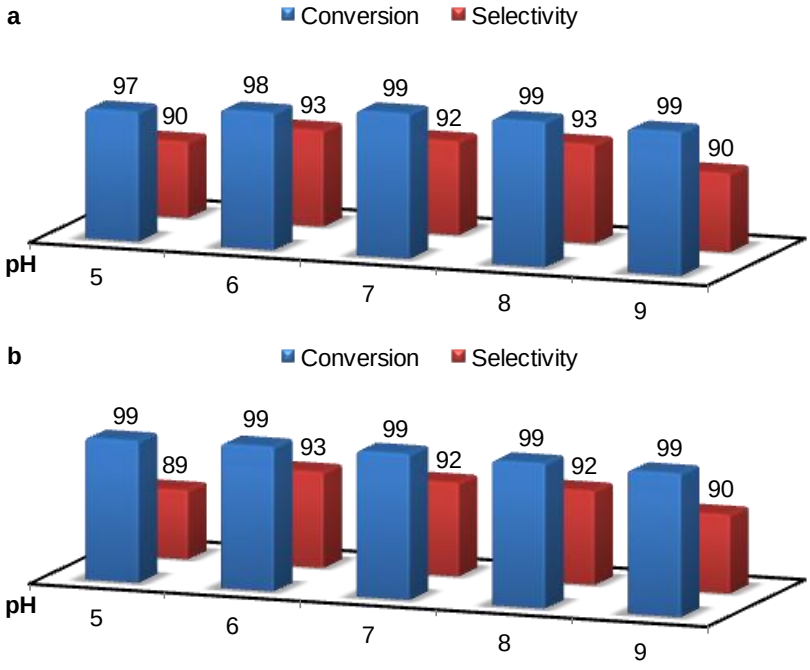

Figure 44 pH-dependent chemoselective formation of phenylalanine **34** with a) **17'** ⊂ S112H and b) **17'** ⊂ K121H. Reactions were carried out at 55°C for 12 h with 1 mol% complex *vs.* substrate: 680 μM final metal concentration and 68 mM substrate with 0.33 mol% tetrameric S112H (corresponding to 916 μM biotin binding sites) or 458 μM final metal concentration 45.8 mM substrate, with 0.50 mol% tetrameric K121H (corresponding to 916 μM biotin binding sites), with 4.90 M NH_4COOH in a total reaction volume of 200 μL.

Both metalloenzymes exhibited high conversion and chemoselectivity for the production of phenylalanine **34**. In contrast to the work reported by Fukuzumi and coworkers,[173] the results highlighted the modest influence of pH on the outcome of the reaction. Encouraged by the catalytic activity demonstrated by artificial metalloenzymes **17'** ⊂ S112H and **17'** ⊂ K121H, the enantioselective reductive amination of phenylpyruvic acid was investigated next.

4.2.2. Catalytic Activity of Artificial Metalloenzymes as Catalyst for the Synthesis of Enantiopure Phenylalanine

4.2.2.1. pH Optimization

The pH dependence of both artificial metalloenzymes **17'** ⊂ S112H and **17'** ⊂ K121H towards the synthesis of phenylalanine **34** was investigated and the results are summarized in Table 10.

Table 10 Influence of pH on the synthesis of phenylalanine **34** with hybrid catalysts **17'** ⊂ S112H and **17'** ⊂ K121H.[a]

Entry	Metalloenzyme	pH	Conversion (%)	Yield (%)	Selectivity (%)	*ee* (%)
1	**17'** ⊂ S112H	5	quant.	84	84	rac.
2	**17'** ⊂ S112H	6	quant.	90	90	rac.
3	**17'** ⊂ S112H	7	quant.	89	89	rac.
4	**17'** ⊂ S112H	8	quant.	87	87	rac.
5	**17'** ⊂ S112H	9	quant.	90	90	rac.
6	**17'** ⊂ K121H	5	quant.	89	89	13 (*S*)
7	**17'** ⊂ K121H	6	quant.	92	92	13 (*S*)
8	**17'** ⊂ K121H	7	quant.	92	92	18 (*S*)
9	**17'** ⊂ K121H	8	quant.	91	91	24 (*S*)
10	**17'** ⊂ K121H	9	quant.	93	93	13 (*S*)

[a] Reactions were carried out at 55°C for 12 h using 1 mol% complex *vs.* substrate: 680 μM final metal concentration, 68 mM substrate and 0.33 mol% tetrameric S112H (corresponding to 916 μM biotin binding sites) or 458 μM final metal concentration, 45.8 mM substrate and 0.50 mol% tetrameric K121H (corresponding to 916 μM biotin binding sites) with 4.90 M NH_4COOH in a total reaction volume of 200 μL.

The results suggest that the pH does not influence either the activity or the selectivity of either **17'** ⊂ S112H or **17'** ⊂ K121H in the reductive amination of phenylpyruvic acid **33**. However, the enantioselectivity of the reductive amination of **33** was found to be pH-dependent: while hybrid catalyst **17'** ⊂ S112H yielded racemic mixtures, the metalloenzyme **17'** ⊂ K121H yielded (*S*)-phenylalanine in modest enantioselectivity. Subsequently, further investigations were conducted with hybrid catalyst **17'** ⊂ K121H.

4.2.2.2. Temperature Optimization

Our previous work demonstrated that temperature had a strong influence on the outcome of the ATH reaction: lowering the temperature lead to a decrease of the enantioselectivity of imine reduction. The results for the reductive amination using hybrid catalyst **17'** ⊂ K121H at different temperatures (5°C, 25°C, 37°C and 55°C) are summarized in Table 11.

Table 11 Temperature optimization with hybrid catalyst **17'** ⊂ K121H.[a]

Entry	Temperature (°C)	Conversion (%)	Yield (%)	Selectivity (%)	*ee* (%)
1	5	5	5	-[b]	32 (*S*)
2	25	7	5	-[b]	21 (*S*)
3	37	10	10	-[b]	18 (*S*)
4	55	quant.	93	93	22 (*S*)

[a] Reactions were carried out at pH 8.0 for 12 h with 1 mol% complex *vs.* substrate (458 μM final metal concentration, 45.8 mM substrate and 0.50 mol% tetrameric K121H (corresponding to 916 μM biotin binding sites) with 4.90 M NH_4COOH in a total reaction volume of 200 μL. [b] Peaks were too small to determine selectivity.

The temperature had a strong influence on the activity of the metalloenzyme **17'** ⊂ K121H: a dramatic decrease in conversion was observed upon lowering the temperature (see Table 11, entry 1). However, the enantioselectivity increased upon lowering the temperature to 5°C

(32% *ee* for (*S*)-Phe, see Table 11, entry 1). Unfortunately, prolonging the reaction time to 96 h did not increase significantly the yield.

4.2.2.3. Catalyst Loading

In order to gain a better insight in the catalytic performance of **17'** ⊂ K121H, loading of the metal complex was varied, keeping the concentration of phenylpyruvic acid **33** constant. The TON of the artificial metalloenzyme was then determined at two different temperatures (5°C see Table 12 and 55°C, see Table 13).

Table 12 Results of loading investigation of the hybrid catalyst **17'** ⊂ K121H at 5°C.[a]

Entry	Loading (%)	Complex concentration (mM)	Conversion (%)	Yield (%)	Selectivity (%)	*ee* (%)
1	2	0.916	28	28	quant.	43 (*S*)
2	1	0.458	8	8	quant.	39 (*S*)
3	0.5	0.229	2	2	-[b]	31 (*S*)
4	0.1	0.0458	<1	<1	-[b]	20 (*S*)

[a] Reactions were carried out at 5°C for 96 h at pH 8.0 using fixed substrate concentration (45.8 mM with 0.50 mol% tetrameric K121H) with 4.90 M NH_4COOH in a total reaction volume of 200 µL. [b] Peaks were too small to determine selectivity.

The study clearly highlighted the modest catalytic performance of the artificial metalloenzyme **17'** ⊂ K121 in the reductive amination of phenylpyruvic acid **33** at 5°C: only 14 turnovers were achieved after 96 h of reaction with a substrate/metal ratio of 50/1 (see Table 12, entry 1).

Table 13 Results of loading investigation of the hybrid catalyst **17'** ⊂ K121H at 55°C.[a]

Entry	Loading (%)	Complex concentration (mM)	Conversion (%)	Yield (%)	Selectivity (%)	*ee* (%)
1	2	0.916	quant.	90	90	24 (*S*)
2	1	0.458	quant.	92	92	19 (*S*)
3	0.5	0.229	24	24	-[b]	rac.
4	0.1	0.0458	17	17	-[b]	rac.

[a] Reactions were carried out at pH 8.0 for 12 h using fixed substrate concentration (45.8 mM with 0.50 mol% tetrameric K121H) with 4.90 M NH_4COOH in a total reaction volume of 200 µL. [b] Peaks were too small to determine selectivity.

The study demonstrated the promising activity for the production of phenylalanine **34** with the artificial metalloenzyme **17'** ⊂ K121 at 55°C: the (*S*)-enantiomer was obtained with up to 45 TONs and 24% *ee*.

4.2.2.4. Genetic Optimization

With the aim of gaining structural insight into the artificial transfer hydrogenases, *in silico* investigations were carried out by Maurus Schmid. Guided by previous docking experiments (see Chapter 3) and based on the work of Reetz *et al.* on directed evolution of enantioselective hybrid catalysts,[174] position 110 was selected for a second round of genetic optimization. Indeed, qualitative inspection of the docked complex **17'** inside K121H suggested that position 110 was close-lying to the metal center (see Figure 45). Subsequently, the double mutants, K121H-L110X were selected for production. The proteins were produced with the "small-scale purification" method (SSP, work carried out by Elisa Nogueira). The catalysis experiments performed with double mutants involving K121H-L110X are summarized in Table 14. The double mutant K121H-S112H was also tested.

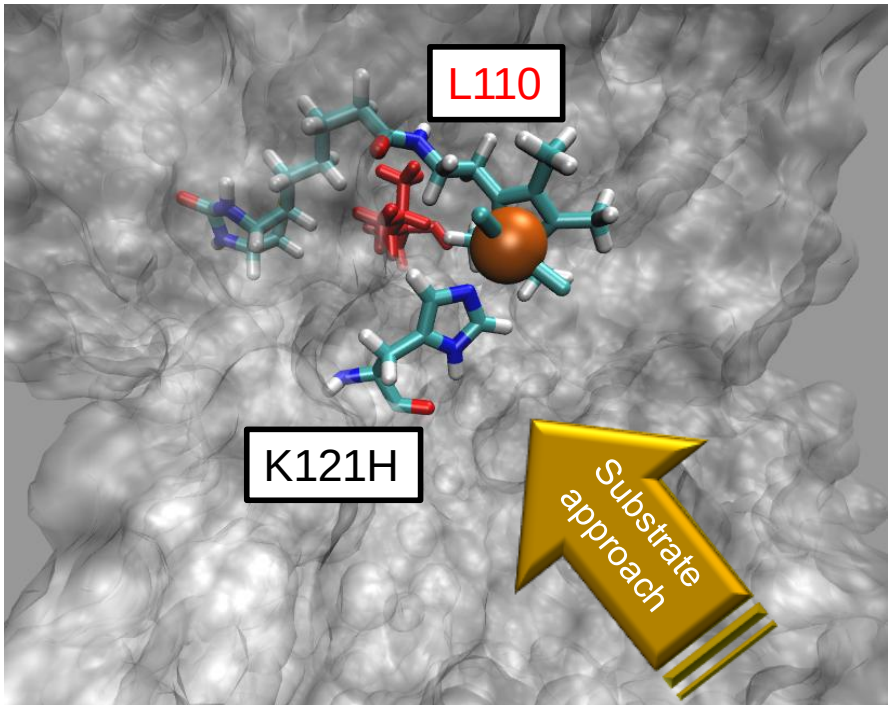

Figure 45 Model of the biotinylated rhodium catalyst **17'** embedded into K121H host protein. Residue 110 is highlighted in red.

Table 14 Results for the preparation of phenylalanine **34** using hybrid catalysts **17'** ⊂ K121H-L110X.[a], [b]

Entry	Protein[d]	Protein concentration (μM)	Conversion (%)	Yield (%)	Selectivity (%)	*ee* (%)
1	K121H-L110A	110	86	73	85	rac.
2	K121H-L110E	180	83	68	82	rac.
3	K121H-L110K	215	84	68	81	rac.
4	K121H-L110D	50	60	44	74	rac.
5	K121H-L110C	90	91	82	90	25 (*S*)
6	K121H-S112H	105	quant.	82	82	rac.

[a] Reactions were carried out at 55°C for 12 h at pH 8.0 with 2 mol% complex *vs.* substrate (1 mol% tetrameric Sav isoforms) with 4.90 M NH_4COOH in a total reaction volume of 200 μL. [d] Proteins obtained from the SSP protocol.

The catalysis experiments carried out with the different double mutants yielded modest to good conversions and only the hybrid catalyst **17'** ⊂ K121H-L110C yielded (*S*)-phenylalanine with 25% *ee* (see Table 14, entry 5). Interestingly, the metalloenzyme **17'** ⊂ K121H-S112H yielded racemic phenylananie **34** (see Table 14, entry 6). This result could be explained by the possible coordination of the metal by the two histidine residues.

This screening effort led to the identification of a new active artificial metalloenzyme: **17'** ⊂ K121H-L110C. Subsequently, production and isolation of pure protein, K121H-L110C was performed by Elisa Nogueira. With large amounts of this double mutant, catalysis experiments were performed at two different temperatures (5°C and 55°C, see Table 15).

Table 15 Comparison of hybrid catalysts bearing single and double mutants.[a], [c]

Entry	Protein	Temperature (°C)	Conversion (%)	Yield (%)	Selectivity (%)	*ee* (%)
1	K121H-L110C[d]	55[e]	91	82	90	25 (*S*)
2	K121H-L110C	55[e]	quant.	97	97	24 (*S*)
3	K121H	55[e]	quant.	90	90	24 (*S*)
4	K121H-L110C	5[f]	74	74	quant.	30 (*S*)
5	K121H	5[f]	28	28	quant.	43 (*S*)

[a] Reactions were carried out at pH 8 with 2 mol% complex (458 μM final metal concentration, 1 mol% tetrameric Sav isoforms), with 4.90 M NH_4COOH in a total reaction volume of 200 μL. [d] Proteins obtained from the SSP protocol. [e] Reactions were carried out for 12 h. [f] Reactions were carried out for 96h.

The catalysis experiments using the pure protein K121H-L110C demonstrated that the metalloenzyme **17'** ⊂ K121H-L110C was able to nearly quantitatively produce (*S*)-Phe in 24% *ee* at 55°C (see Table 15, entry 2). The latter result confirmed the trend observed with K121H-L110C produced with the SSP method (see Table 15, entry 1), thus supporting the reliability of the method. Moreover, increased activity was observed with **17'** ⊂ K121H-L110C

when compared to **17'** ⊂ K121H (see Table 15, entries 2, 3, 4 and 5). However, **17'** ⊂ K121H displayed better enantioselectivity at 5°C than the double mutant (see Table 15, entries 4 and 5). Although the selectivity of the double mutant was slightly lower than that of single mutant, its activity at 5°C was markedly higher, thus highlighting the importance of both first and second coordination sphere contacts in determining both the activity and the selectivity of artificial metalloenzymes.

4.2.2.5. Towards the Enantioselective Synthesis of Unnatural Amino Acid (uAA) Catalyzed by 17' ⊂ K121H

The metalloenzyme **17'** ⊂ K121H was investigated for its capacity to perform reductive amination of benzoylformic acid **36** to yield phenylglycine **37** (PhGly, see Scheme 29). This unnatural amino acid was selected because it represents an important component in marketed drugs.[175]

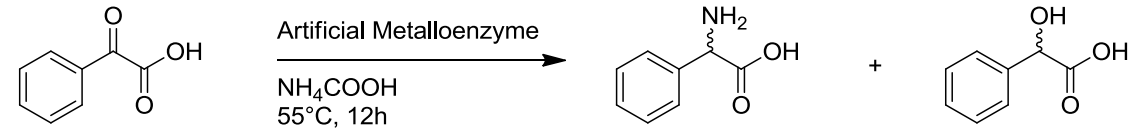

36 benzoylformic acid

37 α-phenylglycine

38 α-mandelic acid

Scheme 29 Reductive amination of benzoylformic acid **36**.

The hybrid catalyst **17'** ⊂ K121H displayed low activity for the preparation of phenylglycine **37** at 55°C (2% loading, 19% yield). However, interesting enantioselectivity was observed: the phenylglycine was formed with 25% *ee* in favor of the (*R*)-enantiomer. This result highlighted the versatility of catalyst **17'** ⊂ K121H to transform different α-keto acid into non-natural amino acids.

4.2.3. Incorporation of Biotinylated Bidentate Catalysts into Streptavidin for the Enantioselective Synthesis of α-Amino Acids

4.2.3.1. Ethylenediamine Rhodium and Iridium Catalysts

With the aim of creating novel active and enantioselective metalloenzymes in reductive amination, the incorporation of biotinylated catalyst bearing bidentate ligands into a Sav host protein was investigated. The catalysis experiments were carried out with *in situ* prepared rhodium **31** and iridium **32** complexes (see Figure 46) for the synthesis of phenylglycine. The resulting piano stool complexes were combined with Sav mutants (WT Sav, P64G-L124V, V47G, S112A) that were selected based on previous work in the Ward group (see Table 16).[160, 169, 176]

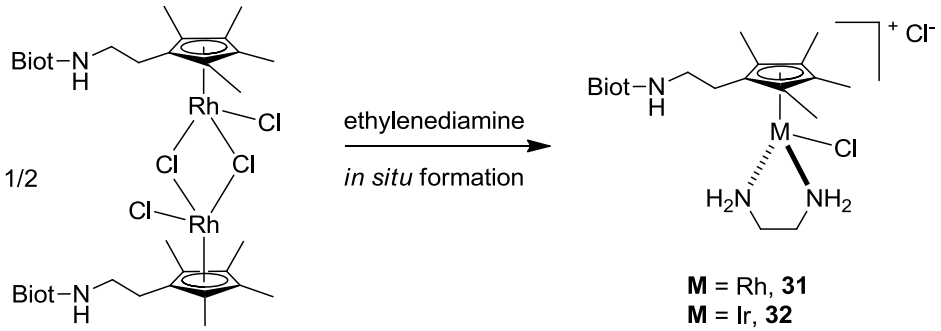

M = Rh, **17**
M = Ir, **18**

M = Rh, **31**
M = Ir, **32**

Figure 46 *In situ* prepared Rh and Ir biotinylated catalysts bearing ethylenediamine ligand **31** and **32**.

Table 16 Results for the synthesis of phenylglycine **37** using hybrid catalyst involving *in situ* prepared rhodium **31** and iridium **32** complexes [a]

Entry	Complex	Protein	Conversion (%)	Yield (%)	Selectivity (%)	*ee* (%)
1	**31**	no	56	13	24	rac.
2	**31**	WT Sav	8	1	14	rac.
3	**31**	S112A	13	3	27	rac.
4	**31**	V47G	5	5	-[b]	rac.
5	**31**	P64G-L124V	quant.	24	24	26 (*S*)
6	**32**	no	16	7	43	rac.
7	**32**	WT Sav	6	2	34	rac.
8	**32**	S112A	3	3	-[b]	rac.
9	**32**	V47G	12	12	-[b]	rac.
10	**32**	P64G-L124V	76	27	35	29 (*S*)

[a] Reactions were carried out at 55°C for 12 h at pH 8.0 with 2 mol% complex *vs.* substrate: 458 µM final metal concentration, 22.9 mM substrate and 1 mol% tetrameric Sav (corresponding to 916 µM biotin binding sites), with 4.90 M NH_4COOH in a total reaction volume of 200 µL. [b] Peaks were too small to determine selectivity.

The screening of four Sav isoforms lead to the identification of P64G-L124V as a potential host protein for both ethylenediamine rhodium complex **31** (24% yield and 26% *ee* for the (*S*)-enantiomer) and iridium complex **32** (27% yield and 29% *ee* for the (*S*)-enantiomer).

4.2.3.2. Chemical Optimization

Encouraged by the results obtained with both metalloenzymes **31** ⊂ P64G-L124V and **32** ⊂ P64G-L124V, different bidentate ligands (depicted in Figure 47) were screened. The results are summarized in Table 17.

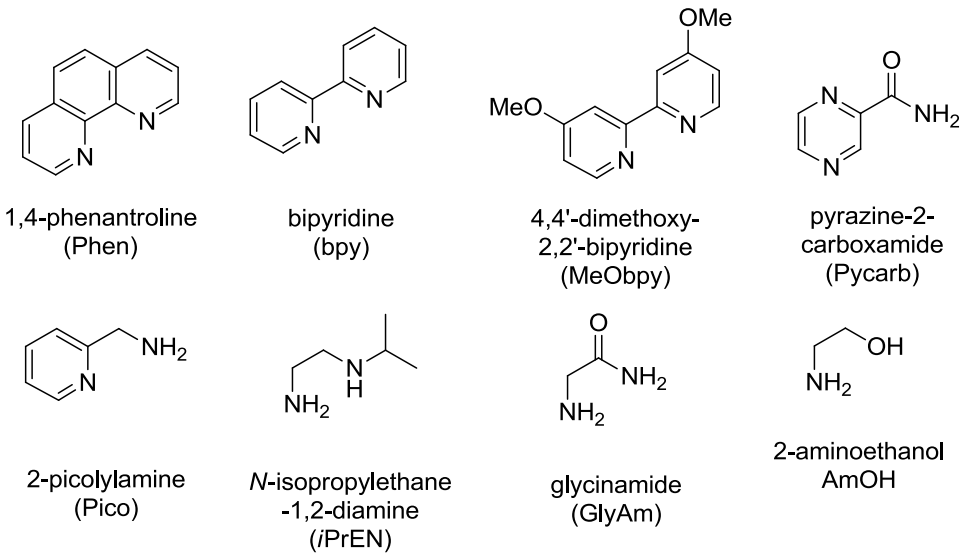

Figure 47 Bidentate ligands selected for the chemical optimization.

Table 17 Screening of bidentate ligands with **17** and **18** for the synthesis of phenylglycine **37** in the presence of P64G-L124V.[a]

Entry	Complex	Ligand	Conversion (%)	Yield (%)	Selectivity (%)	*ee* (%)
1	**17**	Phen	4	4	quant.	16 (*S*)
2	**17**	Bpy	3	3	quant.	9 (*S*)
3	**17**	MeObpy	10	1	10	rac.
4	**17**	Pycarb	25	9	38	rac.
5	**17**	Pico	quant.	17	17	16 (*S*)
6	**17**	*i*PrEN	60	11	19	rac.
7	**17**	GlyAm	quant.	16	16	rac.
8	**17**	AmOH	quant.	17	17	10 (*S*)
9	**18**	Phen	3	<1	31	6 (*S*)
10	**18**	Bpy	5	1	24	10 (*S*)
11	**18**	MeObpy	10	5	50	rac.
12	**18**	Pycarb	25	9	38	rac.
13	**18**	Pico	quant.	7	7	15 (*S*)

14	**18**	*i*PrEN	2	<1	11	7 (*S*)
15	**18**	GlyAm	54	6	10	rac.
16	**18**	AmOH	37	3	7	rac

[a] Reactions were carried out at 55°C for 12 h at pH 8.0 with 2 mol% complex: 458 µM final metal concentration, 22.9 mM substrate and 1 mol% tetrameric Sav (corresponding to 916 µM biotin binding sites), with 4.90 M NH_4COOH in a total reaction volume of 200 µL.

The results highlighted the poor performance of the artificial metalloenzymes towards the synthesis of phenylglycine **37**. The best enantioselectivity was observed for catalysis experiments carried out with hybrid catalysts combining Phen-**17**, Pico-**17** and Pico-**18** (see Table 17, entries 1, 5 and 13). The rhodium complex **17** bearing the picolylamine ligand was found to be the only bidentate complex capable of both quantitatively transforming benzoylformic acid **36** and providing interesting enantioselectivity (see Table 17, entries 5). However, very low yield for the desired α-uAA was observed. Indeed, the major product obtained was the corresponding α-hydroxy acid (mandelic acid **38**), suggesting that the ketone reduction is favored over the reductive amination for this substrate (see Scheme 30).

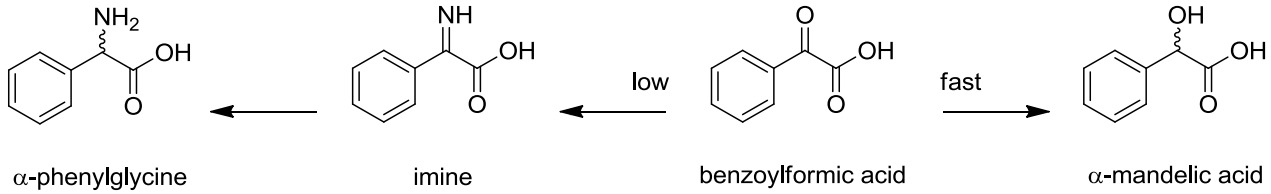

Scheme 30 Ketone reduction faster than imine reduction for the reductive amination of benzoylformic acid **36**.

The results highlighted the importance of the first coordination sphere: only the smallest ligand ethylenediamine was able to provide interesting yield and *ee.* This focused chemical screening of ligand did not allow identification of an additional catalyst for the reductive amination reaction.

4.2.3.3. Genetic Optimization

In order to improve the *ee* and the conversion in reductive amination of benzoylformic acid **36**, genetic optimization was performed using the rhodium complex bearing an additional bidentate ligand **31**. To confirm that both mutations in P64G-L124V were important, catalysis experiments using single mutants P64G and L124V Sav were performed. In addition, single mutants bearing neutral alkyl side chain such as L124G, L124A and L124F were also investigated (see Table 18).

Table 18 Influence of neutral alkyl side chain at position P64 and L124 for the synthesis of phenylglycine **37** using complex **31**.[a]

Entry	Complex	Protein	Conversion (%)	Yield (%)	Selectivity (%)	*ee* (%)
1	**31**	P64G-L124V	quant.	24	24	26 (*S*)
2	**31**	P64G	quant.	25	25	rac.
3	**31**	L124V	quant.	6	6	34 (*S*)
4	**31**	L124G	59	9	16	8 (*S*)
5	**31**	L124A	quant.	15	15	8 (*S*)
6	**31**	L124F	quant.	17	17	21 (*S*)

[a] Reactions were carried out at 55°C for 12 h at pH 8.0 with 2 mol% complex *vs.* substrate: 458 μM final metal concentration, 22.9 mM substrate and 1 mol% tetrameric P64G-124V (corresponding to 916 μM biotin binding sites), with 4.90 M NH_4COOH in a total reaction volume of 200 μL.

This focused genetic screening highlighted that mutation at position P64G was not important for the enantioselection (see Table 18, entry 2). We conclude that in the double-mutant P64G-L124V, only the mutation L124V plays a key role in enantioselection (34% *ee* in favor of the (*S*)-enantiomer, see Table 18, entry 3). However, the double mutant P64G-L124V leads to better activity and selectivity than the single mutant L124V. It appears that small

variations at position 124 play a determinant role in enantioselectivity, thus suggesting the close contact between the catalyst and this side chain.

4.2.3.4. Temperature Optimization

The metalloenzyme **31** ⊂ L124V was identified as the best catalyst in terms of enantioselectivity. In order to test the previously observed trend concerning the temperature, the reductive amination with **31** ⊂ L124V was investigated at different temperatures (5°C, 25°C, 37°C and 55°C, see Table 19).

Table 19 Temperature optimization using **31** ⊂ L124V for the enantioselective production of phenylglycine **37**.[a]

Entry	Complex	Temp. (°C)	Conversion (%)	Yield (%)	Selectivity (%)	*ee* (%)
1	**31**	5	30	4	12	73 (*S*)
2	**31**	25	50	8	15	56 (*S*)
3	**31**	37	quant.	15	15	50 (*S*)
4	**31**	55	quant.	6	6	34 (*S*)

[a] Reactions were carried out for 12 h at pH 8.0 with 2 mol% complex *vs.* substrate: 458 μM final metal concentration, 22.9 mM substrate and 1 mol% tetrameric 124V (corresponding to 916 μM biotin binding sites), with 4.90 M NH_4COOH in a total reaction volume of 200 μL.

As expected, lowering the temperature lead to an increase in enantioselectivity for the metalloenzyme consisting of **31** ⊂ L124V (up to 73% *ee* in favor of the (*S*)-enantiomer). Unfortunately, both the yield and the selectivity were very low (see Table 19, entry 1).

4.3. Conclusion

In summary, we reported the first non-enzymatic enantioselective reductive amination for the preparation of unprotected natural (phenylalanine, **34**) and non-natural (phenylglycine, **37**) α-amino acids by two different artificial metalloenzymes.

We demonstrated the capacity of the metalloenzyme **17'** ⊂ K121H to catalyze the reductive amination of phenylpyruvic acid **33** in water to afford (*S*)-phenylalanine (24% *ee*) with promising activity (TON = 45 at 55°C). The studies also highlighted an unexpected result: compared to the ATH reaction, hybrid catalyst **17'** ⊂ S112H afforded racemic material in the reductive amination. We speculate that the ammonium group of the close-lying lysine in position 121 may interact differently depending on the substrate (salsolidine precursor or phenylpyruvic acid **33**):

Furthermore, we confirmed that low temperatures leads to increase enantioselectivity: up to 43% *ee* was obtained with the hybrid catalyst **17'** ⊂ K121H for the reductive amination of phenylpyruvic acid **33**. However, the metalloenzyme suffers from low TONs (14 at 5°C *vs.* 45 at 55°C)

In order to increase the yield and the *ee*, genetic optimization was investigated using a small-scale purification process, "SSP". This strategy allowed the identification of K121H-L110C as attractive double mutant (TON = 49). The combination of the rhodium dimer **17** with pure K121H-L110C exhibited increased activity even at 5°C (TON = 37) when compared to the single-mutated metalloenzyme, **17'** ⊂ K121H (TON = 14). These results confirmed the validity of the mutant production strategy as genetic screening combined with qualitative *in silico* investigations. Although precise information about the enantioselection mechanism is difficult to achieve with such method (which is also the case with X-ray structure), *in silico* studies have been found to be a useful tool in guiding the design of artificial metalloenzymes.

We also identified additional metal complex/protein assemblies that were competent in the synthesis of the unnatural α-amino acid, phenylglycine **37**. Indeed, rhodium piano stool complexes bearing an ethylenediamine ligand displayed promising properties with Sav

mutants P64G-L124V, L124V and L124F: up to 73% *ee* for (*S*)-PhGly. Future efforts towards improving the yield and the selectivity are underway in the group.

.

5. General Conclusion and Outlook

5.1. General Conclusion

The biotin-streptavidin technology has proven to be a remarkable tool for the design of effective artificial metalloenzymes. Two main properties contributing to the usefulness of the technology are: i) the exceptional strength and precision of the supramolecular anchoring and ii) the possibilities offered through chemical derivatization of the biotinylated cofactor with metal-complexes. These properties allow the resulting artificial metalloproteins to catalyze diverse processes (oxidation and reduction reactions). Furthermore, large organometallic guests can be effectively combined with a macromolecular host in order to also achieve unexplored processes (at least with metalloproteins) such as drug delivery. In addition, the nature of the host can also be fine-tuned by genetic modification, providing a very powerful chemo-genetic approach for optimization of catalytic or binding properties of the assembly.

In the first chapter, we demonstrated that the combination of a metallodrug (i.e. biotinylated ruthenium piano stool) with a presenter protein (i.e. streptavidin) provided a supramolecular assembly able to modulate the affinity and selectivity towards DNA telomers *in vitro*. The recognition profile through the provision of additional non-covalent interactions was effective even in the presence of competing targets (such as glutathione and dsDNA).

As concerns supramolecular assemblies with catalytic activity, as described in the second part of this thesis, in most cases the artificial metalloenzymes display low activity (few turnovers, see Table 20). In general, one challenge remains to develop highly active catalysts for specific embedding into host biomolecules. We addressed this challenge by implementing an effective synthetic platform for a straightforward chemical optimization of biotinylated complexes (see Table 20, blue row).

Table 20 Comparison of metalloenzymes in reduction reactions.

Catalyzed reaction	Anchoring	Macromolecule	Complex or ligand	*ee* (%)	TON	Group
Transfer Hydrogenation	Supramolecular	Sav P64G-L124V	[η^6-(*p*-cymene)Ru(Biot-*p*-L)Cl]	98 (*R*)	100	Ward[169]
		Sav S112A	[Cp*Ir(Biot-*p*-L)Cl]	96 (*R*)	4000	Ward[160]
	Dative and Supramolecular	Sav K121H	[(η^5-Me$_4$Cp(CH$_2$)$_2$-*N*-Biot)RhCl$_2$]$_2$	77 (*R*)	240	this thesis
Hydrogenation	Supramolecular	Sav S112W	[Rh(Biot-(*R*)-Pro-amino-diphosphine)(COD)]BF$_4$	95 (*S*)	100	Ward[177]
		Sav N49V	[Rh(Biot-amino-diphosphine)(COD)]BF$_4$	65 (*R*)	500	Reetz[178]
		Avidin	[Rh(Biot-amino-diphosphine)(NBD)]Tf	41 (*S*)	>500	Whitesides[179]
			[Rh-(*S*,*S*)-pyrphos (COD)]BF$_4$	48 (*R*)	32	Chan[180]
		Antibody 1G8	[Rh(aminodiphosphine) (COD)]ClO$_4$	98 (*S*)	854	Yamaguchi[181]
	Dative	Carbonic anhydrase	[Rh(COD)$_2$]BF$_4$	20:1[a]	100	Kazlauskas[115a]
	Covalent	Papain	[Rh(COD)$_2$]BF$_4$	-	400	de Vries[182]
				-	800	de Vries[183]
		Photoactive Yellow Protein	[Rh(COD)(MeCN)$_2$]BF$_4$	n.d.	n.d.	Kamer[184]

[a] Selectivity for *cis*-stilbene over *trans*-stilbene

In this thesis a d^6-piano stool rhodium and iridium complexes with a tethered-Cp* directly attached to biotin for incorporation into streptavidin were designed. Combination of a chemically optimized cofactor (by varying the linker, the metal and/or its ligand for example) with fine-tuning of the second coordination sphere (designed evolution and directed evolution approaches) allowed us to identify a new generation of active biocatalysts, summarized as follows:

i) Incorporation of biotinylated d^6-piano stool (rhodium and iridium) complexes bearing bidentate ligands into L124 Sav mutants displayed promising activity in ATH. Particularly interesting was the hybrid catalyst consisting of L124V and rhodium-piano stool complexes bearing an ethylenediamine ligand, which was competent in the non-enzymatic

enantioselective synthesis of unprotected non-natural α-amino acids, with up to 73% *ee* for the (*S*)-enantiomer of phenylglycine.

ii) Rational ligand design with genetic optimization of the biomolecular host allowed the design of the first active metalloenzyme based on the biotin-streptavidin technology using a dual anchoring strategy, with both supramolecular and dative anchoring. Both (*S*)- and (*R*)-enantiomers could be obtained with the same metal complex depending on the host protein employed: incorporation of biotinylated piano stool rhodium complex **17** into K121H provided (*R*)-salsolidine with up to 240 TONs and remarkable enantioselectivity (77% *ee*); the complementary metalloenzyme, **17'** ⊂ S112H yielded (*S*)-product with up to 170 TONs, and promising enantioselectivity (60% *ee*). We also demonstrated the capacity of metalloenzyme **17'** ⊂ K121H to catalyze the reductive amination of phenylpyruvic acid in water to afford (*S*)-phenylalanine (24% *ee*) with promising activity (TON = 45 at 55°C). This is the first example of enantioselective synthesis of unprotected α-amino acids in water.

In conclusion, the facile chemical optimization of these catalysts potentially allows to elaborate highly active and selective hybrid catalysts for a given reaction.

5.2. Outlook

5.2.1. Optimization of a Drug Delivery System

In the present form, such assemblies cannot be delivered easily into cells, thus hampering *in vivo* studies. To overcome this challenge, current alternative strategies include the following:

i) Appending cell penetrating peptide (CPP) sequences to the presenter protein. CPPs allow cell-impermeable compounds to reach intracellular targets. Recent advances in the field have demonstrated that some CPPs can exhibit cell specificity.[185]

ii) Exploiting endogenous host proteins overexpressed in cancer cells as presenter proteins, such as lysozyme or carbonic anhydrase[186]. The latter would thus only require cell penetration of the metallo-prodrug.

5.2.2. Use of Artificial Metalloenzymes in Challenging Reactions

Enantioselective transfer hydrogenation reactions (keto and imine reduction) have been effectively implemented in organic media. However, reactions involving hydride transfers remain challenging and enantioselective reductive amination of ketones and keto acids in aqueous media remain underdeveloped: Thus, the novel artificial enzymes described in this thesis have great potential in developing interesting enantioselective reductive amination reactions, for example for future effective synthesis of high-value enantiopure compounds including:

i) Optically active amines yielded by enantioselective reduction of imines (see Figure 48). The asymmetric hydrogenation of acyclic imines in which R^2 is distinct from methyl or both groups are alkyl is particularly challenging.[76c] There is an increasing demand for catalysts providing high enantioselectivities in the reduction of dialkyl imines or phenyl substituted quinolines. Moreover, in the hydrogenation of cyclic imines such as quinolines, isoquinolines, and quinoxalines the nature of the substituent R^4 influences the efficiency of the reduction reaction. For example, when R^4 is a bulky substituent such as aryl, the enantioselectivity dropped significantly.

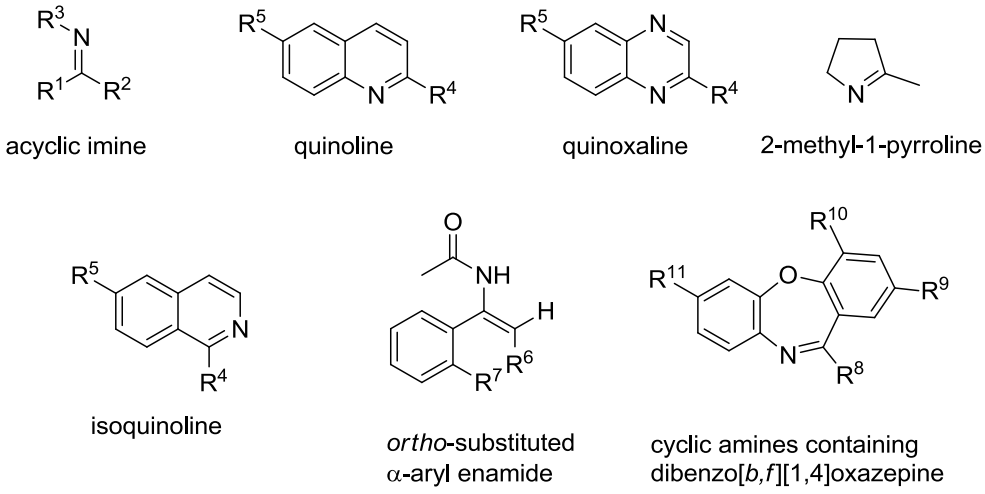

Figure 48 Interesting imine and enamide substrates for the ATH

An additional interesting scaffold is the enamide class: the *ortho*-substituted enamides are particularly difficult to reduce.[76d] This is exemplified by *ortho*-fluorophenyl enamide (when R^7 = F). The *ortho*-substituted-α-aryl enamide has been intermittently reported on but deserves attention because the products more closely mimic alkaloid or drug-like structures.

The optically active (*R)*-2-methylpyrrolidine is useful as a chiral building block of H_3 histamine receptor antagonist, ABT-239.[187] Consequently reduction of 2-methyl-1-pyrroline represents a relevant but challenging reaction. Finally, the chemistry of dibenzo[*b,f*][1,4]oxazepine derivatives has attracted much attention since they are found in many physiologically active compounds.[188]

ii) Non-protected α- and ß-amino acids. Generally, α-amino acids are prepared under their protected form. The challenge remains to efficiently and enantioselectively produce natural and unnatural amino acids that would not require a further deprotection step. Among the unnatural amino acids, α-allylglycine is found in different bioactive molecules such as binaphthyl-supported macrocycles that display antibacterial activity.[189] In this particular case, α-allylglycine is involved in a ring-closing metathesis reaction. Furthermore, (*S*)-allylglycine and (*R*)-allylglycine were found inhibit proteinase K.[190] Additional interesting unnatural α-amino acids are the substituted phenylalanine such as *O*-methyl-*L*-tyrosine (see Figure 49) which enters in the composition of Puromycin (PM).[191] PM is an aminoacyl nucleoside antibiotic is categorized as a mimic of aminoacyl-tRNA (aa-tRNA), acts as an inhibitor of protein synthesis.[192]

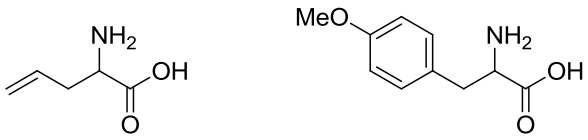

α-allylglycine *O*-methyl-tyrosine

Figure 49 Interesting unnatural α-amino acids.

Enantiomerically pure ß-amino acids are present in a number of natural products that possess a wide range of biological activities.[193] Thus, synthesis of ß-amino acids is a challenging target for organic chemists.[194]

In summary, the studies described in this thesis provide the first example of synthetic enantioselective reductive amination for the preparation of a range of unprotected chiral α-amino acids in water, thus demonstrating the great potential of artificial metalloenzymes to complement both homogeneous and enzymatic catalysts.

.

List of Abbreviations

⊂	included in
ACN	acetonitrile
AcOEt	ethyl acetate
Å	Angström
Ar	arene
Avi	avidin
ATH	Asymmetric Transfer Hydrogenation
Biot	biotin(yl)
B_4F	biotin-4-fluoresceine
BNHS	biotin *N*-hydroxysuccinimide ester
Boc	*tert*-butoxycarbonyl
BPFP	biotin pentafluorophenyl ester
4,4'diMeObpy	4,4'-dimethoxy-2,2'-bipyridine
bpy	bipyridine
Conv.	conversion
COD	1,5-cyclooctadiene
Cp*	pentamethylcyclopentadienyl
DEA	diethylamine
DMF	dimethylformamide
DMSO	dimethylsulfoxide
DNA	deoxyribonucleic acid
ds-DNA	double stranded DNA
dsOnc	double stranded oncogenic DNA
ss-DNA	single stranded DNA
EDTA	ethylenediaminetetraacetic acid
ee	enantiomeric excess

e. g.	*exempli gratia,* for example
EMSA	Electrophoretic Mobility Shift Assay
EN	ethylendiamine
eq.	equivalent(s)
ESI	Electron Spray Ionisation
Et	ethyl
EtOH	ethanol
Et_2O	diethyl ether
Et_3N	triethylamine
G4A	G-quadruplex telomeric DNA
GSH	glutathione
HABA	4-hydroxyazobenzene-2-carboxylic acid
HPLC	High Performance Liquid Chromatography
i. e.	*id est*, that is
ITC	isothermal titration calorimetry
M	metal
Me	methyl
Me_4Cp	tetratamethylcyclopentadienyl
min.	minute(s)
MES	2-(*N*-morpholino)ethanesulfonic acid
MOPS	3-(*N*-morpholino)propanesulfonic acid
MS	Mass Spectrometry
NMR	Nuclear Magnetic Resonance
NBD	norbornadiene
PDB	Protein Data Bank
ppm	parts-per-million
*i*Pr	isopropyl

*i*PrEN	*N*-isopropylethylene diamine
Sav	streptavidin
scG4A	“scrambled” telomeric sequence
R.T.	room temperature
t_1, t_2	retention times (min.)
Temp.	temperature
THF	tetrahydrofuran
TH	Transfer hydrogenation
TFA	trifuoroacetic acid
TfO^-	trifluoromethanesulfonate
TOF	turnover number
TON	turnover frequency
TS	transition state
TsEN	*N*-tosylethylenediamine
TsDPEN	*N*-(*p*-toluenesulfony1)-1,2-diphenylethylenediamine
vs.	*versus*
VMD	Visual Molecular Dynamics
WT	wild-type

7. Experimental Section

7.1. Chemical Synthesis

7.1.1. Synthesis of Biotinylated Piano Stool Metallodrugs Used in DNA Recognition

(3*R*,4*R*)-*N*-benzyl-3,4-dihydropyrrolidin-2,5-dione (**8**)[136]

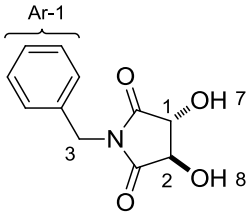

Benzylamine (125.25 ml, 1.309 mol) and (*L*)-tartaric acid (50 g, 333.13 mmol) were azeotropically dehydrated with boiling *o*-xylene (120 ml) in a Dean-Stark trap (until the formation of 4.95 ml of water). After cooling, the crystalline (yellowish color) precipitate was filtered, washed with acetone and recrystallized in EtOH to yield compound **8** as a white solid (58.9 g, 80% yield). The product was characterized according to the ^{1}H NMR described in literature[136]:

^{1}H NMR (400 MHz, MeOD) δ 7.36-7.15 (m, 5H, **Ar-1**), 4.07-4.03 (m, 2H, 4.87 (s, 2H, **H^3**), 4.64 (s, 2H, **H^1**, **H^2**).

(3*S*,4*S*)-*N*-benzyl-3,4-dihydropyrrolidine (**9**)[136]

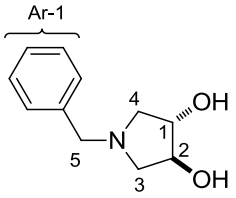

To a solution of compound **8** (10 g, 45.21 mmol) and the BF_3/Et_2O (22.51 ml, 177.66 mmol) in dimethylester diglycol (100 ml) was added $NaBH_4$ (4.5 g, 118.89 mmol) in small portions during 1 h at 0°C. When the evolution of hydrogen had stopped, the mixture was allowed to come to RT followed by heating for 2 h at 70°C. After cooling to RT, HCl (6N, 60 ml) was

slowly added, then the reaction was heated again for 15 min at 70°C. NaF (27.71 g) was then added in one portion with vigorous stirring. The mixture was immediately acidified by adding HCl, 6N (45 ml) to pH 1.0 followed by heating for 30 min at 100°C. After cooling to RT NaOH, 20% (60 ml) was added (pH 9.0-10.0). The salts were removed by filtration and the organic and the aqueous phases were separated. The organic phase was concentrated to afford a colorless solid. This residue was dissolved H_2O (35 ml) and extracted 10 times with Et_2O. The combined organic phases were dried (Na_2SO_4) and concentrated to a pale yellow oil, which solidified upon standing. Recrystallization from AcOEt (35 ml) provided **9** as a crystalline powder. The water phase was extracted continuously for 8 h with Et_2O. The organic phase was dried and concentrated to give a residue which was recrystallized from AcOEt (35 ml) to afford more **9** (6.20 g, 71% final yield). The product was characterized according to the ^{1}H NMR described in literature:[136]

^{1}H NMR (400 MHz, MeOD) δ 7.52-7.28 (m, 5H, **Ar-1**), 4.07-4.03 (m, 2H, **H^1**, **H^2**), 3.70-3.54 (m, 2H, **H^5**), 2.94/2.48 (dd, *J* = 12.4, 3.4 Hz, 2H, **H^3**, **H^4**).

(3*S*,4*S*)-benzyl-3,4-di(methylsulfonyloxy)pyrrolidine (**10**)[136]

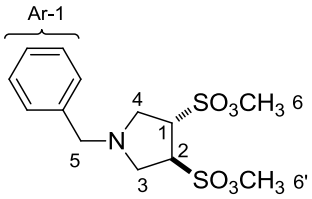

A solution of **9** (10 g, 51.75 mmol) in CH_2Cl_2 (40 ml) was treated with Et_3N (14.42 ml, 103.49 mmol) and stirred at 0°C. Then, methanesulfonylchloride (8.01 ml, 103.49 mmol) was added dropwise. After 30 min stirring at RT, the mixture was washed twice with water (30 ml) and the organic layers were treated with 1 M solution of HCl (190 ml). The aqueous layers formed, were treated with NaOH solution 20% (100 ml). The resulting oil was extracted twice with dichloromethane (2x60 ml). The organic phase was evaporated until dryness and the crude product was used without any further purification for the next step.

(3*R*,4*R*)-*N*-benzyl-pyrrolidine-3,4-diazide (**11**)[136]

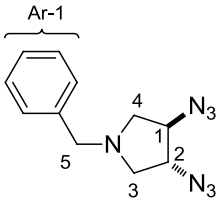

A stirred solution of compound **10** (10 g, 28.65 mmol) and NaN_3 (4.84 g, 74.84 mmol) in dry DMF (150 ml) was heated at 100°C for 4 h. After cooling to room temperature, the white solid was filtered off and the residue (6.47 g) was purified by column chromatography using AcOEt/Heptane (1:1) to afford compound **11** as yellowish oil (6.48 g, 93% yield). The product was characterized according to the ^{1}H NMR described in literature[136]:

^{1}H NMR (400 MHz, MeOD) δ 7.35-7.32 (m, 5H, **Ar-1**), 3.99-3.94 (m, 2H, $\mathbf{H^1}$, $\mathbf{H^2}$), 3.70-3.66 (m, 2H, $\mathbf{H^5}$), 2.99/2.60 (dd, *J* = 12.4, 3.4 Hz, 2H, $\mathbf{H^3}$, $\mathbf{H^4}$).

(3*R*,4*R*)-*N*-benzyl-3,4-diaminopyrrolidine (**12**)[136]

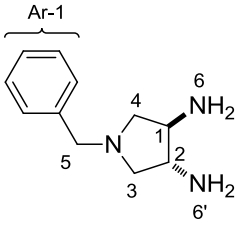

To a solution of compound **12** (500 mg, 2.06 mmol) in degassed EtOH (10 ml) was added Pd/C (10%, 50 mg). The resulting mixture was hydrogenated during 4 h at 5 bar. The solution was then filtered and solvents were evaporated. The crude product was purified by a column chromatography (CH_2Cl_2) to yield compound **12** (292 mg, 74% yield). The product was characterized according to the ^{1}H NMR described in literature[136]:

^{1}H NMR (400 MHz, MeOD) δ 7.35-7.32 (m, 5H, **Ar-1**), 3.65-3.60 (m, 2H, $\mathbf{H^1}$, $\mathbf{H^2}$), 3.05-3.82 (m, 4H, $\mathbf{H^5}$, $\mathbf{H^3}$, $\mathbf{H^4}$), 2.94/2.38 (dd, *J* = 12.4, 3.4 Hz, 2H, $\mathbf{H^3}$, $\mathbf{H^4}$).

(3*R*,4*R*)-*N*-benzyl-3,4-di(*N,N-tert*-butyloxycarbonyl)aminopyrrolidine (**13**)[136]

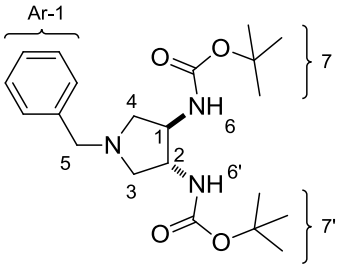

Compound **12** (1.37 g, 7.16 mmol) was dissolved in CH_2Cl_2 (30 ml) and the mixture was cooled to 0°C. Then $(BOC)_2O$ (3.75 g, 17.19 mmol) and Et_3N (3.99 ml, 28.65 mmol) were added. The reaction was stirred overnight at RT. The resulting crude product was purified by column chromatography on silica gel (100% CH_2Cl_2 then CH_2Cl_2/MeOH : 10/1)) to yield compound **13** quantitatively (2.74, 98% yield). The product was characterized according to the ^{1}H NMR described in literature[136]:

^{1}H NMR (400 MHz, MeOD) δ 7.33-7.25 (m, 5H, **Ar-1**), 3.87-3.83 (m, 2H, **H^1**, **H^2**), 3.60 (s, 2H, **H^5**), 2.95/2.41 (dd, *J* = 12.4, 3.4 Hz, 2H, **H^3**, **H^4**), 1.44 (s, 18H, **H^7**, **H$^{7'}$**).

(3*R*,4*R*)-3,4-di(*N,N-tert*-butyloxycarbonyl)aminopyrrolidine (**14**)[136]

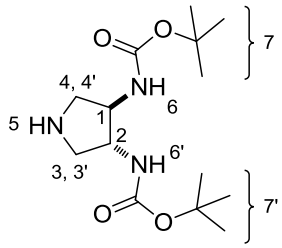

Compound **13** (910 mg, 2.32 mmol) was dissolved on a degassed mixture of 60 ml of AcOEt/EtOH (5 : 1). Pd/C (10 %) and $PdOH_2$ (10 %) were added and the mixture was hydrogenated overnight at 5 bar. After the catalysis finished the crude precipitate was filtered and evaporated to afford compound **14** (678 mg, 97% yield). The product was characterized according to the ^{1}H NMR described in literature[136]:

^{1}H NMR (400 MHz, MeOD) δ 3.91-3.83 (m, 2H, **H^1**, **H^2**), 3.15 (dd, *J* = 12.4, 3.4 Hz, 2H, **H^3**, **H^4**), 2.65 (dd, *J* = 12.3, 3.4 Hz, 2H, **H$^{3'}$**, **H$^{4'}$**), 1.42 (s, 18H, **H^7**, **H$^{7'}$**).

(3*R*,4*R*)-1-biotinyl-3,4-di(*N*,*N*-*tert*-butyloxycarbonyl)aminopyrrolidine (**15**)

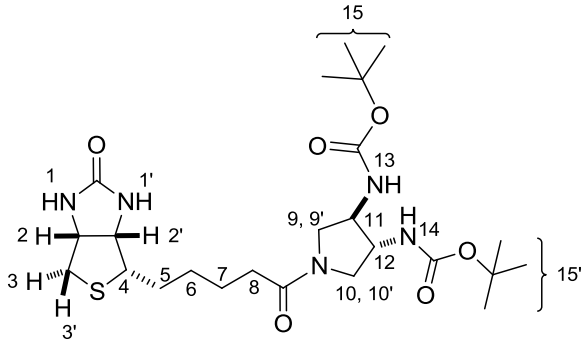

Compound **14** (0.37 g, 1.21 mmol, 1 eq.) was dissolved in DMF (30 mL). Biotin *N*-hydroxysuccinimide ester (0.39 g, 1.21 mmol, 1 eq.) and Et_3N (0.51 mL, 3.63 mmol, 3 eq.) were then added and the mixture was heated at 80°C overnight. The solvent was removed and the product was then purified by column chromatography on silicagel (CH_2Cl_2/MeOH : 10/1.5) to obtain compound **15** as a white solid (383 mg, 95.0% yield).

^{1}H NMR (400 MHz, MeOD): δ 4.49 (dd, *J* = 4.9, 7.6 Hz, 1H, **H^{2}**), 4.31 (dd, *J* = 4.4, 7.7 Hz, 1H, **H$^{2'}$**), 4.10-3.92 (m, 2H, **H^{11}**, **H^{12}**), 3.86 (dd, *J* = 6.8, 12.2 Hz, 1H, **H^{9}**), 3.77 (dd, *J* = 6.9, 12.2 Hz, 1H, **H^{10}**), 3.30-3.36 (m, 1H, **H$^{9'}$**), 3.17-3.25 (m, 2H, **H^{4}**, **H$^{10'}$**), 2.93 (dd, *J* = 4.9, 12.0 Hz, 1H, **H$^{3'}$**), 2.70 (d, *J* = 12.0 Hz, 1H, **H^{3}**), 2.33 (t, *J* = 7.4 Hz, 2H, **H^{8}**), 1.82-1.40 (m, 6H, **H^{5}**, **H^{7}**, **H^{6}**), 1.47 (s, 18H, **H^{15}**, **H$^{15'}$**). ^{13}C NMR (101 MHz, MeOD): δ 173.71, 173.20, 164.85, 157.84 (2C), 79.35 (2C), 62.06, 60.36, 55.70 (2C), 49.83, 39.77, 33.29, 28.57, 28.26, 27.42 (6H), 25.00, 24.44. MS (ESI-MS, pos): *m*/*z* = 549.93 $[M+Na]^+$; calcd. for $C_{24}H_{41}N_5O_6S$, 527.68. See appendix.

(3*R*,4*R*)-1-biotinyl-3,4-diaminopyrrolidine (**16**)

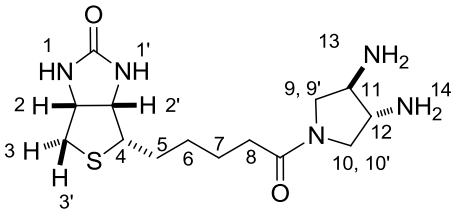

Compound **15** (0.20 g, 0.39 mmol, 1 eq.) was dissolved in CH_2Cl_2 (10 mL). TFA (2 mL, 26.09 mmol, 67 eq.) was added and the mixture was stirred at RT until completion of the reaction as revealed by thin layer chromatography. After evaporation of the volatiles, the crude product was dissolved in water (20 mL), washed three times with CH_2Cl_2 (40 mL) and then the pH adjusted to 9.0. The product was extracted with CH_2Cl_2 (2x40 mL). The organic phase was dried and the crude product was purified by column chromatography (MeOH/CH_2Cl_2 : 7/3) to afford **16** as white solid (34 mg, 57.0 % yield).

^{1}H NMR (400 MHz, MeOD): δ 4.49 (dd, *J* = 4.9, 7.8 Hz, 1H, **H^{2}**), 4.31 (dd, *J* = 4.5, 7.8 Hz, 1H, **H$^{2'}$**), 3.90-3.71 (m, 2H, **H^{9}**, **H^{10}**), 3.27-3.03 (m, 5H, **H^{4}**, **H$^{9'}$**, **H$^{10'}$**, **H^{11}**, **H^{12}**), 2.93 (dd, *J* = 5.0, 12.0 HZ, 1H, **H$^{3'}$**), 2.70 (d, *J* = 12.0 Hz, 1H, **H^{3}**), 2.33 (t, *J* = 7.4 Hz, 2H, **H^{8}**), 1.81-1.53 (m, 4H, **H^{5}**, **H^{7}**), 1.47 (dd, *J* = 7.5, 15.1 Hz, 1H, **H^{6}**). ^{13}C NMR (101 MHz, MeOD): δ 173.39, 166.13, 63.34, 61.63, 59.11, 57.80, 56.00, 54.81, 53.58, 41.04, 34.66, 29.89, 29.54, 25.76. HR-MS (ESI-MS, pos): *m/z* = 328.1793 $[M+H]^+$; calcd. for $C_{14}H_{25}N_5O_2S$, 327.1728. See appendix.

[(η^6-*p*-cymene)Ru(biotin-*N*-(*R,R*)-3,4-diaminopyrrolidine-*N,N*)Cl]CF_3SO_3 (**6**)

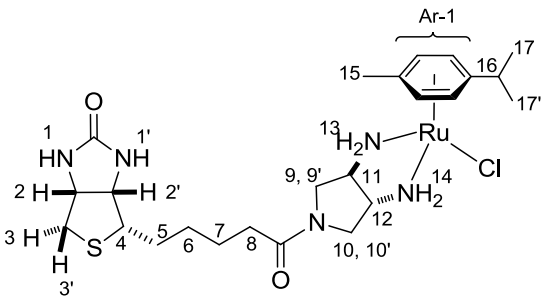

The dimer [(η^6-*p*-cymene)$RuCl_2]_2$ (46.8 mg, 0.0736 mmol, 0.5 eq.) was dissolved in MeOH (5 mL) and $AgCF_3SO_3$ (39.2 mg, 0.1527 mmol, 1 eq.) was added to the solution. The reaction

mixture was then stirred in the dark for 2 h at RT. The AgCl was filtered off and the resulting solution was added to the (3*R,*4*R*)-1-biotinyl-3,4-diaminopyrrolidine (50 mg, 0.1527 mmol, 1 eq.). The mixture was stirred for 2 h and the solvent was evaporated to dryness. The residue was washed with $CHCl_3$ (50 mL), the precipitate was filtered and dried to afford a yellow solid (87 mg, 95 % yield).

^{1}H NMR (400 MHz, MeOD): δ 5.67 (d, *J* = 5.4 Hz, 2H, **Ar-1**), 5.56 (dd, *J* = 5.4 Hz, 2H, **Ar-1**), 4.50 (dd, *J* = 4.8, 7.7 Hz, 1H, **H^{2}**), 4.29 (dd, *J* = 4.4, 7.8 Hz, 1H, **H$^{2'}$**), 3.81-3.49 (m, 2H, **H^{9}**, **H^{10}**), 3.25-3.20 (m, 2H, **H^{4}**, **H$^{9'}$**), 3.09-2.90 (m, 5H, **H$^{10'}$**, **H^{11}**, **H^{12}**, **H$^{3'}$**, **H^{16}**), 2.71 (d, *J* = 12.4, 1H, **H^{3}**), 2.27 (s, 3H, **H^{15}**), 2.32-2.23 (m, 2H, **H^{8}**), 1.74-1.35 (m, 6H, **H^{7}**, **H^{5}**, **H^{6}**), 1.31 (dd, 6H, **H^{17}**, **H$^{17'}$**). ^{13}C NMR (101 MHz, MeOD): δ 173.86, 165.09, 104.37, 97.96, 82.23, 80.73, 63.78, 62.81, 62.34, 60.64, 59.12, 58.13, 56.03, 46.13, 45.30, 40.05, 32.90, 31.04, 28.71, 28.59, 25.51, 22.23, 21.28, 17.21. (ESI-MS, pos): *m*/*z* = 598.1532 $[M]^+$, 562.27 $[M\text{-}Cl]^+$; calcd. for $C_{24}H_{39}ClN_5O_2RuS$, 598.19. See appendix.

3-Phenyl-1,4-cyclohexadiene[139]

Biphenyl (5 g, 32.42 mmol) was added to anhydrous EtOH (50 ml) in a 1 L three-necked flask equipped with loose cotton plugs in the side necks. After the biphenyl was dissolved, liquid ammonia (300 ml) was condensed into the stirred solution. Then sodium (2 g) was added in small pieces. When about 1/3 of the sodium has been added, the white sodium salt of the acid precipitated and there was strong foaming of the reaction mixture. After all the sodium has been consumed, as evidenced by the disappearance of the blue color, NH_4Cl (5.7 g, 106.67 mmol) was added cautiously. The mixture was stirred for an additional hour and then allowed to stand at RT until the ammonia has evaporated. The resulting residue was dissolved in water (150 ml). The solution was poured onto ice (100 g) and acidified (pH 4.0) by addition of 10% HCl (40 ml). The resulting mixture was extracted with portions of ether (4x50 ml), and the combined extracts were washed with saturated aqueous solution of NaCl (25 ml) and dried over $MgSO_4$. The ether solution was separated from the drying agent and concentrated at RT under reduced pressure. The residual oil was distilled from a 25 ml

Claisen flask with an intended neck. The crude material was used directly in the next step without further purification.

$[(\eta^6\text{-biphenyl})RuCl_2]_2$[138]

A mixture of 3-Phenyl-1,4-cyclohexadiene (4.28 g, 12.05 mmol) and $RuCl_3$, x•H_2O (0.25 g, 1.205 mmol) in EtOH (25 ml) was refluxed for 4 h. The resulting precipitate was removed by filtration and washed with EtOH. The combined filtrate and washings were then concentrated to give $[(\eta^6\text{-biphenyl})RuCl_2]_2$.(379 mg, 44% yield). The product was characterized according to the ^{1}H NMR described in literature.

^{1}H NMR (400 MHz, DMSO-d_6) δ 7.85-7.76 (m, 2H), 7.52-7.45 (m, 3H), 6.45 -6.39 (m, 2H), 6.10-6.00 (m, 3H).

$[(\eta^6\text{-biphenyl})Ru(\text{biotin-}N\text{-}(R,R)\text{-3,4-diaminopyrrolidine-}N,N)Cl]CF_3SO_3$ (**7**)

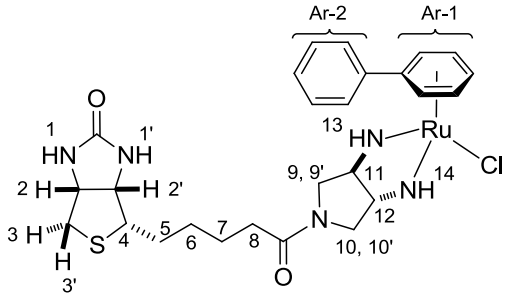

The dimer $[(\eta^6\text{-biphenyl})RuCl_2]_2$ (16 mg, 0.025 mmol 0.4 eq.) was dissolved in dry MeOH (5 mL) and CF_3SO_3Ag (13.8 mg, 0.0626 mmol, 1 eq.) was added to the solution. Then the reaction mixture was stirred for 2 h at RT. The silver salts were filtered and the resulting solution was added to the (3*R,4R*)-1-biotinyl-3,4-diaminopyrrolidine (20.5 mg, 0.626 mmol, 1 eq.). The mixture was stirred 4h and the solvent was evaporated. The residue was washed with $CHCl_3$, the precipitate was filtered and then dried to yield a yellow solid (16 mg, 41% yield).

^{1}H NMR (500 MHz, MeOD): δ 7.70-7.69 (m, 2H, **Ar-2**), 7.43-7.40 (m, 3H, **Ar-2**), 6.12-6.05 (m, 2H, **Ar-1**), 5.91-5.80 (m, 3H, **Ar-1**), 4.41-4.38 (m, 1H, $\mathbf{H^2}$), 4.24-4.14 (m, 1H, $\mathbf{H^{2'}}$), 3.62-3.48 (m, 2H, $\mathbf{H^9}$, $\mathbf{H^{10}}$), 3.15-3.05 (m, 3H, $\mathbf{H^4}$, $\mathbf{H^{9'}}$, $\mathbf{H^{10'}}$), 2.87-2.76 (m, 3H, $\mathbf{H^{3'}}$, $\mathbf{H^{11}}$, $\mathbf{H^{12}}$), 2.60

(d, *J* = 12.7, 1H, **H^{3}**), 2.12-2.08 (m, 2H, **H^{8}**), 1.65-1.40 (m, 4H, **H^{5}**, **H^{7}**), 1.41-1.24 (m, 2H, **H^{6}**). HR-MS (ESI-MS, pos): *m*/*z* = 618.1238 $[M]^+$, 582.15 $[M\text{-}Cl]^+$; calcd. for $C_{26}H_{35}ClN_5O_2RuS$, 618.1243. The carbon ^{13}C NMR could not be obtained since not enough material was available. See appendix

7.1.2. Synthesis of Biotinylated Piano Stool Complexes Used in ATH

(2,3,4,5-tetramethylcyclopentadienyl)acetonitrile (**20**)[162]

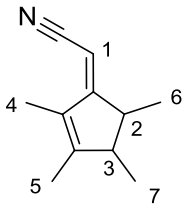

To a solution of ACN (1.88 mL, 35.8 mmol) in THF (40 mL) cooled to -80°C was added *n*-BuLi in hexane (14.3 mL of a 2.5 M solution, 35.88 mmol). After 15 min 2,3,4,5-tetramethylcyclopent-2-enone **19** (4.85 mL, 4.5 g, 32.6 mmol) was added at -80°C over a period of 45 min. Over 3 h the temperature was allowed to rise to 0°C. Water (10 mL) was added, and the organic layer was washed with two portions of water (10 mL). Then, HCl (2N, 10 mL) was added, the mixture was extracted, and after 16 h the layers were separated. The organic phase was washed with brine, dried over Na_2SO_4, and concentrated. The product was then purified by column chromatography (cyclohexane/AcOEt : 50/1) to yield a transparent oil (4.72 g, 90% yield).

NMR data of the major isomer (2,3,4,5-tetramethylcyanomethylenecyclopent-2-ene): ^{1}H NMR (400 MHz, $CDCl_3$) δ 4.81 (d, *J* = 1.8 Hz,1H, **H^{1}**), 2.52 (br q, *J* = 7.2 Hz, 1H, **H^{2}**), 2.19 (br q, *J* = 7.2 Hz, 1H, **H^{3}**), 1.76 (br s, 3H, **H^{4}**), 1.62 (br s, 3H, **H^{5}**), 1.19 (d, *J* = 7.2 Hz, 3H, **H^{6}**), 1.02 (d, *J* = 7.1 Hz, 3H, **H^{7}**). ^{13}C NMR (101 MHz, $CDCl_3$) δ 177.13, 158.26, 131.43, 119.31, 82.20, 52.03, 45.34, 19.94, 19.06, 14.22, 10.08. MS (ESI-MS, pos): *m*/*z* = 162.30 $[M+H]^+$, 184.10 $[M+Na]^+$; calcd. for $C_{11}H_{15}N$, 161.28; (additional peak: 345.1, impurity from the instrument).

2-(2,3,4,5-tetramethylcyclopentadienyl)ethylamine (**21**)[162]

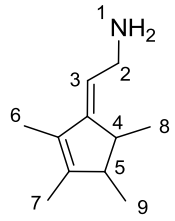

Solid $LiAlH_4$ (0.304 g, 8.02 mmol) was added to dry THF (5 mL). The reaction mixture was allowed to stir until a homogeneous slurry was formed. Solid $AlCl_3$ (1.069 g, 8.02 mmol) was then added to the slurry. The reaction was then cooled to 0°C and a solution of 2-(2,3,4,5-tetramethylcyclopentadienyl)ethylamine **20** (862 mg, 5.35 mmol) in THF was added dropwise to the reaction mixture. The reaction was allowed to warm to room temperature, and stirred overnight. Next, the reaction was quenched with NaOH. The mixture was filtered to remove the aluminum salts. The THF was removed under reduced pressure, the deep yellow solution was dissolved in Et_2O and the residual water was dried over Na_2SO_4. The crude product was used for the next step.

$[(\eta^5\text{-}Me_4Cp(CH_2)_2NH_3)RhCl_2]_2Cl_2$ (**22**)[161]

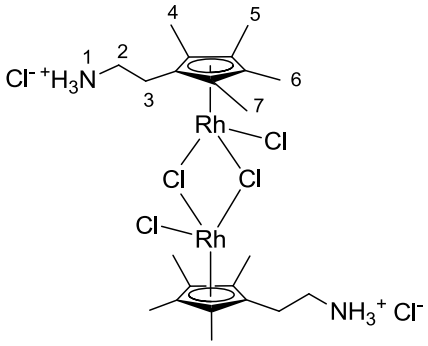

2-(2,3,4,5-tetramethylcyclopentadienyl)ethyl-amine **21** (tautomer mixture, 500 mg, 3.03 mmol) was dissolved in Et_2O (10 mL) and treated with HCl (1.78 mL, 5.95 mmol, 4 M in dioxane). Hexane (20 mL) was added to this solution until a white precipitate formed, which was filtered off and washed twice with hexane. The white solid was dissolved in EtOH (50 mL) and $RhCl_3 \cdot nH_2O$ (186 mg, 0.705 mmol) was added. The reaction mixture was refluxed for 4 days and thereafter stored at -20°C overnight. The precipitate was filtered off and

washed with hexane, Et_2O and cold EtOH to yield the pure product as an orange powder (214 mg, 90% yield).

^{1}H NMR (400 MHz, DMSO-d_6): δ 8.02 (br s, 6H, **H^1**), 2.95-2.85 (m, 4H, **H^2**), 2.46-2.42 (m, 4H, **H^3**), 1.71/1.62 (s, 24H, **H^4**, **H^5**, **H^6**, **H^7**). ^{13}C NMR (101 MHz, DMSO-d_6) δ 97.35, 92.51, 86.23, 37.10, 22.33, 9.23 (2C), 9.11 (2C) HR-MS (ESI-MS, pos): *m*/*z* = 639.0058 $[M\text{-}Cl]^+$, calcd. for $C_{22}H_{36}Cl_4N_2Rh_2$, 673.9742.

$[(\eta^5\text{-}Me_4Cp(CH_2)_2\text{-}N\text{-Biot})RhCl_2]_2$ (**17**)

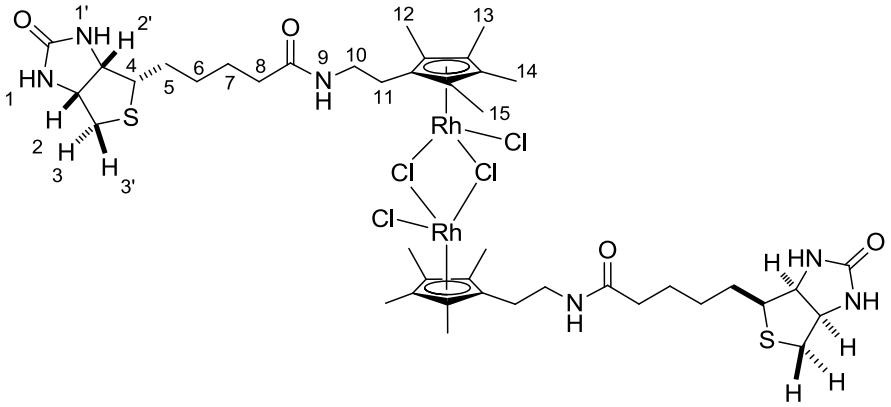

$[(\eta^5\text{-}Me_4Cp(CH_2)_2NH_3)RhCl_2]_2Cl_2$ **22** (100 mg, 0.148 mmol) was suspended in DMF (10 mL) and biotin *N*-hydroxysuccinimide (151 mg, 0.444 mmol) and Et_3N (0.416 mL, 2.96 mmol) were added. The reaction mixture was left to stir at RT overnight. The solvent was removed under reduced pressure and the brown solid was resuspended in CH_2Cl_2. The solid was filtered and washed with CH_2Cl_2. Then the solid was resuspended in a minimum amount of DMF, stirred for few minutes and finally filtered to yield a brown-red powder (125 mg, 75% yield).

^{1}H NMR (500 MHz, DMSO-d_6) δ 10.55 (s, 1H, COOH-biotin), 7.97 (t, *J* = 6.0 Hz, 2H, **H^9**), 6.44 (s, *2*H, **H$^{1'}$**), 6.37 (s, *2*H, **H^1**), 4.35-4.27 (m, 2H, **H^2**), 4.15-4.09 (m, 2H, **H$^{2'}$**), 3.22 (dt, *J* = 13.4, 6.9 Hz, 4H, **H^{10}**), 3.11-3.09 (m, 2H, **H^4**), 2.83 (dd, *J* = 12.4, 5.0 Hz, 2H, **H$^{3'}$**), 2.59 (d, *J* = 12.4 Hz, 2H, **H^3**), 2.27 (t, *J* = 6.9 Hz, 4H, **H^{11}**), 2.21 (t, *J* = 7.4 Hz, 1H, biotin), 2.03 (t, *J* = 7.4 Hz, 4H, **H^8**), 1.68/1.64 (s, 24H, **H^{12}**, **H^{13}**, **H^{14}**, **H^{15}**), 1.80-1.21 (m, 12H, **H^5**, **H^6**, **H^7**).

Remark: Presence of residual biotin can be highlighted by the presence of a triplet at 2.21 ppm as well as the proton from the carboxylic group at 10.55 ppm.

Alternative synthesis of $[(\eta^5\text{-}Me_4Cp(CH_2)_2\text{-}N\text{-Biot})RhCl_2]_2$ (**17**)

$[(\eta^5\text{-}Me_4Cp(CH_2)_2NH_3)RhCl_2]_2Cl_2$ **22** (200 mg, 0.296 mmol) was suspended in DMF (20 mL) and biotin pentafluorophenyl ester (231 mg, 0.562 mmol) and Et_3N (0.831 mL, 5.920 mmol) were added. The compound rapidly dissolved to give a dark red solution and was stirred at RT overnight. The solvent was removed and the reddish solid was suspended in hexane. The solid was filtered and washed with hexane (3x15 mL) then with CH_2Cl_2 (4x15 mL) to afford 284 mg of brown-red powder (85% yield).

^{1}H NMR (500 MHz, DMSO-d_6) δ 7.97 (t, *J* = 6.0 Hz, 2H, **H^{9}**), 6.44 (s, *2*H, **H$^{1'}$**), 6.37 (s, *2*H, **H^{1}**), 4.35-4.27 (m, 2H, **H^{2}**), 4.15-4.09 (m, 2H, **H$^{2'}$**), 3.22 (dt, *J* = 13.4, 6.9 Hz, 4H, **H^{10}**), 3.11-3.09 (m, 2H, **H^{4}**), 2.83 (dd, *J* = 12.4, 5.0 Hz, 2H, **H$^{3'}$**), 2.59 (d, *J* = 12.4 Hz, 2H, **H^{3}**), 2.27 (t, *J* = 6.9 Hz, 4H, **H^{11}**), 2.03 (t, *J* = 7.4 Hz, 4H, **H^{8}**), 1.68/1.64 (s, 24H, **H^{12}**, **H^{13}**, **H^{14}**, **H^{15}**), 1.80-1.21 (m, 12H, **H^{5}**, **H^{6}**, **H^{7}**). ^{13}C NMR (126 MHz, DMSO-d_6) δ 172.05 (2C), 162.68 (2C), 100.40 (4C), 99.04 (4C), 96.78 (2C), 61.01 (2C), 59.15 (2C), 55.37 (2C), 54.89 (2C), 35.65 (2C), 35.05 (2C), 28.19 (2C), 28.00 (2C), 25.07 (2C), 24.13 (2C), 8.70 (4C), 8.59 (4C). HR-MS (ESI-MS, pos): *m/z* = 1093.1555 $[M\text{-}Cl]^+$; calcd. for $C_{42}H_{64}Cl_4N_6O_4Rh_2S_2$, 1126.1451 (additional peaks: 492.12 $[(M\text{-}2Cl)/2]^{2+}$, 528.10 $[(M\text{-}Cl)/2]^+$). See appendix.

[(η^5-$Me_4Cp(CH_2)_2NH_3$)$IrCl_2$]$_2Cl_2$ (**23**)

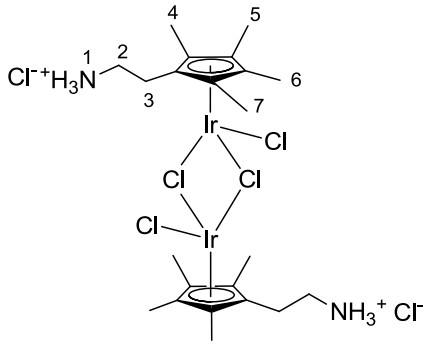

2-(2,3,4,5-tetramethylcyclopentadienyl)ethyl amine **21** (tautomer mixture, 91.1 mg, 0.551 mmol) was dissolved in Et_2O (2 mL) and treated with HCl (0.272 mL, 1.09 mmol, 4 M in dioxane). Hexane (4 mL) was added to this solution until a white precipitate formed, which was filtered and washed twice with hexane. The white solid was dissolved in MeOH (5 mL) and introduced into a 10 mL Schlenk tube. Then, $[Ir(COD)Cl]_2$ (100 mg, 0.149 mmol) and a solution of concentrated HCl (0.8 mL of 37% solution in water) was added. This mixture was refluxed under nitrogen; after 30 min the initial orange-red suspension turned to a clear orange solution. A few minutes later, orange crystals began to precipitate and the reaction mixture was refluxed overnight. The compound was filtered off, washed with MeOH and dried to yield a bright orange powder (116.8 mg, 60% yield).

^{1}H NMR (400 MHz, DMSO-d_6) δ 8.23 (br s, 6H, **H^1**), 2.95-2.84 (m, 4H, **H^2**), 2.43-2.39 (m, 4H, **H^3**), 1.74/1.64 (s, 24H, **H^4**, **H^5**, **H^6**, **H^7**). ^{13}C NMR (101 MHz, DMSO-d_6) δ 97.34, 92.50, 86.22, 37.10, 22.32, 9.23 (2C), 9.11 (2C). HR-MS (ESI-MS, pos): *m*/*z* = 819.1130 $[M\text{-}Cl]^+$; calcd. for $C_{22}H_{36}Cl_4N_2Rh_2$, 854.0891 (additional peak: 642.22 $[(M\text{-}Cl)/2]^+$). See appendix.

[(η^5-$Me_4Cp(CH_2)_2$-*N*-Biot)$IrCl_2]_2$ (**18**)

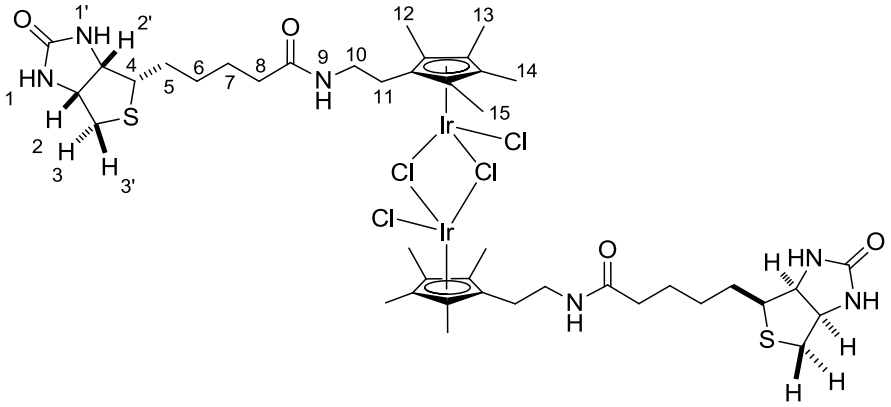

[(η^5-$Me_4Cp(CH_2)_2NH_3)IrCl_2]_2(Cl)_2$ **23** (200 mg, 0.234 mmol) was suspended in DMF (20 mL) and biotin pentafluorophenyl ester (182 mg, 0.445 mmol) and Et_3N (0.658 µL, 4.68 mmol) was added. The compounds rapidly dissolved to give a clear yellow solution. It was left to stir at RT overnight. The solvent was removed and the brown solid was suspended in hexane. The solid was filtered and washed with hexane (3x15 mL) then with CH_2Cl_2 (4x15 mL) to afford a pale yellow powder (66 mg, 80% yield).

^{1}H NMR (400 MHz, DMSO-d_6) δ 7.94 (t, *J* = 5.9 Hz, 2H, **H^9**), 6.41 (s, *2*H, **H$^{1'}$**), 6.35 (s, *2*H, **H^1**), 4.32-4.24 (m, 2H, **H^2**), 4.11-4.09 (m, 2H, **H$^{2'}$**), 3.19 (dt, *J* = 13.2, 6.9 Hz, 4H, **H^{10}**), 3.14-3.02 (m, 2H, **H^4**), 2.80 (dd, *J* = 12.5, 5.0 Hz, 2H, **H$^{3'}$**), 2.55 (d, *J* = 12.5 Hz, 2H, **H^3**), 2.15 (t, *J* = 6.9 Hz, 4H, **H^{11}**), 2.02 (t, *J* = 7.4 Hz, 4H, **H^8**), 1.67/1.61 (s, 24H, **H^{12}**, **H^{13}**, **H^{14}**, **H^{15}**), 1.73-1.20 (m, 12H, **H^5**, **H^6**, **H^7**). ^{13}C NMR (126 MHz, DMSO-d_6) δ 171.99 (2C), 162.76 (2C), 94.45 (4C), 92.12 (4C), 88.99 (2C), 61.01 (2C), 59.15 (2C), 55.59 (2C), 39.61 (2C), 35.91 (2C), 35.14 (2C), 28.15 (2C), 27.93 (2C), 25.25 (2C), 23.95 (2C), 8.36 (4C), 8.24 (4C). HR-MS (ESI-MS, pos): *m*/*z* = 1271.2703 [M-Cl]$^+$, 618.1216 [M/2-Cl]$^+$; calcd. for $C_{42}H_{64}Cl_4Ir_2N_6O_4S_2$, 1306.2443. See appendix.

The biotinylated diimine complexes were synthesized following the procedure of Freedman *et al.*.[167]

[(η^5-$Me_4Cp(CH_2)_2$-*N*-Biot)Rh(bpy)Cl]Cl (**24**)

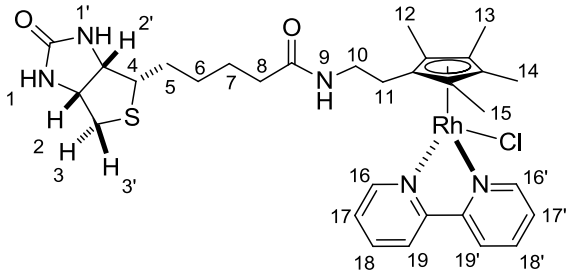

[(η^5-$Me_4Cp(CH_2)_2$-*N*-Biot)$RhCl_2]_2Cl_2$ **17** (20 mg, 0.0177 mmol) and 2,2'-bipyridine (4.4 mg, 0.0282 mmol) were added to ACN (5 mL, HPLC grade, used without further purification). The resulting slurry was purged with nitrogen for 20 min and then refluxed for 4h. The precipitate was filtered and washed with ACN to yield a brownish powder (13.5 mg, 70% yield).

^{1}H NMR (400 MHz, DMSO-d_6) δ 8.99 (d, *J* = 5.0 Hz, 2H, **H^{19}**, **H$^{19'}$**), 8.72 (d, *J* = 8.1 Hz, 2H, **H^{16}**, **H$^{16'}$**), 8.35 (td, *J* = 8.0, 1.3 Hz, 2H, **H^{18}**, **H$^{18'}$**), 8.11 (t, *J* = 6.0 Hz, 1H, **H^{9}**), 7.93-7.85 (m, 2H, **H^{17}**, **H$^{17'}$**), 6.42 (s, 1H, **H$^{1'}$**), 6.38 (s, 1H, **H^{1}**), 4.35-4.27 (m, 1H, **H^{2}**), 4.19-4.08 (m, 1H, **H$^{2'}$**), 3.27-3.17 (m, 2H, **H^{10}**), 3.13-3.05 (m, 1H, **H^{4}**), 2.82 (dd, *J* = 12.4, 5.1 Hz, 1H, **H$^{3'}$**), 2.58 (d, *J* = 12.4 Hz, 2H, **H^{3}**), 2.30 (t, *J* = 6.7 Hz, 2H, **H^{11}**), 2.04 (t, *J* = 7.4 Hz, 2H, **H^{8}**), 1.69/1.67 (s, 12H, **H^{12}**, **H^{13}**, **H^{14}**, **H^{15}**), 1.76-1.19 (m, 6H, **H^{5}**, **H^{6}**, **H^{7}**). ^{13}C NMR (101 MHz, DMSO-d_6) δ 172.18, 162.67, 153.93 (2C), 152.37 (2C), 140.37 (2C), 128.41 (2C), 123.83 (2C), 98.71 (2C), 97.00 (2C), 95.11, 61.01, 59.17, 55.37, 55.33, 35.53, 34.87, 28.19, 28.02, 25.05, 23.56, 8.59 (2C), 8.45 (2C). HR-MS (ESI-MS, pos): *m*/*z* = 684.1643 $[M]^+$; calcd. for $C_{31}H_{40}ClN_5O_2RhS$, 684.1646; (additional peak: 528.10 corresponding to traces of dimer **17**). See appendix.

[(η^5-$Me_4Cp(CH_2)_2$-*N*-Biot)Ir(bpy)Cl]Cl (**25**)

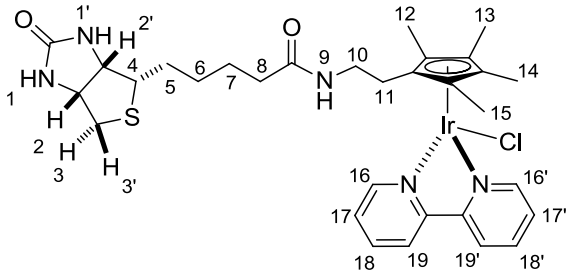

[(η^5-$Me_4Cp(CH_2)_2$-*N*-Biot)$IrCl_2]_2Cl_2$ **23** (50 mg, 0.0382 mmol) and 2,2'-bipyridine (13.1 mg, 0.0841 mmol) were added to ACN (10 mL, HPLC grade, used without further purification). The resulting slurry was purged with nitrogen for 20 min and then refluxed for 4h. The precipitate was filtered and washed with ACN to yield a brownish powder (24.7 mg, 80% yield).

^{1}H NMR (400 MHz, DMSO-d_6) δ 8.99 (d, *J* = 5.3 Hz, 2H, **H^{19}**, **H$^{19'}$**), 8.80 (d, *J* = 8.0 Hz, 2H, **H^{16}**, **H$^{16'}$**), 8.34 (td, *J* = 7.9, 1.4 Hz, 2H, **H^{18}**, **H$^{18'}$**), 8.05 (t, *J* = 5.9 Hz, 1H, **H^{9}**), 7.90-7.84 (m, 2H, **H^{17}**, **H$^{17'}$**), 6.42 (s, 1H, **H$^{1'}$**), 6.38 (s, 1H, **H^{1}**), 4.32 (m, 1H, **H^{2}**), 4.13 (m, 1H, **H$^{2'}$**), 3.23 (dt, *J* = 12.6, 6.4 Hz, 1H, **H^{10}**), 3.12-3.05 (m, 1H, **H^{4}**), 2.82 (dd, *J* = 12.4, 5.1 Hz, 1H, **H$^{3'}$**), 2.58 (d, *J* = 12.4 Hz, 1H, **H^{3}**), 2.23 (t, *J* = 6.4 Hz, 2H, **H^{11}**), 2.05 (t, *J* = 7.3 Hz, 2H, **H^{8}**), 1.70/1.67 (s, 12H, **H^{12}**, **H^{13}**, **H^{14}**, **H^{15}**), 1.73-1.26 (m, 6H, **H^{5}**, **H^{6}**, **H^{7}**). ^{13}C NMR (101 MHz, DMSO-d_6) δ 172.09, 162.47, 154.86 (2C), 152.13 (2C), 140.38 (2C), 128.97 (2C), 124.13 (2C), 91.55 (2C), 88.93 (2C), 85.84, 61.01 (2C), 55.37 (2C), 35.02, 28.20, 28.02, 26.38, 25.28, 25.01, 8.26 (2C), 8.12 (2C). HR-MS (ESI-MS, pos): *m*/*z* = 774.2175 $[M]^+$; calcd. for $C_{31}H_{40}ClN_5O_2IrS$, 774.2220. See appendix.

[(η^5-$Me_4CpCH_2)_2$-*N*-Biot)Rh(4,4'-diMeObpy)Cl]Cl (**26**)

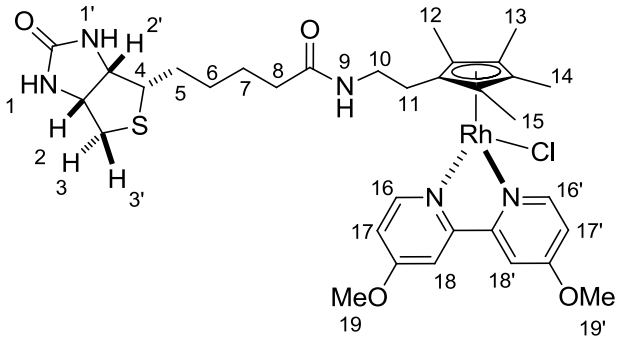

[(η^5-$Me_4Cp(CH_2)_2$-*N*-Biot)$RhCl_2]_2Cl_2$ **17** (20 mg, 0.0177 mmol) and 4,4'-dimethoxy-2,2'-bipyridine (7.05 mg, 0.0354 mmol) were added to ACN (5 mL, HPLC grade, used without further purification). The resulting slurry was purged with nitrogen for 20 min and then refluxed for 4h. The precipitate was filtered and washed with ACN yield a bright orange powder (22.4 mg, 85% yield).

^{1}H NMR (400 MHz, MeOD) δ 8.71 (d, *J* = 6.5 Hz, 2H, **H^{16}**, **H$^{16'}$**), 8.10 (d, *J* = 2.7 Hz, 2H, **H^{18}**, **H$^{18'}$**), 7.39 (dd, *J* = 6.5, 2.7 Hz, 2H, **H^{17}**, **H$^{17'}$**), 4.48 (dd, *J* = 7.7, 5.0 Hz, 1H, **H^{2}**), 4.33-4.23 (m, 1H, **H$^{2'}$**), 4.09 (s, 6H, **H^{19}**, **H$^{19'}$**), 3.37 (t, *J* = 7.0 Hz, 2H, **H^{10}**), 3.20 (dt, *J* = 10.2, 5.7 Hz, 1H, **H^{4}**), 2.93 (dd, *J* = 12.7, 4.8 Hz, 1H, **H$^{3'}$**), 2.70 (d, *J* = 12.7 Hz, 1H, **H^{3}**), 2.40 (t, *J* = 6.9 Hz, 2H, **H^{11}**), 2.18 (t, *J* = 7.6 Hz, 2H, **H^{8}**), 1.75/1.72 (s, 12H, **H^{12}**, **H^{13}**, **H^{14}**, **H^{15}**), 1.81-1.35 (m, 6H, **H^{5}**, **H^{6}**, **H^{7}**). ^{13}C NMR (101 MHz, MeOD) δ 172.80, 168.00, 162.74 (2C), 155.38 (2C), 153.02 (2C), 114.25 (2C), 110.34 (2C), 99.49 (2C), 98.56 (2C), 95.34, 61.03, 59.18, 57.01 (2C), 55.37, 48.55, 45.35, 34.96, 28.18, 27.99, 25.17, 25.02, 8.56 (2C), 8.41 (2C). MS (ESI-MS, pos): *m*/*z* = 707.7374 $[M\text{-}Cl]^+$, 742.6812 $[M]^+$; calcd. for $C_{33}H_{44}ClN_5O_4RhS$, 742.1857. See appendix.

[(η^5-$Me_4Cp(CH_2)_2$-*N*-Biot)Ir(4,4'-diMeObpy)Cl]Cl (**27**)

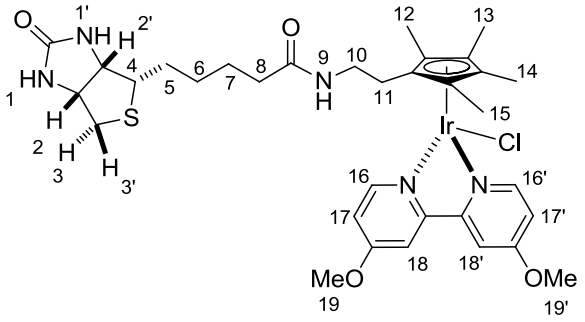

$[(\eta^5\text{-}C_5Me_4(CH_2)_2\text{-}N\text{-Biot})IrCl_2]_2Cl_2$ **18** (20 mg, 0.0153 mmol) and 4,4'-dimethoxy-2,2'-bipyridine (6.62 mg, 0.0306 mmol) were added to ACN (5 mL HPLC grade, used without further purification). The resulting slurry was purged with nitrogen for 20 min and then refluxed for 4h. The precipitate was filtered and washed with ACN yield a bright orange powder (20.4 mg, 80% yield).

^{1}H NMR (400 MHz, MeOD) δ 8.73 (d, *J* = 6.6 Hz, 2H, **H^{16}**, **H$^{16'}$**), 8.19 (d, *J* = 2.7 Hz, 2H, **H^{18}**, **H$^{18'}$**), 7.39 (dd, *J* = 6.6, 2.7 Hz, 2H, **H^{17}**, **H$^{17'}$**), 4.49 (dd, *J* = 7.9, 5.0 Hz, 1H, **H^{2}**), 4.33-4.31 (m, 1H, **H$^{2'}$**), 4.14 (s, 1H, **H^{19}**, **H$^{19'}$**), 3.40 (t, *J* = 6.9 Hz, 2H, **H^{10}**), 3.19 (dt, *J* = 10.1, 5.7 Hz, 1H, **H^{4}**), 2.94 (dd, *J* = 12.7, 4.9 Hz, 1H, **H$^{3'}$**), 2.72 (d, *J* = 12.8 Hz, 1H, **H^{3}**), 2.32 (t, *J* = 6.9 Hz, 2H, **H^{11}**), 2.29 (t, *J* = 7.6 Hz, 2H, **H^{8}**), 1.77/1.73 (s, 12H, **H^{12}**, **H^{13}**, **H^{14}**, **H^{15}**), 1.81-1.35 (m, 6H, **H^{5}**, **H^{6}**, **H^{7}**).^{13}C NMR (101 MHz, MeOD) δ 170.16, 161.67, 158.37 (2C), 153.89 (2C), 151.20 (2C), 115.90 (2C), 111.57 (2C), 101.36 (2C), 92.62 (2C), 86.92, 66.92, 61.65, 57.71 (2C), 57.03, 47.71, 41.13, 36.68, 29.73, 26.68, 25.35, 25.10, 9.00 (2C), 8.63 (2C). HR-MS (ESI-MS, pos): *m/z* = 834.2418 $[M]^+$; calcd. for $C_{33}H_{44}ClN_5O_4IrS$, 834.2431. See appendix.

[(η^5-$Me_4Cp(CH_2)_2$-*N*-Biot)Rh(Phen)Cl]Cl (**28**)

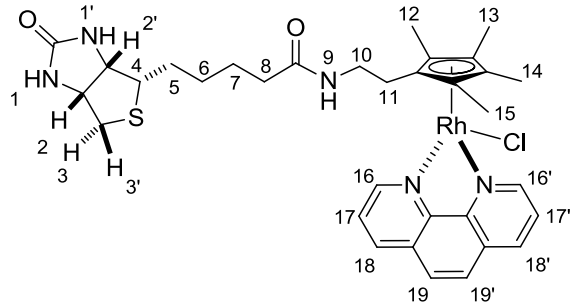

[(η^5-$Me_4Cp(CH_2)_2$-*N*-Biot)$RhCl_2]_2Cl_2$ **17** (50 mg, 0.0443 mmol) and 1,10-phenanthroline monohydrate (14.1 mg, 0.0704 mmol) were added to ACN (10 mL, HPLC grade, used without further purification). The resulting slurry was purged with nitrogen for 20 min and then refluxed for 4h. The precipitate was filtered and washed with ACN to yield a bright orange powder (31mg, 62% yield).

^{1}H NMR (400 MHz, MeOD) δ 9.38 (dd, *J* = 5.2, 1.1 Hz, 2H, **H^{16}**, **H$^{16'}$**), 8.86 (dd, *J* = 8.2, 1.2 Hz, 2H, **H^{18}**, **H$^{18'}$**), 8.22 (s, 2H, **H^{19}**, **H$^{19'}$**), 8.18 (dd, *J* = 8.2, 5.2 Hz, 2H, **H^{17}**, **H$^{17'}$**), 4.48 (dd, *J* = 7.9, 4.7 Hz, 1H, **H^{2}**), 4.28 (dd, *J* = 7.9, 4.6 Hz, 1H, **H$^{2'}$**), 3.42 (t, *J* = 6.9 Hz, 1H, **H^{10}**), 3.19 (dt, *J* = 9.9, 4.5 Hz, 1H, **H^{4}**), 2.90 (dd, *J* = 12.7, 5.0 Hz, 1H, **H$^{3'}$**), 2.70 (d, *J* = 12.7 Hz, 1H, **H^{3}**), 2.51 (t, *J* = 6.8 Hz, 2H, **H^{11}**), 2.19 (t, *J* = 7.3 Hz, 2H, **H^{8}**), 1.85/1.82 (s, 12H, **H^{12}**, **H^{13}**, **H^{14}**, **H^{15}**), 1.89-1.34 (m, 6H, **H^{5}**, **H^{6}**, **H^{7}**). ^{13}C NMR (101 MHz, MeOD) δ 172.26, 163.43, 152.56 (2C), 145.73 (2C), 139.51 (2C), 131.23 (2C), 127.97 (2C), 127.15 (2C), 93.70 (2C), 88.66 (2C), 84.20, 62.38, 60.61, 56.00, 40.03, 36.45, 35.60, 28.48, 25.63, 25.28, 24.38, 8.40 (2C), 8.06 (2C). HR-MS (ESI-MS, pos): *m/z* = 708.1635 $[M]^+$; calcd. for $C_{33}H_{40}ClN_5O_2RhS$, 708.1646; (additional peak: 528.10 corresponding to traces of dimer **17**). See appendix.

[(η^5-$Me_4Cp(CH_2)_2$-*N*-Biot)Rh(4,7-diOHPhen)Cl]Cl (**29**)

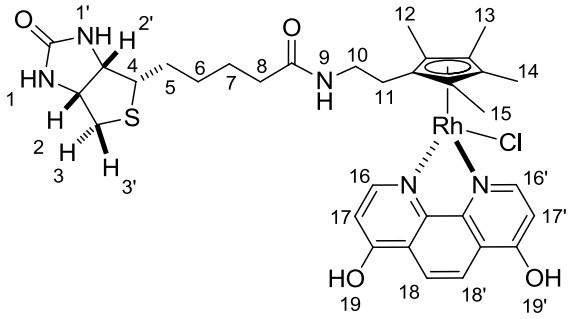

[(η^5-$Me_4Cp(CH_2)_2$-*N*-Biot)$RhCl_2]_2Cl_2$ **17** (30 mg, 26.2 µmol), and 8.97 mg of 4,7-dihydroxy-1,10-phenanthroline (42.3 µmol) were added to anhydrous ACN (6 mL, degassed for 20 min). The mixture was refluxed for 4h. The precipitate was filtered and washed with ACN to yield a brownish powder (17.6 mg, 56.1 % yield).

^{1}H NMR (400 MHz, DMSO-d_6) δ 12.25 (s, 1H, **H$^{19'}$**), 11.83 (s, 1H, **H^{19}**), 8.71 (d, *J* = 4.9 Hz, 1H, **H^{16}**), 8.06-8.04 (m, 1H, **H$^{16'}$**), 7.97 (t, *J* = 6.0 Hz, 1H, **H^{9}**), 7.92-7.89 (m, 2H, **H^{18}**, **H$^{18'}$**), 7.11 (d, *J* = 5.0 Hz, 1H, **H$^{17'}$**), 6.43 (s, 1H, **H$^{1'}$**), 6.37 (s, 1H, **H$^{1'}$**), 6.26 (d, *J* = 7.3 Hz, 1H), 4.33-4.27 (m, 1H, **H^{2}**), 4.15-4.09 (m, 1H, **H$^{2'}$**), 3.21 (dd, *J* = 13.5, 6.9 Hz, 2H, **H^{10}**), 3.09 (dt, *J* = 8.7, 6.2 Hz, 1H, **H^{4}**), 2.82 (dd, *J* = 12.4, 5.1 Hz, 1H, **H$^{3'}$**), 2.58 (d, *J* = 12.4 Hz, 1H, **H^{3}**), 2.26 (t, *J* = 6.9 Hz, 2H, **H^{11}**), 2.03 (t, *J* = 7.4 Hz, 2H, **H^{8}**), 1.68/1.63 (s, 12H, **H^{12}**, **H^{13}**, **H^{14}**, **H^{15}**), 1.72-1.21 (m, 6H, **H^{5}**, **H^{6}**, **H^{7}**). HR-MS (ESI-MS, pos): *m*/*z* = 740.1536 $[M]^+$; calcd. for $C_{33}H_{40}ClN_5O_4RhS$, 740.1544.

The carbon ^{13}C NMR could not be obtained since not enough material was available_See appendix.

7.2. DNA

Oligonucleotides (desalted) were purchased from Microsynth (Switzerland). DNA stocks were dissolved in water and carefully quantified spectrophotometrically at 260 nm. The DNA was then prepared for experiments by heat denaturation at 95°C for 10 minutes, in 375 mM MOPS buffer with KOH (50 mM) at pH 6.5 and allowed to cool down to room temperature. G4A oligonucleotide:[142a] catggtggtttgggttagggttagggttagggttaccac; dsDNA:

ctagctacagagaaatctcga and complementary strand (this dsDNA contained the common Braf V599E oncogenic mutation);[195] trinucleotide: ggg; ss12mer: gag gag aga aga; scrambled G4A (scG4A): gtgagtgttgctgtgtaggtgtagtacgtgtggagtcac.

7.3. Isothermal Titration Calorimetry (ITC).

7.3. Isothermal Titration Calorimetry (ITC).

To study the interaction of **6** embedded in tetrameric Sav with G-quadruplex telomeric DNA (G4A) experiments were carried out at 25°C with in 75 mM MOPS buffer with KOH (10 mM) at pH 6.5 using a VP-ITC titration calorimetry (MicroCal, Northampton, MA, USA). At least two titration experiments were performed for each sample set to evaluate reproducibility. All solutions were thoroughly degassed before use titrations. Before each experiment, the ITC sample cell was washed several times with MOPS buffer solution (containing KOH). The sample cell was loaded with 1.5 ml of G4A solution (25 μM) and the reference cell contained MOPS solution (containing KOH). The titration was carried out using a 300 μL syringe filled with the **6** ⊂ Sav solution or Sav solution, with stirring at 300rpm. The solution **6** ⊂ Sav was made by mixing two equivalents of complex **6** with one equivalent of tetrameric Sav. Injections were started after baseline stability had been achieved. A titration experiment consisted of 50 consecutive injections of 5 μl volume and 10 s duration each, with a 10 min interval between each injection. The titration was carried out with a **6** ⊂ Sav concentration of 0.375 mM or Sav concentration of 0.375 mM. Heats of dilution of **6** ⊂ Sav solution into the buffer alone were used to adjust total observed heats of binding, although the heat released by dilution of **6** ⊂ Sav in MOPS was negligible. Heats of dilution of the complex/protein were determined by injecting **6** ⊂ Sav solution or SAV alone into the buffer and the total observed heats of binding were corrected for the heat of dilution. The resulting data were fitted using MicroCal ORIGIN software supplied with the instrument.

7.4. Electrophoretic Mobility Shift Assays (Work Carried Out by Alessia Sardo)

EMSA were carried out on 1.2 % agarose gels containing ethidium bromide (5 µg per 100 ml of gel) in standard Tris-Borate-EDTA (TBE) buffer. Five hundred nanograms (500 ng) of DNA, previously refolded after heat denaturation, were incubated at 37 °C for 30 min with the desired amount of protein and metal complex mixture to give a final concentration of 3.3 µM oligonucleotide and 75 mM MOPS buffer with KOH (10 mM) at pH 6.5. The protein and metal complex mixtures were prepared by mixing two equivalents of metal complex with one equivalent of tetrameric Sav. After incubation, loading buffer consisting only of 40 % sucrose was added to a final 1/6 of total volume before charging the gels. Electrophoresis was typically carried out at 45 V for 20-30 min. A DNA marker with blue dye (DNA Molecular Weight Marker X, 0.07-12.2 Kb.p., Roche) was used solely for the purpose of confirming similar running conditions between gels. Binding constants were estimated from EMSA by using the concentrations of incubation at which the DNA migrated approximately equally-distributed between the slow mobility (ternary complex) and high mobility (free DNA) species in titration experiments, according to simple visual inspection. One major shifted species was always observed by EMSA, with only small amounts of slower mobility species under specific experimental conditions (*i.e.* when scDNA was used as target; in fully-loaded **6** ⊂ Sav, with four Ru per tetramer; in the presence of competing ssDNA). Values estimated assume in all cases a 1 : 1 stoichiometry. Gels were repeated three times to ensure reproducibility of EMSA titrations. According to the observed single-site binding stoichiometry :

$$K_d = [Sav]_0 - \frac{1}{2}[DNA]_0$$

Where $[Sav]_0$ and $[DNA]_0$ correspond to the initial concentration of Sav and DNA in which DNA was seen to migrate approximately equally-distributed between the slow mobility and fast mobility species. In the case of **6** ⊂ Sav binding to G4A, a 1 : 1 stoichiometry of **6** ⊂ Sav

to DNA target was observed and only an upper estimate of Kd could be determined by EMSA.

7.5. Protein Expression and Purification

7.5.1. Protein Expression and Purification for ATH of Imines (Work Carried Out by Alessia Sardo)

Site-directed mutagenesis was carried out using the Quick-Change mutagenesis kit (Stratagene) on the pET11b-Sav plasmid.[113] Recombinant T7-tagged streptavidin, was expressed in the cytoplasm of Escherichia coli BL21(DE3)pLysS grown in a 10 L fermentor and the protein purified as previously described.[113]

7.5.2. Protein Expression and Purification for Reductive Amination of α-Keto Acids (Work Carried Out by Livia Knörr and Elisa Nogueira)

7.5.2.1. Production and Purification of Recombinant Sav for Pure Proteins

Expressions and purification of Sav mutants as described in Humbert *et al.*[196] and Klein *et al.*[197]

7.5.2.2. Sav Protein Purification in SSP (Work Carried Out by Elisa Nogueira)

The pellet (~3 g from a 50 mL culture) was thawed and resuspended in distilled H_2O (3x wet cell weight). 1 µL of 10 mg/mL DNase I (Roche Diagnostics, Switzerland) and 1 mM phenylmethylsulfonyl fluoride (Applichem, Switzerland) were added and the resuspended cells were incubated first at 37°C for 2 h and then at RT under vigorous shaking until total degradation of nucleic acids. The proteic extract was centrifuged (18 000 x *g*, 30 min, 4°C) to remove cell debris. The pH was adjusted to 9.8 by addition of 5 M Na_2CO_3, pH 9.8 to prepare

the proteic extract for affinity chromatography. A suspension of 2-iminobiotin sepharose (0.5 mL, Affiland, Belgium) which was equilibrated at pH 9.8 (50 mM Na_2CO_3, 0.5 M NaCl), was added to the extract (1.5 mL). Pure streptavidin was eluted with 1 % v/v formic acid. The eluted protein was immediately brought to pH 8.0 using NH_3 (32 %). The purified protein was quantified by Nanodrop (ε = 41.490 M^{-1} cm^{-1}, $MW_{monomer}$ = 16,430 Da), and shock frozen using liquid nitrogen, lyophilized, and stored at 4°C until use.

The protein was resuspended in NH_4COOH and the concentration was confirmed by Nanodrop.

7.6. VMD Docking Studies (Work Carried Out by Maurus Schmid)

The structure of the ligand was optimized with Density Functional Theory (DFT)[198] using Gaussian[199] and the hybrid B3LYP functional.[200] The atomic basis sets consisted of an effective core potential (LanL2DZ)[201] for the metal and the explicit 6-31G(d,p) basis for all remaining atoms.

The optimized structure of the ligand was docked into the protein (PDB code 1MK5) using Autodock Vina. The structure with the best docking score was used subsequently. Simulations were performed in NAMD[202] using the CHARMM27 force-field with custom parameters developed previously (paper in preparation). The metal was treated with a simple bonded model. For the metal binding η^5-carbons, only a bond was assumed, no angular or dihedral parameters were considered. Charges (Mulliken charges) were taken from the DFT calculation above. The system was set using VMD. The protein was mutated to the respective mutant. An additional bond from the metal to the histidine nitrogen Nε was introduced to mimic the histidine bound metal complex. Simulation was carried out using the interactive molecular dynamics plugin (AutoIMD) of VMD. Only the complex and residues within 5 Angstrom were free to move during the simulation. The rest of the atoms were fixed. Interactive molecular dynamics simulations were performed.[203] As a final step, the structure

was minimized. The resulting structure was considered as the docked structure of the complex.

7.7. Catalysis Experiments

All experiments were carried out using standard Schlenk techniques, with thoroughly degassed solutions (nitrogen-flushed).

7.7.1. Preparation of Stock Solutions

Sodium formate (3.4 g, 0.05 mol, 4 M) and MOPS (8.37 g, 0.04 mol, 3.2 M) were dissolved in milli-Q water (12.5 mL) and the pH was adjusted to 5.0 using concentrated HCOOH solution. The isolated biotinylated complexes and the dimeric metal complex **17** and **18** were dissolved in DMSO (0.05 M) and stored under air at 4°C prior to use. For *in situ* complexes, stock solutions of bidentate ligands were prepared in DMSO (0.05 M). A stock solution of the substrate was prepared dissolving 6,7-dimethoxy-1-methyl-3,4-dihydroisoquinoline in milli-Q water to a final concentration of 2 M.

7.7.2. Procedure for the Synthesis of Salsolidine 5 by ATH

7.7.2.1. General Procedure for ATH Performed with Isolated Biotinylated Piano Stool Complexes and *in situ* prepared to be Embedded within Sav Isoforms at pH 5

Streptavidin was directly weighed into the reaction tubes (0.916 mM final biotin binding site concentration). A solution of formate/MOPS (193 µL) from the stock solution was added. The mixture was stirred for 5-10 min until the protein was completely dissolved. The biotinylated complex from the stock solution (2.74 µL, final metal concentration 680 µM; 0.75 equivalents [M] *vs*. Sav free binding sites) was added and the mixture was stirred for 15 min. Finally, the substrate stock solution was added (6.8 µL, final concentration, 68 mM). The test tubes were

placed in a magnetically stirred multireactor (RR 98072, Radleys Discovery Technologies) which was purged three times with nitrogen heated to the appropriate temperature and time.

7.7.2.2. General Procedure for ATH Performed with Hybrid Catalysts 17 ⊂ Sav Isoforms and 18 ⊂ Sav Isoforms

Streptavidin was directly weighed into the reaction tubes (0.916 mM final biotin binding site concentration). A solution of formate/MOPS (192 µL) from the stock solution was added. The mixture was stirred for 5-10 min until the protein was completely dissolved. The dimer precursor complex from the stock solution (1.37 µL, final metal concentration 680 µM; 0.75 equivalents [M] *vs*. Sav free binding sites) was added and the mixture was stirred for 15 min. Finally, the substrate stock solution was added (6.8 µL, final concentration, 68 mM). The test tubes were placed in a magnetically stirred multireactor (RR 98072, Radleys Discovery Technologies) which was purged three times with nitrogen heated to the appropriate temperature and time.

7.7.2.3. General Procedure ATH Performed with *In situ* Complexes to be Embedded within Sav Isoforms at pH 6.5

Streptavidin was directly weighed into the reaction tubes, (0.916 mM final biotin binding site concentration). A solution of formate/MOPS (193 µL) from the stock solution was added. The mixture was stirred for 5-10 min until the protein was completely dissolved. The dimer precursor complex from the stock solution (1.37 µL, final metal concentration, 680 µM; 0.75 equivalents [M] *vs.* Sav free binding sites) was premixed with the bidentate ligand from the stock solution (3.6 µL, final concentration, 900 µM; 1.3 equivalent excess *vs.* metal) The mixture was stirred for 30 min at RT. This premix was then added to the protein solution and stirred for 15 min. Finally, the substrate stock solution was added (6.8 µL, final concentration, 68 mM). The test tubes were placed in a magnetically stirred multireactor (RR 98072,

Radleys Discovery Technologies) which was purged three times with nitrogen heated to the appropriate temperature and time.

7.7.2.4. General Procedure for ATH Performed with 17' ⊂ S112H and 17' ⊂ K121H (Optimized Conditions)

Streptavidin was directly weighed into the reaction tubes, (0.916 mM final biotin binding site concentration). A solution of formate/MOPS (193 µL) from the stock solution was added. The mixture was stirred for 5-10 min until the protein was completely dissolved. The dimer precursor complex from the stock solution was added: For reactions carried out with **17'** ⊂ S112H (1.37 µL, final metal concentration, 680 µM; 0.75 equivalents [Rh] *vs.* Sav free binding sites). Alternatively, reactions carried out with **17'** ⊂ K121H (0.92 µL, final metal concentration, 458 µM; 0.5 equivalents [Rh] *vs.* Sav free binding sites). The reaction mixture was stirred for 15 min. Finally, the substrate stock solution was added: For catalysis experiments performed with **17'** ⊂ S112H (6.8 µL, final concentration, 68 mM) and for catalysis experiments performed with **17'** ⊂ K121 (4.58 µL, final concentration, 45.8 mM). The test tubes were placed in a magnetically stirred multireactor (RR 98072, Radleys Discovery Technologies) which was purged three times with nitrogen heated to the appropriate temperature and time.

7.7.2.5. Sample Workup

After reaction completion, milli-Q water (0.5 mL) and NaOH (60 µL of 20 %) were added to the reaction mixture, which was then extracted 3 times with CH_2Cl_2 (2 mL). The organic phase was dried over Na_2SO_4, filtered with a syringe filter and subjected to HPLC analysis.

7.7.2.6. Analytical Data

The conversion and the *ee* of the reduction products were determined by chiral HPLC using a Chiralpak IC column (20 µm, 250 x 4.5 mm, Daicel Chemical Industries, Tokyo) with CH_2Cl_2/iPrOH/DEA 98:2:0.1 as an eluent at 1 mL/min (UV-detection at 280 nm). The absolute configurations were assigned by comparison with commercial enantiopure samples of (*rac*)-salsolidine **5**:

(R)-6,7-dimethoxy-1-methyl-1,2,3,4-tetrahydroisoquinoline, t = 10.19 min

(S)-6,7-dimethoxy-1-methyl-1,2,3,4-tetrahydroisoquinoline, t = 6.86 min

6,7-dimethoxy-1-methyl-3,4-dihydroisoquinoline, t = 8.37 min

The conversion was determined thanks to the response factor (1.946) reported in previous work carried out by Dr. Thibaud Rossel.[160]

7.7.3. Procedure for the Synthesis of α-Amino Acids by Reductive Amination of α-Keto Acids

7.7.3.1. Preparation of Stock Solutions

Ammonium formate (6.3 g, 0.1 mol, 5 M) were dissolved in milli-Q water (20 mL) and the pH was adjusted to 8.0 using a concentrated ammonia solution (18 M). From the stock solution, the dimer metal complex $[\eta^5\text{-}Me_4Cp\text{-}(CH_2)_2\text{-}N\text{-Biot})RhCl_2]_2$ **17** was dissolved in DMSO (0.05 M) and stored under air at 4°C prior to use. For preformed and *in situ* complexes, stock solutions of bidentate ligands were prepared in DMSO (0.05 M).

7.7.3.2. General Procedure for Reductive Amination Performed with 17' ⊂ S112H and 17' ⊂ K121H

Streptavidin was directly weighed into the reaction tubes, (0.916 mM final biotin binding site concentration). A solution of NH_4COOH (194.5 µL) from the stock was added. The mixture was stirred for 5-10 min until the protein was completely dissolved. The metal complex stock solution was added: for reactions carried out with **17'** ⊂ K121H, 0.92 µL of dimer precursor complex stock solution was added (final metal concentration, 458 µM; 0.5 equivalents [Rh] *vs.* Sav free binding sites); respectively reactions carried out with **17'** ⊂ S112H, 1.37 µL of dimer precursor complex stock solution was added (final metal concentration, 680 µM; 0.75 equivalents [Rh] *vs.* Sav free binding sites). Finally, the substrate solution* was added (4.58 µL, final concentration 45.8 mM). The test tubes were placed in a magnetically stirred multireactor (RR 98072, Radleys Discovery Technologies) which was purged three times with nitrogen heated to the appropriate temperature and time.

*The substrate solution was prepared dissolving α-keto acid in NH_4COOH solution to a final concentration of 2 M and let to stir 1h in order to favor the imine formation.

7.7.3.3. General Procedure for Reductive Amination Performed with *In situ* Prepared Rhodium and Iridium Complexes Embedded Within Sav Isoforms

Streptavidin was directly weighed into the reaction tubes (0.916 mM final biotin binding site concentration). A solution of NH_4COOH (194.5 µL) from the stock was added. The mixture was stirred for 5-10 min until the protein was completely dissolved. The metal complex stock solution was added: 0.92 µL of dimer precursor complex stock solution (final metal concentration, 458 µM; 0.5 equivalents [M] *vs.* Sav free binding sites) was premixed with 3.6 µL bidentate ligand stock solution (final concentration, 900 µM; 1.3 equivalent excess *vs.* metal). The mixture was stirred for 30 min at RT. This premix was then added to the protein solution and stirred for 15 min. Finally, the substrate solution* was added (4.58 µL, final

concentration 45.8 mM). The test tubes were placed in a magnetically stirred multireactor (RR 98072, Radleys Discovery Technologies) which was purged three times with nitrogen heated to the appropriate temperature and time.

7.7.3.4. Sample Workup

After completion, 1.2 mL of MeOH was added to the reaction mixture. The resulting suspension was stirred for 15 min. The mixture was centrifugated and 600 µL of the supernatant was dissolved in a 1:1 ratio with an aqueous solution containing $CuSO_4$ (2mM). The resulting solution was subjected to HPLC analysis.

7.7.3.5. Analytical Data

The conversion, selectivity and the *ee* of the reduction products were determined by chiral HPLC using a Chirex 3126 (*D*)-penicillamine LC Column (5 µm, 50 x 4.6 mm, Phenomenex) with different eluents depending on the α-keto acid. The yield was calculated by multiplying the selectivity by the conversion.

7.7.3.5.1. Phenylalanine

HPLC method (see Table 21: Line A ($MeOH/H_2O/CuSO_4$: 80/20/2mM) and in Line B ($H_2O/CuSO_4$, 2mM). A gradient method allowed separation of (*rac*)-phenylalanine **34**, phenylpyruvic acid **36** and (*rac*)-phenyllactic acid **35** at 1.25 mL/min with a column heated at 40°C (UV-detection at 247 nm).

Table 21 HPLC method for the reductive amination of phenylpyruvic acid **36**.

Time (min)	Line A (%)	Line B (%)
0.00	22	78
12.00	22	78
14.00	37	63
40.00	37	63

The absolute configurations were assigned by comparison with commercial enantiopure samples:

-(*S*)-phenylalanine t = 7.51 min

-(*R*)-phenylalanine t = 10.11 min

-phenylpyruvic acid t = 5.93 min

-(*S*)-phenyllactic acid t = 27.79 min

-(*R*)-phenyllactic acid t = 33.58 min

Calibration curve: to determine the conversion, a response factor was determined, taking into account the different UV responses of the α-keto acids and the amino acids. Therefore; 3 mg of phenylpyruvic acid **36** and 3 mg of (*rac*)-phenylalanine **34** were dissolved in 3 mL of an aqueous solution containing $CuSO_4$ (2mM). Different molar ratios of keto acid and amino acid were prepared and subjected to HPLC analysis. The ratio of the peak areas keto acid/amino acid was plotted against the molar ratio keto acid/amino acid. The slope of the regression line allows the determination of the response factor.

Table 22 Conditions used to determine the response factor between phenylpyruvic acid **36** and (*rac*)-phenylalanine **34**.

Area of **36**	Area of **34**	Concentration of **36** (mM)	Concentration of **34** (mM)
2671	529	3.04	0.37
1212	1050	1.52	0.75
550	1930	0.76	1.51
369	3549	0.38	3.02

Response factor for phenylalanine at 247 nm: 1.6021.

The same procedure was applied to the keto acid and the (*rac*)-hydroxy acid. Therefore, 3 mg of phenylpyruvic acid **36** and (*rac*)-phenyllactic acid **35** were dissolved in 3 mL of an aqueous solution containing $CuSO_4$ (2 mM). Different molar ratios of keto acid and amino acid were prepared and subjected to HPLC analysis. The ratio of the peak areas hydroxy acid/keto acid was plotted against the molar ratio hydroxy acid/keto acid. The slope of the regression line allows determining the response factor.

Table 23 Conditions used to determine the response factor between phenylpyruvic acid **36** and (*rac*)-phenyllactic acid **35**.

Area of **36**	Area of **35**	Concentration of **36** (mM)	Concentration of **35** (mM)
2671	743	3.05	0.38
1212	1423	1.52	0.75
550	2727	0.76	1.50
369	4888	0.38	3.01

Response factor for phenyllactic acid at 247 nm: 2.2601.

7.7.3.5.2. Phenylglycine

HPLC method (see Table 24): Line A ($MeOH/H_2O/CuSO_4$: 80/20/2mM) and in Line B ($H_2O/CuSO_4$, 2 mM). A gradient method allowed separation of (*rac*)-phenylglycine **37**, benzoylformic acid **36** and (*rac*)-mandelic acid **38** at 1.25 mL/min with a column heated at 40°C (UV-detection at 247 nm).

Table 24 HPLC method for the reductive amination of benzoylformic acid **36**.

Time (min)	Line A (%)	Line B (%)
0.00	22	78
12.00	22	78
15.00	37	63
25.00	37	63

The absolute configurations were assigned by comparison with commercial enantiopure samples:

(*S*)-phenylglycine t = 2.90 min

(*R*)-phenylglycine t = 4.44 min

benzoylformic acid t = 7.71 min

(*S*)- mandelic acid t = 18.57 min

(*R*)-mandelic acid t = 23.36 min

Undetermined impurity t = 11.02 min

Calibration curve: to determine the conversion, a response factor was determined, taking into account the different UV responses for the keto acid and the amino acid. Therefore, 3.2 mg of benzoylformic acid **36** were dissolved in 3.2 mL of an aqueous solution containing $CuSO_4$ (2 mM) and 3 mg of (*rac*)-phenylglycine **37** were dissolved in 13 mL of an aqueous solution containing $CuSO_4$ (2 mM). Different molar ratios of keto acid and amino acid were prepared

and subjected to HPLC analysis. The ratio of the peak areas hydroxy acid/keto acid was plotted against the molar ratio hydroxy acid/keto acid. The slope of the regression line allows the determination of the response factor.

Table 25 Conditions used to determine the response factor between benzoylformic acid **36** and (*rac*)-phenylglycine **37**.

Area of **36**	Area of **37**	Concentration of **36** (mM)	Concentration of **37** (mM)
97322	618	6.66	0.19
51583	1203	3.33	0.38
25985	2441	1.67	0.76
8678	4868	0.83	1.53

Response factor for phenylglycine at 247 nm: 0.2222.

To determine the selectivity, a response factor was determined, taking into account the different UV responses for the keto acid and the (*rac*)-hydroxy acid. Therefore, 3.2 mg of benzoylformic acid **36** were dissolved in 3.2 mL of an aqueous solution containing $CuSO_4$ (2 mM) and 2.5 mg of (*rac*)-mandelic acid **38** were dissolved in 2.5 mL of an aqueous solution containing $CuSO_4$ (2 mM). Different molar ratios of keto acid and (*rac*)-hydroxy acid were prepared and subjected to HPLC analysis. The ratio of the peak areas hydroxy acid/keto acid was plotted against the molar ratio hydroxy acid/keto acid. The slope of the regression line allowed the determination of the response factor.

Table 26 Conditions used to determine the response factor between phenylpyruvic acid **36** and (*rac*)-mandelic acid **38**.

Area of **36**	Area of **38**	Concentration of **36** (mM)	Concentration of **38** (mM)
97323	2171	6.66	0.82
51583	4359	3.33	1.64
25985	8793	1.67	3.29
8678	17476	0.83	6.57

Response factor for mandelic acid at 247 nm: 0.1810.

8. Bibliography

[1] a) R. H. Fish, G. Jaouen, *Organometallics* **2003**, *22*, 2166-2177; b) J. Halpern, *Pure Appl. Chem.* **2001**, *73*, 209-220.

[2] H. Brunner, *Angew. Chem., Int. Ed.* **1999**, *38*, 1194-1208.

[3] a) H. Brunner, *Eur. J. Inorg. Chem.* **2001**, 905-912; b) C. Ganter, *Chem. Soc. Rev.* **2003**, *32*, 130-138.

[4] a) K. B. Sharpless, *Angew. Chem., Int. Ed. Engl.* **2002**, *41*, 2024-2032; b) R. Noyori, *Angew. Chem., Int. Ed. Engl.* **2002**, *41*, 2008-2022; c) W. S. Knowles, *Angew. Chem., Int. Ed. Engl.* **2002**, *41*, 1998-2007.

[5] L. Liu, D. Wang, in *Handbook of Green Chemistry*, Wiley-VCH Verlag GmbH & Co. KGaA, **2010**.

[6] G. Gasser, I. Ott, N. Metzler-Nolte, *J. Med. Chem.* **2010**, *54*, 3-25.

[7] a) S. Hashiguchi, A. Fujii, J. Takehara, T. Ikariya, R. Noyori, *J. Am. Chem. Soc.* **1995**, *117*, 7562-7563; b) R. Noyori, S. Hashiguchi, *Acc. Chem. Res.* **1997**, *30*, 97-102.

[8] a) P. Kacer, M. Kuzma, E. Leitmannova, L. Cerveny, Nova Science Publishers, Inc., **2010**, 373-401; b) R. Noyori, S. Hashiguchi, *Acc. Chem. Res.* **1997**, *30*, 97-102.

[9] a) X. Wu, X. Li, A. Zanotti-Gerosa, A. Pettman, J. Liu, A. J. Mills, J. Xiao, *Chem. Eur. J.* **2008**, *14*, 2209-2222; b) A. Robertson, T. Matsumoto, S. Ogo, *Dalton Trans.* **2011**, *40*, 10304-10310.

[10] a) R. Kawahara, K.-i. Fujita, R. Yamaguchi, *Adv. Synth. Catal.* **2011**, *353*, 1161-1168; b) K. Fujita, T. Fujii, R. Yamaguchi, *Org. Lett.* **2004**, *6*, 3525-3528; c) O. Saidi, A. J. Blacker, M. M. Farah, S. P. Marsden, J. M. J. Williams, *Chem. Commun.* **2010**, *46*, 1541-1543.

[11] a) T. P. Brewster, J. D. Blakemore, N. D. Schley, C. D. Incarvito, N. Hazari, G. W. Brudvig, R. H. Crabtree, *Organometallics* **2011**, *30*, 965-973; b) J. F. Hull, D. Balcells, J. D. Blakemore, C. D. Incarvito, O. Eisenstein, G. W. Brudvig, R. H. Crabtree, *J. Am. Chem. Soc.* **2009**, *131*, 8730-8731.

[12] a) K.-i. Fujita, T. Yoshida, Y. Imori, R. Yamaguchi, *Org. Lett.* **2011**, *13*, 2278-2281; b) T. Suzuki, T. Matsuo, K. Watanabe, T. Katoh, *Synlett* **2005**, 1453-1455.

[13] A. Levina, A. Mitra, P. A. Lay, *Metallomics* **2009**, *1*, 458-470.

[14] Z. Liu, A. Habtemariam, A. M. Pizarro, S. A. Fletcher, A. Kisova, O. Vrana, L. Salassa, P. C. A. Bruijnincx, G. J. Clarkson, V. Brabec, P. J. Sadler, *J. Med. Chem.* **2011**, *54*, 3011-3026.

[15] T. R. Ward, *Acc. Chem. Res.* **2011**, *44*, 47-57.

[16] a) G. Sava, A. Bergamo, S. Zorzet, B. Gava, C. Casarsa, M. Cocchietto, A. Furlani, V. Scarcia, B. Serli, E. Iengo, E. Alessio, G. Mestroni, *Eur. J. Cancer* **2002**, *38*, 427-435; b) J. M. Rademaker-Lakhai, D. van den Bongard, D. Pluim, J. H. Beijnen, J. H. M. Schellens, *Clin. Cancer Res.* **2004**, *10*, 3717-3727; c) A. Bergamo, R. Gagliardi, V. Scarcia, A. Furlani, E. Alessio, G. Mestroni, G. Sava, *J. Pharmacol. Exp. Ther.* **1999**, *289*, 559; d) G. Sava, I. Capozzi, K. Clerici, G. Gagliardi, E. Alessio, G. Mestroni, *Clin. Exp. Metastasis* **1998**, *16*, 371-379; e) L. Morbidelli, S. Donnini, S. Filippi, L. Messori, F. Piccioli, P. Orioli, G. Sava, M. Ziche, *Br. J. Cancer* **2003**, *88*, 1484-1491; f) B. K. Keppler, W. Rupp, U. M. Juhl, H. Endres, R. Niebl, W. Balzer, *Inorg. Chem.* **1987**, *26*, 4366-4370; g) C. G. Hartinger, M. A. Jakupec, S. Zorbas-Seifried, M. Groessl, A. Egger, W. Berger, H. Zorbas, P. J. Dyson, B. K. Keppler, *Chem. Biodiversity* **2008**, *5*, 2140-2155; h) T. Pieper, K. Borsky, B. K. Keppler, *Top. Biol. Inorg. Chem.* **1999**, *1*, 171.

[17] A. Bergamo, G. Sava, *Dalton Trans.* **2011**, *40*, 7817-7823.

[18] I. Kostova, *Curr. Med. Chem.* **2006**, *13*, 1085-1107.

[19] L. D. Dale, J. H. Tocher, T. M. Dyson, D. I. Edwards, D. A. Tocher, *Anti-Cancer Drug Des.* **1992**, *7*, 3-14.

[20] a) W. H. Ang, A. Casini, G. Sava, P. J. Dyson, *J. Organomet. Chem.* **2011**, *696*, 989-998; b) S. J. Dougan, P. J. Sadler, *Chimia* **2007**, *61*, 704-715.

[21] a) A. F. A. Peacock, P. J. Sadler, *Chem.--Asian J.* **2008**, *3*, 1890-1899; b) E. Reisner, V. B. Arion, B. K. Keppler, A. J. L. Pombeiro, *Inorg. Chim. Acta* **2008**, *361*, 1569-1583.

[22] W. H. Ang, *Chimia* **2007**, *61*, 140-142.
[23] Y. K. Yan, M. Melchart, A. Habtemariam, P. J. Sadler, *Chem. Commun.* **2005**, 4764-4776.
[24] a) P. C. A. Bruijnincx, P. J. Sadler, *Curr. Opin. Chem. Biol.* **2008**, *12*, 197-206; b) F. Wang, J. Xu, A. Habtemariam, J. Bella, P. J. Sadler, *J. Am. Chem. Soc.* **2005**, *127*, 17734-17743; c) F. Wang, A. Habtemariam, E. P. L. van der Geer, R. Fernández, M. Melchart, R. J. Deeth, R. Aird, S. Guichard, F. P. A. Fabbiani, P. Lozano-Casal, I. D. H. Oswald, D. I. Jodrell, S. Parsons, P. J. Sadler, *Proc. Natl. Acad. Sci. U.S.A.* **2005**, *102*, 18269-18274; d) T. Bugarcic, A. Habtemariam, J. Stepankova, P. Heringova, J. Kasparkova, R. J. Deeth, R. D. L. Johnstone, A. Prescimone, A. Parkin, S. Parsons, V. Brabec, P. J. Sadler, *Inorg. Chem.* **2008**, *47*, 11470-11486.
[25] A. Habtemariam, M. Melchart, R. Fernández, S. Parsons, I. D. H. Oswald, A. Parkin, F. P. A. Fabbiani, J. E. Davidson, A. Dawson, R. E. Aird, D. I. Jodrell, P. J. Sadler, *J. Med. Chem.* **2006**, *49*, 6858-6868.
[26] a) R. Fernández, M. Melchart, A. Habtemariam, S. Parsons, P. J. Sadler, *Chem. Eur. J.* **2004**, *10*, 5173-5179; b) C. Scolaro, A. Bergamo, L. Brescacin, R. Delfino, M. Cocchietto, G. Laurenczy, T. J. Geldbach, G. Sava, P. J. Dyson, *J. Med. Chem.* **2005**, *48*, 4161-4171; c) C. Scolaro, A. B. Chaplin, C. G. Hartinger, A. Bergamo, M. Cocchietto, B. K. Keppler, G. Sava, P. J. Dyson, *Dalton Trans.* **2007**, *43*, 5065.
[27] a) O. Novakova, H. Chen, O. Vrana, A. Rodger, P. J. Sadler, V. Brabec, *Biochemistry* **2003**, *42*, 11544-11554; b) H.-K. Liu, F. Wang, J. A. Parkinson, J. Bella, P. J. Sadler, *Chem. Eur. J.* **2006**, *12*, 6151-6165.
[28] S. Neidle, *Nucleic Acid Structure and Recognition*, Oxford University Press, **2001**.
[29] R. E. Aird, J. Cummings, A. A. Ritchie, M. Muir, R. E. Morris, H. Chen, P. J. Sadler, D. I. Jodrell, *Br. J. Cancer* **2002**, *86*, 1652-1657.
[30] F. Wang, J. Bella, J. Parkinson, P. Sadler, *J. Biol. Inorg. Chem.* **2005**, *10*, 147-155.
[31] J. Reedijk, *Proc. Natl. Acad. Sci. U.S.A.* **2003**, *100*, 3611.
[32] S. Betanzos-Lara, A. Habtemariam, G. J. Clarkson, P. J. Sadler, *Eur. J. Inorg. Chem.* **2011**, *2011*, 3257-3264.
[33] C. Gossens, A. Dorcier, P. J. Dyson, U. Rothlisberger, *Organometallics* **2007**, *26*, 3969-3975.
[34] a) P. J. Dyson, *Chimia* **2007**, *61*, 698-703; b) A. Bergamo, A. Masi, P. J. Dyson, G. Sava, *Int. J. Oncol.* **2008**, *33*, 1281-1289.
[35] A. Casini, G. Mastrobuoni, W. H. Ang, C. Gabbiani, G. Pieraccini, G. Moneti, P. J. Dyson, L. Messori, *ChemMedChem* **2007**, *2*, 631-635.
[36] A. Casini, C. Gabbiani, F. Sorrentino, M. P. Rigobello, A. Bindoli, T. J. Geldbach, A. Marrone, N. Re, C. G. Hartinger, P. J. Dyson, L. Messori, *J. Med. Chem.* **2008**, *51*, 6773-6781.
[37] S. Chatterjee, S. Kundu, A. Bhattacharyya, C. Hartinger, P. Dyson, *J. Biol. Inorg. Chem.* **2008**, *13*, 1149-1155.
[38] G. Suss-Fink, *Dalton T* **2010**, *39*, 1673-1688.
[39] W. H. Ang, E. Daldini, L. Juillerat-Jeanneret, P. J. Dyson, *Inorg. Chem.* **2007**, *46*, 9048-9050.
[40] W. H. Ang, E. Daldini, C. Scolaro, R. Scopelliti, L. Juillerat-Jeannerat, P. J. Dyson, *Inorg. Chem.* **2006**, *45*, 9006.
[41] C. Sanchez-Cano, M. J. Hannon, *Dalton Trans.* **2009**, 10702-10711.
[42] H.-K. Liu, P. J. Sadler, *Acc. Chem. Res.* **2011**, *44*, 349-359.
[43] X. Cai, P. J. Gray Jr, D. D. Von Hoff, *Cancer Treat. Rev.* **2009**, *35*, 437-450.
[44] B. M. Zeglis, V. C. Pierre, J. K. Barton, *Chem. Commun.* **2007**, 4565-4579.
[45] P. J. Perry, T. C. Jenkins, *Expert Opin. Ther. Pat.* **1999**, *8*, 1981-2008.
[46] a) E. H. Blackburn, *Nature* **2000**, *408*, 53-56; b) J. Karlseder, A. Smogorzewska, T. de Lange, *Science* **2002**, *295*, 2446-2449; c) H. Takai, A. Smogorzewska, T. de Lange, *Curr. Biol.* **2003**, *13*, 1549-1556; d) T. De Lange, *Cold Spring Harbor Symposia on Quantitative Biology* **2005**, *70*, 197-204.
[47] T. de Lange, *Oncogene* **2002**, *21*, 532-540.
[48] J. W. Shay, W. E. Wright, *Nat. Rev. Mol. Cell Biol.* **2000**, *1*, 72-76.
[49] J. A. Londoño-Vallejo, *Biochimie* **2008**, *90*, 73-82.

[50] N. Kim, M. Piatyszek, K. Prowse, C. Harley, M. West, P. Ho, G. Coviello, W. Wright, S. Weinrich, J. Shay, *Science* **1994**, *266*, 2011-2015.
[51] N. H. Campbell, G. N. Parkinson, *Methods* **2007**, *43*, 252-263.
[52] G. N. Parkinson, M. P. H. Lee, S. Neidle, *Nature* **2002**, *417*, 876-880.
[53] Y. Wang, D. J. Patel, *Structure* **1993**, *1*, 263-282.
[54] a) A. T. Phan, V. Kuryavyi, K. N. Luu, D. J. Patel, *Nucleic Acids Res.* **2007**, *35*, 6517-6525; b) K. N. Luu, A. T. Phan, V. Kuryavyi, L. Lacroix, D. J. Patel, *J. Am. Chem. Soc.* **2006**, *128*, 9963-9970.
[55] A. Arola, R. Vilar, *Curr. Top. Med. Chem.* **2008**, *8*, 1405-1415.
[56] a) J. T. Davis, *Angew. Chem. Int. Ed. Engl.* **2004**, *43*, 668-698; b) S. Burge, G. N. Parkinson, P. Hazel, A. K. Todd, S. Neidle, *Nucleic Acids Res.* **2006**, *34*, 5402-5415.
[57] A. M. Zahler, J. R. Williamson, T. R. Cech, D. M. Prescott, *Nature* **1991**, *350*, 718-720.
[58] J.-L. Mergny, J.-F. Riou, P. Mailliet, M.-P. Teulade-Fichou, E. Gilson, *Nucleic Acids Res.* **2002**, *30*, 839-865.
[59] R. Noyori, T. Ohkuma, *Angew. Chem., Int. Ed.* **2001**, *40*, 40.
[60] a) H. Meerwein, R. Schmidt, *Justus Liebigs Ann. Chem.* **1925**, *444*, 221-238; b) A. Verley, *Bull. Soc. Chim. Fr.* **1925**, *37*, 537-542; c) W. Ponndorf, *Angew. Chem., Int. Ed.* **1926**, *39*, 138-143.
[61] a) T. Ikariya, K. Murata, R. Noyori, *Org. Biomol. Chem.* **2006**, *4*, 393; b) S. Gladiali, E. Alberico, *Chem. Soc. Rev.* **2006**, *35*, 226-236; c) J. S. M. Samec, J.-E. Backvall, P. G. Andersson, P. Brandt, *Chem. Soc. Rev.* **2006**, *35*, 237-248; d) K. Everaere, A. Mortreux, J.-F. Carpentier, *Adv. Synth. Catal.* **2003**, *345*, 67-77; e) H.-U. Blaser, C. Malan, B. Pugin, F. Spindler, H. Steiner, M. Studer, *Adv. Synth. Catal.* **2003**, *345*, 103-151; f) C. Wang, X. F. Wu, J. L. Xiao, *Chem. Asian J.* **2008**, *3*, 1750-1770; g) O. Saidi, J. M. J. Williams, *Topics in Organometallic Chemistry* **2011**, *34*, 77-106.
[62] X. Wu, J. Xiao, *Chem. Commun.* **2007**, 2449-2466.
[63] C. Bubert, J. Blacker, S. M. Brown, J. Crosby, S. Fizjohn, J. P. Muxworthy, T. Thorpe, J. M. J. Williams, *Tetrahedron Lett.* **2001**, *42*, 4037-4039.
[64] S. Ogo, T. Abura, Y. Watanabe, *Organometallics* **2002**, *21*, 2964-2969.
[65] X. Wu, X. Li, F. King, J. Xiao, *Angew. Chem. Int. Ed.* **2005**, *44*, 3407-3411.
[66] a) S. E. Clapham, A. Hadzovic, R. H. Morris, *Coord. Chem. Rev.* **2004**, *248*, 2201-2237; b) R. Noyori, M. Yamakawa, S. Hashiguchi, *J. Org. Chem.* **2001**, *66*, 7931-7944; c) O. Pàmies, J.-E. Bäckvall, *Chem. Eur. J.* **2001**, *7*, 5052-5058.
[67] M. Yamakawa, H. Ito, R. Noyori, *J. Am. Chem. Soc.* **2000**, *122*, 1466-1478.
[68] S. Gladiali, R. Taras, in *Modern Reduction Methods*, Wiley-VCH Verlag GmbH & Co. KGaA, **2008**, 135-157.
[69] a) M. Breuer, K. Ditrich, T. Habicher, B. Hauer, M. Keßeler, R. Stürmer, T. Zelinski, *Angew. Chem. Int. Ed. Engl.* **2004**, *43*, 788-824; b) U. T. Bornscheuer, M. Hohn, *Chemcatchem* **2009**, *1*, 42-51.
[70] a) F. Fache, E. Schulz, M. L. Tommasino, M. Lemaire, *Chem. Rev.* **2000**, *100*, 2159-2231; b) Y.-M. He, Q.-H. Fan, *Org. Biomol. Chem.* **2010**, *8*, 2497-2504; c) Y. Gnas, F. Glorius, *Synthesis* **2006**, 1899-1930; d) J. Brazier, N. Tomkinson, *Vol. 291* (Ed.: B. List), Springer Berlin / Heidelberg, **2009**, 281-347.
[71] R. Grigg, T. R. B. Mitchell, N. Tongpenyai, *Synthesis* **1981**, *1981*, 442,444.
[72] H. A. Brune, J. Unsin, R. Hemmer, M. Reichhardt, *J. Organomet. Chem.* **1989**, *369*, 335-342.
[73] C. P. Casey, S. W. Singer, D. R. Powell, R. K. Hayashi, M. Kavana, *J. Am. Chem. Soc.* **2001**, *123*, 1090.
[74] a) J. S. M. Samec, J.-E. Backvall, *Chem. Eur. J.* **2002**, *8*, 2955-2961; b) C. P. Casey, J. B. Johnson, *J. Am. Chem. Soc.* **2005**, *127*, 1883-1894.
[75] N. Uematsu, A. Fujii, S. Hashiguchi, T. Ikariya, R. Noyori, *J. Am. Chem. Soc.* **1996**, *118*, 4916-4917.
[76] a) C. Q. Li, J. L. Xiao, *J. Am. Chem. Soc.* **2008**, *130*, 13208-13209; b) L. Evanno, J. Ormala, P. M. Pihko, *Chem. Eur. J.* **2009**, *15*, 12963-12967; c) N. Fleury-Bregeot, V. de la Fuente, S. Castillon, C. Claver, *Chemcatchem* **2010**, *2*, 1346-1371; d) T. C. Nugent, M. El-Shazly, *Adv. Synth. Catal.*

2010, *352*, 753-819; e) M. Wills, *Imino Reductions by Transfer Hydrogenation*, Wiley-VCH Verlag GmbH & Co. KGaA, **2008**; f) J. Mao, D. C. Baker, *Org. Lett.* **1999**, *1*, 841-843.

[77] J. S. Wu, F. Wang, Y. P. Ma, X. C. Cui, L. F. Cun, J. Zhu, J. G. Deng, B. L. Yu, *Chem. Commun.* **2006**, 1766-1768.

[78] J. Canivet, G. Suss-Fink, *Green Chemistry* **2007**, *9*, 391-397.

[79] C. Wang, C. Q. Li, X. F. Wu, A. Pettman, J. L. Xiao, *Angew. Chem., Int. Ed.* **2009**, *48*, 6524-6528.

[80] a) J. B. Aberg, J. S. M. Samec, J.-E. Backvall, *Chem. Commun.* **2006**, 2771-2773; b) C. P. Casey, T. B. Clark, I. A. Guzei, *J. Am. Chem. Soc.* **2007**, *129*, 11821-11827; c) D. G. Blackmond, M. Ropic, M. Stefinovic, *Org. Process Res. Dev.* **2006**, *10*, 457-463.

[81] a) R. M. Bullock, *Chem. Eur. J.* **2004**, *10*, 2366-2374; b) C. Wang, B. Villa-Marcos, J. Xiao, *Chem. Commun.* **2011**, *47*, 9773-9785.

[82] a) K.-J. Haack, S. Hashiguchi, A. Fujii, T. Ikariya, R. Noyori, *Angew. Chem., Int. Ed.* **1997**, *36*, 285-288; b) D. A. Alonso, P. Brandt, S. J. M. Nordin, P. G. Andersson, *J. Am. Chem. Soc.* **1999**, *121*, 9580-9588.

[83] C. Wang, A. Pettman, J. Basca, J. Xiao, *Angew. Chem., Int. Ed.* **2010**, *49*, 7548-7552, S7548/7541-S7548/7129.

[84] J. E. D. Martins, G. J. Clarkson, M. Wills, *Org. Lett.* **2009**, *11*, 847-850.

[85] A. B. Hughes, Editor, *Amino Acids, Peptides And Proteins In Organic Chemistry, Volume 1 - Origins And Synthesis Of Amino Acids*, Wiley-VCH Verlag GmbH & Co. KGaA, **2009**.

[86] S. V. Bhat, B. A. Nagasampagi, M. Sivakumar, *Chemistry of natural products*, Springer Verlag ; Narosa Publishing House, **2005**.

[87] Y. S. Tsantrizos, *Acc. Chem. Res.* **2008**, *41*, 1252-1263.

[88] a) Vadim A. Soloshonok, K. Izawa, *Asymmetric Synthesis and Application of α-Amino Acids, Vol. 1009*, American Chemical Society, **2009**; b) W. M. Robert, C. M.Burnett, in *Asymmetric Synthesis and Application of α-Amino Acids, Vol. 1009*, American Chemical Society, **2009**, 420-442; c) L.-W. Xu, Y. Lu, *Org Biomol Chem* **2008**, *6*, 2047-2053; d) J. Kaiser, S. S. Kinderman, B. C. J. van Esseveldt, F. L. van Delft, H. E. Schoemaker, R. H. Blaauw, F. P. J. T. Rutjes, *Org. Biomol. Chem.* **2005**, *3*, 3435-3467; e) D. B. Jose L. Vicario, Luisa Carrillo, Efraim Reyes, Juan Etxebarria, *Curr. Org. Chem.* **2005**, *9*, 219-235; f) L. Wang, P. G. Schultz, *Angew. Chem. Int. Ed. Engl.* **2005**, *44*, 1-1; g) G. Helmchen, A. Pfaltz, *Acc. Chem. Res.* **2000**, *33*, 336-345; h) F. P. J. T. Rutjes, L. B. Wolf, H. E. Schoemaker, *J. Chem. Soc., Perkin Trans. 1* **2000**, 4197-4212; i) F. J. Sardina, H. Rapoport, *Chem. Rev.* **1996**, *96*, 1825-1872.

[89] D. J. Ager*, Vol. 1*, Wiley-VCH Verlag GmbH & Co. KGaA, **2009**, 495-526.

[90] A. Menzel, H. Werner, J. Altenbuchner, H. Gröger, *Engineering in Life Sciences* **2004**, *4*, 573-576.

[91] A. S. Bommarius*, Vol. 3*, Wiley-VCH Verlag GmbH, **2002**, 1047-1063.

[92] P. H. Boyle, A. P. Davis, K. J. Dempsey, G. D. Hosken, *Tetrahedron: Asymmetry* **1995**, *6*, 2819-2828.

[93] D. A. Evans, T. C. Britton, *J. Am. Chem. Soc.* **1987**, *109*, 6881-6883.

[94] H. Gröger, *Chem. Rev.* **2003**, *103*, 2795-2828.

[95] C. Nájera, J. M. Sansano, *Chem. Rev.* **2007**, *107*, 4584-4671.

[96] E. R. Jarvo, S. J. Miller, *Tetrahedron* **2002**, *58*, 2481-2495.

[97] a) D. Imao, S. Fujihara, T. Yamamoto, T. Ohta, Y. Ito, *Tetrahedron* **2005**, *61*, 6988-6992; b) L. Xing, C. Cheng, R. Zhu, B. Zhang, X. Wang, Y. Hu, *Tetrahedron* **2008**, *64*, 11783-11788; c) N. Azizi, E. Akbari, A. K. Amiri, M. R. Saidi, *Tetrahedron Lett.* **2008**, *49*, 6682-6684; d) P. S. Reddy, S. Kanjilal, S. Sunitha, R. B. N. Prasad, *Tetrahedron Lett.* **2007**, *48*, 8807-8810; e) A. Heydari, S. Khaksar, J. Akbari, M. Esfandyari, M. Pourayoubi, M. Tajbakhsh, *Tetrahedron Lett.* **2007**, *48*, 1135-1138; f) C. D. Gutierrez, V. Bavetsias, E. McDonald, *Tetrahedron Lett.* **2005**, *46*, 3595-3597; g) M. Beller, M. Eckert, *Angew. Chem. Int. Ed. Engl.* **2000**, *39*, 1010-1027; h) J. Martens, *Chemcatchem* **2010**, *2*, 379-381.

[98] a) W. S. Emerson, *Organic Reactions* **1947**, *4*, 174-255; b) M. L. Moore, *Organic Reactions* **1948**, *5*, 301-330; c) A. F. AbdelMagid, K. G. Carson, B. D. Harris, C. A. Maryanoff, R. D. Shah, *J. Org. Chem.* **1996**, *61*, 3849-3862.

[99] a) L. Mark'o, J. Bakos, *J. Organomet. Chem.* **1974**, *81*, 411-414; b) M. V. Klyuev, M. L. Khidekel, *Transition Metal Chemistry* **1980**, *5*, 134-139.

[100] H.-U. Blaser, *Rend. Fis. Acc. Lincei* **2007**, *18*, 281-304.

[101] H.-U. Blaser, H.-P. Buser, H.-P. Jalett, B. Pugin, F. Spindler, *Synlett* **1999**, *1999*, 867,868.

[102] Y. Chi, Y.-G. Zhou, X. Zhang, *J. Org. Chem.* **2003**, *68*, 4120-4122.

[103] a) R. Kadyrov, T. H. Riermeier, *Angew. Chem., Int. Ed.* **2003**, *115*, 5630-5632; b) V. I. Tararov, R. Kadyrov, T. H. Riermeier, C. Fischer, A. Börner, *Adv. Synth. Catal.* **2004**, *346*, 561-565.

[104] C. Li, B. Villa-Marcos, J. Xiao, *J. Am. Chem. Soc.* **2009**, *131*, 6967-6969.

[105] K. Harada*, Vol. 5*, Academic, **1985**, 345-383.

[106] V. I. Tararov, R. Kadyrov, T. H. Riermeier, A. Borner, *Chem. Commun.* **2000**, 1867-1868.

[107] S. Ogo, K. Uehara, T. Abura, S. Fukuzumi, *J. Am. Chem. Soc.* **2004**, *126*, 3020-3021.

[108] J. Steinreiber, T. R. Ward, *Coord. Chem. Rev.* **2008**, *252*, 751-766.

[109] G. Roelfes, *Mol. Biosyst.* **2007**, *3*, 126-135.

[110] Y. Lu, N. Yeung, N. Sieracki, N. M. Marshall, *Nature* **2009**, *460*, 855-862.

[111] W. F. DeGrado, C. M. Summa, V. Pavone, F. Nastri, A. Lombardi, *Annu. Rev. Biochem.* **1999**, *68*, 779-819.

[112] L. Jiang, E. A. Althoff, F. R. Clemente, L. Doyle, D. Röthlisberger, A. Zanghellini, J. L. Gallaher, J. L. Betker, F. Tanaka, C. F. Barbas, 3rd, D. Hilvert, K. N. Houk, B. L. Stoddard, D. Baker, *Science* **2008**, *319*, 1387-1391.

[113] M. Creus, A. Pordea, T. Rossel, A. Sardo, C. Letondor, A. Ivanova, I. Le_Trong, R. E. Stenkamp, T. R. Ward, *Angew. Chem., Int. Ed.* **2008**, *47*, 1400-1407.

[114] a) M. Ohashi, T. Koshiyama, T. Ueno, M. Yanase, H. Fujii, Y. Watanabe, *Angew. Chem., Int. Ed.* **2003**, *42*, 1005-1008; b) A. Mahammed, Z. Gross, *J. Am. Chem. Soc.* **2005**, *127*, 2883-2887.

[115] a) Q. Jing, K. Okrasa, R. J. Kazlauskas, *Chem. Eur. J.* **2009**, *15*, 1370-1376; b) A. Fernández-Gacio, A. Codina, J. Fastrez, O. Riant, P. Soumillion, *ChemBioChem* **2006**, *7*, 1013-1016.

[116] E. Kaiser, D. Lawrence, *Science* **1984**, *226*, 505-511.

[117] J. R. Carey, S. K. Ma, T. D. Pfister, D. K. Garner, H. K. Kim, J. A. Abramite, Z. Wang, Z. Guo, Y. Lu, *J. Am. Chem. Soc.* **2004**, *126*, 10812-10813.

[118] a) T. Ueno, T. Koshiyama, M. Ohashi, K. Kondo, M. Kono, A. Suzuki, T. Yamane, Y. Watanabe, *J. Am. Chem. Soc.* **2005**, *127*, 6556-6562; b) T. Ueno, T. Koshiyama, S. Abe, N. Yokoi, M. Ohashi, H. Nakajima, Y. Watanabe, *J. Organomet. Chem.* **2007**, *692*, 142-147.

[119] M. Skander, C. Malan, A. Ivanova, T. R. Ward, *Chem. Commun.* **2005**, 4815-4817.

[120] M. Wilchek, E. A. Bayer, in *Methods in Enzymology, Vol. 184*, Academic Press, San Diego, **1990**.

[121] A. Loosli, U. E. Rusbandi, J. Gradinaru, K. Bernauer, C. W. Schläpfer, M. Meyer, S. Mazurek, M. Novic, T. R. Ward, *Inorg. Chem.* **2006**, *45*, 660-668.

[122] a) M. Gonzàlez, C. E. Argaraña, G. D. Fidelio, *Biomol. Eng.* **1999**, *16*, 67-72; b) N. M. Green, *Adv. Protein Chem.* **1975**, *29*, 85-133; c) T. Sano, M. W. Pandori, X. Chen, C. L. Smith, C. R. Cantor¶, *J. Biol. Chem.* **1995**, *270*, 28204-28209.

[123] a) T. Sano, C. R. Cantor, *Proc. Natl. Acad. Sci. USA* **1990**, *87*, 142-146; b) A. Zocchi, N. Humbert, T. Berta, T. R. Ward, *Chimia* **2003**, *57*, 589-592.

[124] D. Häring, M. D. Distefano, *Bioconjugate Chem.* **2001**, *12*, 385-390.

[125] J. Steinreiber, T. Ward*, Vol. 25* (Ed.: T. Ward), Springer Berlin / Heidelberg, **2009**, 93-112.

[126] a) F. H. Arnold, *Acc. Chem. Res.* **1998**, *31*, 125-131; b) J. C. Moore, F. H. Arnold, *Nat. Biotechnol.* **1996**, *14*, 458.

[127] a) M. T. Reetz, *Tetrahedron* **2002**, *58*, 6595-6602; b) M. T. Reetz, *Proc. Natl. Acad. Sci. U. S. A.* **2004**, *101*, 5716-5722; c) M. T. Reetz, C. Torre, A. Eipper, R. Lohmer, M. Hermes, B. Brunner, A. Maichele, M. Bocola, M. Arand, A. Cronin, Y. Genzel, A. Archelas, R. Furstoss, *Org. Lett.* **2003**, *6*, 177-180.

[128] a) C. A. Tracewell, F. H. Arnold, *Curr. Opin. Chem. Biol.* **2009**, *13*, 3-9; b) N. J. Turner, *Nat. Chem. Biol.* **2009**, *5*, 567-573; c) M. Reetz, *Vol. 25* (Ed.: T. Ward), Springer Berlin / Heidelberg, **2009**, 63-92; d) D. H. Appella, *Nat. Chem. Biol.* **2010**, *6*, 87-88.

[129] M. T. Reetz, M. Bocola, J. D. Carballeira, D. Zha, A. Vogel, *Angew. Chem., Int. Ed.* **2005**, *44*, 4192-4196.

[130] M. T. Reetz, J. J.-P. Peyeralans, A. Maichele, Y. Fu, M. Maywald, *Chem. Commun.* **2006**, 4318-4320.

[131] M. Creus, T. R. Ward, *Org. Biomol. Chem.* **2007**, *5*, 1835-1844.

[132] a) J. Panek, T. Ward, A. Jezierska-Mazzarello, M. Novič, *J. Comput. Aided Mol. Des.* **2010**, *24*, 719-732; b) T. R. Ward, *Angew. Chem., Int. Ed.* **2008**, *47*, 7802-7803.

[133] a) R. E. Morris, R. E. Aird, P. d. S. Murdoch, H. Chen, J. Cummings, N. D. Hughes, S. Parsons, A. Parkin, G. Boyd, D. I. Jodrell, P. J. Sadler, *J. Med. Chem.* **2001**, *44*, 3616-3621; b) C. S. Allardyce, P. J. Dyson, D. J. Ellis, S. L. Heath, *Chem. Commun.* **2001**, 1396-1397.

[134] H.-K. Liu, S. J. Berners-Price, F. Wang, J. A. Parkinson, J. Xu, J. Bella, P. J. Sadler, *Angew. Chem., Int. Ed. Engl.* **2006**, *45*, 8153-8156.

[135] a) I. W. McNae, K. Fishburne, A. Habtemariam, T. M. Hunter, M. Melchart, F. Wang, M. D. Walkinshaw, P. J. Sadler, *Chem. Commun.* **2004**, 1786-1787; b) P. Heffeter, K. Böck, B. Atil, M. Reza Hoda, W. Körner, C. Bartel, U. Jungwirth, B. Keppler, M. Micksche, W. Berger, G. Koellensperger, *J. Biol. Inorg. Chem.* **2010**, *15*, 737-748; c) B. Wu, M. S. Ong, M. Groessl, Z. Adhireksan, C. G. Hartinger, P. J. Dyson, C. A. Davey, *Chem. Eur. J.* **2011**, *17*, 3562-3566; d) X. Sun, C.-N. Tsang, H. Sun, *Metallomics* **2009**, *1*, 25-31.

[136] D. W. P. M. Löwik, M. D. Weingarten, M. Broekema, A. J. Brouwer, W. C. Still, R. M. J. Liskamp, *Angew. Chem. Int. Ed. Engl.* **1998**, *37*, 1846-1850.

[137] a) J. M. Becker, M. Wilchek, *Biochim. Biophys. Acta* **1972**, *264*, 165-&; b) E. Bayer, M. Wilchek, in *Methods in Enzymology, Vol. Volume 34* (Ed.: B. C. Raymond), Academic Press, **1974**, 265-267.

[138] M. A. Bennett, A. K. Smith, *J. Chem. Soc., Dalt. Trans.* **1974**, 233-241.

[139] A. J. Birch, *J. Chem. Soc.* **1946**, 593-597.

[140] P. C. Weber, D. H. Ohlendorf, J. J. Wendoloski, F. R. Salemme, *Science* **1989**, *243*, 85-88.

[141] A. P. Silverman, W. Bu, S. M. Cohen, S. J. Lippard, *J. Biol. Chem.* **2002**, *277*, 49743-49749.

[142] a) F. X. Han, R. T. Wheelhouse, L. H. Hurley, *J. Am. Chem. Soc.* **1999**, *121*, 3561-3570; b) S. N. Georgiades, N. H. Abd Karim, K. Suntharalingam, R. Vilar, *Angew. Chem., Int. Ed.* **2010**, *49*, 4020-4034.

[143] M. Morpurgo, A. Radu, E. A. Bayer, M. Wilchek, *J. Mol. Recognit.* **2004**, *17*, 558-566.

[144] O. Novakova, H. Chen, O. Vrana, A. Rodger, J. Sadler Peter, V. Brabec, *Biochemistry* **2003**, *42*, 11544-11554.

[145] C. Gossens, I. Tavernelli, U. Rothlisberger, *J. Am. Chem. Soc.* **2008**, *130*, 10921-10928.

[146] P. Buczek, M. P. Horvath, *J. Mol. Biol.* **2006**, *359*, 1217-1234.

[147] D. L. Theobald, S. C. Schultz, *EMBO J.* **2003**, *22*, 4314-4324.

[148] a) C. G. Hartinger, A. Casini, C. Duhot, Y. O. Tsybin, L. Messori, P. J. Dyson, *J. Inorg. Biochem.* **2008**, *102*, 2136-2141; b) F. Wang, S. Weidt, J. Xu, C. Mackay, P. Langridge-Smith, P. Sadler, *J. Am. Soc. Mass Spectrom.* **2008**, *19*, 544-549.

[149] a) L. Kelland, *Nat. Rev. Cancer* **2007**, *7*, 573-584; b) J. Reedijk, *Chem. Rev.* **1999**, *99*, 2499-2510; c) D. Wang, S. J. Lippard, *Nat. Rev. Drug Discovery* **2005**, *4*, 307-320.

[150] H. H. W. Chen, M. T. Kuo, *Met.-Based Drugs* **2010**.

[151] J. Reedijk, *Eur. J. Inorg. Chem.* **2009**, *2009*, 1303-1312.

[152] a) D. E. Draper, *J. Mol. Biol.* **1999**, *293*, 255-270; b) J. Tan, C. Vonrhein, O. S. Smart, G. Bricogne, M. Bollati, Y. Kusov, G. Hansen, J. R. Mesters, C. L. Schmidt, R. Hilgenfeld, *PLoS Pathog.* **2009**, *5*.

[153] H. Chen, J. A. Parkinson, S. Parsons, R. A. Coxall, R. O. Gould, P. J. Sadler, *J. Am. Chem. Soc.* **2002**, *124*, 3064-3082.

[154] R. Briesewitz, G. Ray, T. Wandless, G. Crabtree, *Proc. Natl. Acad. Sci. U.S.A.* **1999**, *96*, 1953.

[155] a) L. A. Banaszynski, C. W. Liu, T. J. Wandless, *J. Am. Chem. Soc.* **2005**, *127*, 4715-4721; b) O. Nováková, A. A. Nazarov, C. G. Hartinger, B. K. Keppler, V. Brabec, *Biochem. Pharmacol.* **2009**, *77*, 364-374; c) W. H. Ang, A. De Luca, C. Chapuis-Bernasconi, L. Juillerat-Jeanneret, M. Lo Bello, P. J. Dyson, *ChemMedChem* **2007**, *2*, 1799-1806; d) K. R. Barnes, A. Kutikov, S. J. Lippard, *Chem. Biol.* **2004**, *11*, 557-564; e) G. Jaouen, S. Top, A. Vessieres, G. Leclercq, M. J. McGlinchey, *Curr. Med. Chem.* **2004**, *11*, 2505-2517.

[156] a) A. R. Timerbaev, C. G. Hartinger, S. S. Aleksenko, B. K. Keppler, *Chem. Rev.* **2006**, *106*, 2224-2248; b) A. Casini, C. Gabbiani, E. Michelucci, G. Pieraccini, G. Moneti, P. Dyson, L. Messori, *J. Biol. Inorg. Chem.* **2009**, *14*, 761-770.

[157] F. Kratz, *J. Controlled Release* **2008**, *132*, 171-183.

[158] B. Wu, P. Droge, C. A. Davey, *Nat. Chem. Biol.* **2008**, *4*, 110-112.

[159] C. Letondor, N. Humbert, T. R. Ward, *Proc. Natl. Acad. Sci. U. S. A.* **2005**, *102*, 4683-4687.

[160] M. Dürrenberger, T. Heinisch, Y. M. Wilson, T. Rossel, E. Nogueira, L. Knörr, A. Mutschler, K. Kersten, M. J. Zimbron, J. Pierron, T. Schirmer, T. R. Ward, *Angew. Chem., Int. Ed.* **2011**, *13*, 3026–3029.

[161] T. Reiner, D. Jantke, A. Raba, A. N. Marziale, J. Eppinger, *J. Organomet. Chem.* **2009**, *694*, 1934-1937.

[162] D. van Leusen, D. J. Beetstra, B. Hessen, J. H. Teuben, *Organometallics* **2000**, *19*, 4084-4089.

[163] W. F. McCalmont, J. R. Patterson, M. A. Lindenmuth, T. N. Heady, D. M. Haverstick, L. S. Gray, T. L. Macdonald, *Bioorg. Med. Chem.* **2005**, *13*, 3821-3839.

[164] a) V. A. Korshun, N. B. Pestov, E. V. Nozhevnikova, I. A. Prokhorenko, S. V. Gontarev, Y. A. Berlin, *Synth. Commun.* **1996**, *26*, 2531-2547; b) R. Neier, R. Vallinayagam, J. Weber, *Org. Lett.* **2008**, *10*, 4453-4455.

[165] H. Amouri, M. Gruselle, G. Jaouen, *Synth. React. Inorg. Met. Org. Chem.* **1994**, *24*, 395-400.

[166] S. Ogo, N. Makihara, Y. Kaneko, Y. Watanabe, *Organometallics* **2001**, *20*, 4903-4910.

[167] D. A. Freedman, J. K. Evju, M. K. Pomije, K. R. Mann, *Inorg. Chem.* **2001**, *40*, 5711-5715.

[168] V. Parekh, J. A. Ramsden, M. Wills, *Tetrahedron: Asymmetry* **2010**, *21*, 1549-1556.

[169] A. Pordea, M. Creus, C. Letondor, A. Ivanova, T. R. Ward, *Inorg. Chim. Acta* **2010**, *363*, 601-604.

[170] V. Köhler, J. Mao, T. Heinisch, A. Pordea, A. Sardo, Y. M. Wilson, L. Knörr, M. Creus, J.-C. Prost, T. Schirmer, T. R. Ward, *Angew. Chem., Int. Ed* **2011**, *50*, 10863-10866.

[171] T. Wang, L.-G. Zhuo, Z. Li, F. Chen, Z. Ding, Y. He, Q.-H. Fan, J. Xiang, Z.-X. Yu, A. S. C. Chan, *J. Am. Chem. Soc.* **2011**, *133*, 9878-9891.

[172] E. W. Dijk, A. J. Boersma, B. L. Feringa, G. Roelfes, *Org. Biomol. Chem.* **2010**, *8*, 3868-3873.

[173] S. Ogo, K. Uehara, T. Abura, S. Fukuzumi, *J. Am. Chem. Soc.* **2004**, *126*, 3020-3021.

[174] M. T. Reetz, M. Rentzsch, A. Pletsch, M. Maywald, P. Maiwald, J. J. P. Peyralans, A. Maichele, Y. Fu, N. Jiao, F. Hollmann, R. Mondière, A. Taglieber, *Tetrahedron* **2007**, *63*, 6404-6414.

[175] M. A. Wegman, L. M. van Langen, F. van Rantwijk, R. A. Sheldon, *Biotechnol. Bioeng.* **2002**, *79*, 356-361.

[176] M. Skander, N. Humbert, J. Collot, J. Gradinaru, G. Klein, A. Loosli, J. Sauser, A. Zocchi, F. Gilardoni, T. R. Ward, *J. Am. Chem. Soc.* **2004**, *126*, 14411-14418.

[177] U. E. Rusbandi, C. Lo, M. Skander, A. Ivanova, M. Creus, N. Humbert, T. R. Ward, *Adv. Synth. Catal.* **2007**, *349*, 1923-1930.

[178] M. T. Reetz, J. J. P. Peyralans, A. Maichele, Y. Fu, M. Maywald, *Chem. Commun.* **2006**, 4318-4320.

[179] M. E. Wilson, R. G. Nuzzo, G. M. Whitesides, *J. Am. Chem. Soc.* **1978**, *100*, 2269-2270.

[180] C.-C. Lin, C.-W. Lin, A. S. C. Chan, *Tetrahedron: Asymmetry* **1999**, *10*, 1887-1893.

[181] H. Yamaguchi, T. Hirano, H. Kiminami, D. Taura, A. Harada, *Org. Biomol. Chem.* **2006**, *4*, 3571-3573.

[182] L. Panella, J. Broos, J. Jin, M. W. Fraaije, D. B. Janssen, M. Jeronimus-Stratingh, B. L. Feringa, A. J. Minnaard, J. G. de Vries, *Chem. Commun.* **2005**, 5656-5658.

[183] J. G. de Vries, L. Lefort, *Chem. Eur. J.* **2006**, *12*, 4722-4734.

[184] R. den Heeten, B. K. Munoz, G. Popa, W. Laan, P. C. J. Kamer, *Dalton Trans.* **2010**, *39*, 8477-8483.
[185] I. Martin, M. Teixido, E. Giralt, *Pharmaceuticals* **2010**, *3*, 1456-1490.
[186] A. Casini, C. Temperini, C. Gabbiani, C. T. Supuran, L. Messori, *ChemMedChem* **2010**, *5*, 1989-1994.
[187] K. Mitsukura, M. Suzuki, K. Tada, T. Yoshida, T. Nagasawa, *Org. Biomol. Chem.* **2010**, *8*, 4533-4535.
[188] K. Gao, C.-B. Yu, W. Li, Y.-G. Zhou, X. Zhang, *Chem. Commun.* **2011**, *47*, 7845-7847.
[189] D. R. Coghlan, J. B. Bremner, P. A. Keller, S. G. Pyne, D. M. David, K. Somphol, D. Baylis, J. Coates, J. Deadman, D. I. Rhodes, A. D. Robertson, *Bioorg. Med. Chem.* **2011**, *19*, 3549-3557.
[190] N. Hovhannisyan, S. Harutyunyan, A. Hovhannisyan, A. Hambardzumyan, M. Chitchyan, M. Melkumyan, G. Oganezova, N. Avetisyan, *Amino Acids* **2009**, *37*, 531-536.
[191] H. Usuki, Y. Yamamoto, J. Arima, M. Iwabuchi, S. Miyoshi, T. Nitoda, T. Hatanaka, *Org. Biomol. Chem.* **2011**, *9*, 2327-2335.
[192] D. Nathans, *Proc. Natl. Acad. Sci. U. S. A.* **1964**, *51*, 585-592.
[193] a) D. Seebach, A. K. Beck, S. Capone, G. Deniau, U. Grošelj, E. Zass, *Synthesis* **2009**, *2009*, 1,32; b) E. Juaristi, V. A. Soloshonok, Editors, *Enantioselective Synthesis of β-Amino Acids, Second Edition*, John Wiley & Sons, Inc., **2005**.
[194] B. E. Sleebs, N. T. T. Van, A. B. Hughes, *Org. Prep. Proced. Int.* **2009**, *41*, 429-478.
[195] H. Namba, M. Nakashima, T. Hayashi, N. Hayashida, S. Maeda, T. I. Rogounovitch, A. Ohtsuru, V. A. Saenko, T. Kanematsu, S. Yamashita, *J. Clin. Endocrinol. Metab.* **2003**, *88*, 4393-4397.
[196] N. Humbert, A. Zocchi, T. R. Ward, *Electrophoresis* **2005**, *26*, 47-52.
[197] G. Klein, N. Humbert, J. Gradinaru, A. Ivanova, F. Gilardoni, U. E. Rusbandi, T. R. Ward, *Angew. Chem., Int. Ed.* **2005**, *44*, 7764-7767.
[198] P. Hohenberg, W. Kohn, *Physical Rev.* **1964**, *136*, B864.
[199] M. J. Frisch, *Chem Listy* **2006**, *100*, A9-A9.
[200] a) P. J. Stephens, F. J. Devlin, C. F. Chabalowski, M. J. Frisch, *J. Phys. Chem.* **1994**, *98*, 11623-11627; b) A. D. Becke, *J. Chem. Phys.* **1993**, *98*, 5648-5652.
[201] P. J. Hay, W. R. Wadt, *J. Chem. Phys.* **1985**, *82*, 270-283.
[202] J. C. Phillips, R. Braun, W. Wang, J. Gumbart, E. Tajkhorshid, E. Villa, C. Chipot, R. D. Skeel, L. Kalé, K. Schulten, *J. Comput. Chem.* **2005**, *26*, 1781-1802.
[203] P. Grayson, E. Tajkhorshid, K. Schulten, *Biophys. J.* **2003**, *85*, 36-48.

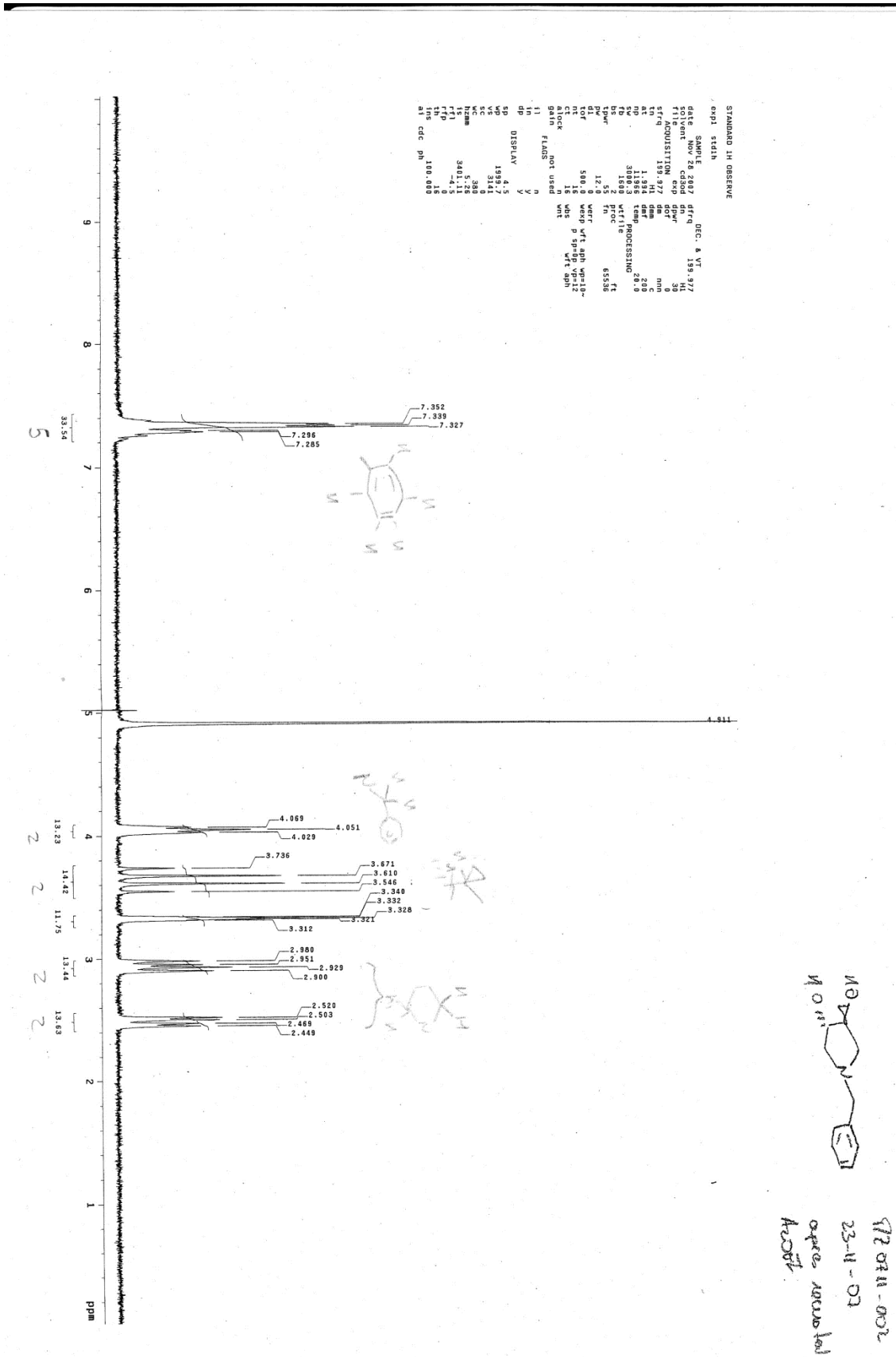
STANDARD 1H OBSERVE
exp1 std1h
SAMPLE
date Nov 28 2007
solvent cd3od
ACQUISITION
sfrq 199.977
tn H1
at 1.994
np 11956
sw 3001.5
fb 1800
bs 2
tdav 1
pw 12.5
d1 0
tof 500.0
nt 16
ct 0
alock n
FLAGS
il n
in y
dp y
DISPLAY
sp 4.5
wp 1999.7
vs 3141
sc 0
wc 380
hzmm 5.26
is 3401.11
rfl -4.5
rfp 0
th 16
ins 1
lb 100.000
ph
cdc
DEC. & VT
dfrq 199.977
dn H1
dpwr 30
dof 0
nnn
dm
dmf 20c
temp 20.0
PROCESSING
wtfile
proc ft
fn 65536
werr
wexp wft aph wp-10~
p sp-10 wp12
wft aph
wnt
7.352
7.339
7.327
7.296
7.285
4.811
4.069
4.051
4.029
3.736
3.671
3.610
3.546
3.340
3.332
3.328
3.321
3.312
2.980
2.951
2.929
2.900
2.520
2.503
2.469
2.449
33.54
13.23
14.42
11.75
13.44
13.63
ppm

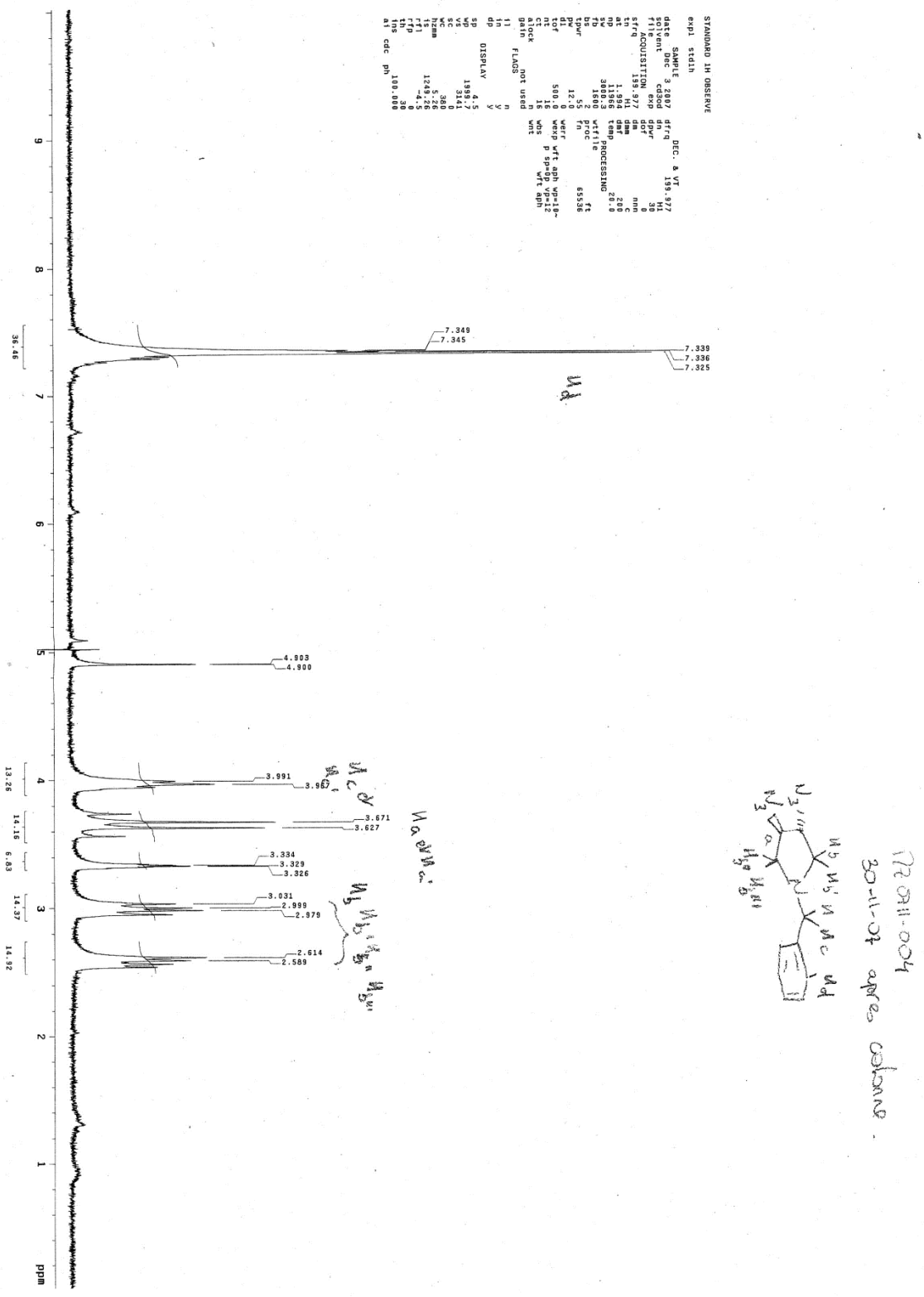
STANDARD 1H OBSERVE
7.349
7.345
7.339
7.336
7.325
4.903
4.900
3.991
3.987
3.671
3.627
3.334
3.329
3.326
3.031
2.999
2.979
2.614
2.589
ppm

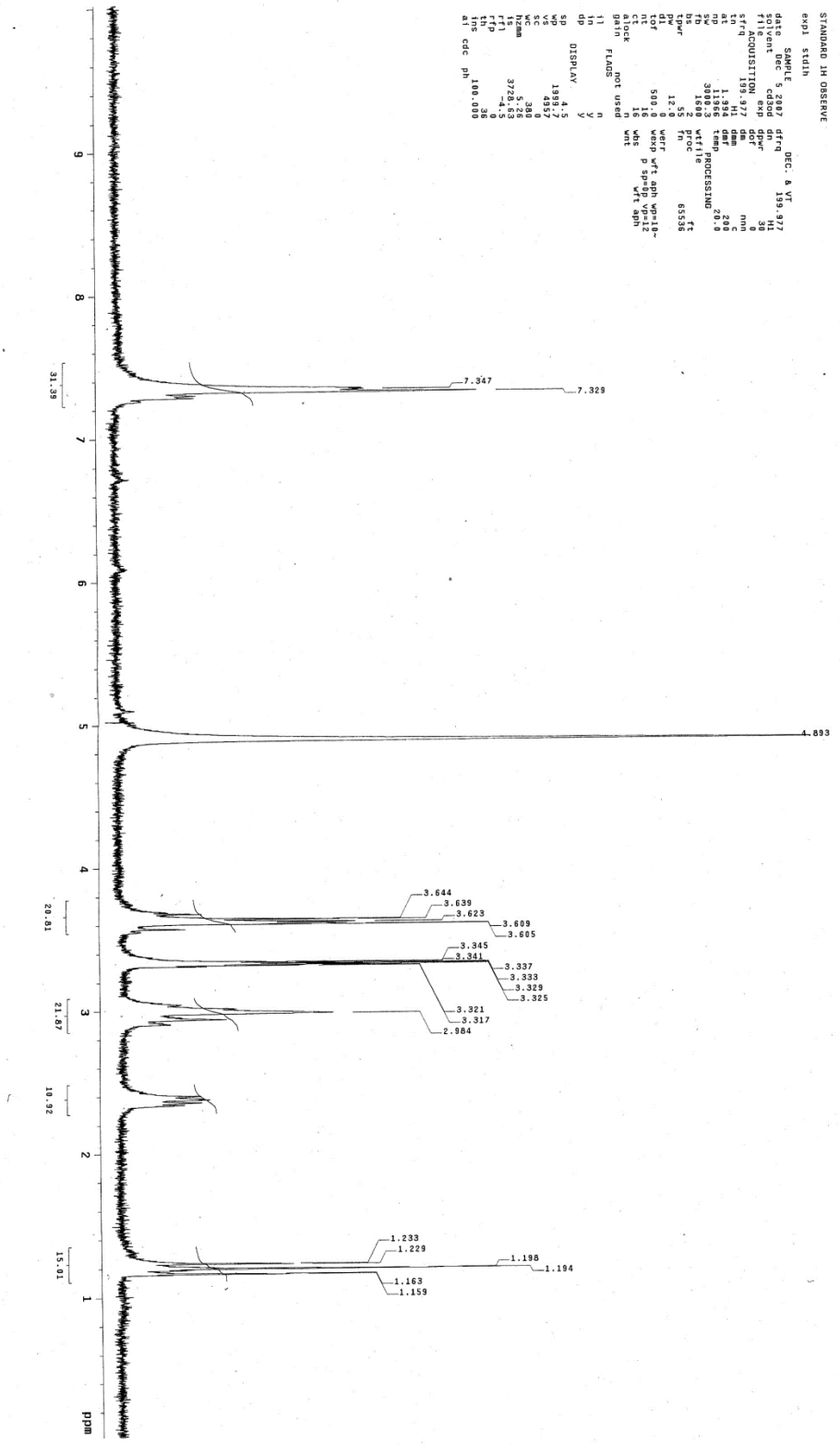

TZ 9HI-006
5-12-07

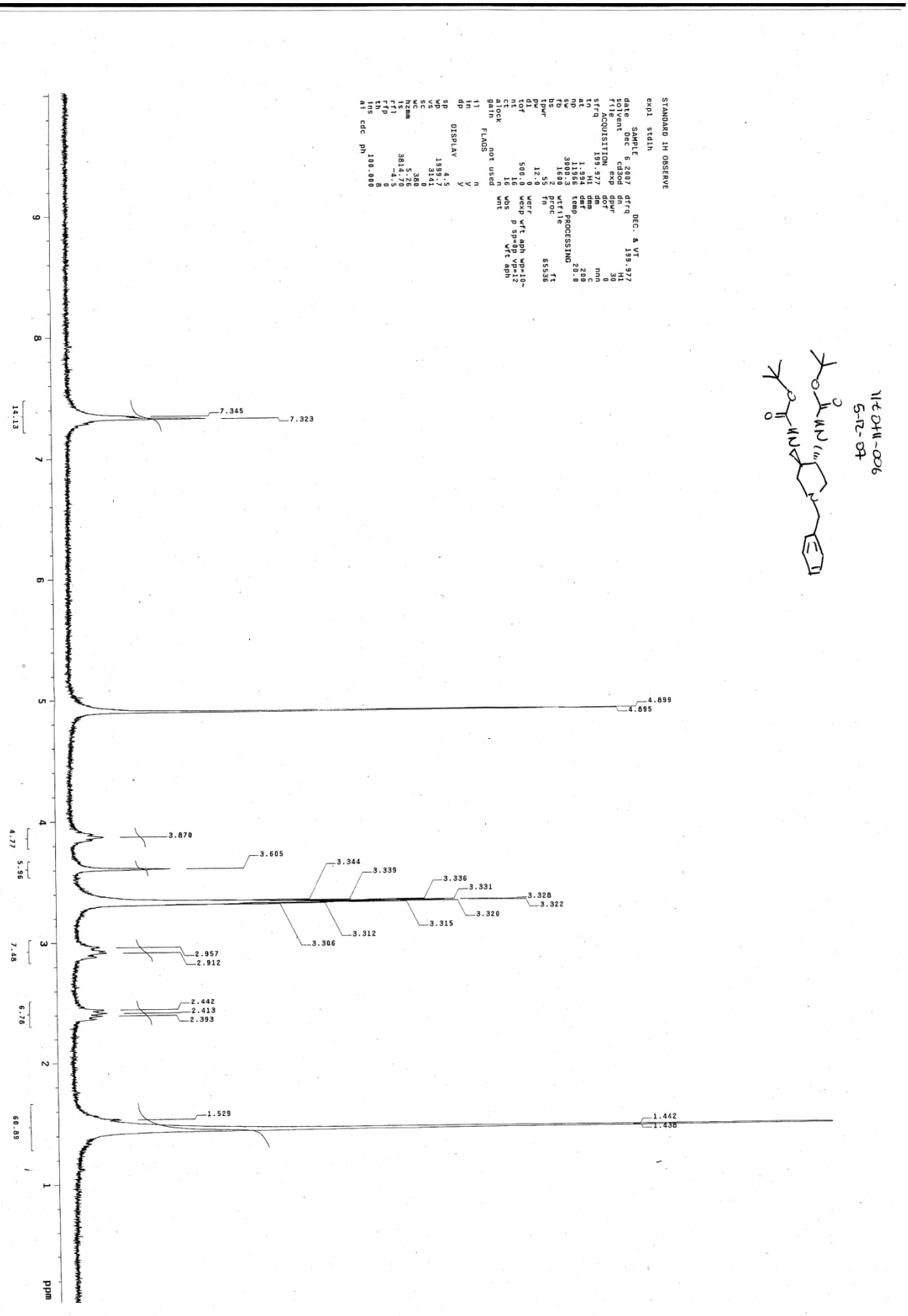
STANDARD 1H OBSERVE
7.345
7.323
4.899
4.895
3.870
3.605
3.344
3.339
3.336
3.331
3.328
3.322
3.320
3.315
3.312
3.306
2.957
2.912
2.442
2.413
2.393
1.529
1.442
1.438
14.13
4.77
5.96
7.48
6.78
60.89
ppm

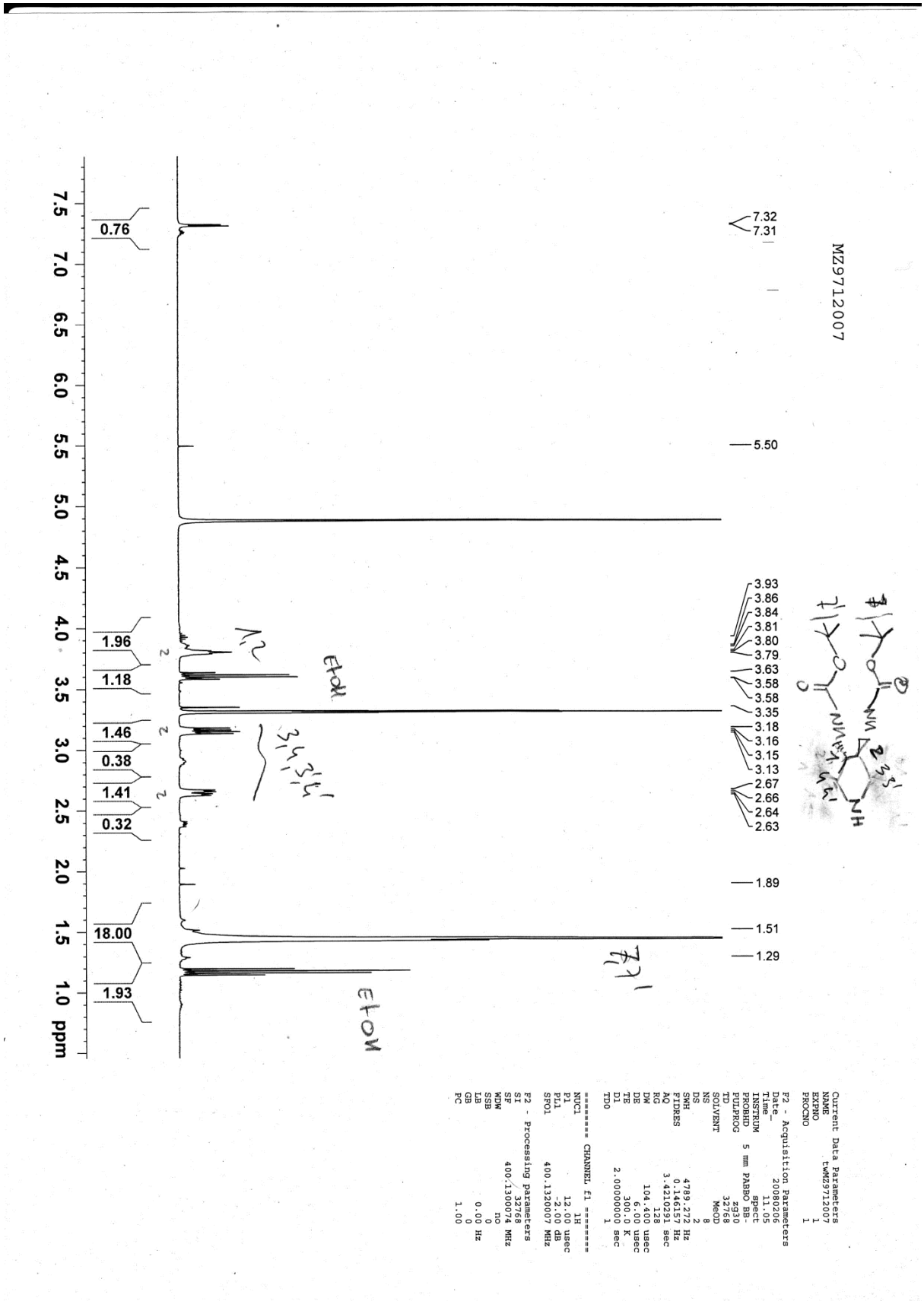
MZ9712007
7.32
7.31
5.50
3.93
3.86
3.84
3.81
3.80
3.79
3.63
3.58
3.58
3.35
3.18
3.16
3.15
3.13
2.67
2.66
2.64
2.63
1.89
1.51
1.29
0.76
1.96
1.18
1.46
0.38
1.41
0.32
18.00
1.93
EtOH
EtOH
7.5 7.0 6.5 6.0 5.5 5.0 4.5 4.0 3.5 3.0 2.5 2.0 1.5 1.0 ppm
Current Data Parameters
NAME tvMZ9712007
EXPNO 1
PROCNO 1
F2 - Acquisition Parameters
Date_ 20080206
Time_ 11.05
INSTRUM spect
PROBHD 5 mm PABBO BB-
PULPROG zg30
TD 32768
SOLVENT MeOD
NS 8
DS 2
SWH 4789.272 Hz
FIDRES 0.146157 Hz
AQ 3.4211228 sec
RG 104.400
DW 104.400 usec
DE 6.00 usec
TE 300.0 K
D1 2.00000000 sec
TD0 1
======== CHANNEL f1 ========
NUC1 1H
P1 12.00 usec
PL1 -2.00 dB
SFO1 400.1320007 MHz
F2 - Processing parameters
SI 131072
SF 400.1300074 MHz
WDW no
SSB 0
LB 0.00 Hz
GB 0
PC 1.00

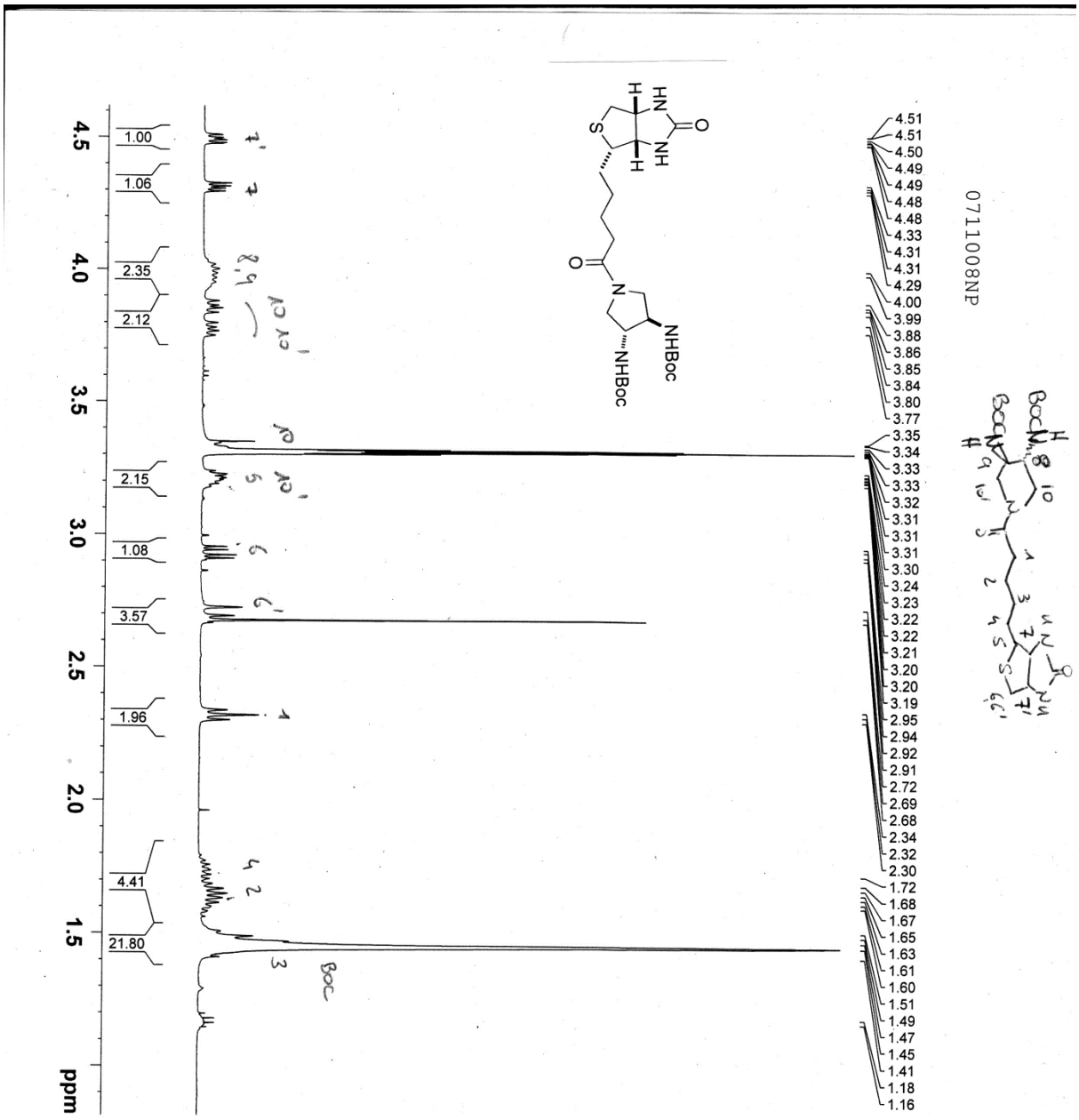


```
Current Data Parameters
NAME                  tw_mz0711008NP
EXPNO                              1
PROCNO                             1

F2 - Acquisition Parameters
Date_                       20080115
Time_                           11.03
INSTRUM                       spect
PROBHD     5 mm PABBO BB-
PULPROG                       zg30
TD                           32768
SOLVENT                       MeOD
NS                               8
DS                               0
SWH                       4795.396 Hz
FIDRES                    0.146344 Hz
AQ                        3.4166601 sec
RG                             256
DW                         104.267 usec
DE                           6.00 usec
TE                          298.2 K
D1                        2.00000000 sec
TD0                              1

========== CHANNEL f1 ==========
NUC1                           1H
P1                           9.34 usec
PL1                        -4.00 dB
SFO1                400.1320150 MHz

F2 - Processing parameters
SI                           32768
SF                  400.1300097 MHz
WDW                             EM
SSB                              0
LB                            0.10 Hz
GB                               0
PC                            1.00
```

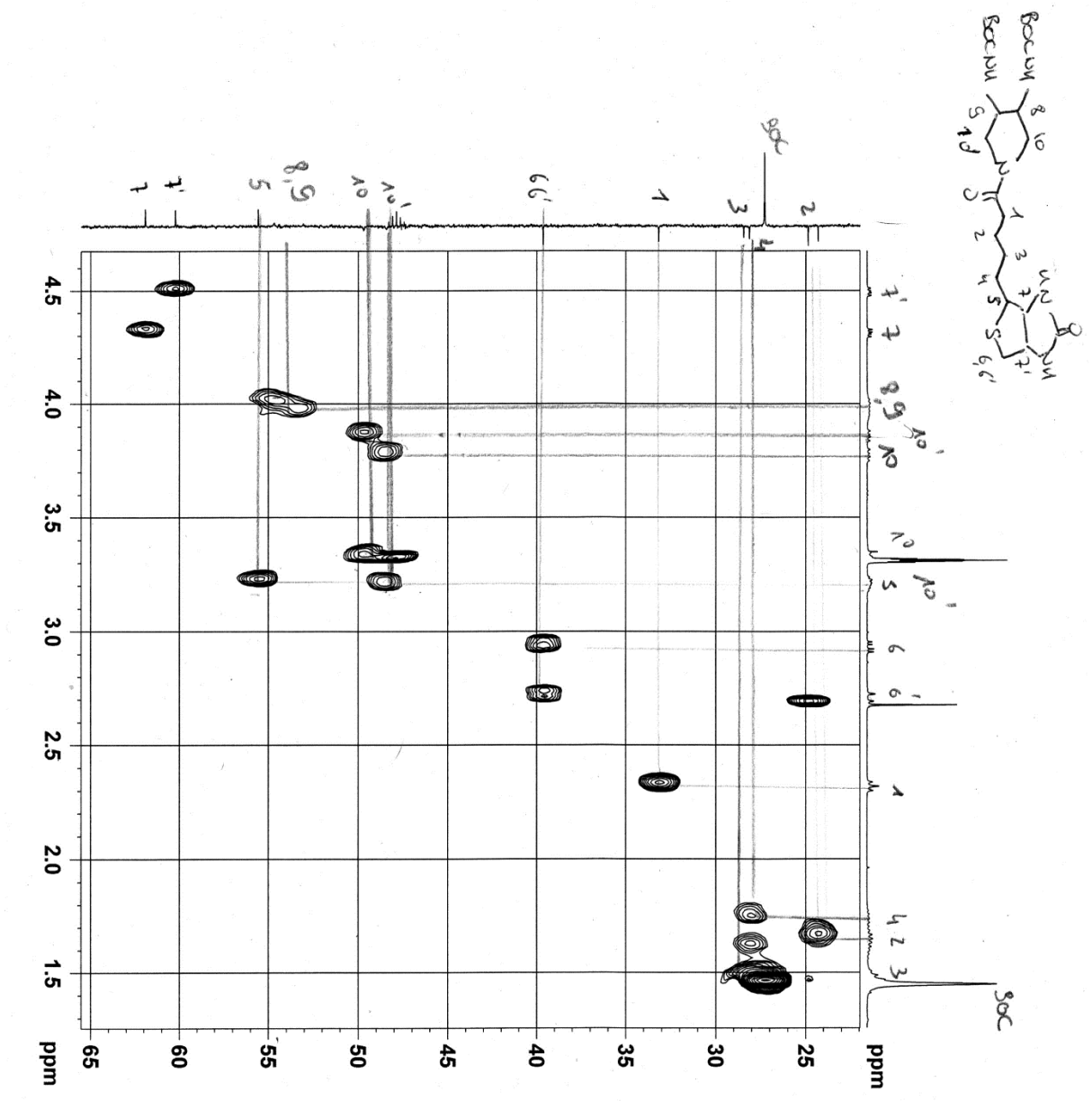


```
Current Data Parameters
NAME                  tw_mz071108NP
EXPNO                            2
PROCNO                           1

F2 - Acquisition Parameters
Date_                     20080115
Time                         11.04
INSTRUM                spect
PROBHD     5 mm PABBO BB-
PULPROG                  hsqcetgp
TD                           1024
SOLVENT                      MeOD
NS                             16
DS                             16
SWH                    5000.000 Hz
FIDRES                    4.882813 Hz
AQ                        0.102400 sec
RG                          1820
DW                       100.000 usec
DE                         6.00 usec
TE                        298.3 K
CNST2                145.0000000
d0                     0.00000300 sec
D1                     1.00000000 sec
d11                    0.03000000 sec
D11                    0.00020000 sec
D16                    0.00020000 sec
d4                     0.00172414 sec
DELTA                  0.00122467 sec
DELTA1                 0.00077614 sec
ID0                    0.00007143 sec
SFICNT                         64
ZGOPTNS

======== CHANNEL f1 ========
NUC1                          1H
P1                         9.34 usec
P2                        18.67 usec
P28                     1000.00 usec
PL1                       4.00 dB
SFO1                400.1320007 MHz

======== CHANNEL f2 ========
CPDPRG2                 garp
NUC2                          13C
P3                         9.30 usec
P4                        18.60 usec
PCPD2                     70.00 usec
PL12                      16.53 dB
PL2                       -1.00 dB
SFO2                100.6218241 MHz

======== GRADIENT CHANNEL =====
GPNAM1               SINE.100
GPNAM2               SINE.100
GPZ1                      80.00 %
GPZ2                      17.00 %
P16                    1000.00 usec

F1 - Acquisition parameters
NUC0                          13C
TD0                           128
SFO1                100.6218 MHz
FIDRES                141.150792 Hz
SW                    180.040 ppm
FnMODE              Echo-Antiecho

F2 - Processing parameters
SI                            1024
SF                  400.1300000 MHz
WDW                        QSINE
SSB                            2
LB                          0.00 Hz
GB                             0
PC                          1.40

F1 - Processing parameters
SI                            1024
MC2                 echo-antiecho
SF                  100.6127690 MHz
WDW                        QSINE
SSB                            2
LB                          0.00 Hz
GB                             0
```

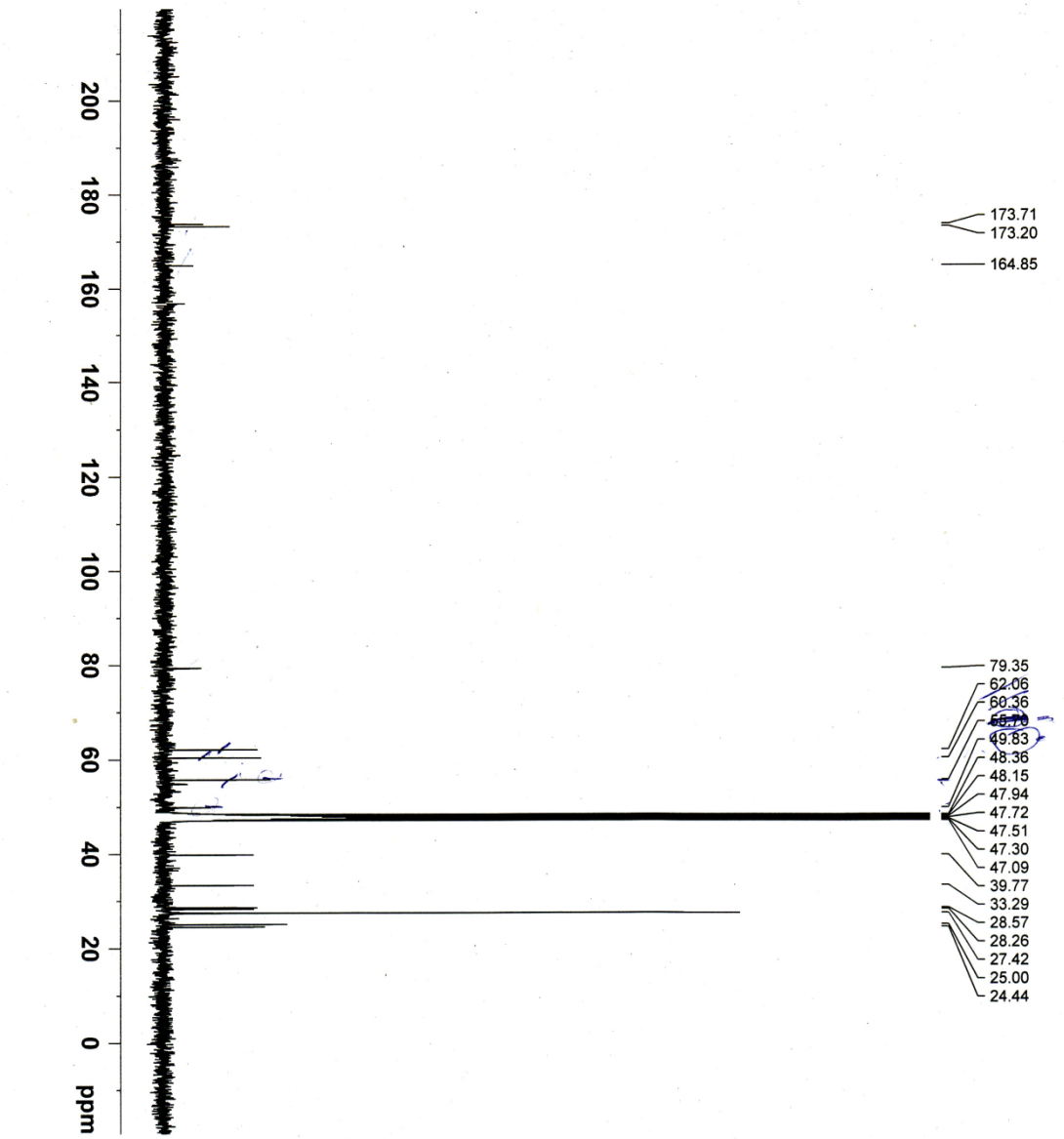


```
Current Data Parameters
NAME          tw_mz071008NP
EXPNO                    4
PROCNO                   1

F2 - Acquisition Parameters
Date_              20080115
Time_                 11.48
INSTRUM                spect
PROBHD  5 mm PABBO BB-
PULPROG              zgpg30
TD                    65536
SOLVENT                MeOD
NS                     1503
DS                        4
SWH               24038.461 Hz
FIDRES                0.366798 Hz
AQ                1.3631988 sec
RG                     1820
DW                  20.800 usec
DE                   6.00 usec
TE                  298.8 K
D1                2.00000000 sec
D11               0.03000000 sec
DELTA             1.89999998 sec
TD0                       1

========== CHANNEL f1 ========
NUC1                    13C
P1                   9.30 usec
PL1                 -1.00 dB
SFO1          100.6228298 MHz

========== CHANNEL f2 ========
CPDPRG2              waltz64
NUC2                    1H
PCPD2                80.00 usec
PL12                14.65 dB
PL13                17.65 dB
PL2                 -1.00 dB
SFO2          400.1316005 MHz

F2 - Processing parameters
SI                      32768
SF            100.6127561 MHz
WDW                        EM
SSB                         0
LB                   2.00 Hz
GB                          0
PC                   1.40
```

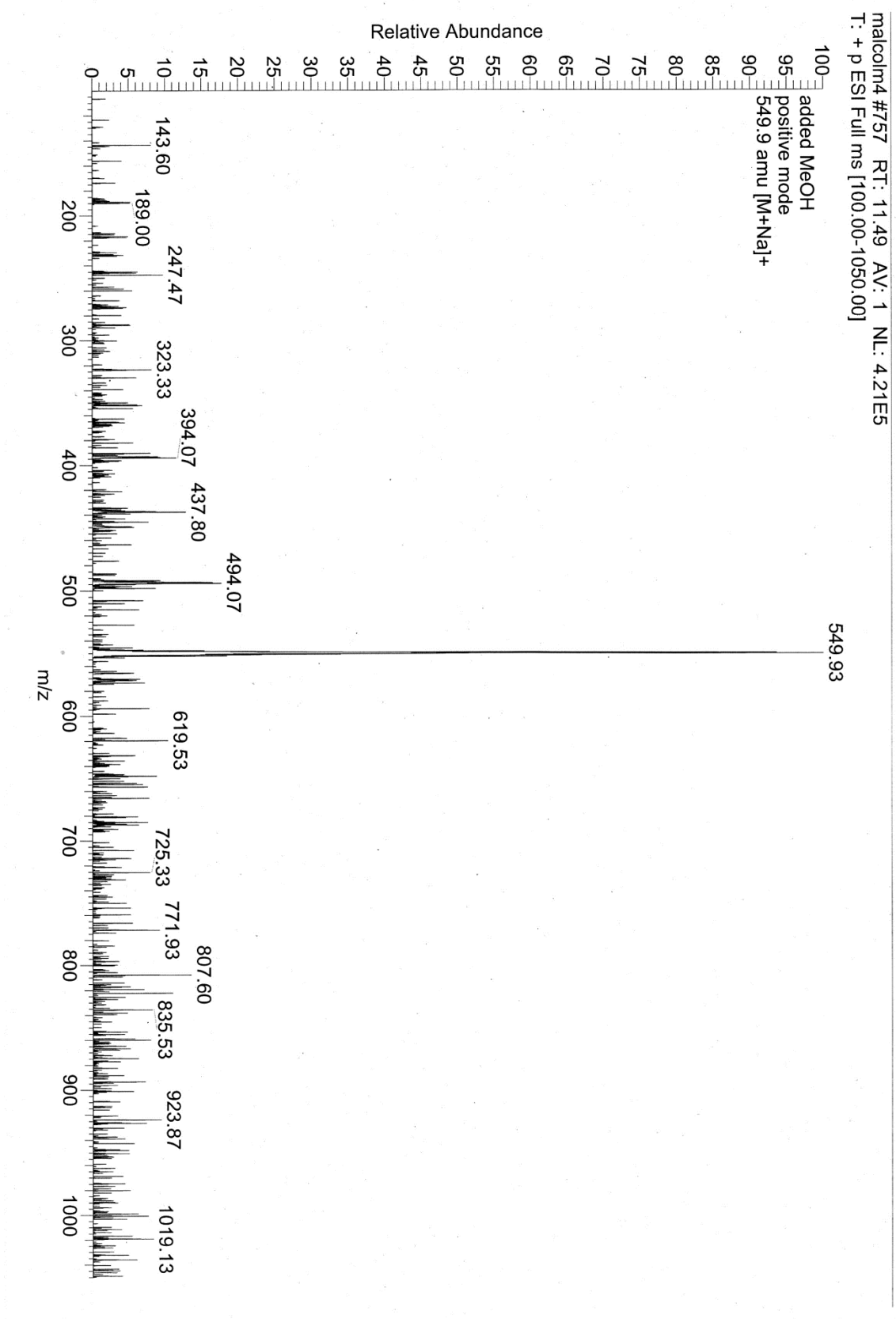
D:\spectres_routine\malcolm4
14.12.2007 10:13:21
MZ 0711008
malcolm4 #757 RT: 11.49 AV: 1 NL: 4.21E5
T: + p ESI Full ms [100.00-1050.00]
added MeOH
positive mode
549.9 amu [M+Na]+
Relative Abundance
m/z
549.93
494.07
437.80
394.07
323.33
247.47
189.00
143.60
619.53
725.33
771.93
807.60
835.53
923.87
1019.13

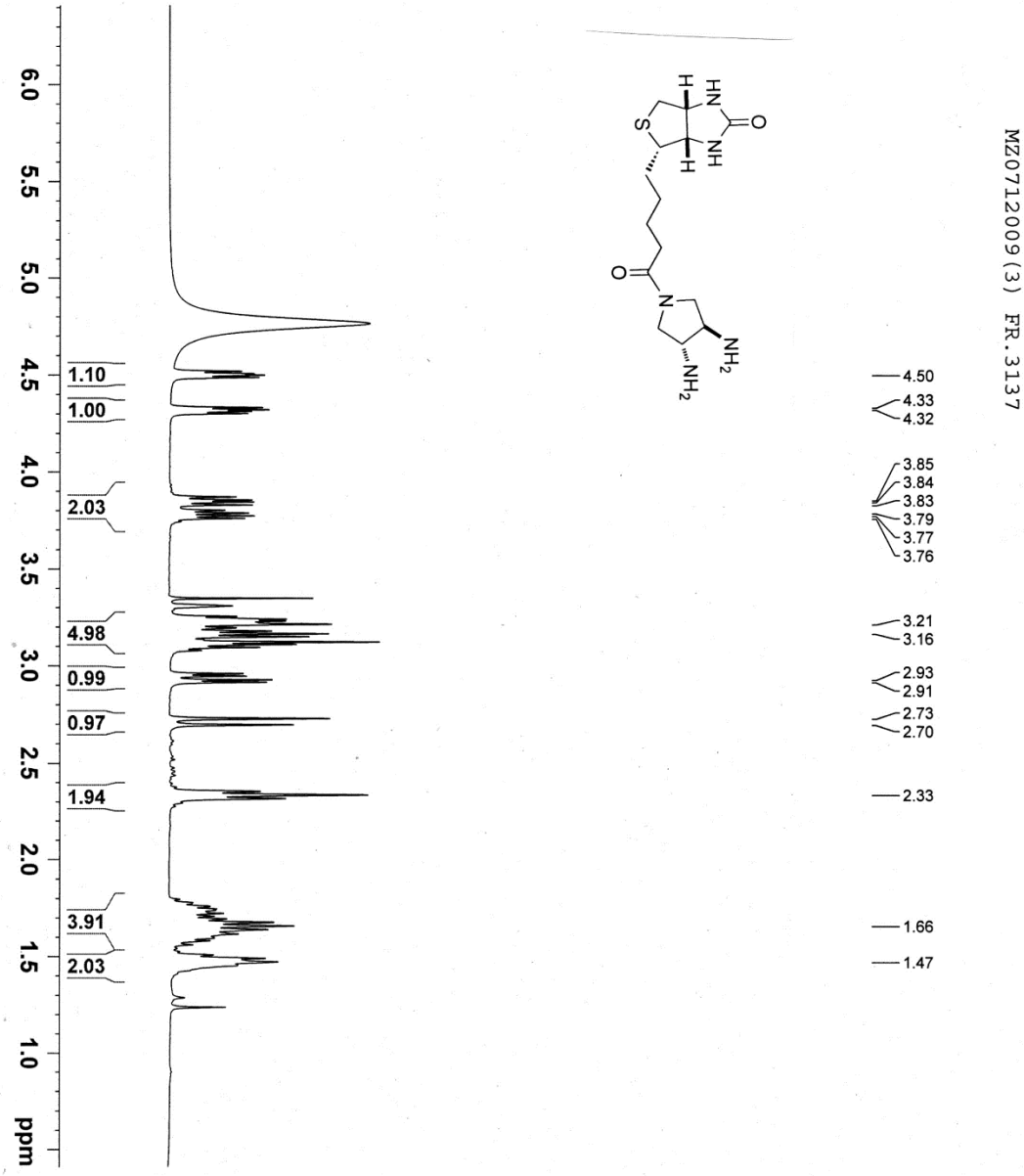


```
Current Data Parameters
NAME                 twmz100308l105
EXPNO                             1
PROCNO                            1

F2 - Acquisition Parameters
Date_                      20080310
Time                           11.11
INSTRUM                         spect
PROBHD     5 mm PABBO BB/
PULPROG                    zg30
TD                            32768
SOLVENT                        MeOD
NS                               32
DS                                0
SWH                        5592.841 Hz
FIDRES                     0.170680 Hz
AQ                         2.9295092 sec
RG                              25.4
DW                         89.400 usec
DE                          6.00 usec
TE                             300.0 K
D1                         2.00000000 sec
TD0                               1

======== CHANNEL f1 ========
NUC1                           1H
P1                         12.00 usec
PL1                        -2.00 dB
SFO1                400.1324008 MHz

F2 - Processing parameters
SI                            32768
SF                  400.1294400 MHz
WDW                              EM
SSB                               0
LB                             0.10 Hz
GB                                0
PC                             1.00
```

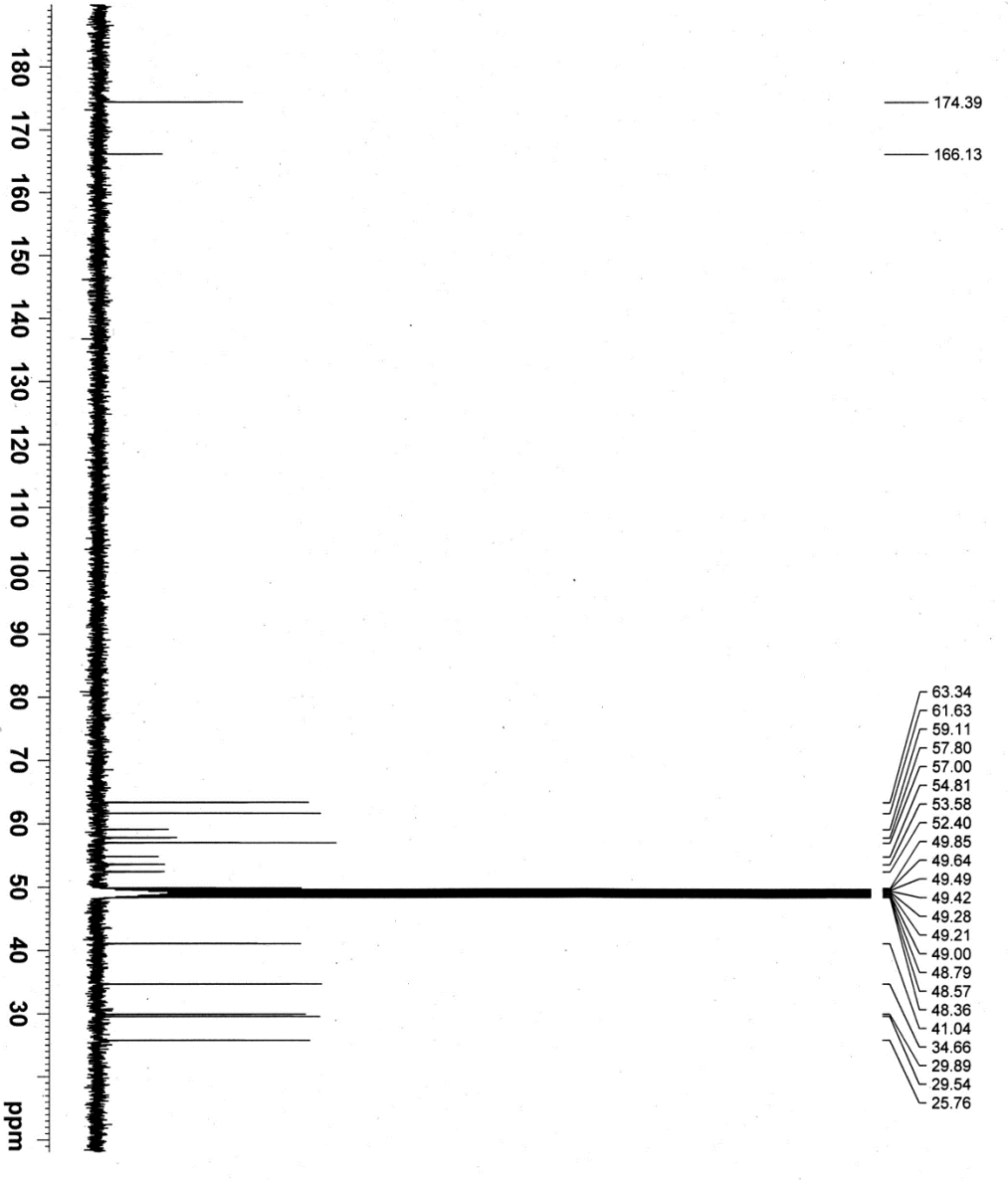


```
Current Data Parameters
NAME                  twMZ074009NP2AC
EXPNO                              5
PROCNO                             1

F2 - Acquisition Parameters
Date_                       20080124
Time_                          15.05
INSTRUM                        spect
PROBHD     5 mm PABBO BB-
PULPROG                     zgpg30
TD                               65536
SOLVENT                       MeOD
NS                               1288
DS                                  4
SWH                        24038.461 Hz
FIDRES                         0.366798 Hz
AQ                         1.3631988 sec
RG                               1820
DW                           20.800 usec
DE                            6.00 usec
TE                             298.7 K
D1                         2.00000000 sec
D11                        0.03000000 sec
DELTA                      1.89999998 sec
TD0                                 1

========== CHANNEL f1 ==========
NUC1                             13C
P1                             9.30 usec
PL1                           -1.00 dB
SFO1                100.6228298 MHz

========== CHANNEL f2 ==========
CPDPRG2                     waltz64
NUC2                             1H
PCPD2                        80.00 usec
PL12                         14.65 dB
PL13                         17.65 dB
PL2                          -1.00 dB
SFO2                400.1316005 MHz

F2 - Processing parameters
SI                               32768
SF                  100.6126286 MHz
WDW                                EM
SSB                                 0
LB                              1.00 Hz
GB                                  0
PC                               1.40
```

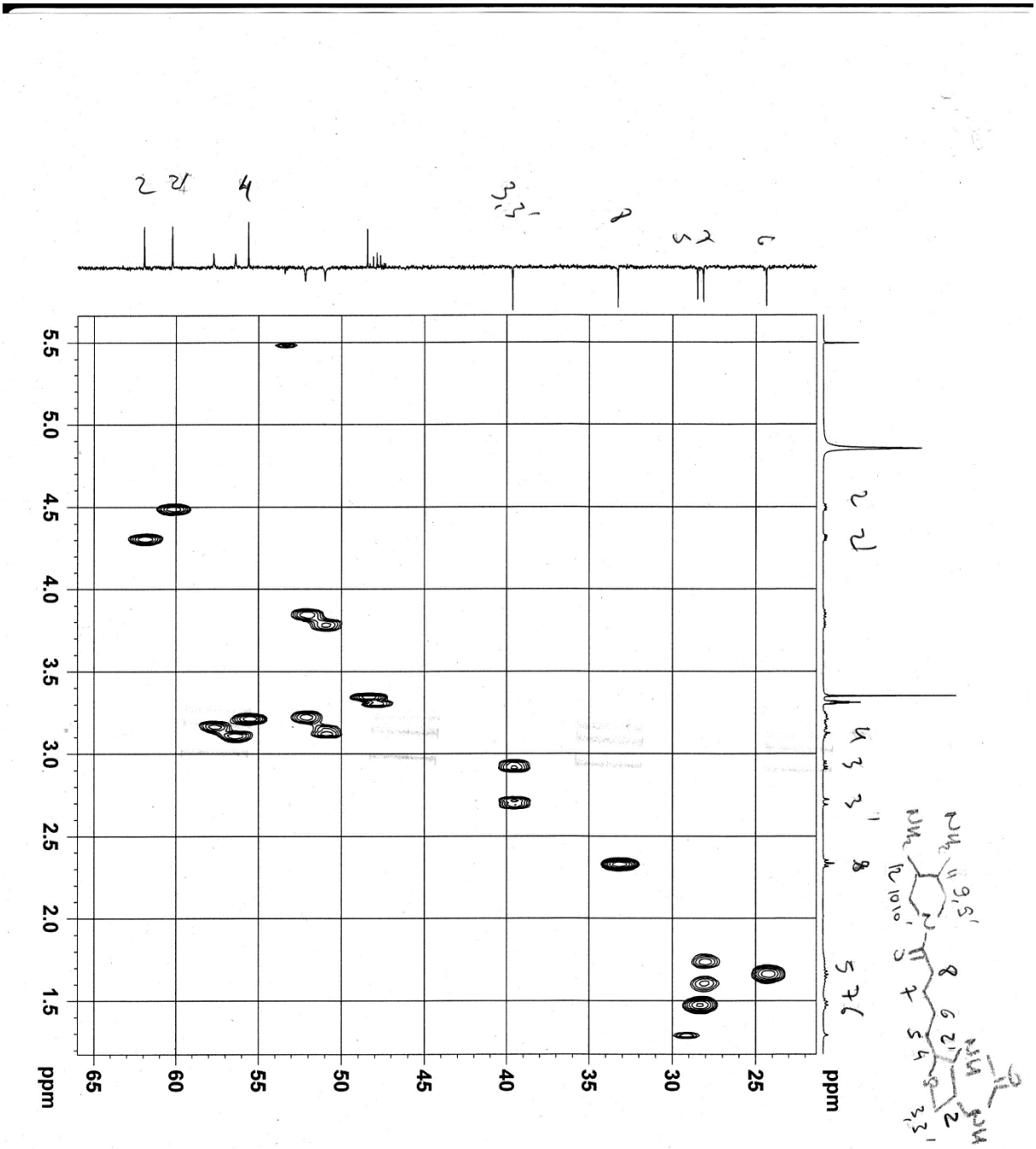


```
Current Data Parameters
NAME          exM20740SNP2AC
EXPNO                      3
PROCNO                     1

F2 - Acquisition Parameters
Date_              20080124
Time               11.40
INSTRUM      5 mm PABBO BB-
PROBHD             hsqcetgp
PULPROG                1024
TD                      16
SOLVENT               MeOD
NS                       8
DS                    5000.000 Hz
SWH                     16.013 Hz
FIDRES                  0.015641 sec
AQ                      1.8220 usec
RG                    100.000 usec
DW                      6.00 usec
DE                    298.0 K
TE                    145.0000000 sec
CNST2                   0.00000300 sec
d0                      1.00000000 sec
D1                      0.00000400 sec
d11                     0.03000000 sec
d13                     0.00020000 sec
D16                     0.00172414 sec
d4                      0.00122467 sec
DELTA                   0.00172414 sec
DELTA1                  0.00002760 sec
IN0
2D-FREQUENCY NUCLEI
======== CHANNEL f1 ========
NUC1                       1H
P1                       9.34 usec
P2                      18.67 usec
PL1                     -4.00 dB
SFO1            400.1320007 MHz
======== CHANNEL f2 ========
CPDPRG2                 garp
NUC2                    13C
P3                       9.30 usec
P4                      18.60 usec
PCPD2                   70.00 usec
PL12                    16.53 dB
PL12                    -1.00 dB
SFO2            100.6218241 MHz
====== GRADIENT CHANNEL =====
GPNAM1               SINE.100
GPNAM2               SINE.100
GPZ1                    80.00 %
GPZ2                    20.10 %
P16                   1000.00 usec

F1 - Acquisition parameters
ND0                        128
TD                        1024
SFO1            100.6218 MHz
FIDRES          141.520792 Hz
SW              159.809 ppm
FnMODE          Echo-Antiecho

F2 - Processing parameters
SI                        1024
SF              400.1300100 MHz
WDW                    QSINE
SSB                         2
LB                       0.00 Hz
GB                          0
PC                       1.40

F1 - Processing parameters
SI                        1024
MC2             echo-antiecho
SF              100.6127690 MHz
WDW                    QSINE
SSB                         2
LB                       0.00 Hz
GB                          0
```

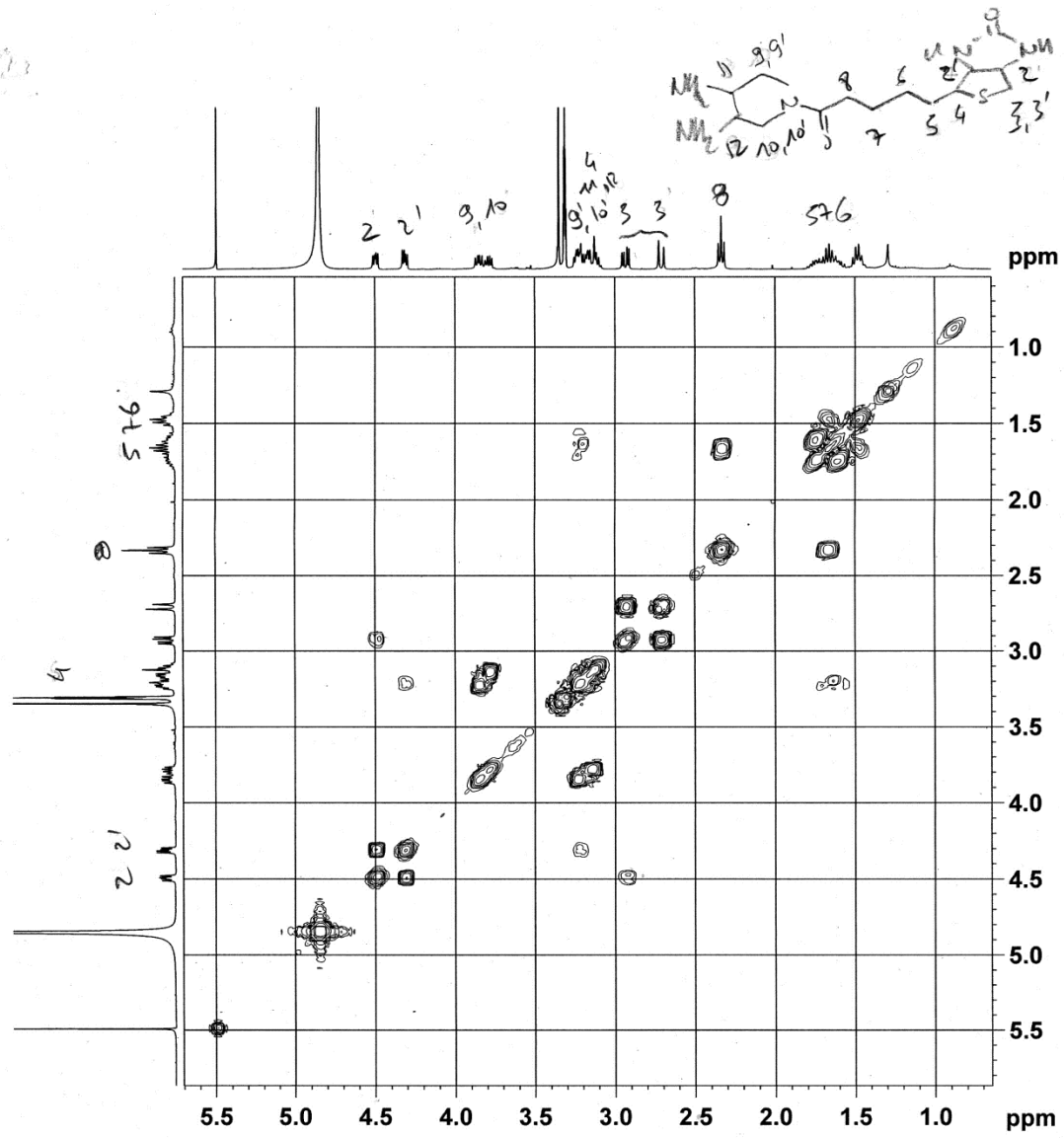


```
Current Data Parameters
NAME      twMZ074009NP2AC
EXPNO                   2
PROCNO                  1

F2 - Acquisition Parameters
Date_            20080124
Time                11.30
INSTRUM             spect
PROBHD    5 mm PABBO BB-
PULPROG          cosygpqf
TD                   1024
SOLVENT              MeOD
NS                      4
DS                      8
SWH              4795.396 Hz
FIDRES           4.683004 Hz
AQ              0.1068191 sec
RG                   1290
DW                104.267 usec
DE                  6.00 usec
TE                 298.1 K
d0              0.00000300 sec
D1              0.96340889 sec
d13             0.00000400 sec
D16             0.00020000 sec
IN0             0.00020855 sec

======== CHANNEL f1 ========
NUC1                   1H
P0                   4.67 usec
P1                   9.34 usec
PL1                 -4.00 dB
SFO1          400.1320007 MHz

====== GRADIENT CHANNEL =====
GPNAM1            SINE.100
GPNAM2            SINE.100
GPZ1                10.00 %
GPZ2                10.00 %
P16               1000.00 usec

F1 - Acquisition parameters
ND0                     1
TD                    128
SFO1              400.132 MHz
FIDRES          37.461040 Hz
SW                11.984 ppm
FnMODE                 QF

F2 - Processing parameters
SI                   1024
SF            400.1300100 MHz
WDW                  SINE
SSB                     0
LB                   0.00 Hz
GB                      0
PC                   0.60

F1 - Processing parameters
SI                   1024
MC2                    QF
SF            400.1300100 MHz
WDW                  SINE
SSB                     0
LB                   0.00 Hz
GB                      0
```

FTMS 4.7T BioAPEX II MS-Service UNI-Fribourg

ESI-MS: MZ0712009

XMASS Mass Analysis for /Data/UNI_BS/ZIMB6214_ESI/3/pdata/1/massanal.res:
XMASS Mass Analysis Constraints

Ion mass = 328.1793870

Charge = +1

#	C	H	N	O	S	mass	DBE	error
*** Mass Analysis for mass 328.1793870								
1	14	26	5	2	1	328.1801722	4.5	7.852e-04
2	16	28	2	3	1	328.1815149	4.0	2.128e-03
3	17	30	1	1	2	328.1763324	3.5	3.055e-03
4	9	26	7	4	1	328.1761495	0.5	3.238e-03
5	11	30	5	2	2	328.1835430	-0.5	4.156e-03
6	13	32	2	3	2	328.1848857	-1.0	5.499e-03
7	20	26	1	1	1	328.1729616	8.5	6.425e-03
8	12	30	3	3	2	328.1723096	-0.5	7.077e-03
9	10	28	6	2	2	328.1709670	0.0	8.420e-03
10	10	28	6	4	1	328.1887255	0.0	9.339e-03

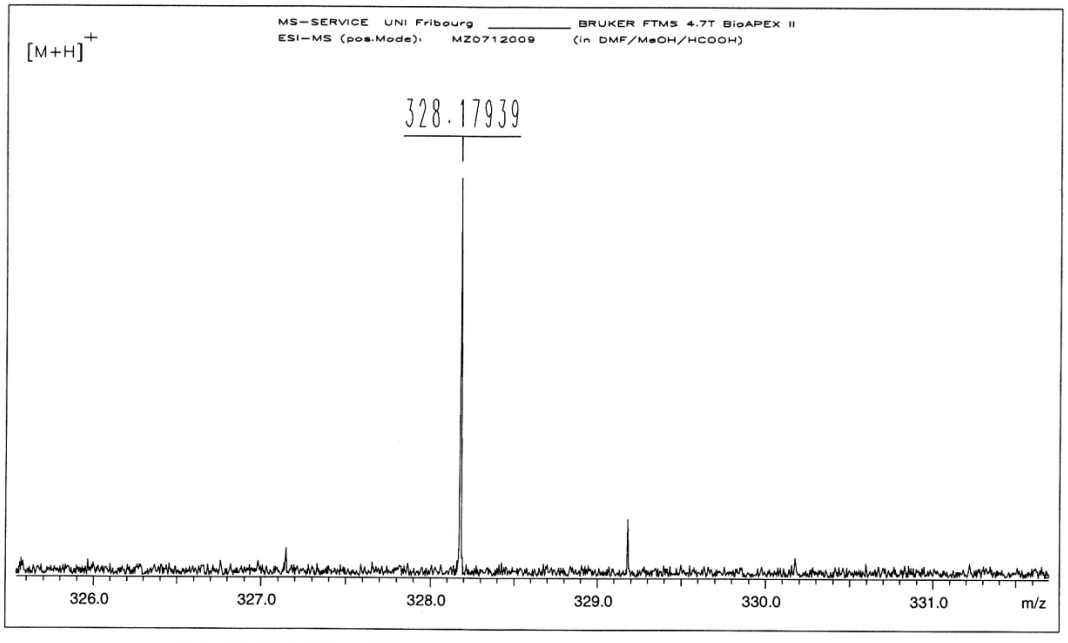

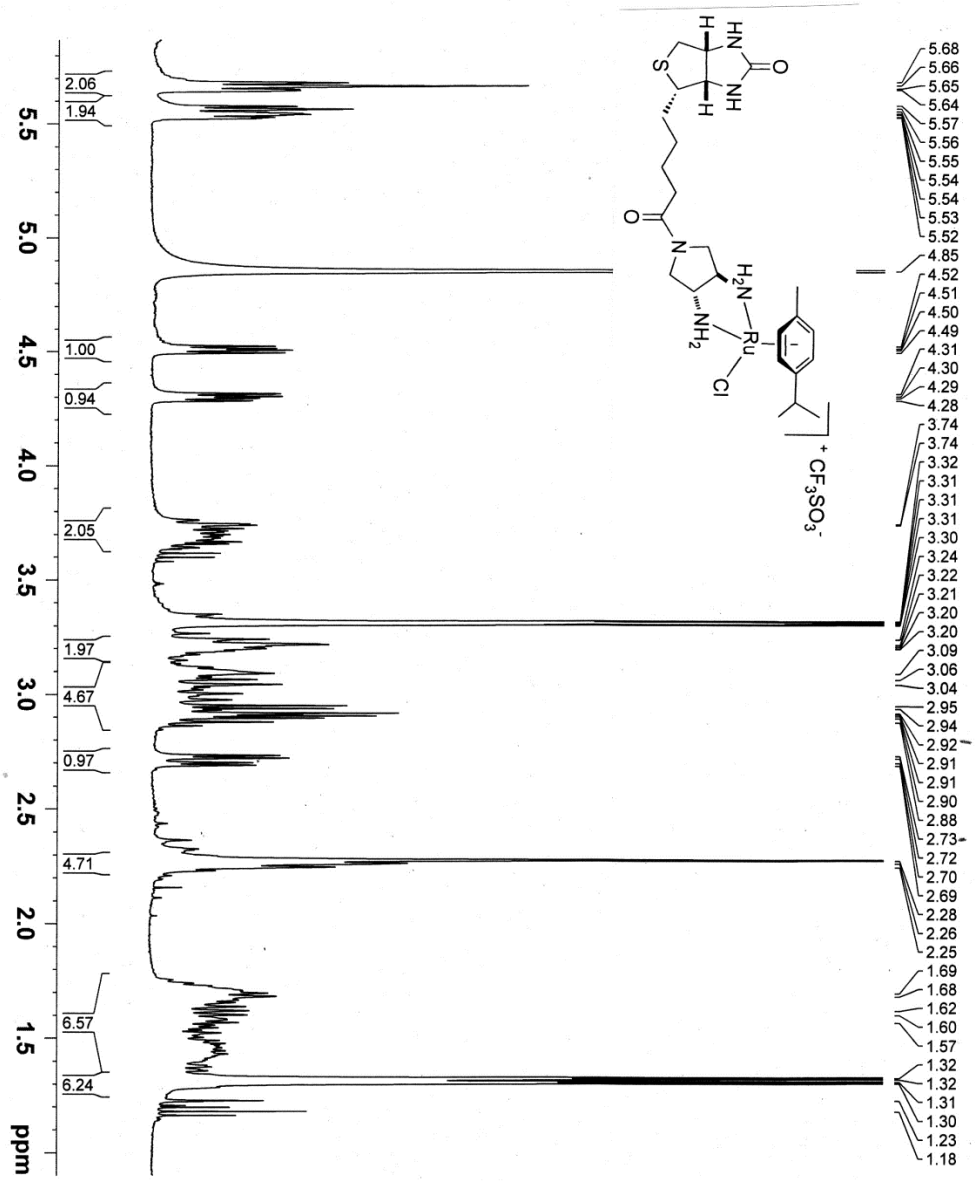


```
Current Data Parameters
NAME                 twmz0712010aCHCl3
EXPNO                             1
PROCNO                            1

F2 - Acquisition Parameters
Date_               20080317
Time_                    10.50
INSTRUM                  spect
PROBHD     5 mm PABBO BB-
PULPROG                 zg30
TD                     32768
SOLVENT                 MeOD
NS                        16
DS                         0
SWH                 4795.396 Hz
FIDRES              0.146344 Hz
AQ                  3.416601 sec
RG                       256
DW                   104.267 usec
DE                     6.00 usec
TE                    298.2 K
D1                    2.00000000 sec
TD0                          1

========== CHANNEL f1 ==========
NUC1                      1H
P1                      9.34 usec
PL1                    -4.00 dB
SFO1          400.1320150 MHz

F2 - Processing parameters
SI                       32768
SF            400.1300097 MHz
WDW                         EM
SSB                          0
LB                        0.10 Hz
GB                           0
PC                        1.00
```

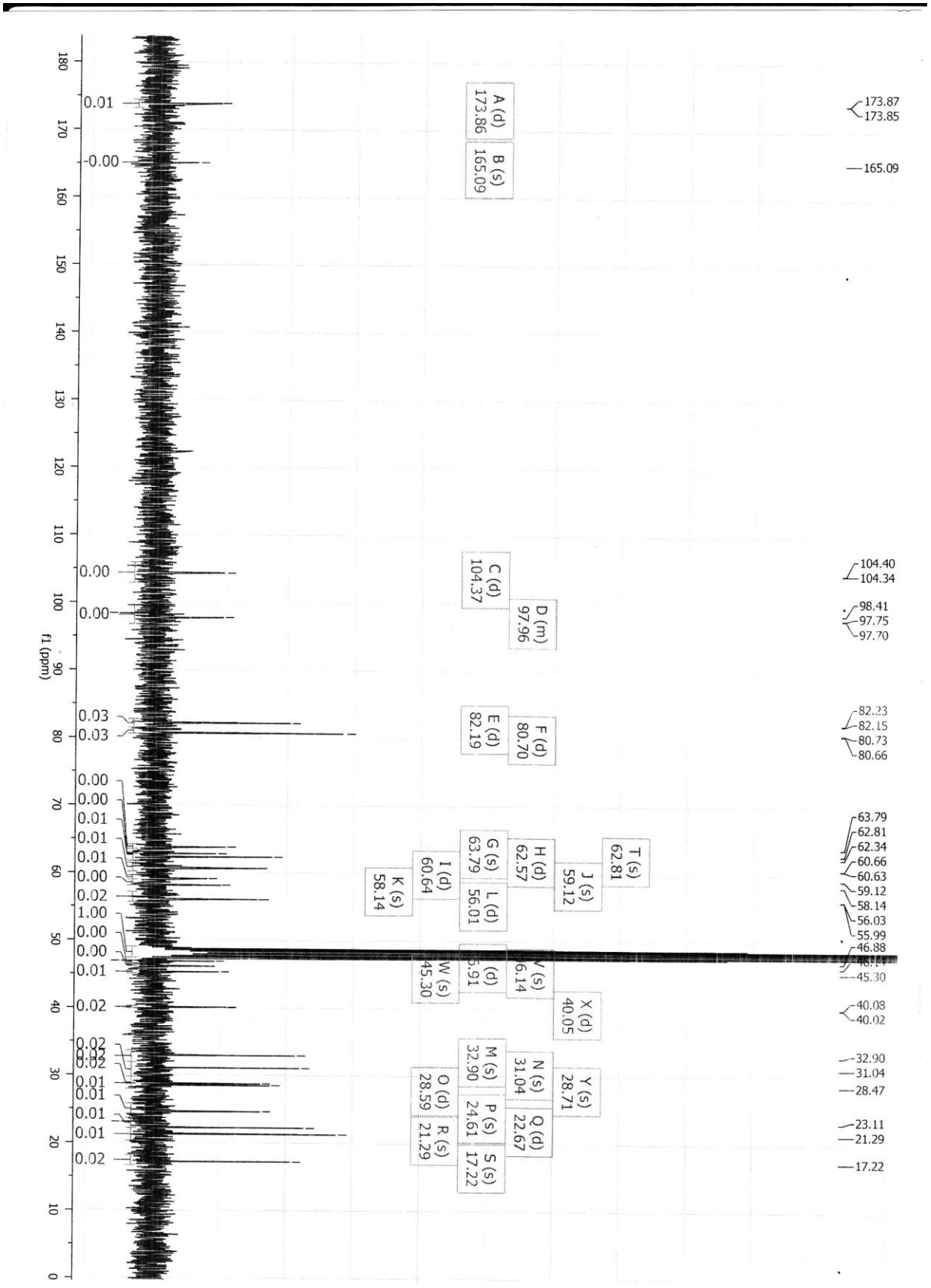
f1 (ppm)
A (d) 173.86
B (s) 165.09
C (d) 104.37
D (m) 97.96
E (d) 82.19
F (d) 80.70
G (s) 63.79
H (d) 62.57
I (d) 60.64
J (s) 59.12
K (s) 58.14
L (d) 56.01
M (s) 32.90
N (s) 31.04
O (d) 28.59
P (s) 24.61
Q (d) 22.67
R (s) 21.29
S (s) 17.22
T (s) 62.81
W (s) 45.30
X (d) 40.05
Y (s) 28.71
173.87
173.85
165.09
104.40
104.34
98.41
97.75
97.70
82.23
82.15
80.73
80.66
63.79
62.81
62.34
60.66
60.63
59.12
58.14
56.03
55.99
46.88
45.30
40.08
40.02
32.90
31.04
28.47
23.11
21.29
17.22

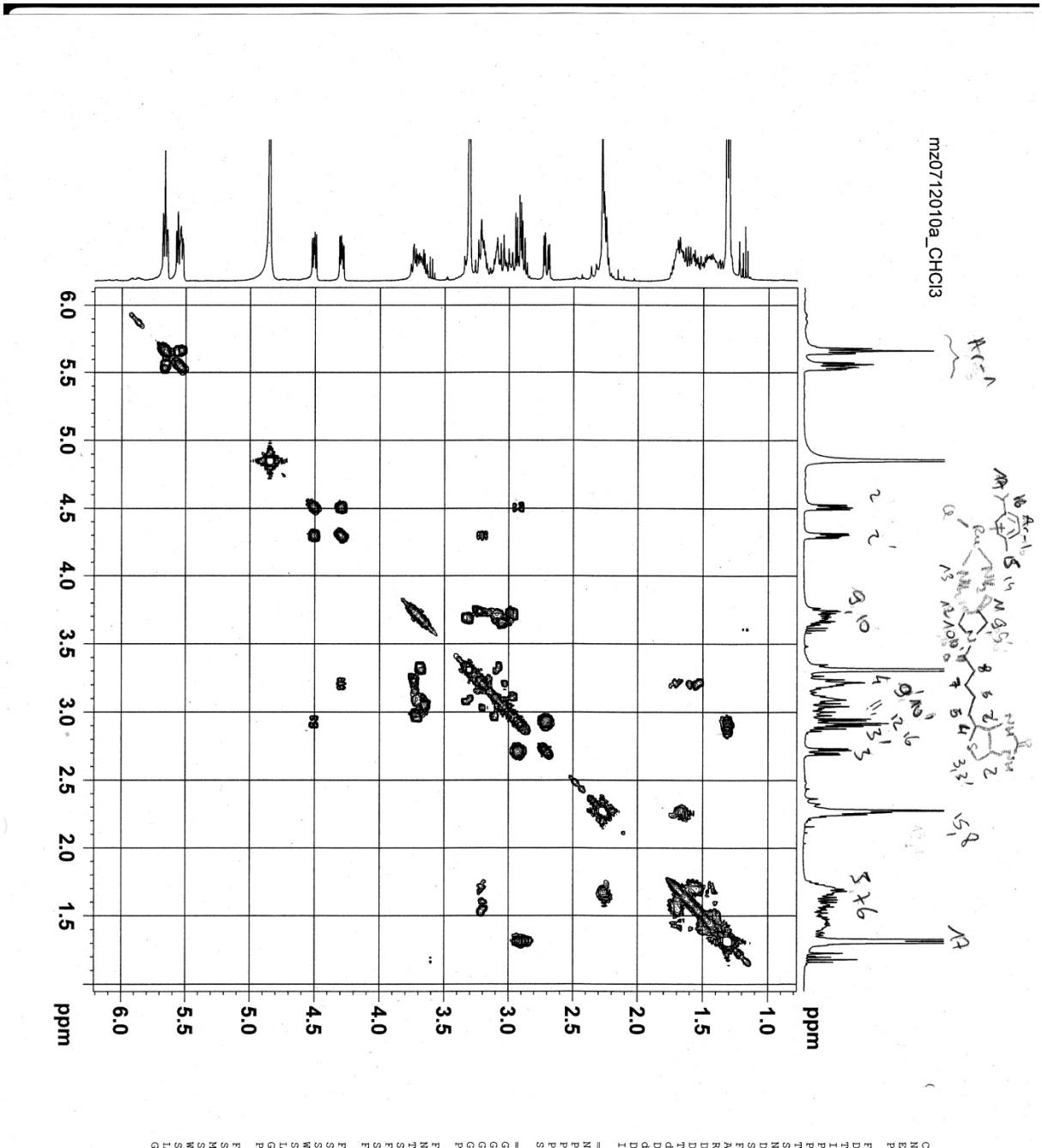


```
Current Data Parameters
NAME                  twmz0712010aCHCl3
EXPNO                                 2
PROCNO                                1

F2 - Acquisition Parameters
Date_              20080317
Time               10.51
INSTRUM              spect
PROBHD     5 mm PABBO BB-
PULPROG              cosygpqf
TD                   1024
SOLVENT              MeOD
NS                      4
DS                      4
SWH                3246.753 Hz
FIDRES             3.170657 Hz
AQ                 0.157760 sec
RG                    90.5
DW                  154.000 usec
DE                    6.00 usec
TE                  298.2 K
d0                  0.00000300 sec
D1                  0.91248202 sec
d13                 0.00000400 sec
D16                 0.00020000 sec
INO                 0.00030800 sec

======== CHANNEL f1 ========
NUC1                  1H
P0                    4.67 usec
P1                    9.34 usec
PL1                  -4.00 dB
SFO1          400.1317842 MHz

====== GRADIENT CHANNEL =====
GPNAM1       SINE.100
GPNAM2       SINE.100
GPZ1                 10.00 %
GPZ2                 10.00 %
P16                1000.00 usec

F1 - Acquisition parameters
NDO                     1
TD                    128
SFO1          400.1318 MHz
FIDRES       25.365259 Hz
SW                 8.114 ppm
FnMODE                QF

F2 - Processing parameters
SI                   1024
SF            400.1300097 MHz
WDW                  SINE
SSB                     0
LB                   0.00 Hz
GB                      0
PC                   0.60

F1 - Processing parameters
SI                   1024
MC2                    QF
SF            400.1300097 MHz
WDW                  SINE
SSB                     0
LB                   0.00 Hz
GB                      0
```

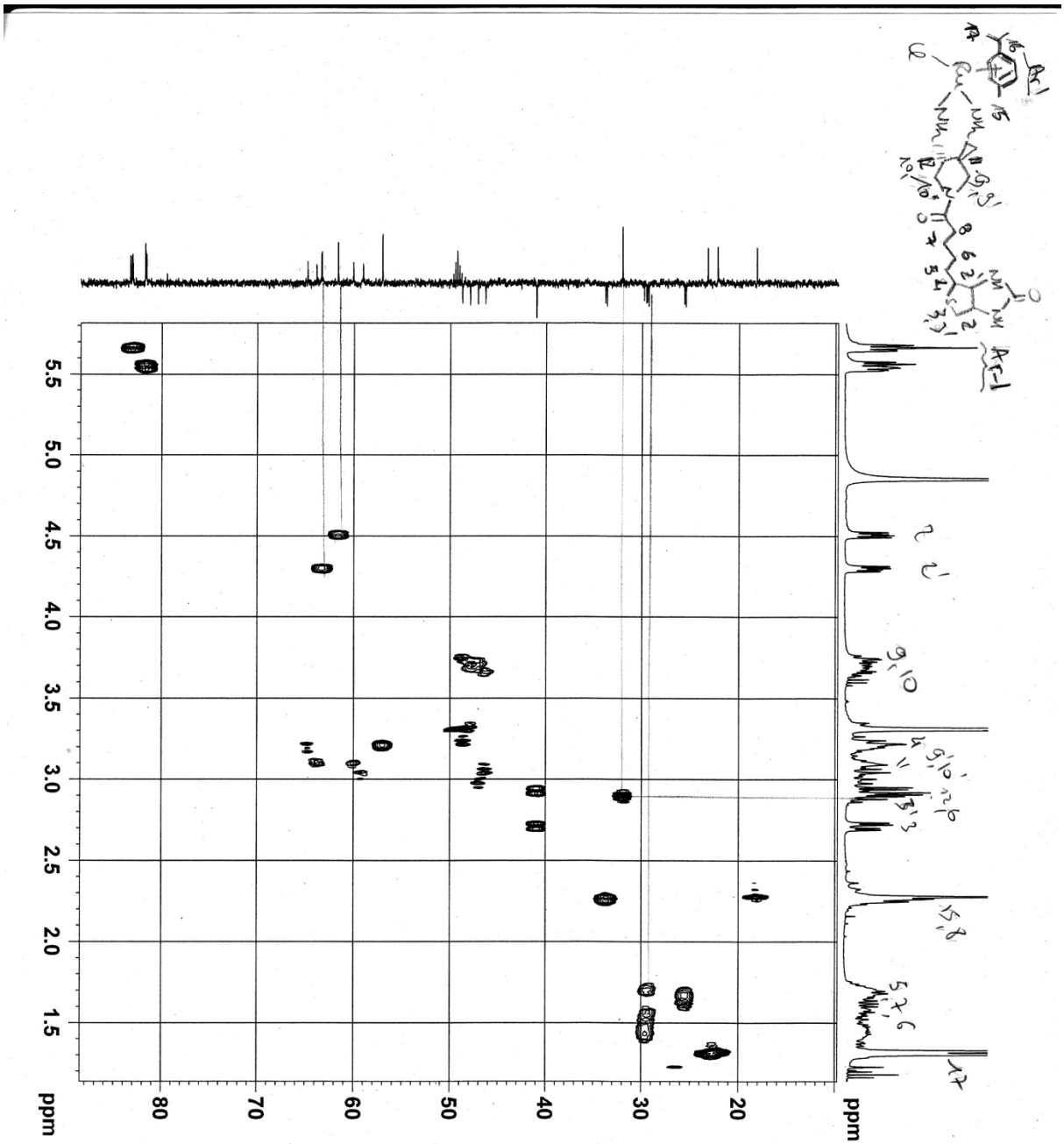


```
Current Data Parameters
NAME                 tum071201OaCHCl3
EXPNO                              4
PROCNO                             1

F2 - Acquisition Parameters
Date_              20080317
Time               11.21
INSTRUM            spect
PROBHD     5 mm PABBO BB-
PULPROG            hsqcetgp
TD                 1024
SOLVENT            MeOD
NS                   16
DS                    2
SWH          1976.285 Hz
FIDRES          1.929965 Hz
AQ           0.2592020 sec
RG                 253.000
DW                 6.00 usec
DE                 6.00 usec
TE                 298.9 K
CNST2              145.0000000
d0           0.0000030000 sec
D1           1.6433280000 sec
d11          0.0300000000 sec
D13          0.0000020000 sec
D16          0.0002000000 sec
d4           0.0017241400 sec
DELTA        0.0012246700 sec
DELTA1       0.0007161400 sec
IN0          0.0000074000 sec
SFICNT             64
ZGOPTNS

======== CHANNEL f1 ========
NUC1               1H
P1                 9.34 usec
P2                18.67 usec
PL1               1.00 dB
SFO1         400.1314050 MHz

======== CHANNEL f2 ========
CPDPRG2          garp
NUC2               13C
P3                 9.30 usec
P4                18.60 usec
PCPD2             70.00 usec
PL12              16.53 dB
PL2               -1.00 dB
SFO2        100.6218241 MHz

======= GRADIENT CHANNEL =====
GPNAM1         SINE.100
GPNAM2         SINE.100
GPZ1              80.00 %
GPZ2              19.51 %
P16             1000.00 usec

F1 - Acquisition parameters
NDO                128
TD                 100.6218 MHz
SFO1          141.530792 Hz
FIDRES          180.040 ppm
SW              Echo-Antiecho
FnMODE

F2 - Processing parameters
SI                1024
SF          400.1300177 MHz
WDW                QSINE
SSB                2
LB                 0.00 Hz
GB                 0.00
PC                 1.40

F1 - Processing parameters
SI                1024
MC2         echo-antiecho
SF          100.6126286 MHz
WDW                QSINE
SSB                2
LB                 0.00 Hz
GB                 0
```

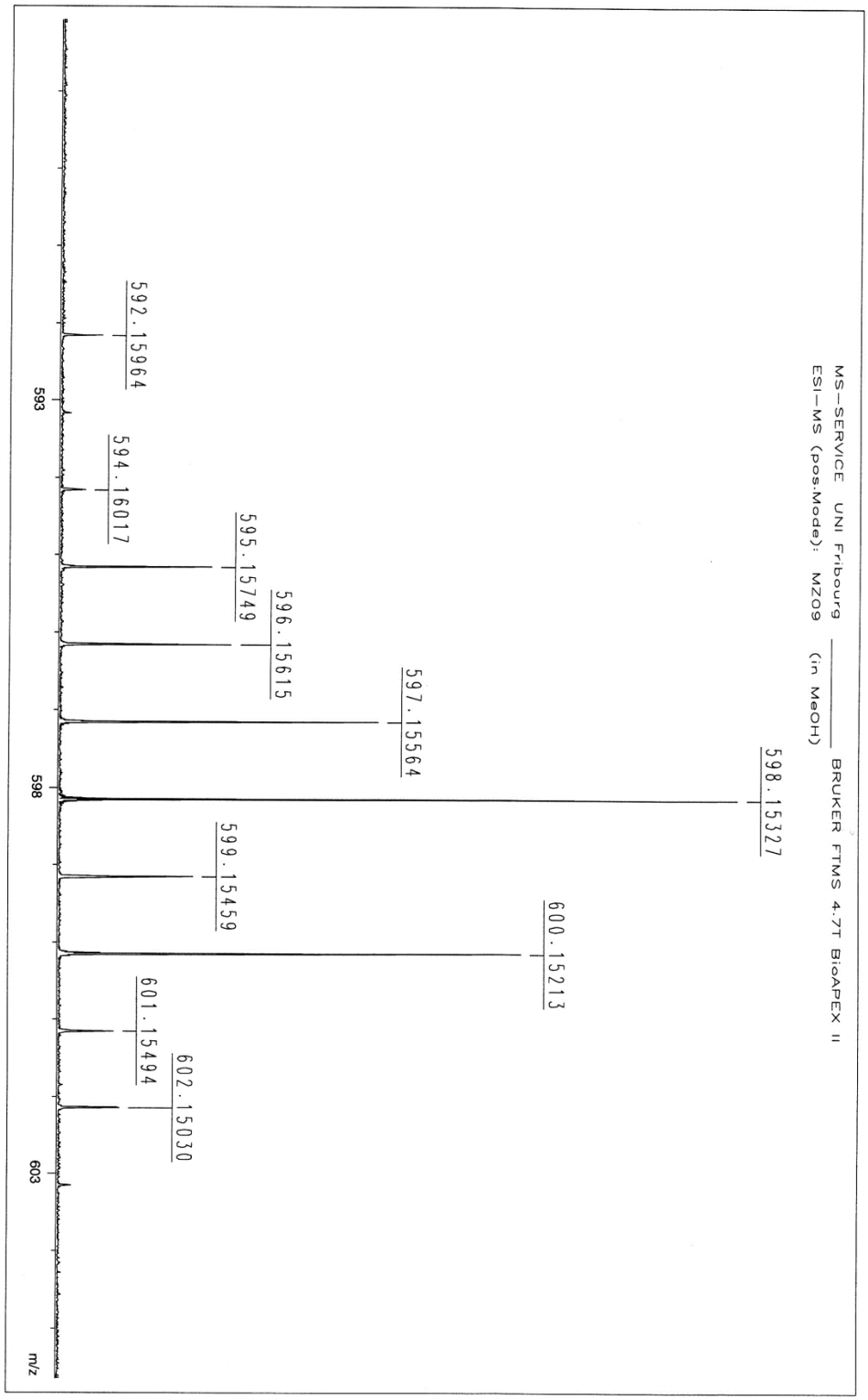
MS-SERVICE UNI Fribourg
ESI-MS (pos.Mode): MZ09 (in MeOH)
BRUKER FTMS 4.7T BioAPEX II
592.15964
593
594.16017
595.15749
596.15615
597.15564
598
598.15327
599.15459
600.15213
601.15494
602.15030
603
m/z
/Data/UNI_BS/ZIMB6167_ESI/10/pdata/1 FTMS USER Thu Nov 17 15:28:41 2011

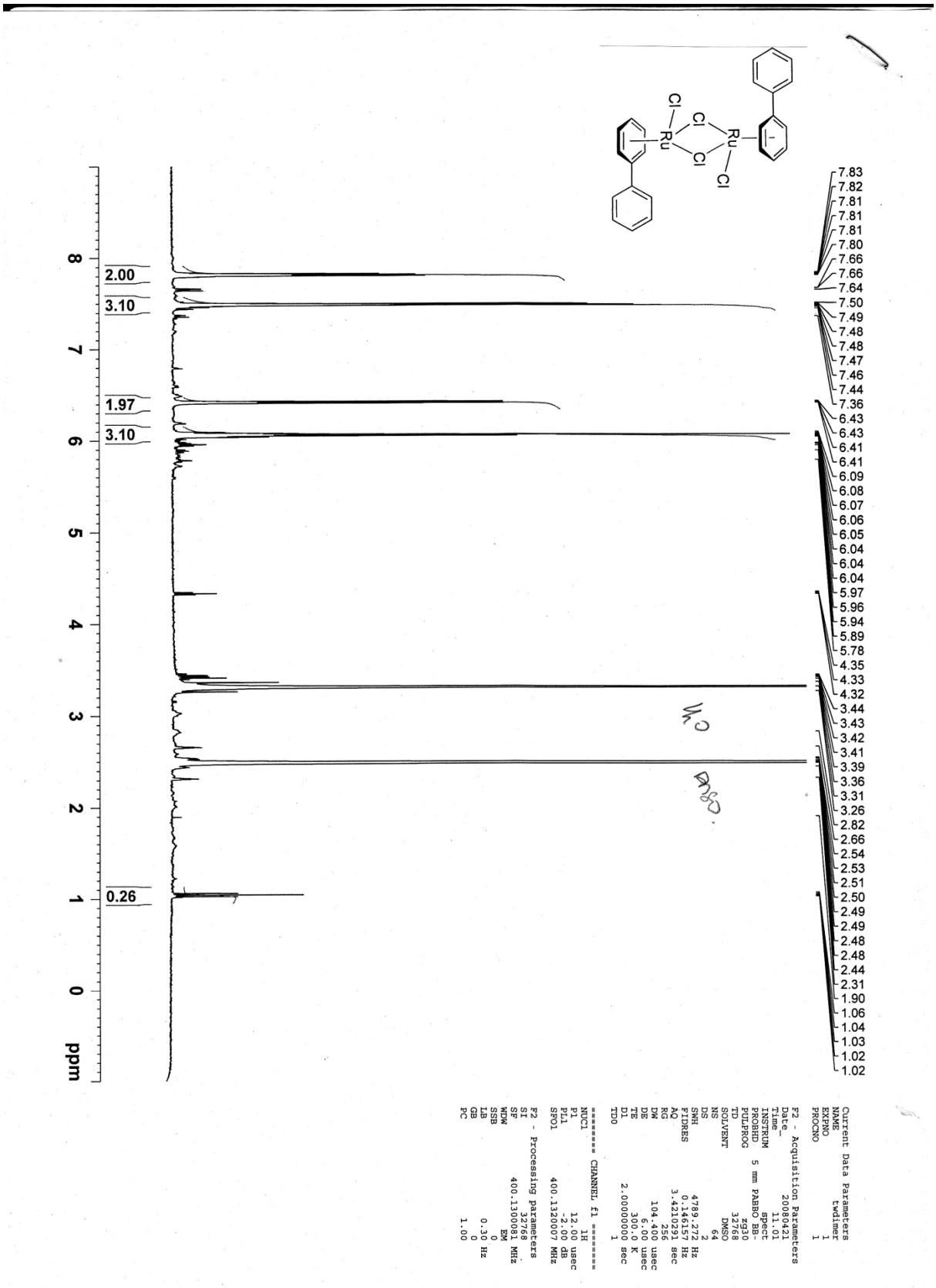
Cl
Cl
Ru
Ru
Cl
Cl
Cl
7.83
7.82
7.81
7.81
7.81
7.80
7.66
7.66
7.64
7.50
7.49
7.48
7.48
7.47
7.46
7.44
7.36
6.43
6.43
6.41
6.41
6.09
6.08
6.07
6.06
6.05
6.04
6.04
6.04
5.97
5.96
5.94
5.89
5.78
4.35
4.33
4.32
3.44
3.43
3.42
3.41
3.39
3.36
3.31
3.26
2.82
2.66
2.54
2.53
2.51
2.50
2.49
2.49
2.48
2.48
2.44
2.31
1.90
1.06
1.04
1.03
1.02
1.02
2.00
3.10
1.97
3.10
0.26
8
7
6
5
4
3
2
1
0
ppm
H2O
DMSO
Current Data Parameters
NAME twdimer
EXPNO 1
PROCNO 1
F2 - Acquisition Parameters
Date_ 20080421
Time_ 11.01
INSTRUM spect
PROBHD 5 mm PABBO BB-
PULPROG zg30
TD 32768
SOLVENT DMSO
NS 64
DS 2
SWH 4789.272 Hz
FIDRES 0.146157 Hz
AQ 3.4210252 sec
RG 228.5
DW 104.400 usec
DE 6.00 usec
TE 300.0 K
D1 2.00000000 sec
TD0 1
======== CHANNEL f1 ========
NUC1 1H
P1 12.00 usec
PL1 -2.00 dB
SFO1 400.1320007 MHz
F2 - Processing parameters
SI 32768
SF 400.1300081 MHz
WDW EM
SSB 0
LB 0.30 Hz
GB 0
PC 1.00

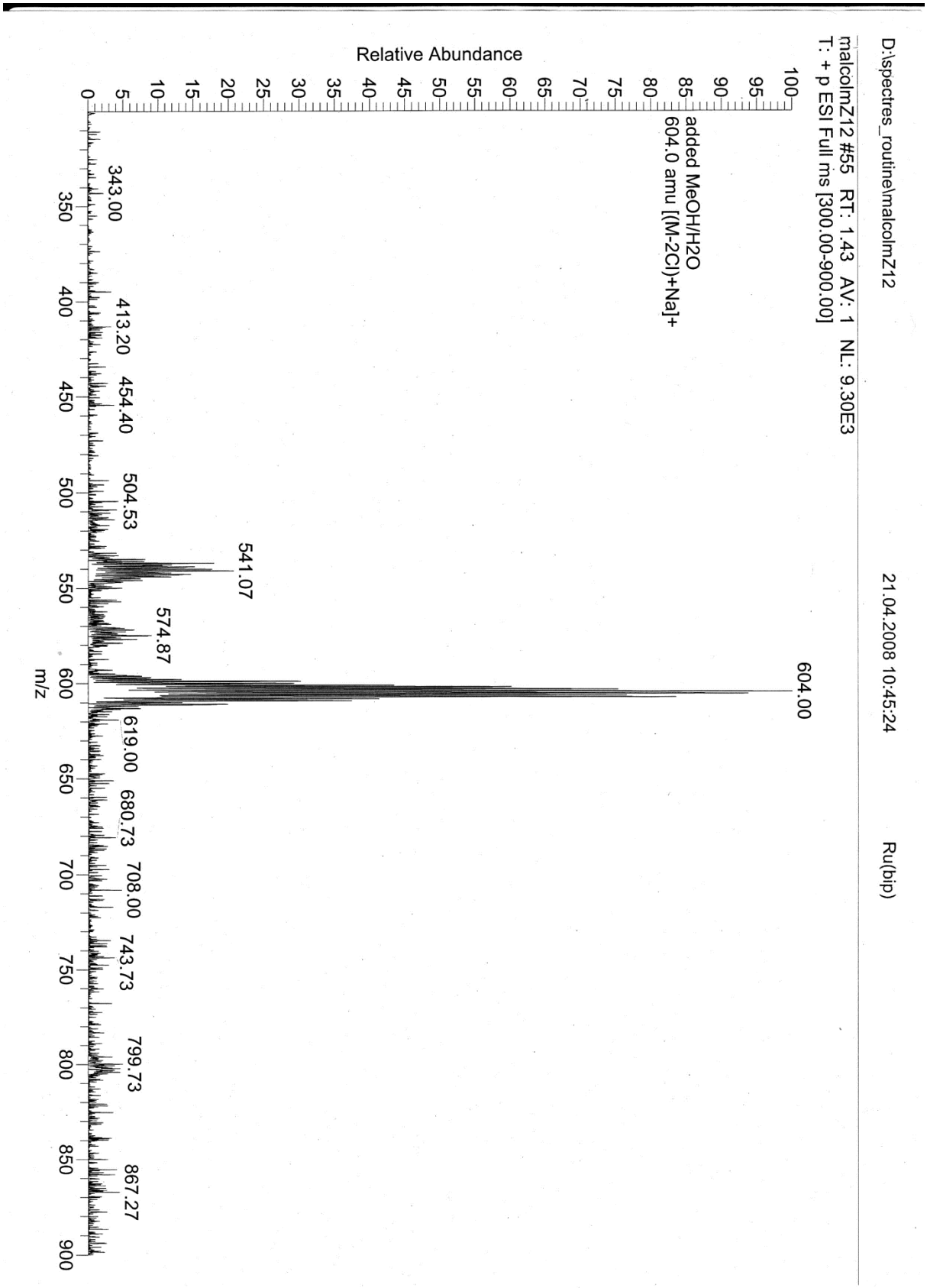
D:\spectres_routine\malcolmZ12
21.04.2008 10:45:24
Ru(bip)
malcolmZ12 #55 RT: 1.43 AV: 1 NL: 9.30E3
T: + p ESI Full ms [300.00-900.00]
Relative Abundance
added MeOH/H2O
604.0 amu [(M-2Cl)+Na]+
604.00
541.07
574.87
343.00
413.20
454.40
504.53
619.00
680.73
708.00
743.73
799.73
867.27
m/z

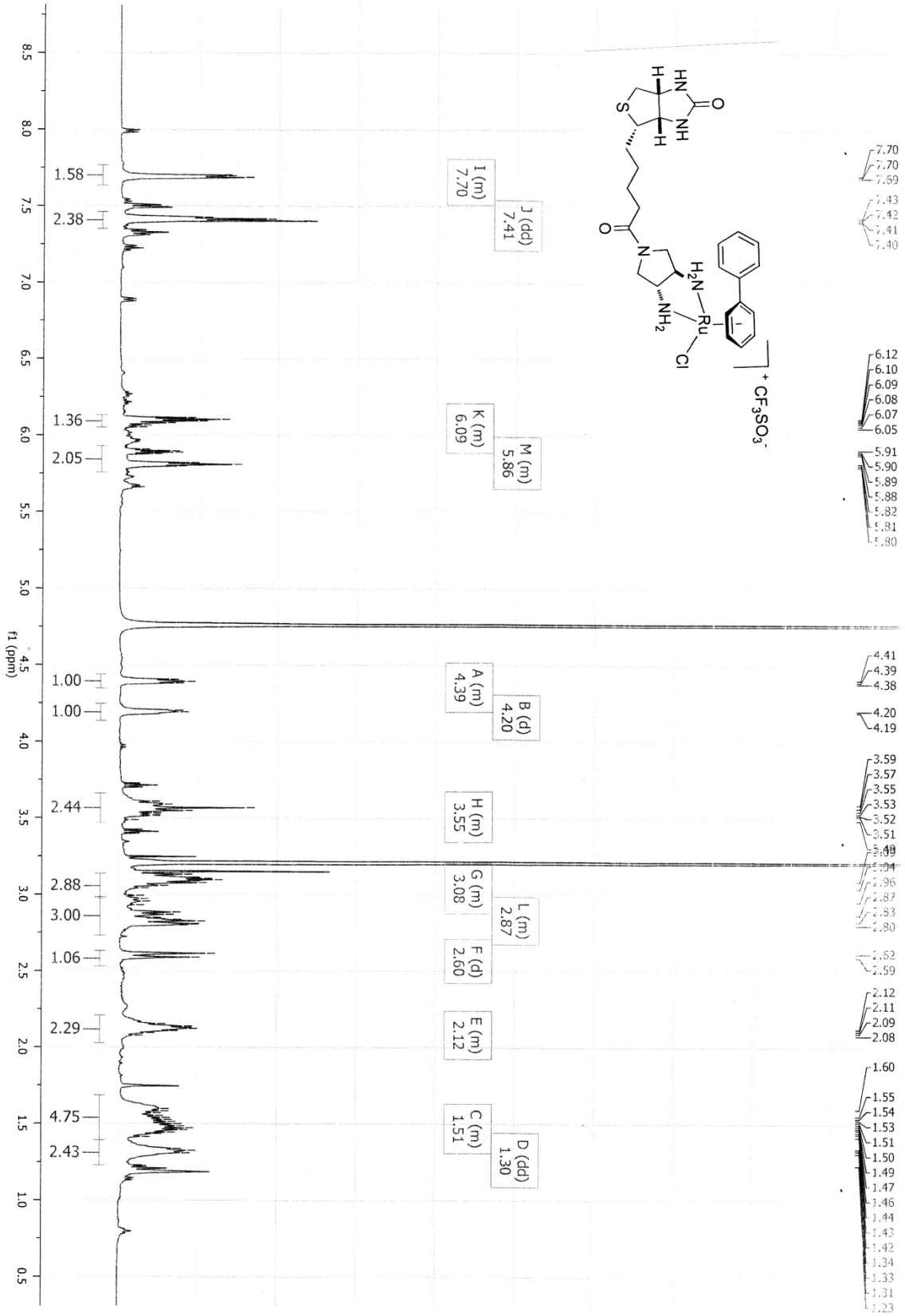
f1 (ppm)
1.58
2.38
1.36
2.05
1.00
1.00
2.44
2.88
3.00
1.06
2.29
4.75
2.43
I (m) 7.70
J (dd) 7.41
K (m) 6.09
M (m) 5.86
A (m) 4.39
B (d) 4.20
H (m) 3.55
G (m) 3.08
L (m) 2.87
F (d) 2.60
E (m) 2.12
C (m) 1.51
D (dd) 1.30
$CF_3SO_3^-$

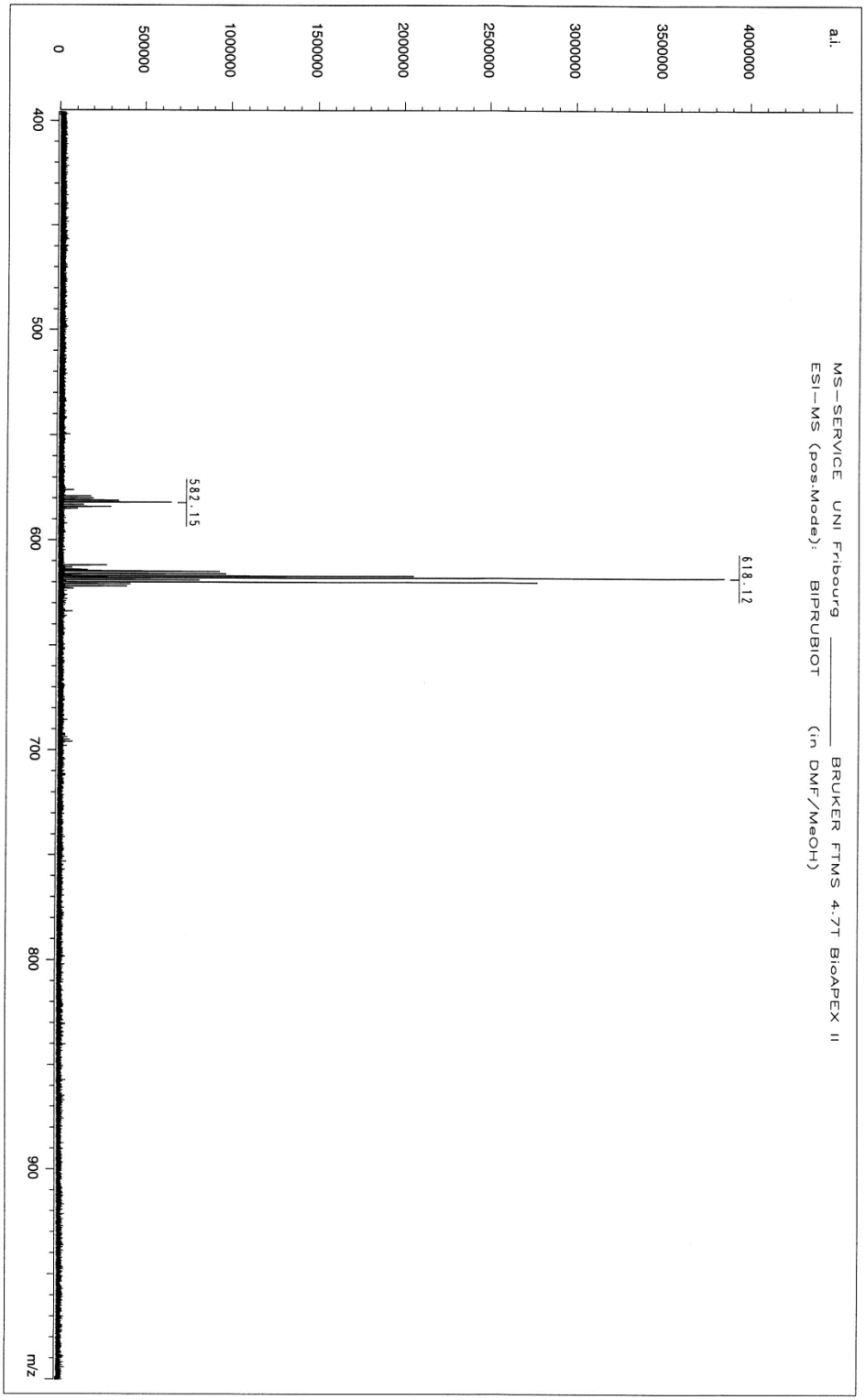
a.i.
MS-SERVICE UNI Fribourg BRUKER FTMS 4.7T BioAPEX II
ESI-MS (pos.Mode): BIPRUBIOT (in DMF/MeOH)
582.15
618.12
m/z
/Data/UNI_BS/ZIMB6210_ESI/1/pdata/1 FTMS USER Wed Dec 7 15:35:10 2011

Breitband

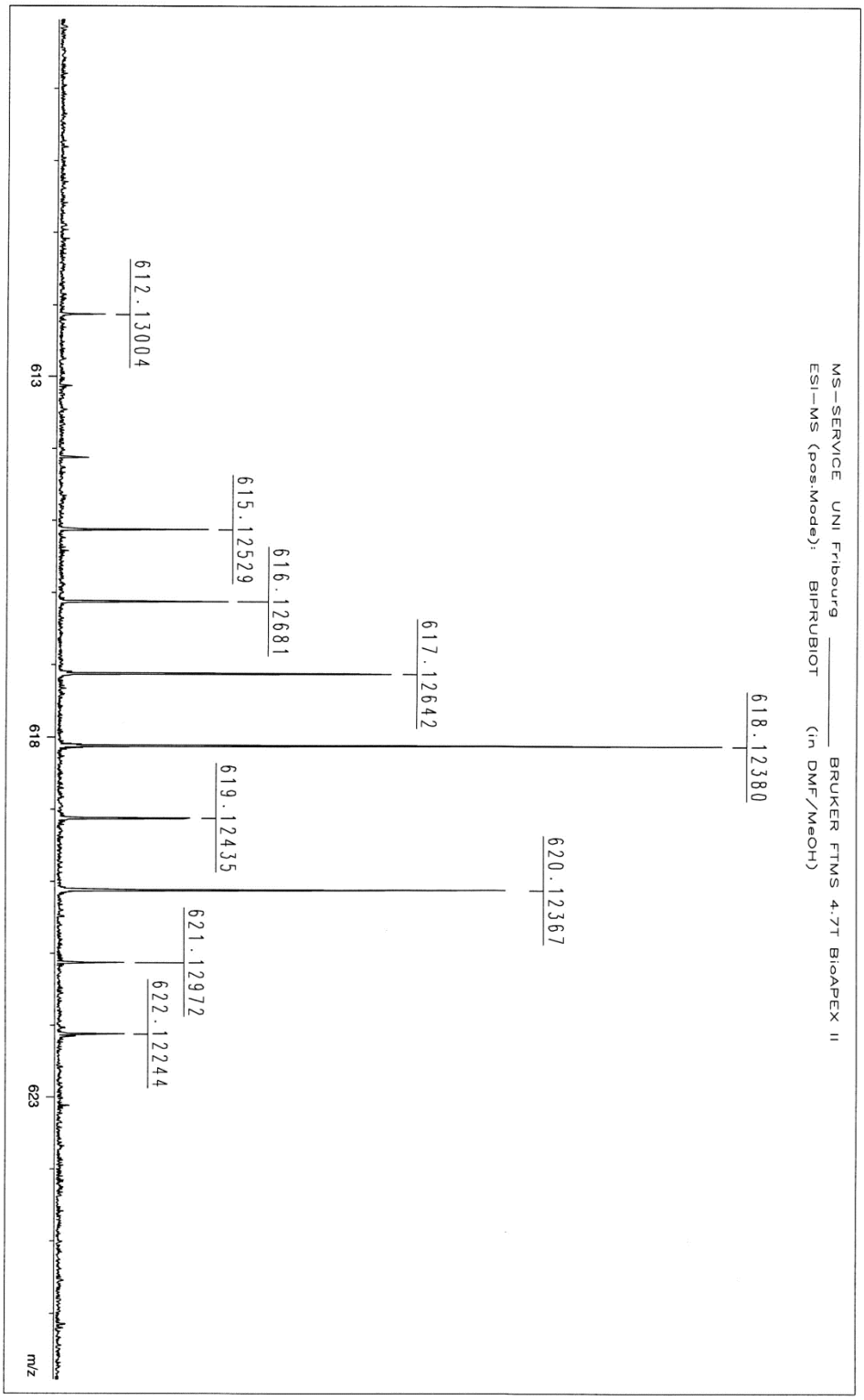
MS-SERVICE UNI Fribourg BRUKER FTMS 4.7T BioAPEX II
ESI-MS (pos-Mode): BIPRUBIOT (in DMF/MeOH)
612.13004
615.12529
616.12681
617.12642
618.12380
619.12435
620.12367
621.12972
622.12244
613
618
623
m/z
/Data/UNI_BS/ZIMB6210_ESI/3/pdata/1 FTMS USER Wed Dec 7 15:33:53 2011

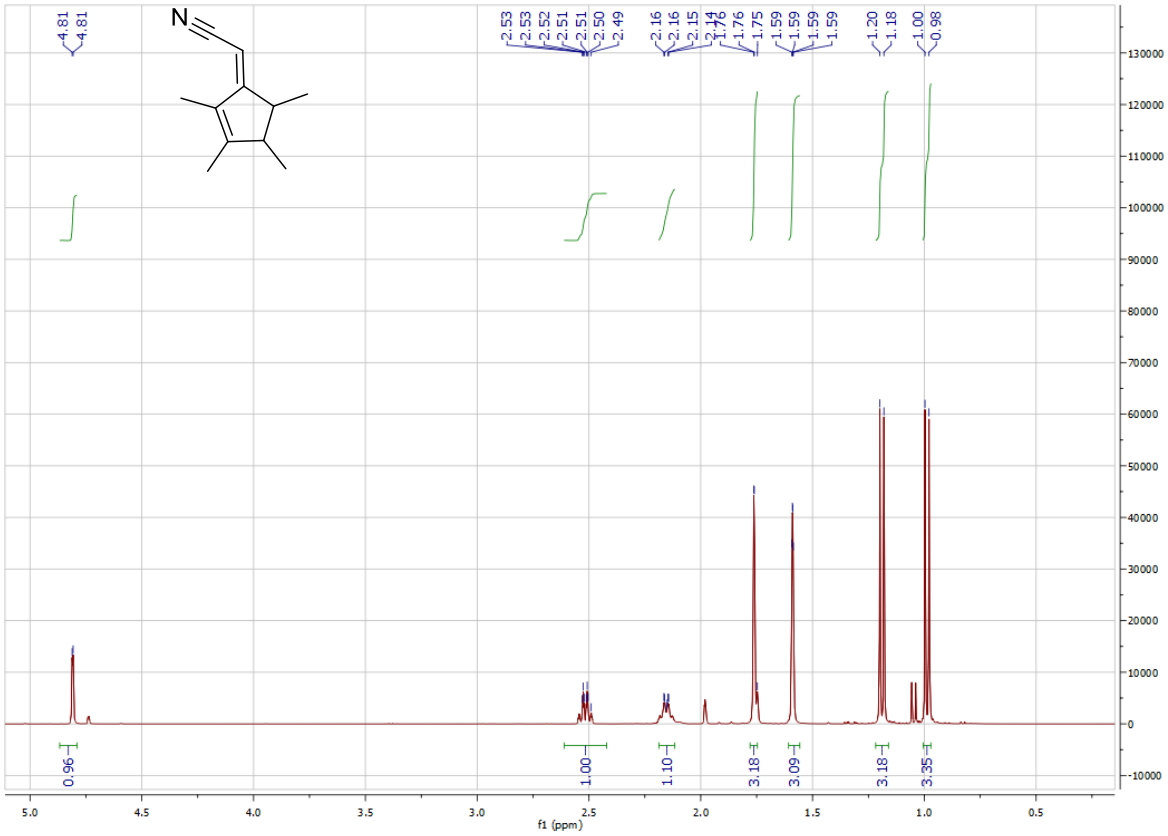
N
4.81
4.81
2.53
2.53
2.52
2.51
2.51
2.50
2.49
2.16
2.16
2.15
2.14
1.76
1.75
1.59
1.59
1.59
1.59
1.20
1.18
1.00
0.98
0.96
1.00
1.10
3.18
3.09
3.18
3.35
f1 (ppm)

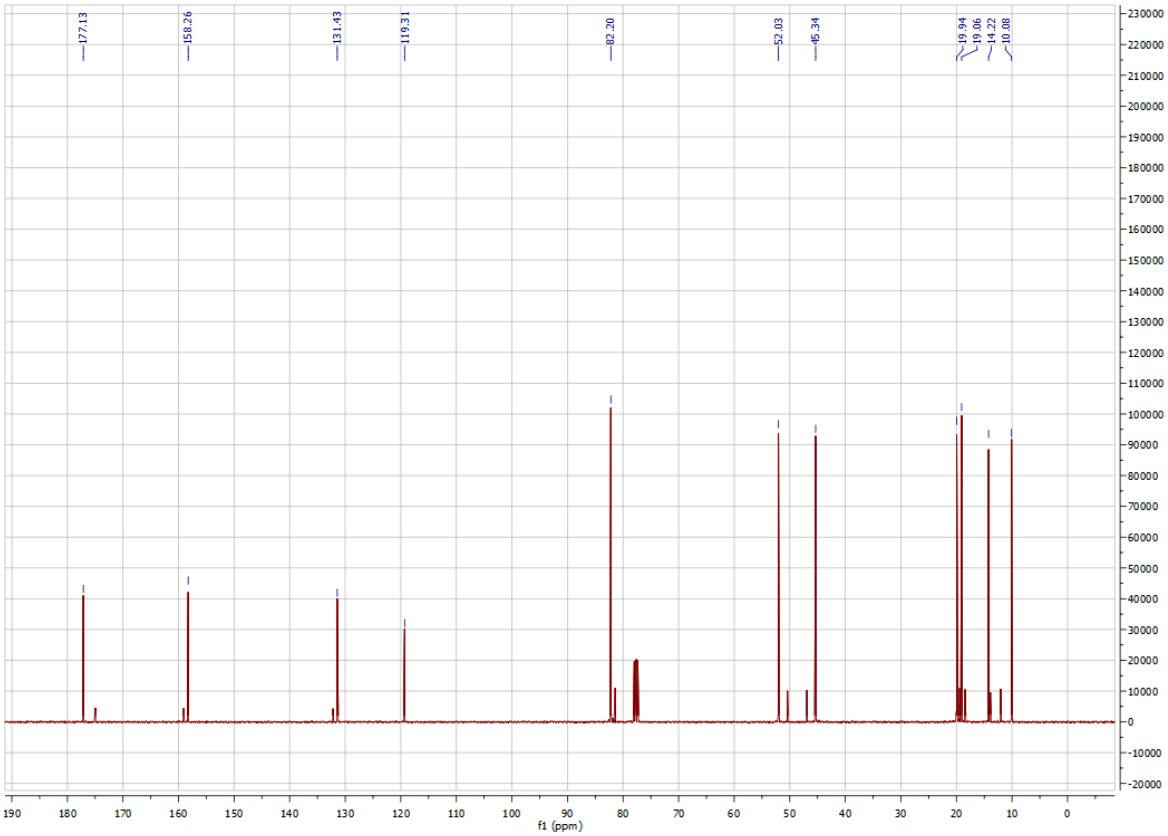
177.13
158.26
131.43
119.31
82.20
52.03
45.34
19.94
19.06
14.22
10.08
f1 (ppm)

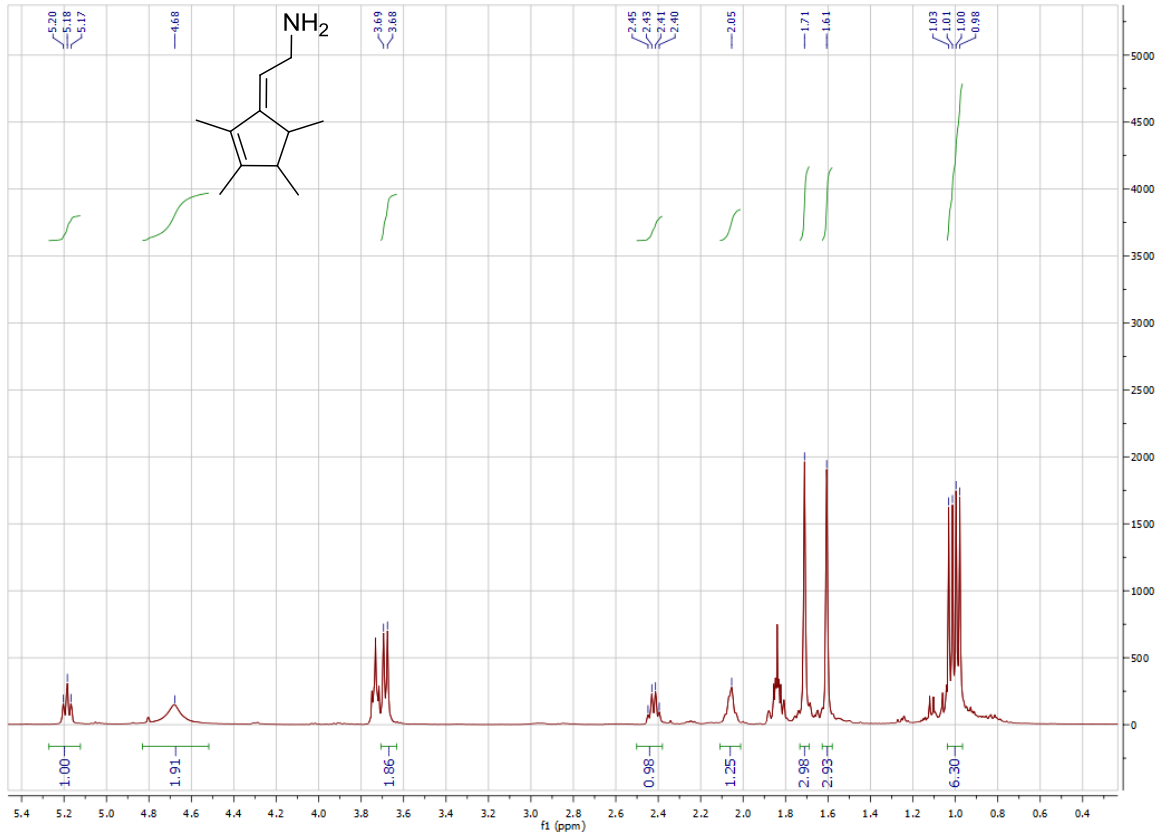
NH2
5.20
5.18
5.17
4.68
3.69
3.68
2.45
2.43
2.41
2.40
2.05
1.71
1.61
1.03
1.01
1.00
0.98
1.00
1.91
1.86
0.98
1.25
2.98
2.93
6.30
f1 (ppm)

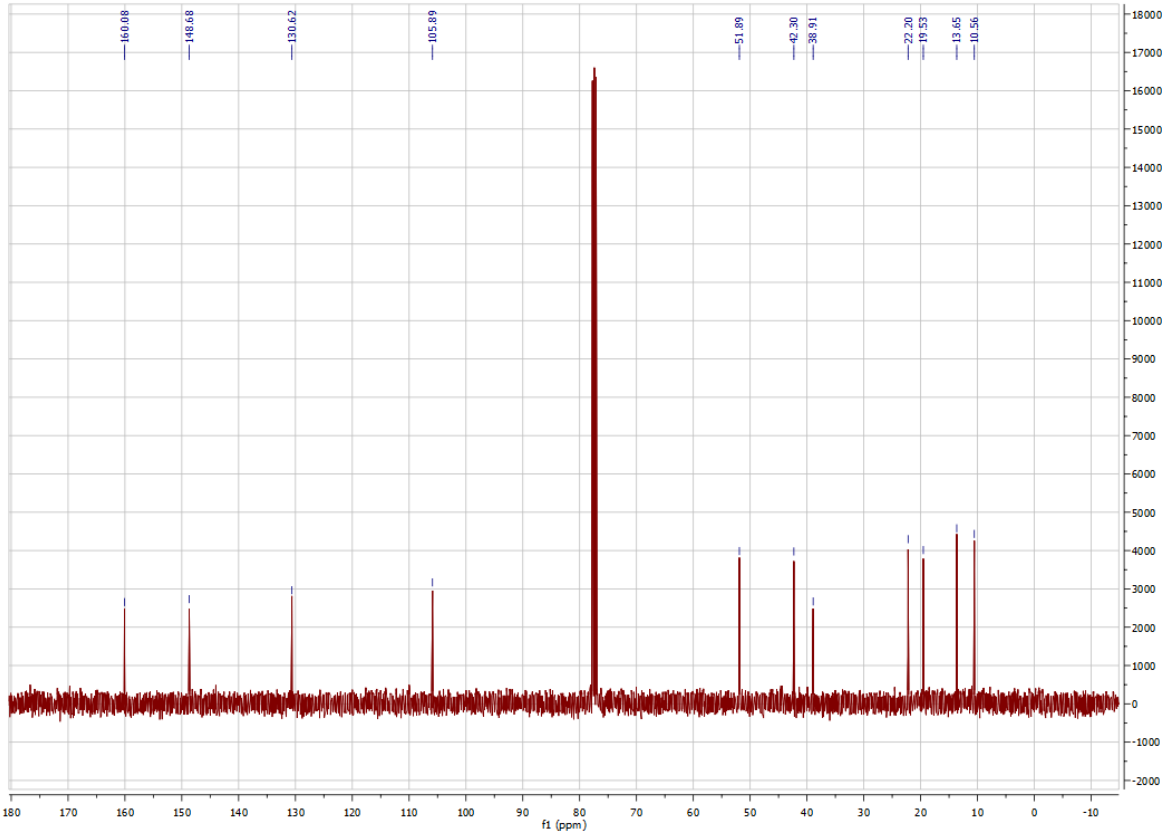
160.08
148.68
130.62
105.89
51.89
42.30
38.91
22.20
19.53
13.65
10.56
f1 (ppm)

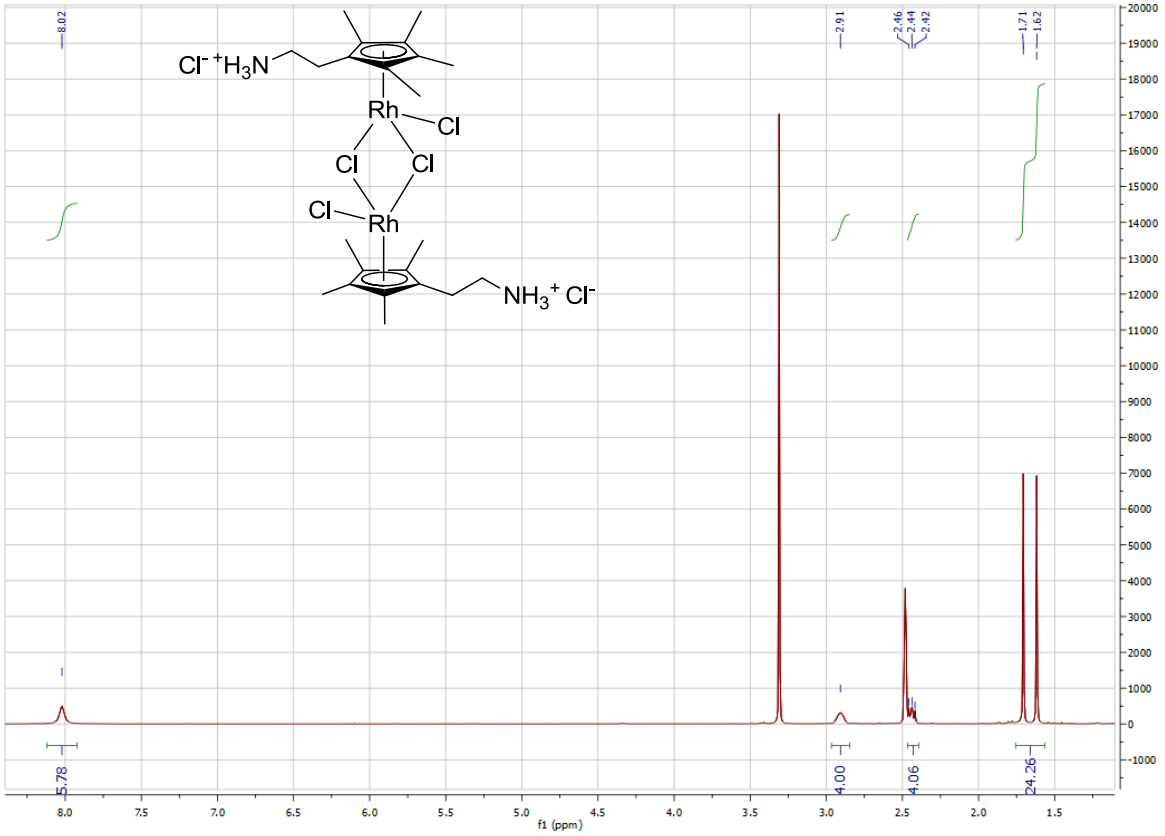
Cl⁻ ⁺H₃N
Rh
Cl
Cl
Cl
Cl
Rh
NH₃⁺ Cl⁻
8.02
2.91
2.46
2.44
2.42
1.71
1.62
5.78
4.00
4.06
24.26
f1 (ppm)

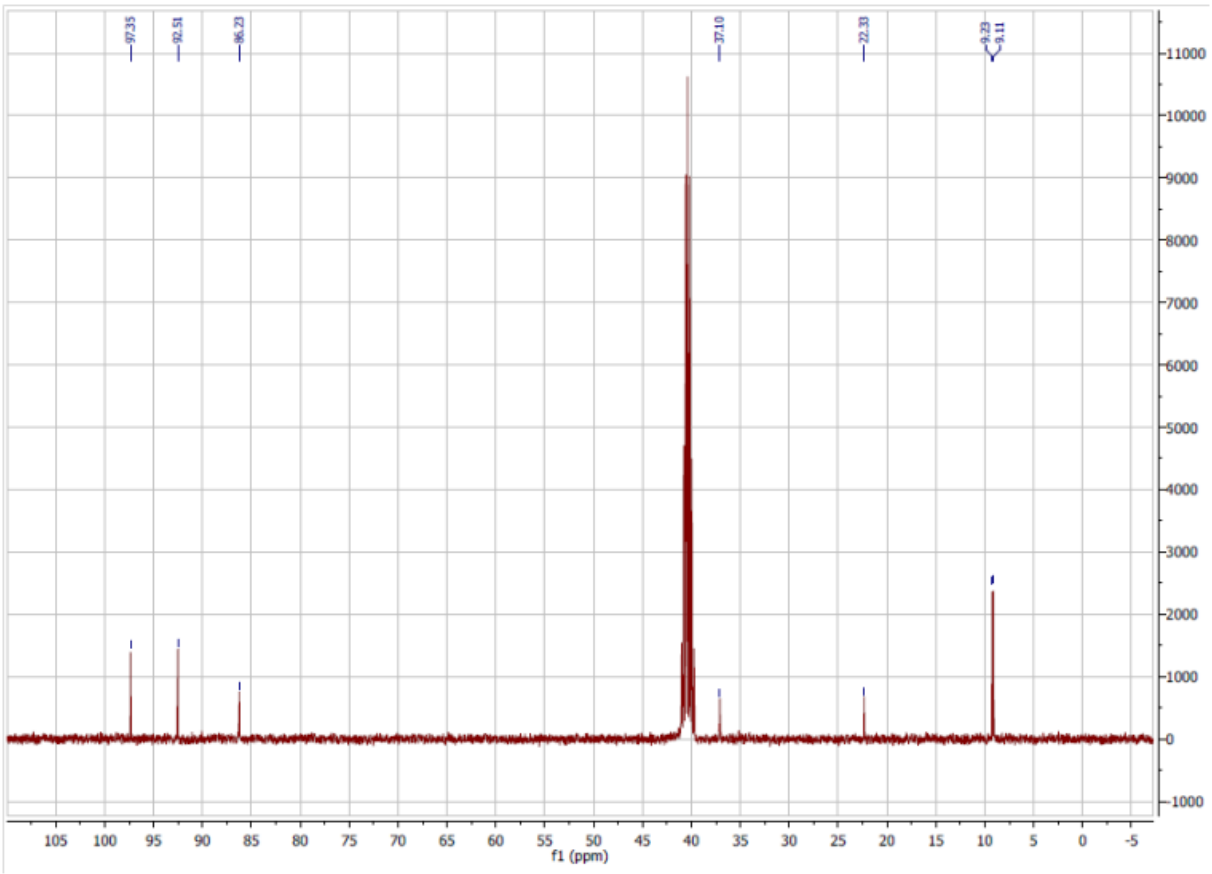
97.35
92.51
86.23
37.10
22.33
9.23
9.11
f1 (ppm)

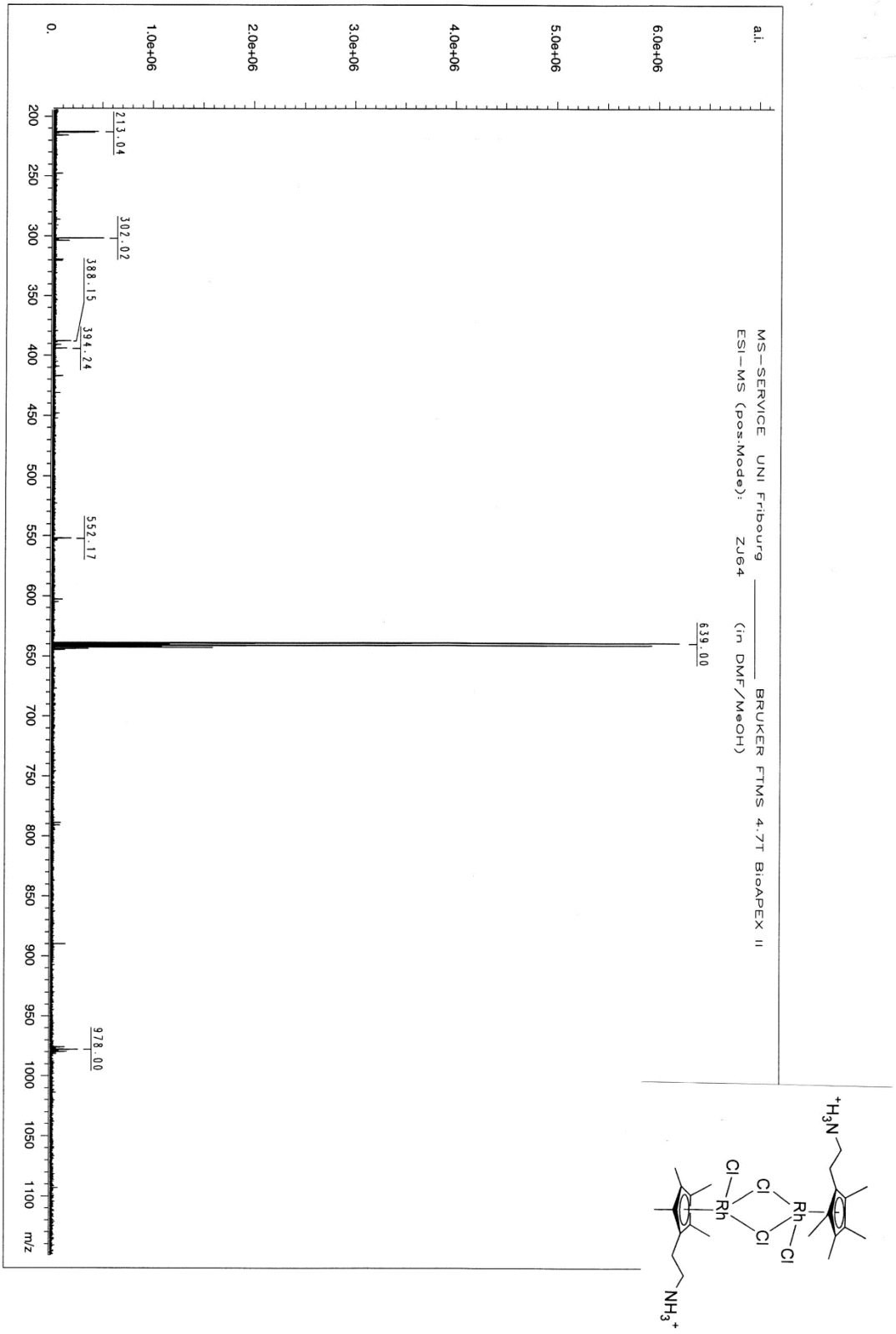
a.i.
MS-SERVICE UNI Fribourg BRUKER FTMS 4.7T BioAPEX II
ESI-MS (pos:Mode): Zu64 (in DMF/MeOH)
213.04
302.02
388.15
394.24
552.17
639.00
978.00
m/z
/Data/UNI_BS/ZIMB5073_ESI/2/pdata/1 FTMS USER Tue Sep 7 13:18:08 2010

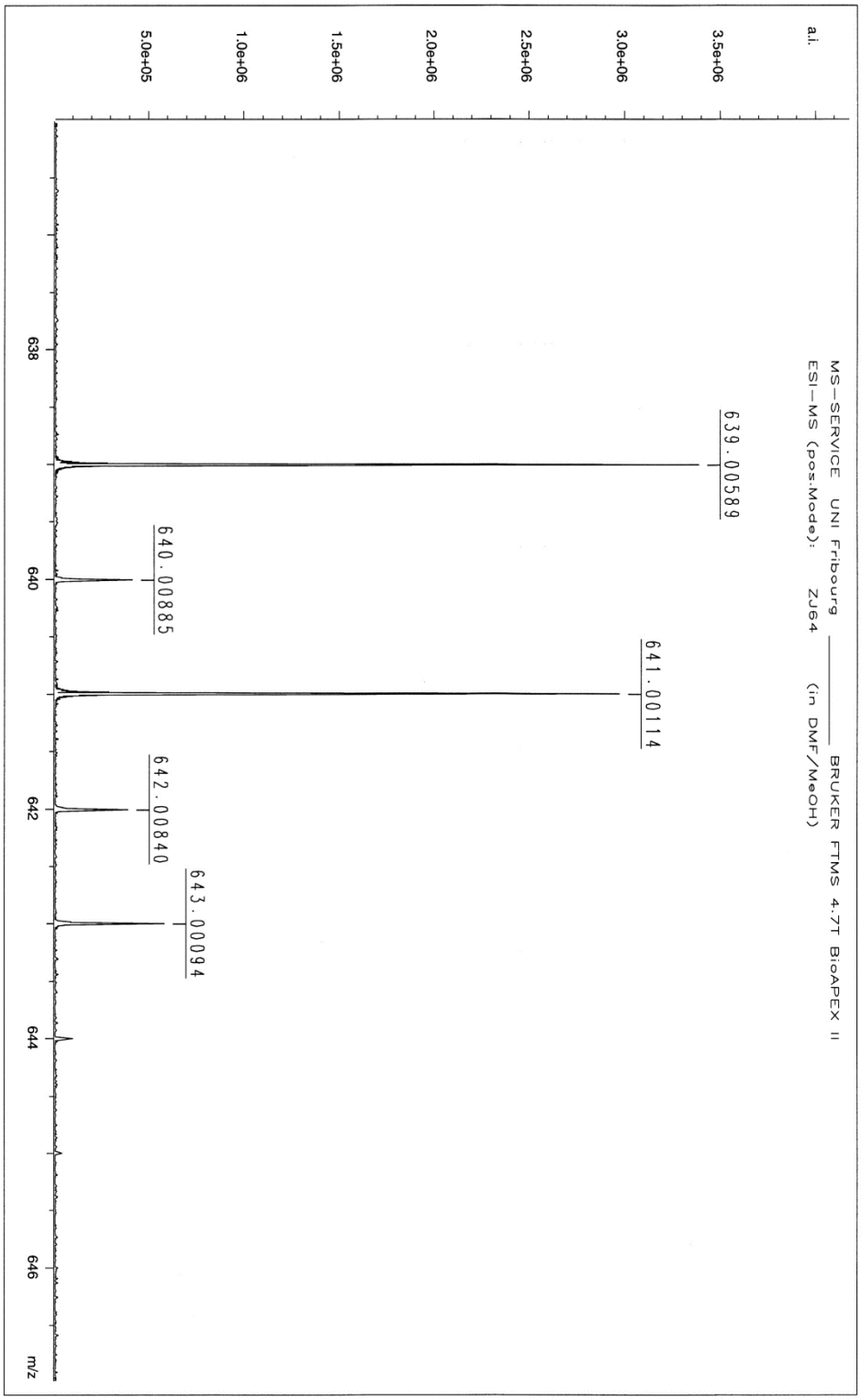
MS-SERVICE UNI Fribourg BRUKER FTMS 4.7T BioAPEX II
ESI-MS (pos:Mode): ZJ64 (in DMF/MeOH)
a.i.
3.5e+06
3.0e+06
2.5e+06
2.0e+06
1.5e+06
1.0e+06
5.0e+05
639.00589
640.00885
641.00114
642.00840
643.00094
638
640
642
644
646
m/z
/Data/UNI_BS/ZIMB5073_ESI/10/pdata/1 FTMS USER Tue Sep 7 13:20:18 2010

exact mass

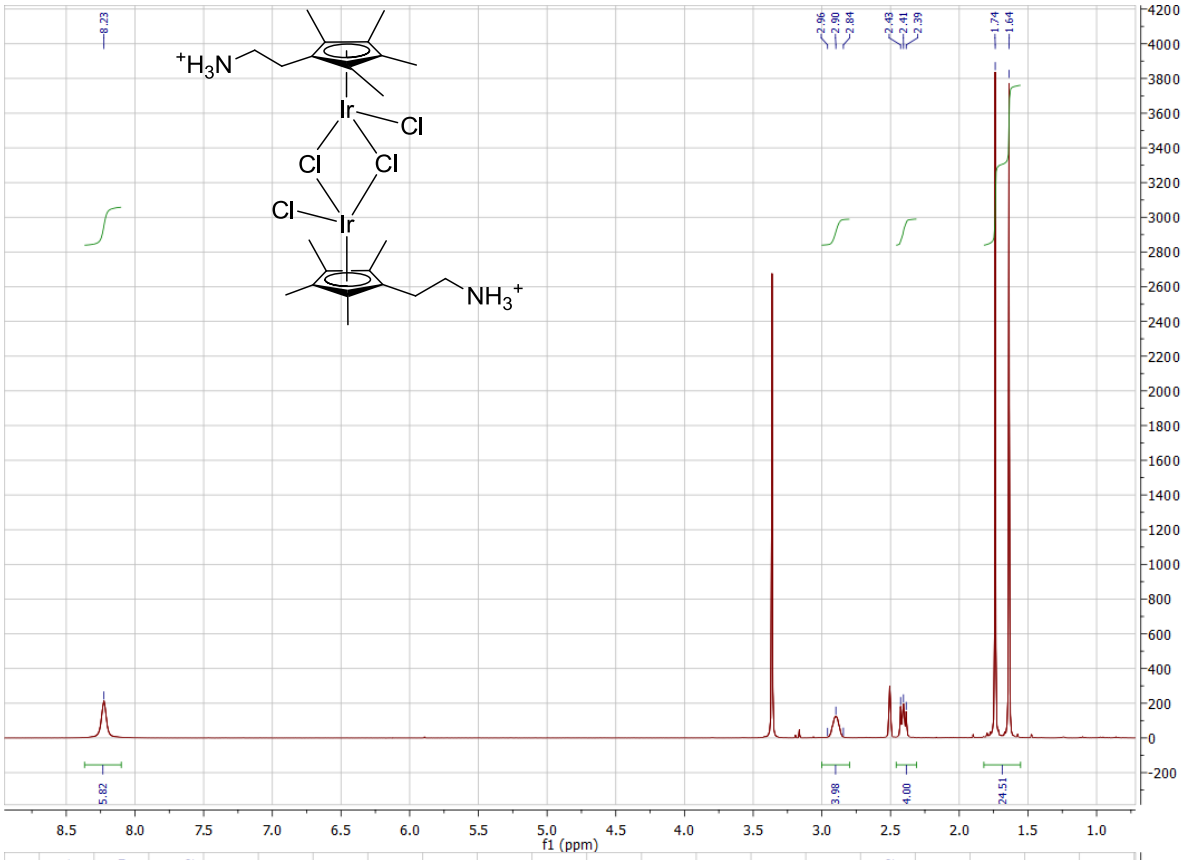
8.23
2.96
2.90
2.84
2.43
2.41
2.39
1.74
1.64
$^{+}H_3N$
Ir
Cl
Cl
Cl
Cl
Ir
NH_3^+
5.82
3.98
4.00
24.51
f1 (ppm)

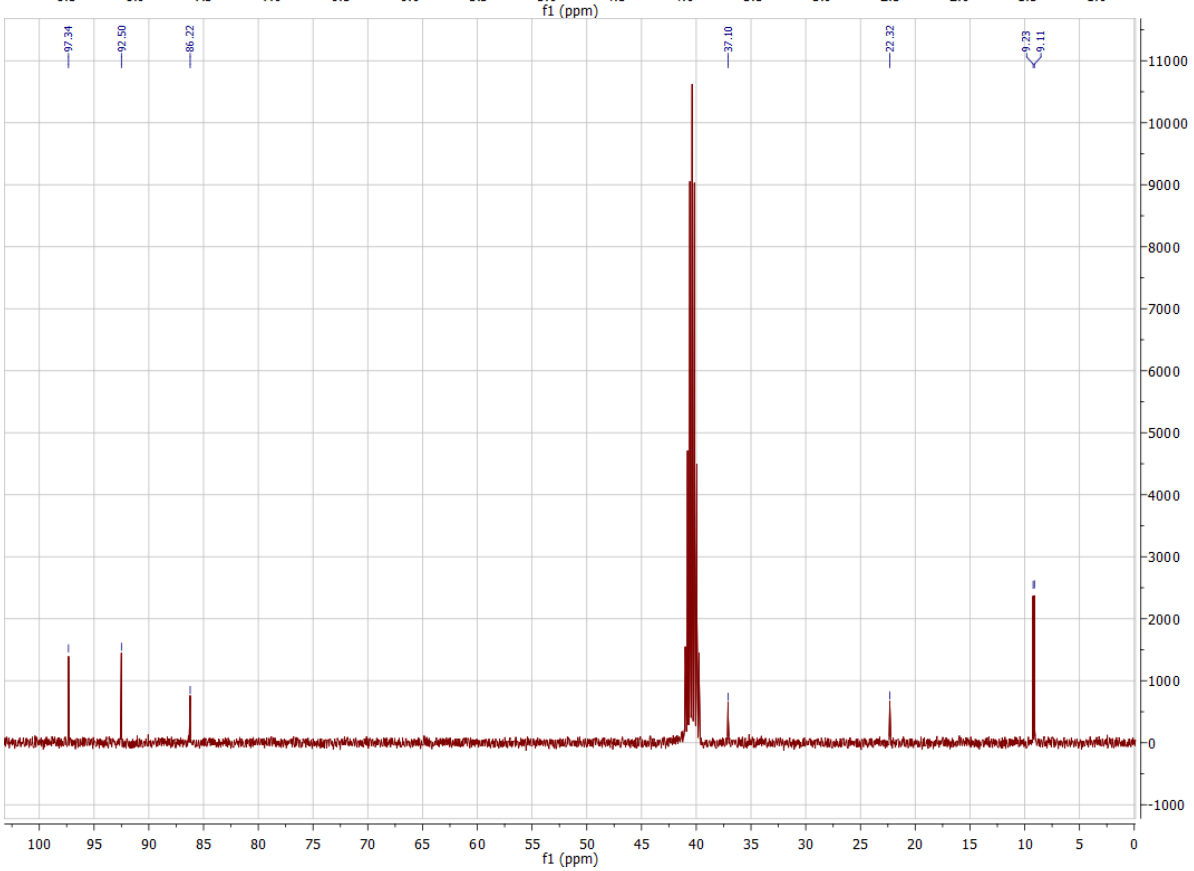
97.34
92.50
86.22
37.10
22.32
9.23
9.11
f1 (ppm)

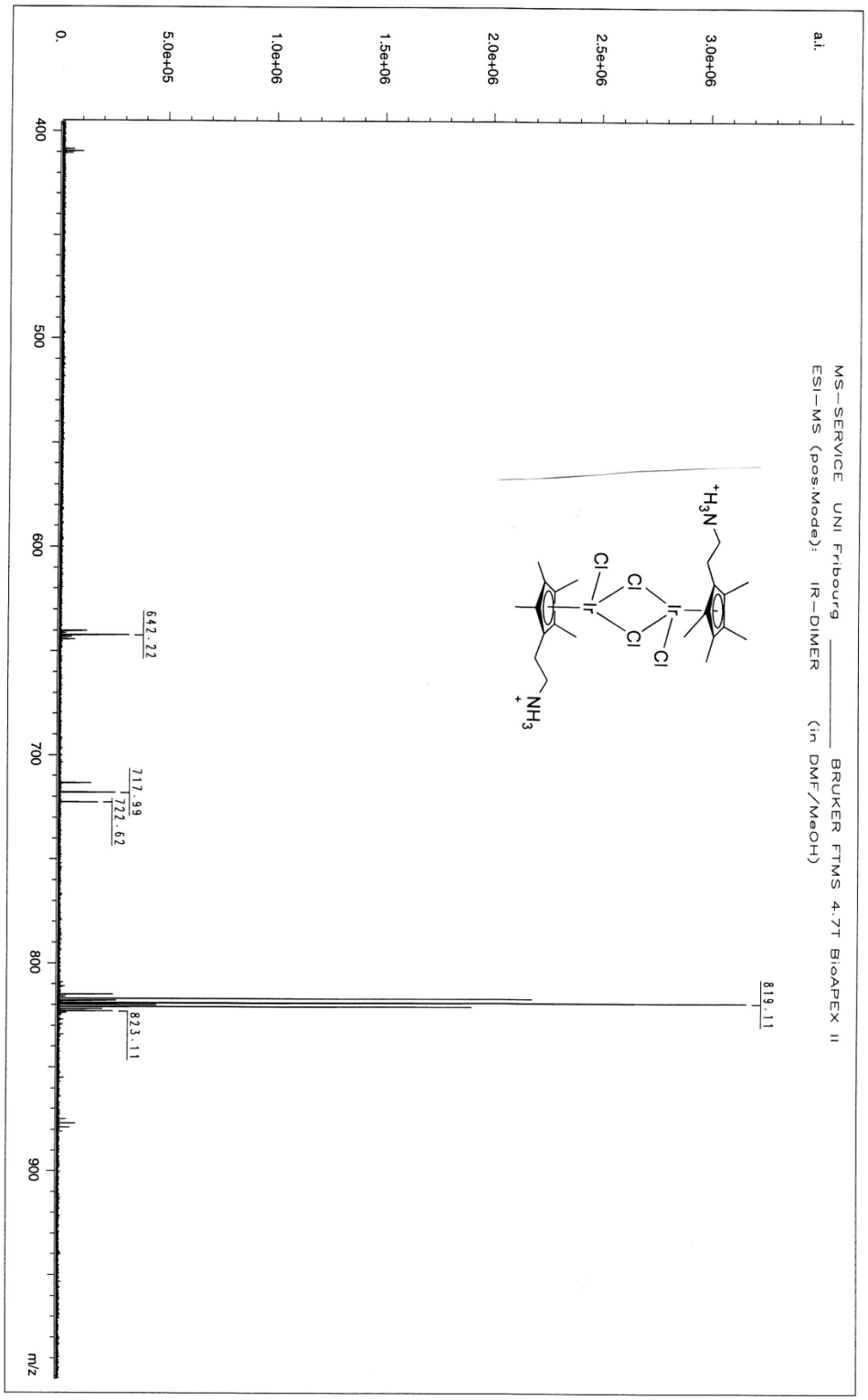
MS-SERVICE UNI Fribourg BRUKER FTMS 4.7T BioAPEX II
ESI-MS (pos.Mode): IR-DIMER (in DMF/MeOH)
a.i.
3.0e+06
2.5e+06
2.0e+06
1.5e+06
1.0e+06
5.0e+05
0.
400
500
600
700
800
900
m/z
642.22
717.99
722.62
819.11
823.11
Cl
Ir
Cl
Cl
Ir
Cl
+H3N
NH3
+
/Data/UNI_BS/ZIMB6209_ESI/1/pdata/1 FTMS USER Wed Dec 7 15:17:05 2011

Breitband

exact mass

23

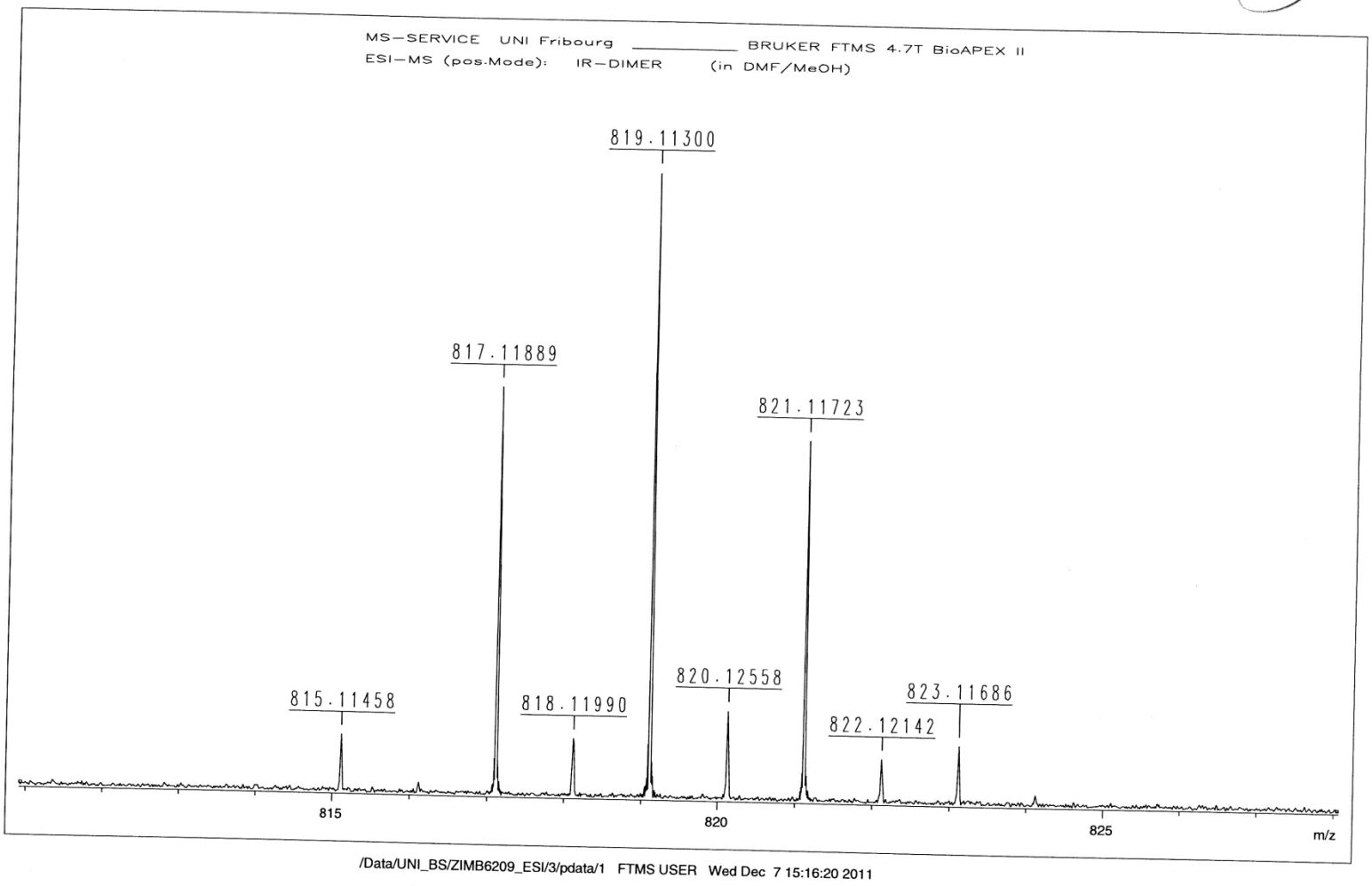

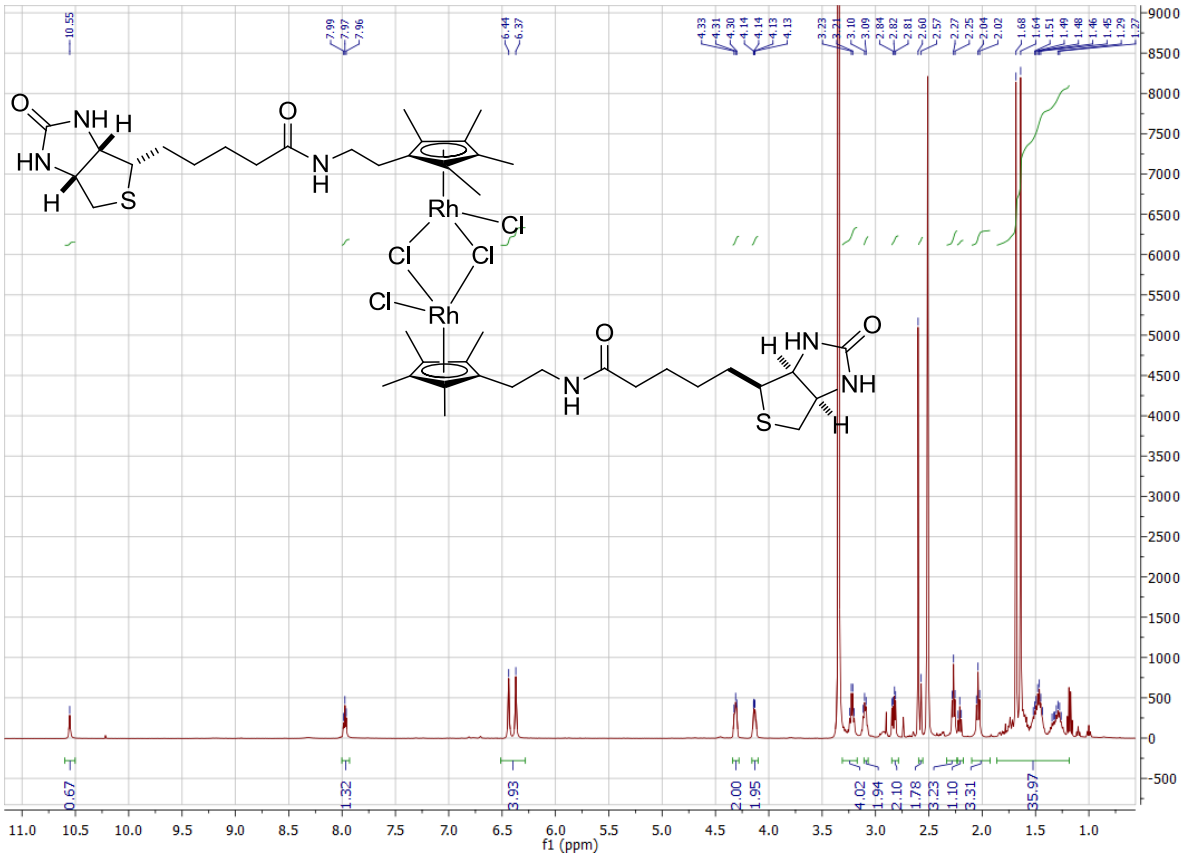
f1 (ppm)

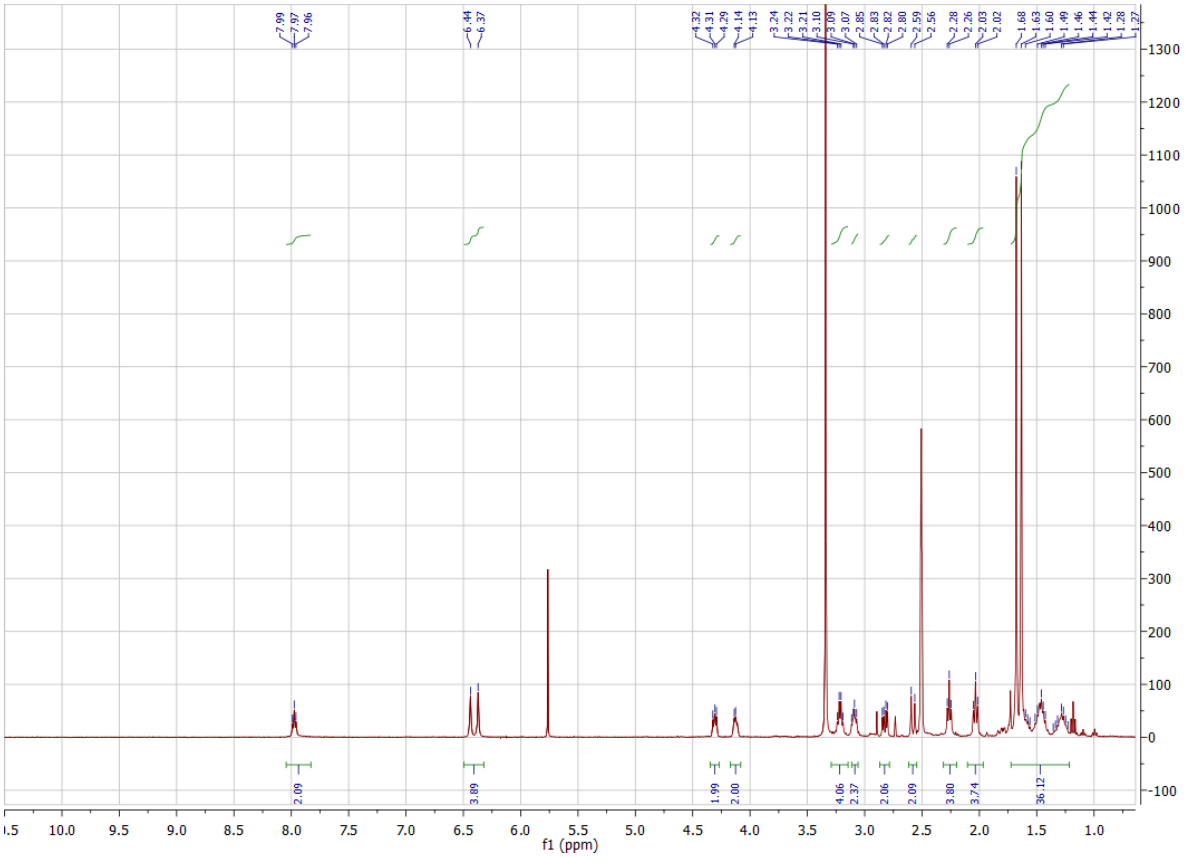
f1 (ppm)

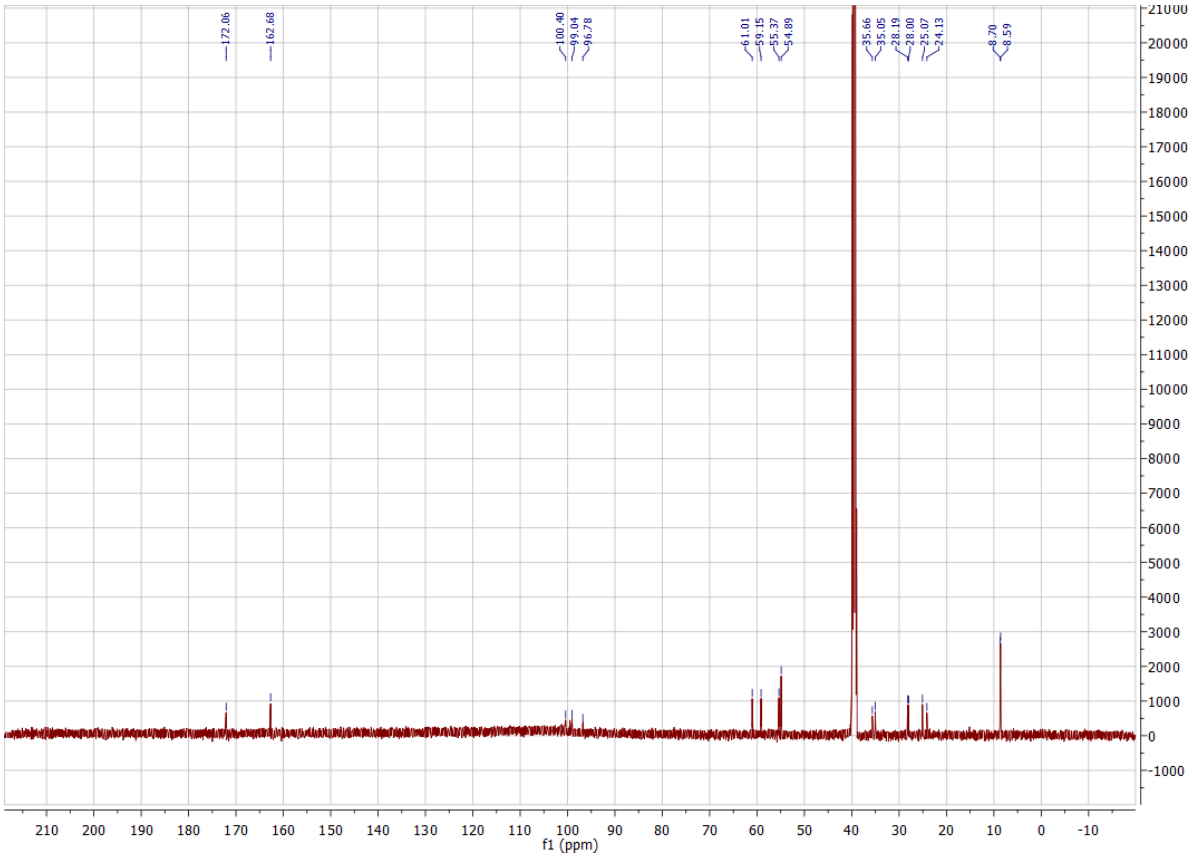
172.06
162.68
100.40
99.04
96.78
61.01
59.15
55.37
54.89
35.66
35.05
28.19
28.00
25.07
24.13
8.70
8.59
f1 (ppm)

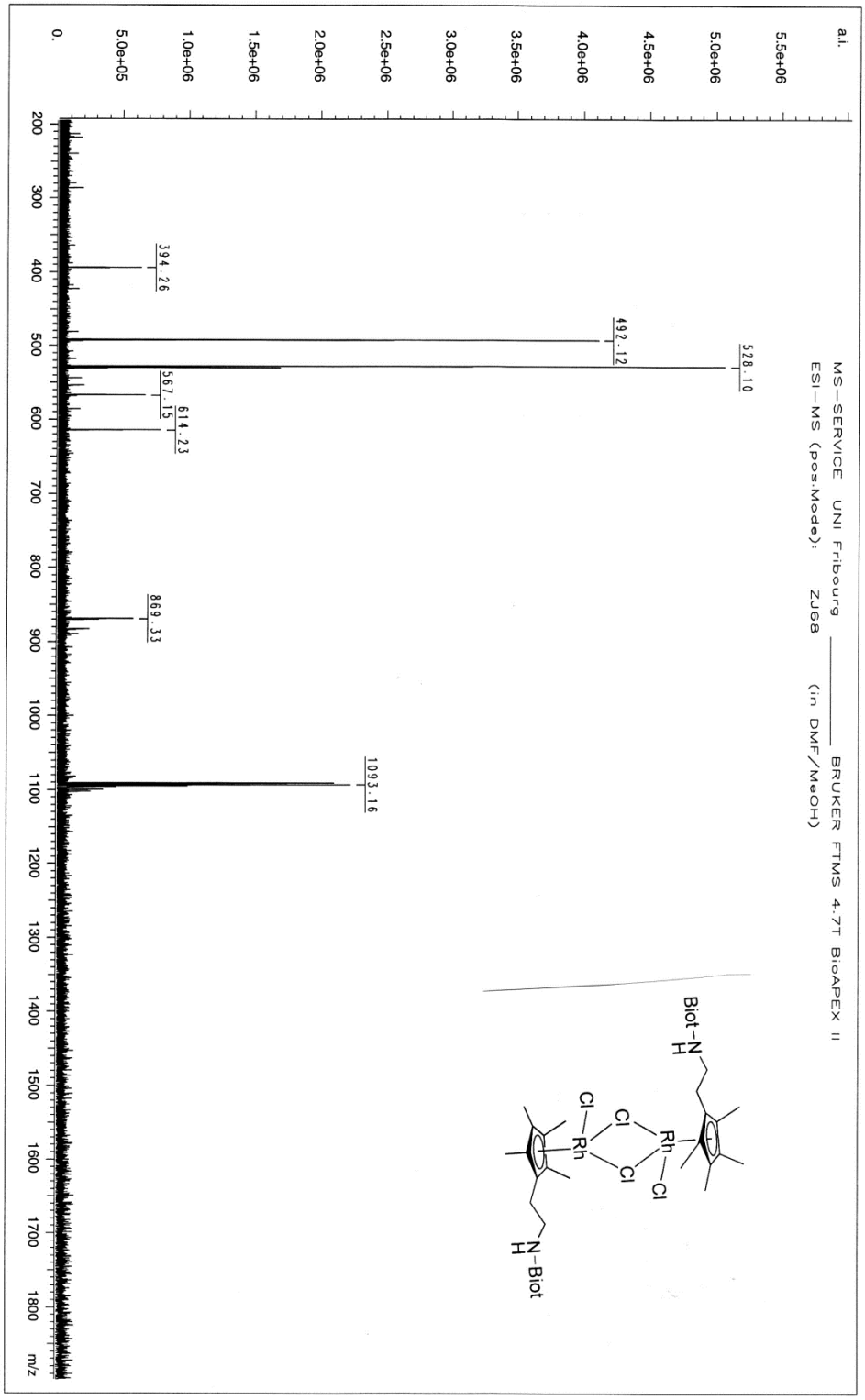
a.i.
MS-SERVICE UNI Fribourg BRUKER FTMS 4.7T BioAPEX II
ESI-MS (pos:Mode): ZJ68 (in DMF/MeOH)
528.10
492.12
394.26
567.15
614.23
869.33
1093.16
Biot-N H
Cl
Rh
Cl
Rh
Cl
Cl
N H -Biot
m/z
/Data/UNI_BS/ZIMB5074_ESI/3/pdata/1 FTMS USER Tue Sep 7 13:00:22 2010

exact mass

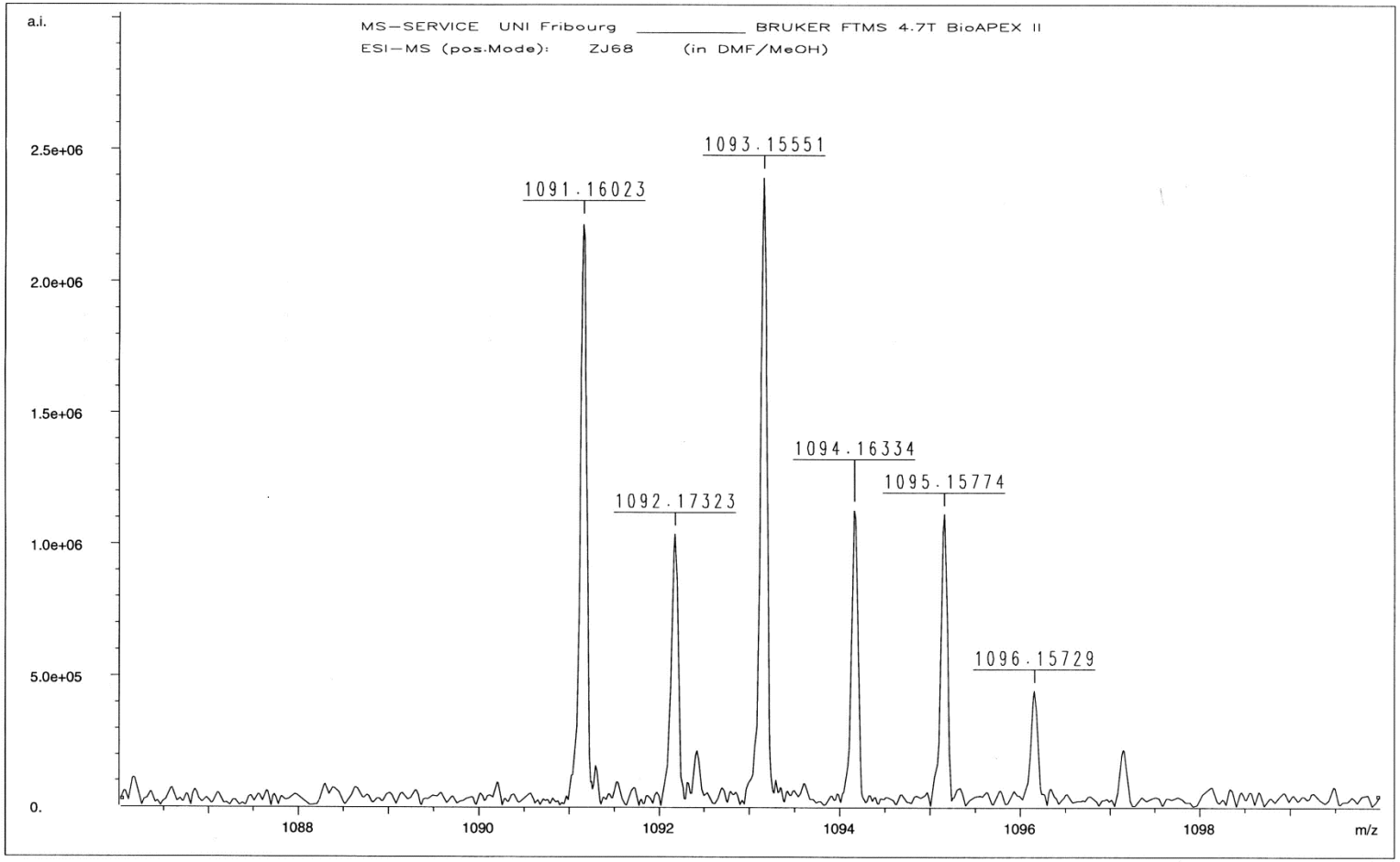
MS—SERVICE UNI Fribourg _____ BRUKER FTMS 4.7T BioAPEX II
ESI—MS (pos.Mode): ZJ68 (in DMF/MeOH)
a.i.
2.5e+06
2.0e+06
1.5e+06
1.0e+06
5.0e+05
0.
1091.16023
1093.15551
1092.17323
1094.16334
1095.15774
1096.15729
1088
1090
1092
1094
1096
1098
m/z
/Data/UNI_BS/ZIMB5074_ESI/4/pdata/1 FTMS USER Tue Sep 7 13:03:10 2010

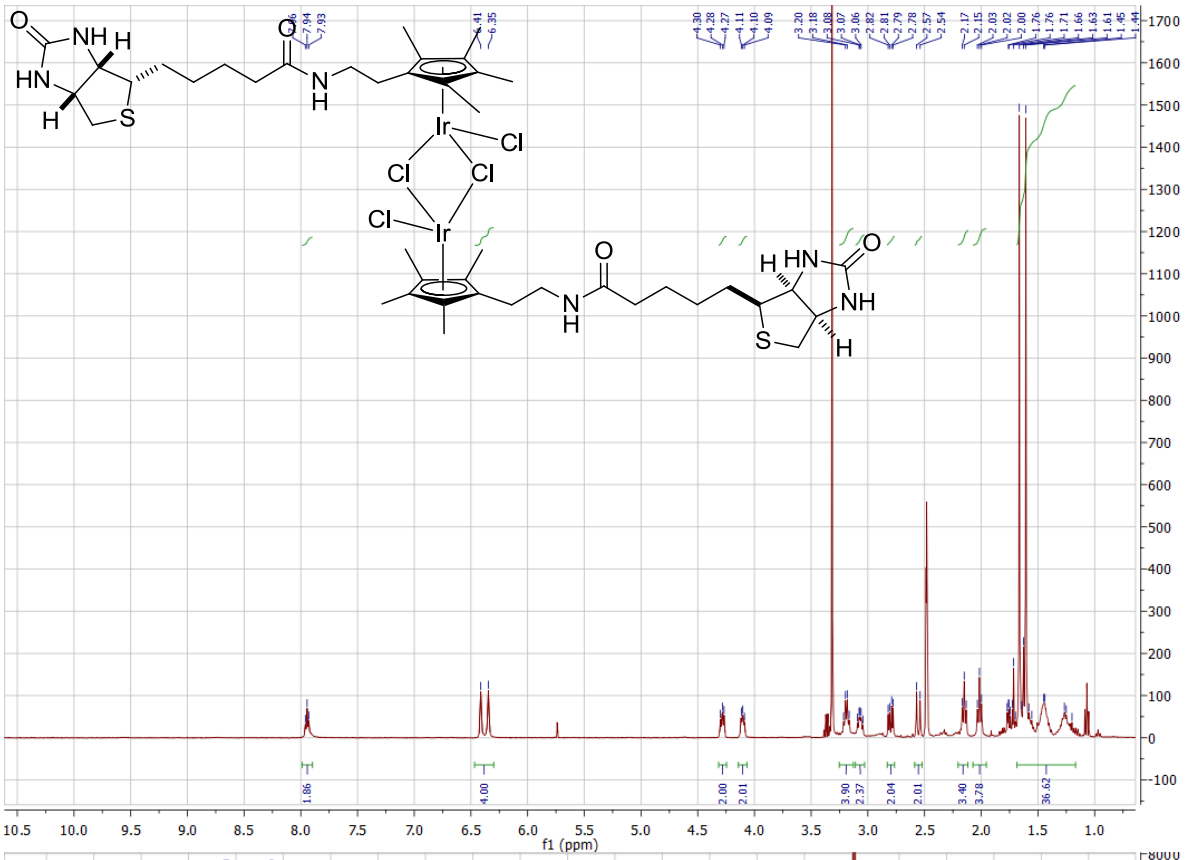
O
NH H
HN
H
S
O
N
H
Ir
Cl
Cl
Cl
Cl
Ir
O
N
H
H HN
O
NH
S
H
f1 (ppm)

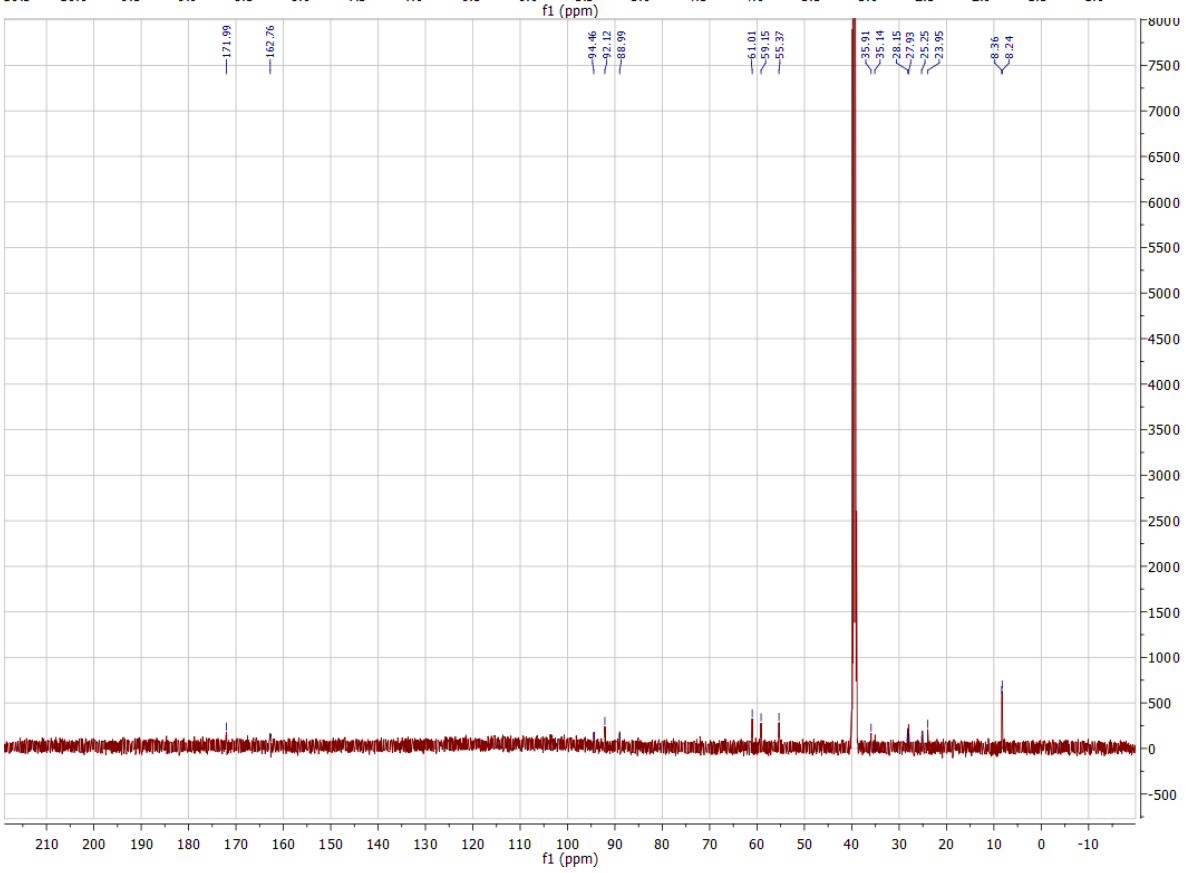
171.99
162.76
94.46
92.12
88.99
61.01
59.15
55.37
35.91
35.14
28.15
27.93
25.25
23.95
8.36
8.24
f1 (ppm)

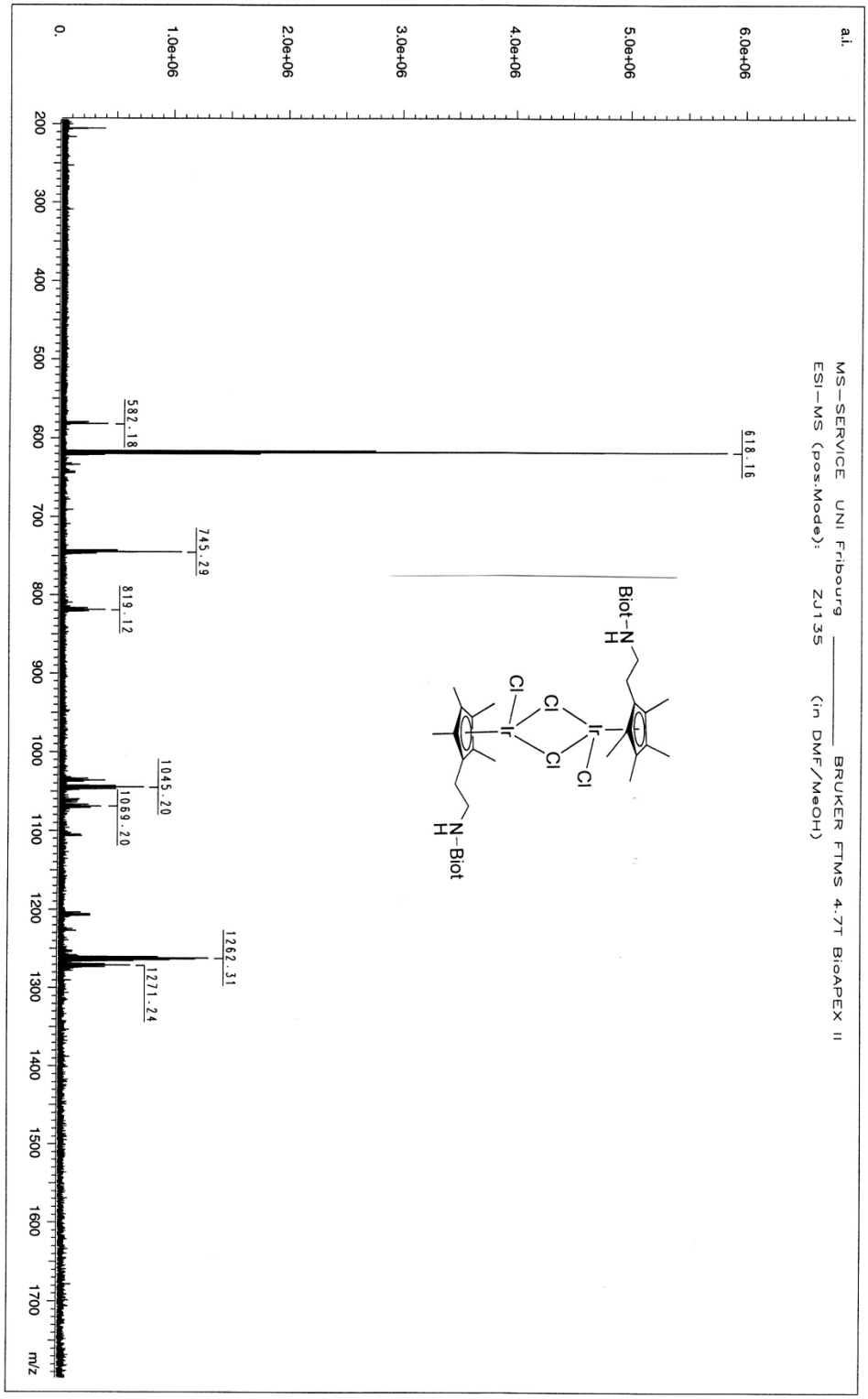
a.i.
MS-SERVICE UNI Fribourg BRUKER FTMS 4.7T BioAPEX II
ESI-MS (pos.Mode): ZJ135 (in DMF/MeOH)
618.16
582.18
745.29
819.12
1045.20
1069.20
1262.31
1271.24
Biot-N H
N H-Biot
Cl
Ir
m/z
/Data/UNI_BS/ZIMB5240_ESI/2/pdata/1 FTMS USER Thu Dec 2 07:45:22 2010

Breitband

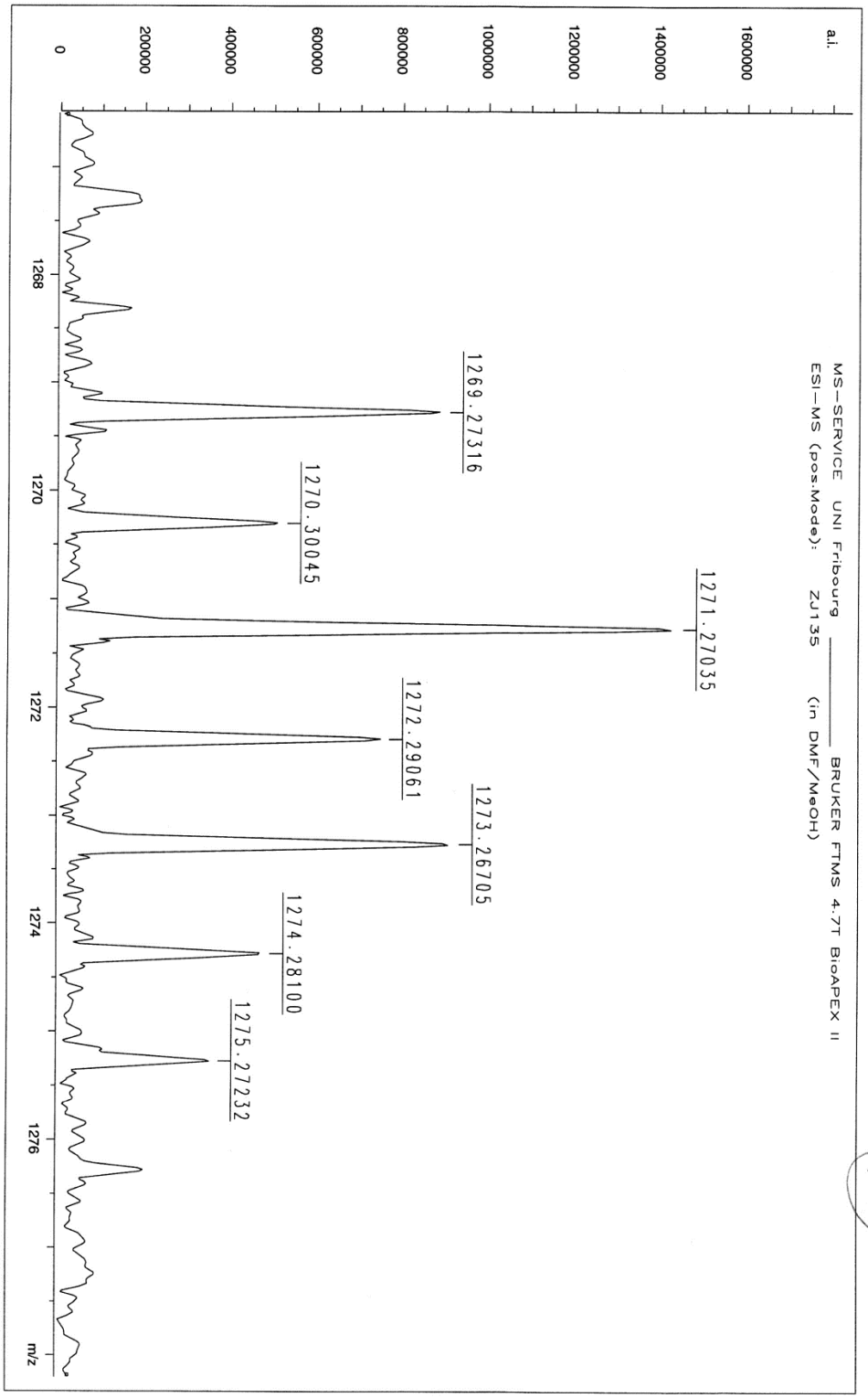
a.i.
MS-SERVICE UNI Fribourg BRUKER FTMS 4.7T BioAPEX II
ESI-MS (pos.Mode): ZJ135 (in DMF/MeOH)
1271.27035
1269.27316
1270.30045
1272.29061
1273.26705
1274.28100
1275.27232
m/z
/Data/UNI_BS/ZIMB5240_ESI/5/pdata/1 FTMS USER Thu Dec 2 07:55:16 2010

exact mass

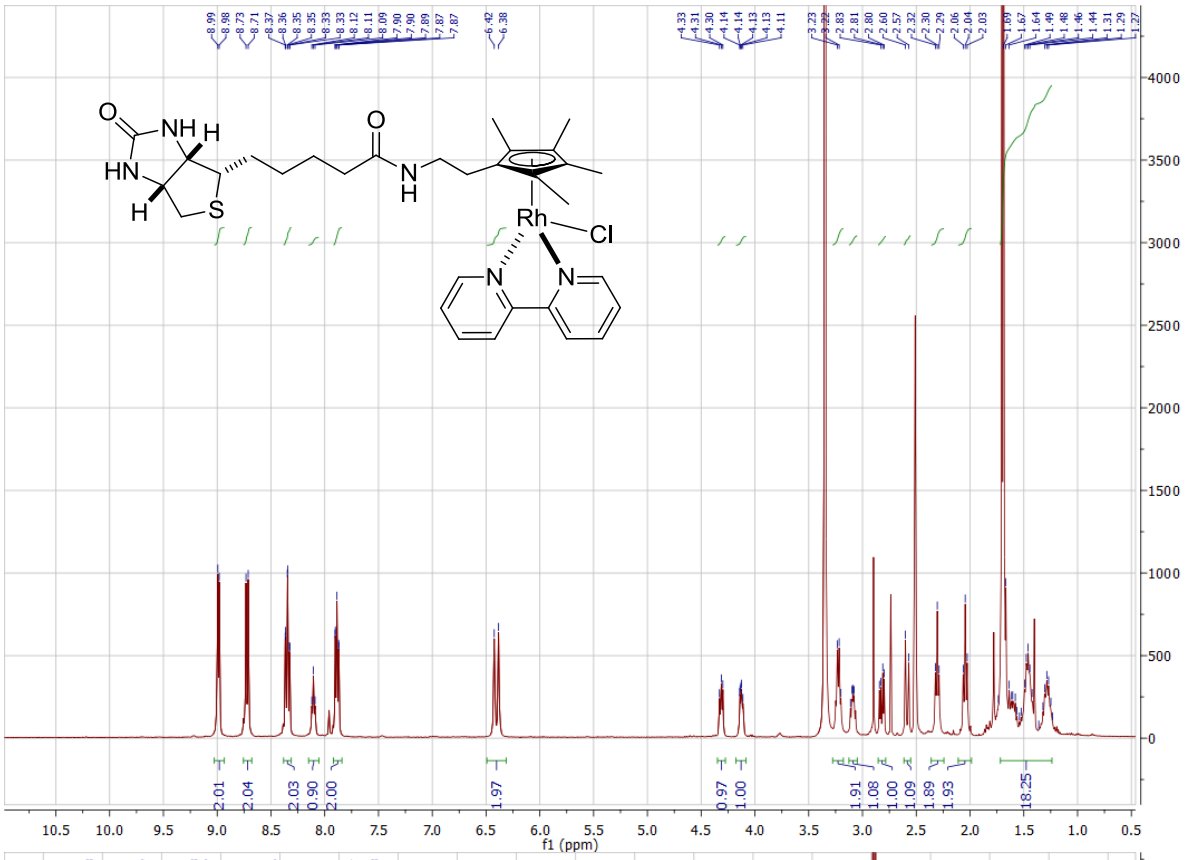
f1 (ppm)

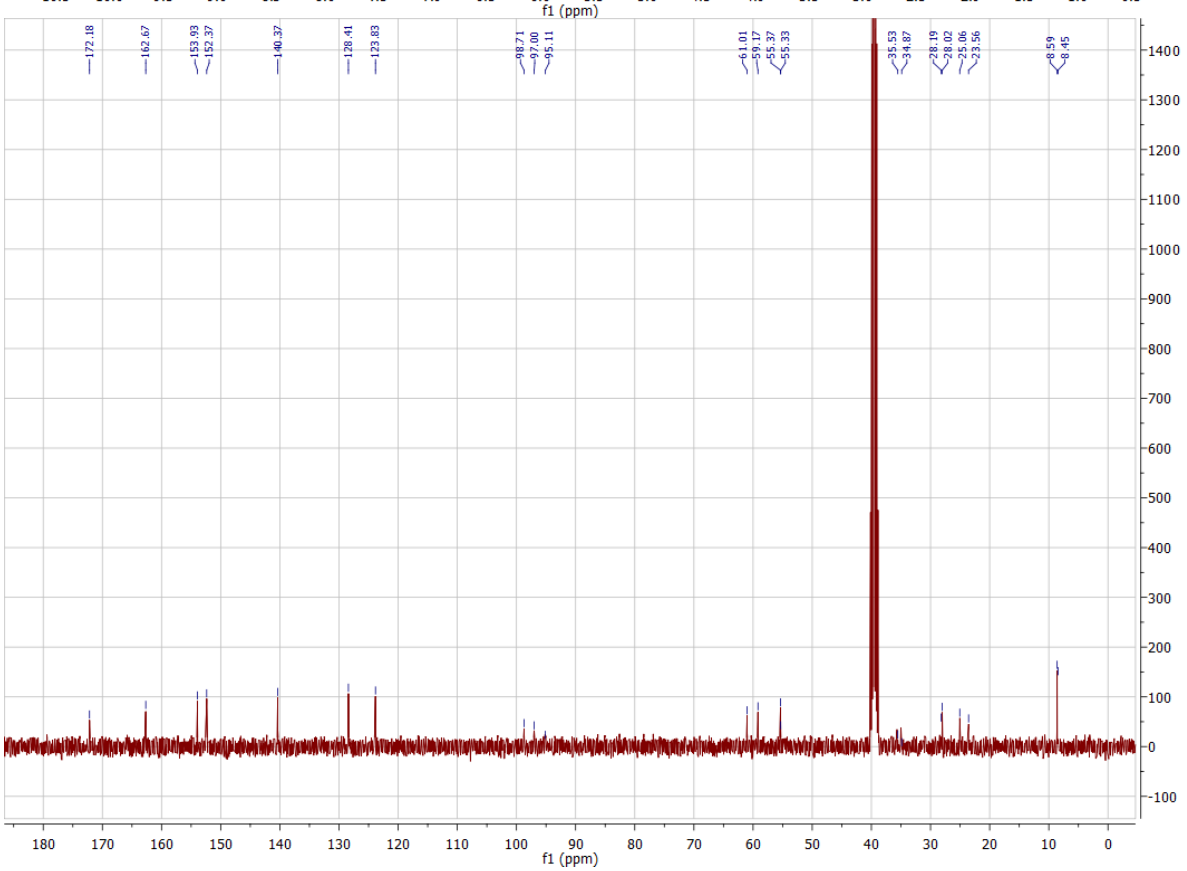
f1 (ppm)

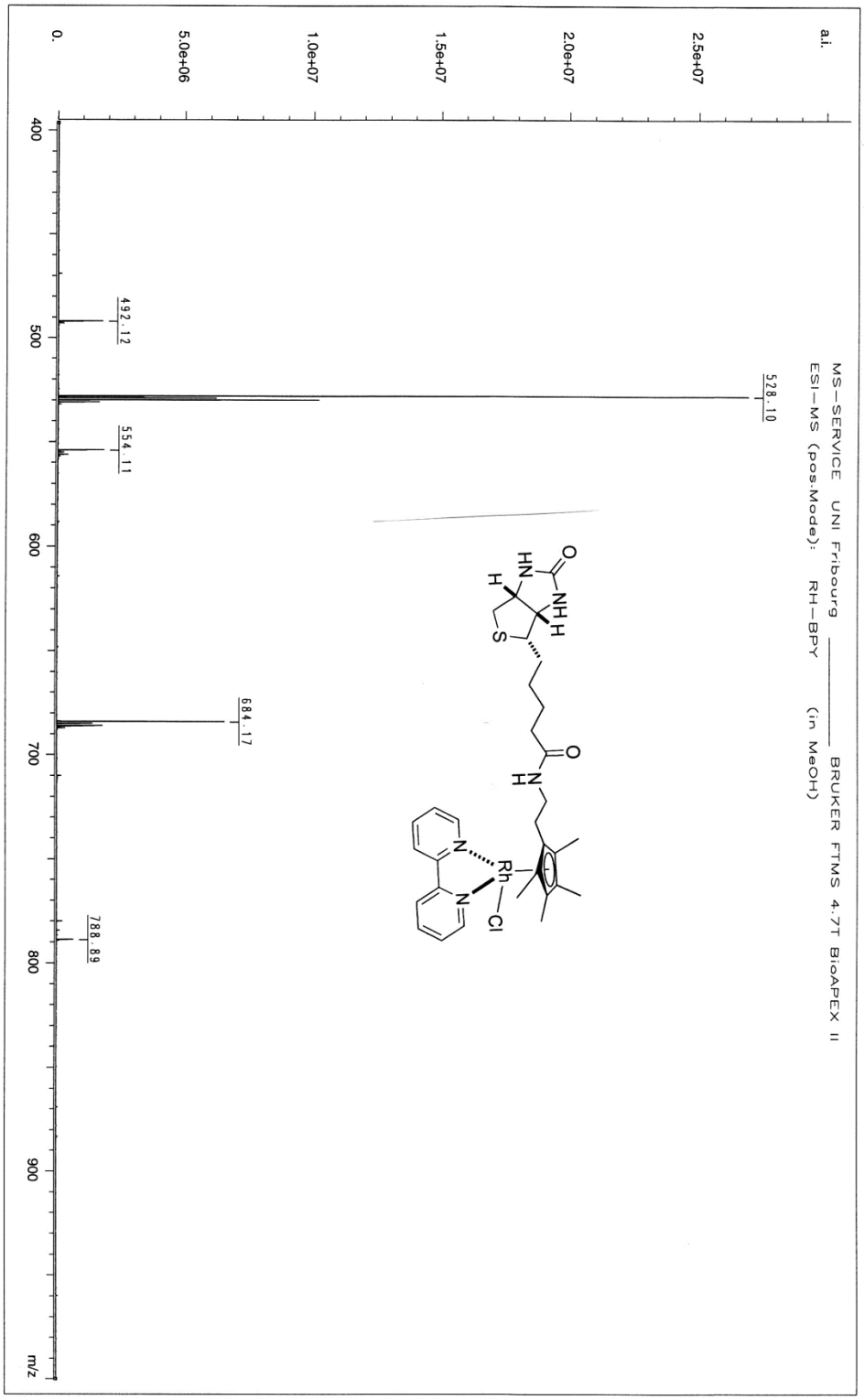
a.i.
MS-SERVICE UNI Fribourg _____ BRUKER FTMS 4.7T BioAPEX II
ESI-MS (pos.Mode): RH-BPY (in MeOH)
528.10
492.12
554.11
684.17
788.89
0.
5.0e+06
1.0e+07
1.5e+07
2.0e+07
2.5e+07
400
500
600
700
800
900
m/z
/Data/UNI_BS/ZIMB6212_ESI/1/pdata/1 FTMS USER Wed Dec 7 15:48:26 2011

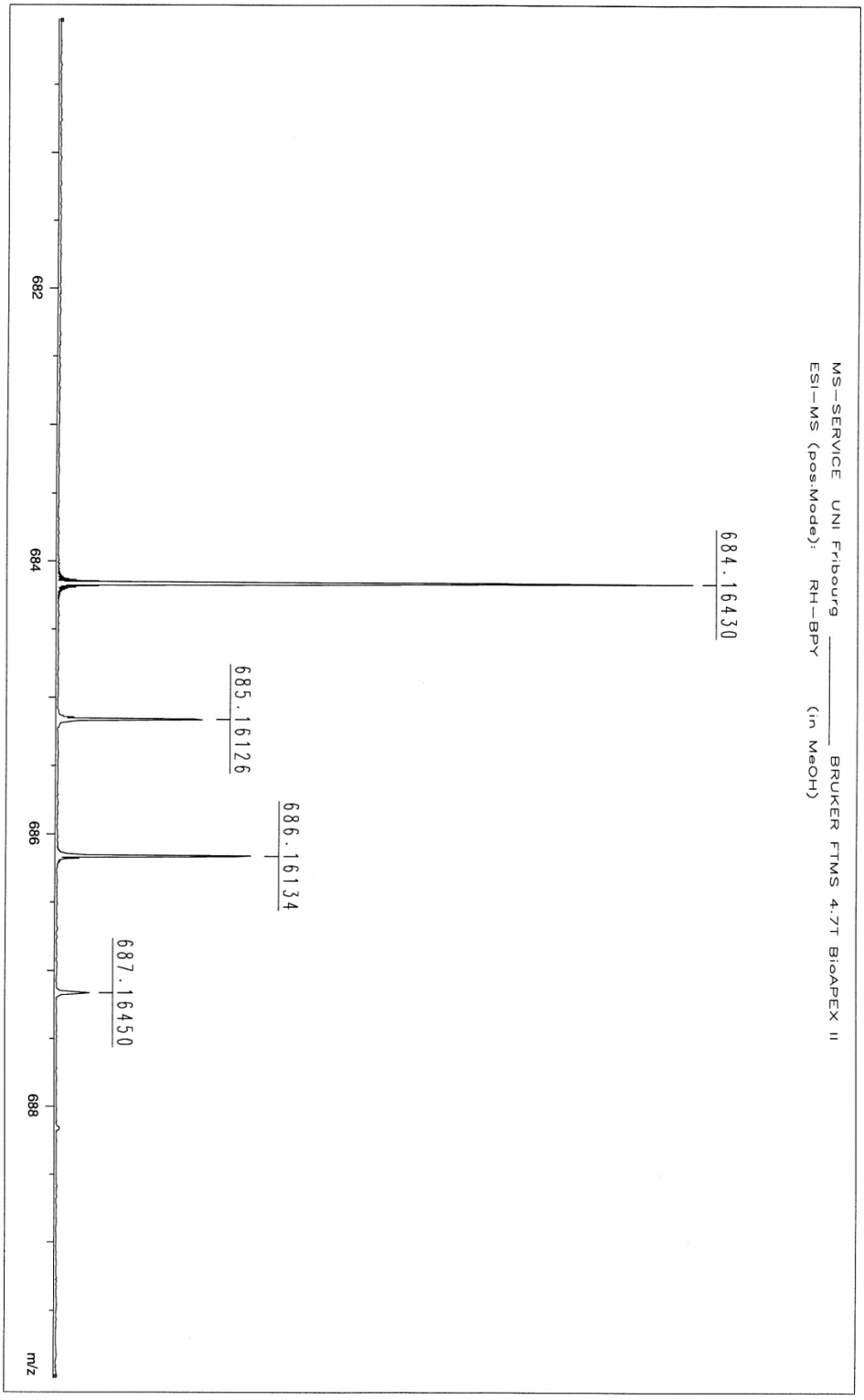
MS-SERVICE UNI Fribourg BRUKER FTMS 4.7T BioAPEX II
ESI-MS (pos.Mode): RH-BPY (in MeOH)
684.16430
685.16126
686.16134
687.16450
682
684
686
688
m/z
/Data/UNI_BS/ZIMB6212_ESI/3/pdata/1 FTMS USER Wed Dec 7 15:47:29 2011

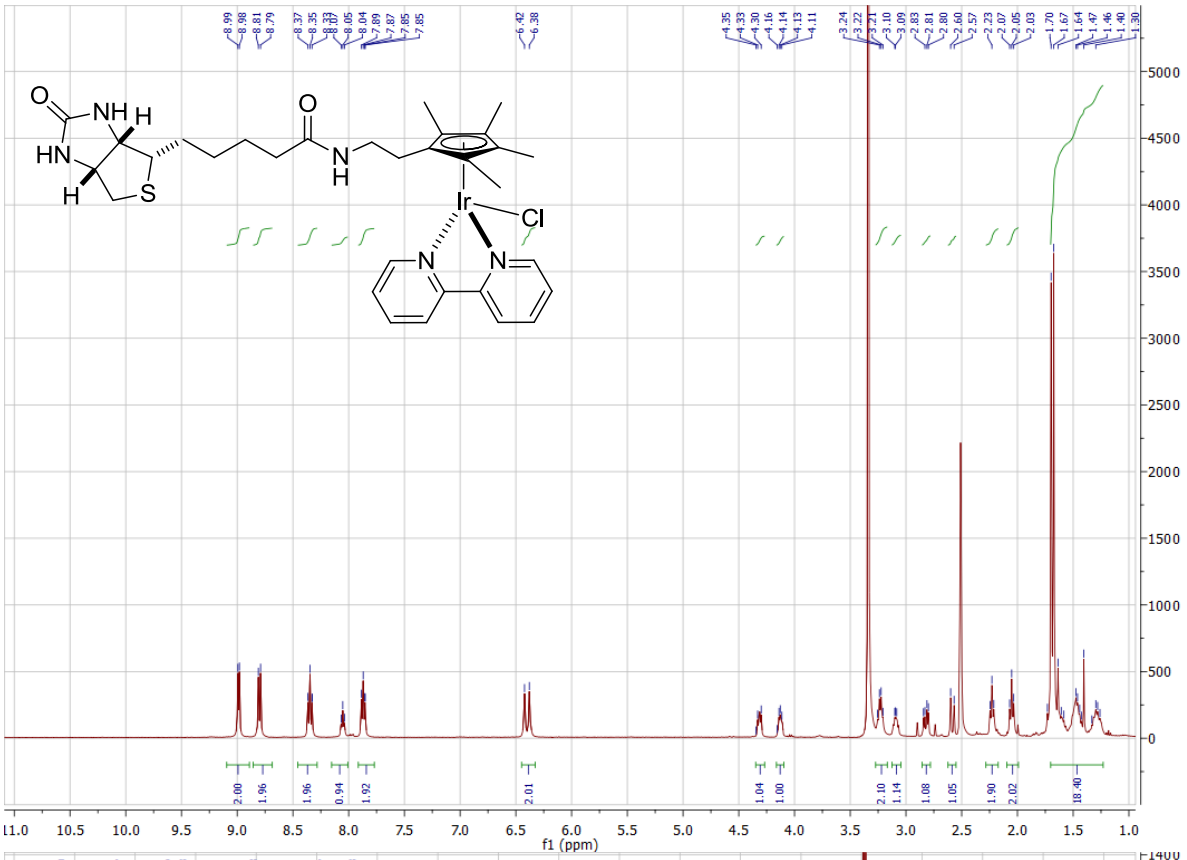
O
NH H
HN
H
S
O
N
H
Ir
Cl
N
N
f1 (ppm)

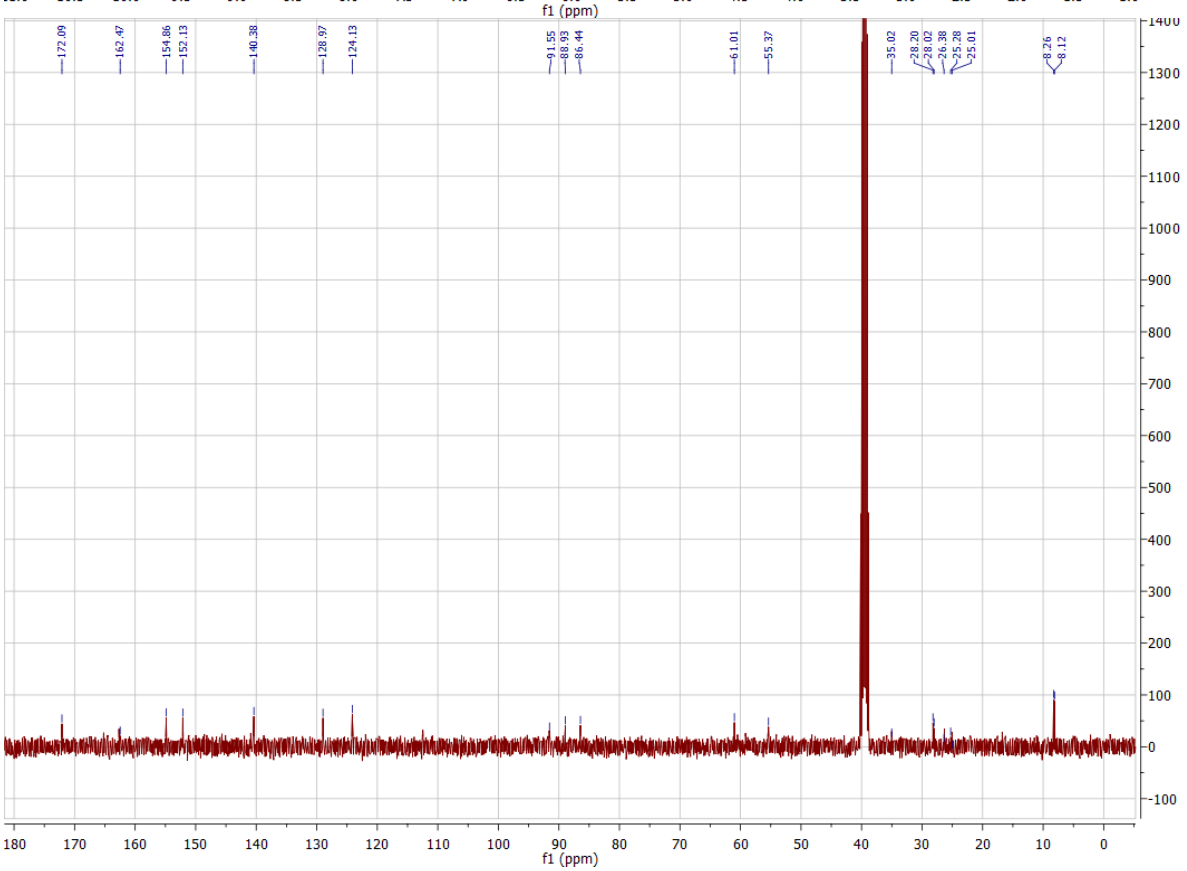
172.09
162.47
154.86
152.13
140.38
128.97
124.13
91.55
88.93
86.44
61.01
55.37
35.02
28.20
28.02
26.38
25.28
25.01
8.26
8.12
f1 (ppm)

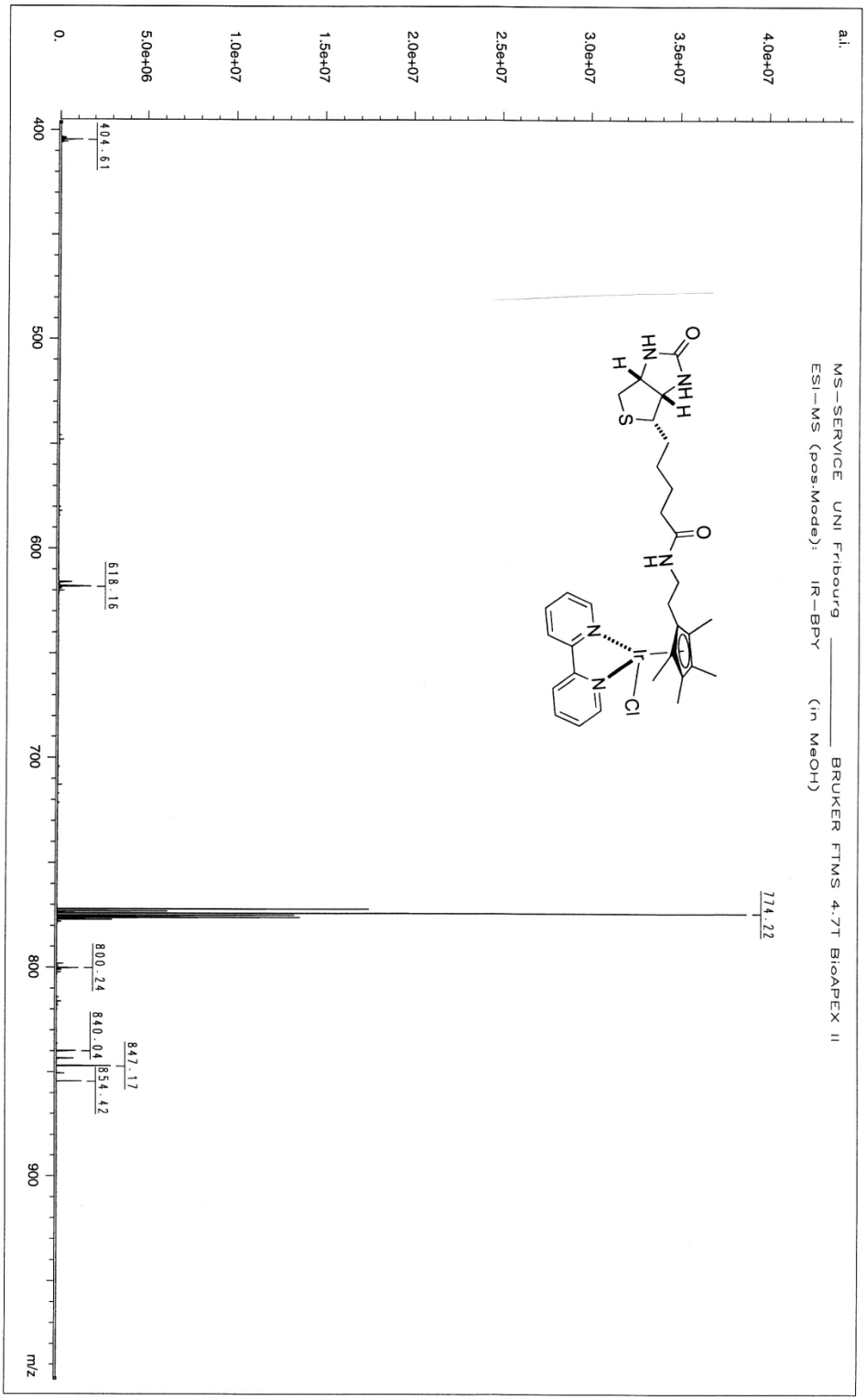
a.i.
MS-SERVICE UNI Fribourg BRUKER FTMS 4.7T BioAPEX II
ESI-MS (pos-Mode): IR-BPY (in MeOH)
4.0e+07
3.5e+07
3.0e+07
2.5e+07
2.0e+07
1.5e+07
1.0e+07
5.0e+06
0.
400
500
600
700
800
900
m/z
404.61
618.16
714.22
800.24
840.04
847.17
854.42
/Data/UNI_BS/ZIMB6213_ESI/1/pdata/1 FTMS USER Wed Dec 7 16:10:22 2011

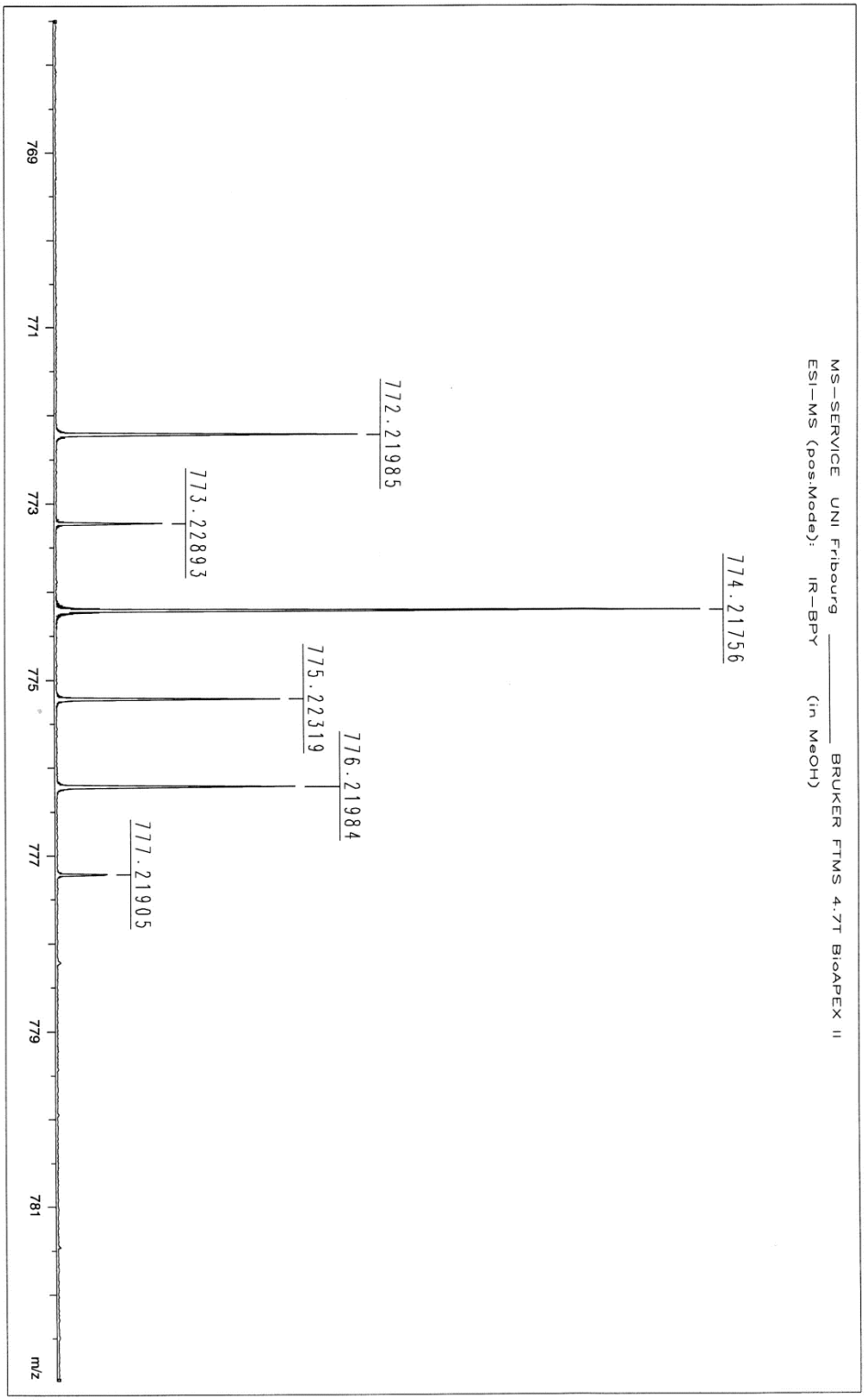
MS-SERVICE UNI Fribourg _____ BRUKER FTMS 4.7T BioAPEX II
ESI-MS (pos.Mode): IR-BPY (in MeOH)
774.21756
772.21985
773.22893
775.22319
776.21984
777.21905
769
771
773
775
777
779
781
m/z
/Data/UNI_BS/ZIMB6213_ESI/3/pdata/1 FTMS USER Wed Dec 7 16:11:00 2011

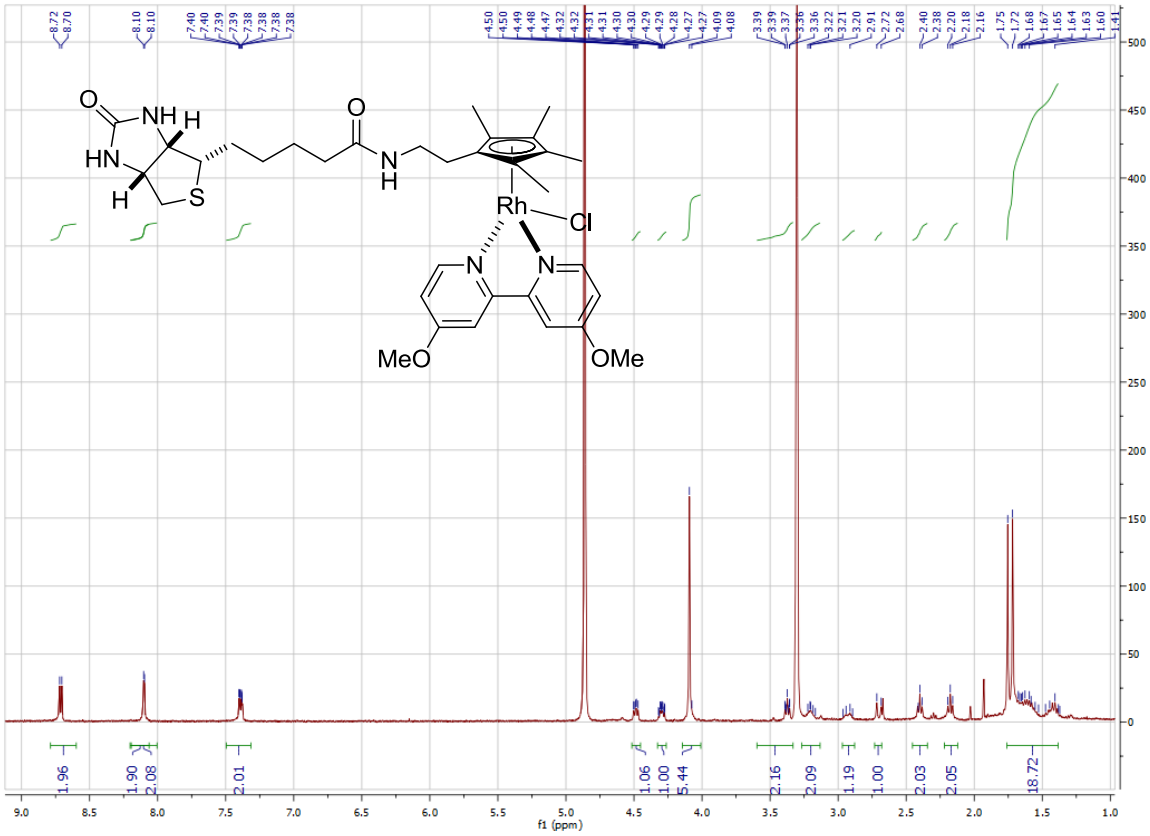
O
NH
H
HN
H
S
O
N
H
Rh
Cl
N
N
MeO
OMe
f1 (ppm)

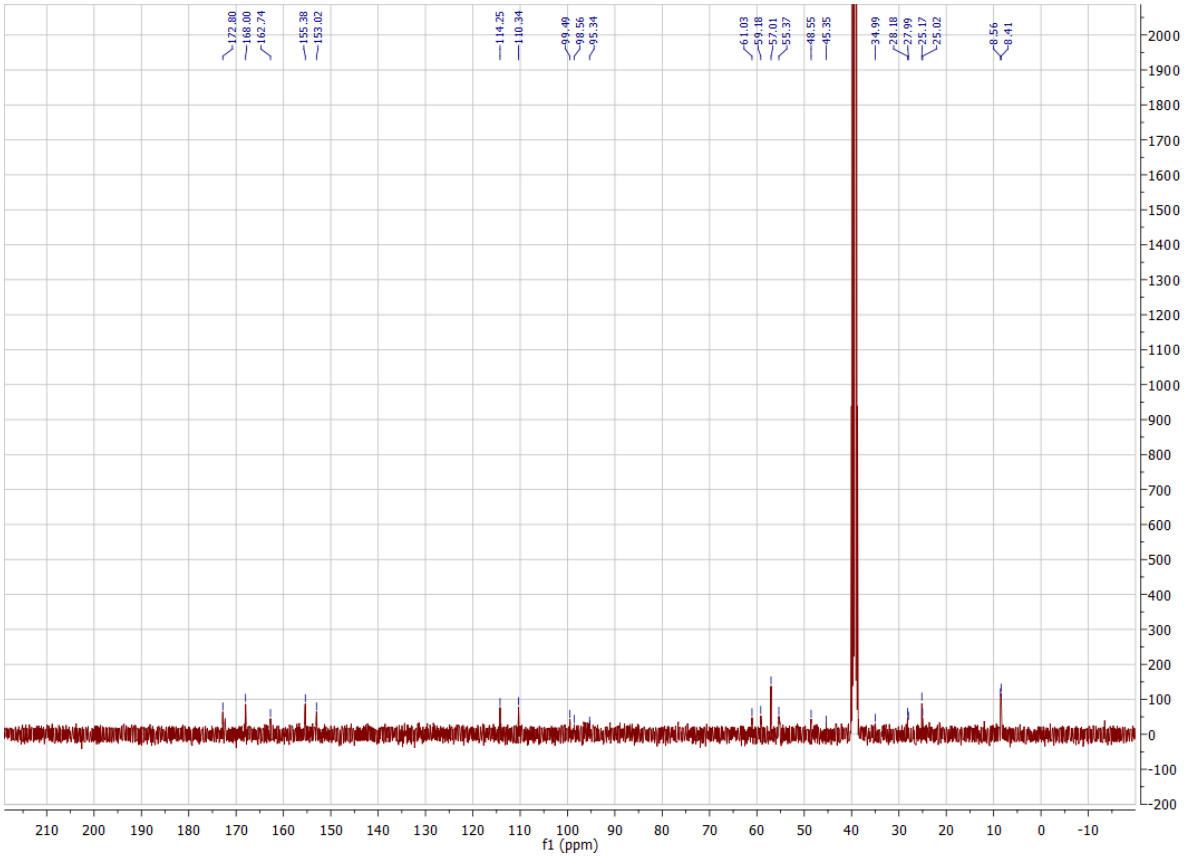
f1 (ppm)

13 march SN 6181

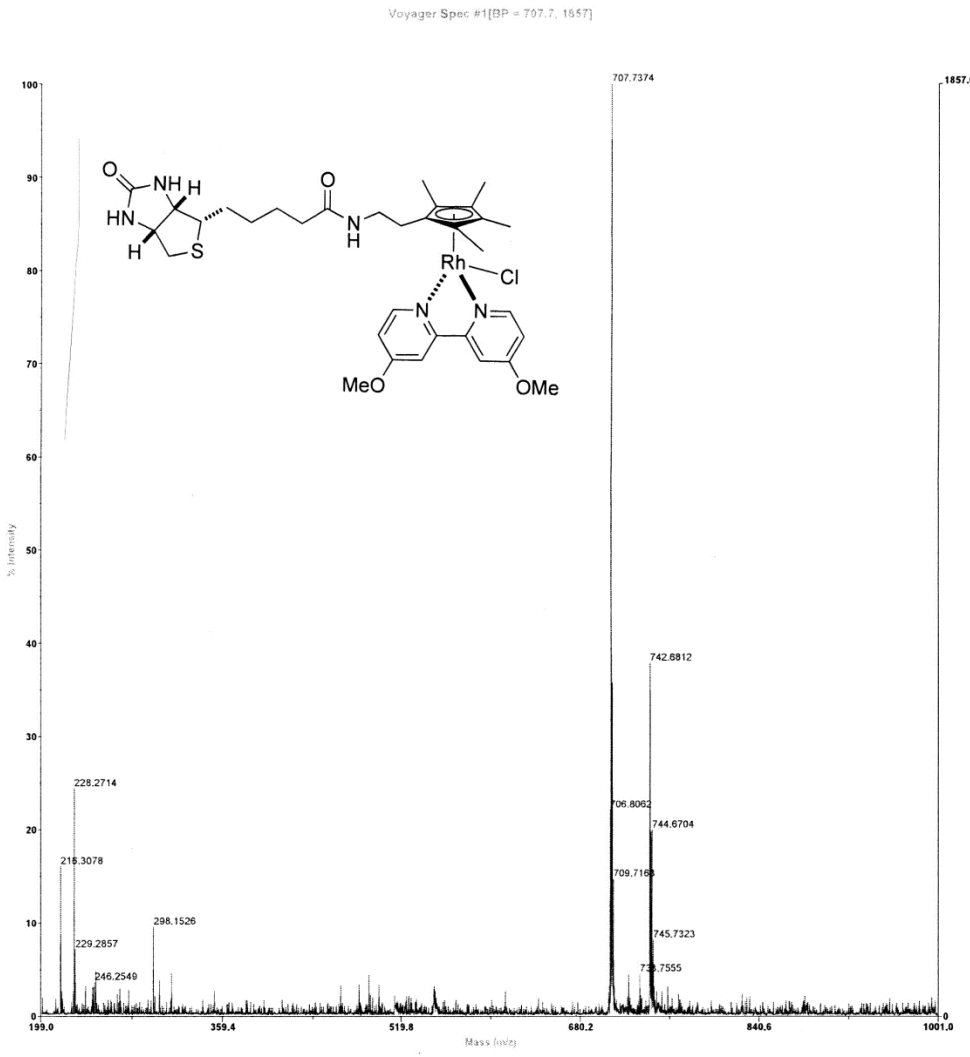

Mode of operation:	Reflector
Extraction mode:	Delayed
Polarity:	Positive
Acquisition control:	Manual
Accelerating voltage:	20000 V
Grid voltage:	75%
Mirror voltage ratio:	1.12
Guide wire 0:	0.1%
Extraction delay time:	50 nsec
Acquisition mass range:	200 -- 1000 Da
Number of laser shots:	200/spectrum
Laser intensity:	1926
Laser Rep Rate:	20.0 Hz
Calibration type:	External -- D:\giese\user\Calibration\porph_pos.cal
Calibration matrix:	2,5-Dihydroxybenzoic acid
Low mass gate:	Off
Timed ion selector:	Off
Digitizer start time:	14.3005
Bin size:	0.5 nsec
Number of data points:	34984
Vertical scale 0:	500 mV
Vertical offset:	0.5%
Input bandwidth 0:	500 MHz
Sample well:	34
Plate ID:	PLATE1
Serial number:	6181
Instrument name:	Voyager-DE PRO
Plate type filename:	C:\VOYAGER\100 well plate.plt
Lab name:	Dep. Chemie
Absolute x-position:	14857.7
Absolute y-position:	33066
Relative x-position:	-1969.78
Relative y-posititon:	998.462
Shots in spectrum:	200
Source pressure:	3.766e-007
Mirror pressure:	1.132e-007
TC2 pressure:	0.003745
TIS gate width:	8
TIS flight length:	687.7

Acquired: 14:38:00, August 13, 2010

Printed: 14:52, August 13, 2010

D:\giese\user\Ward\Malcom\ZJ94_0002.dat

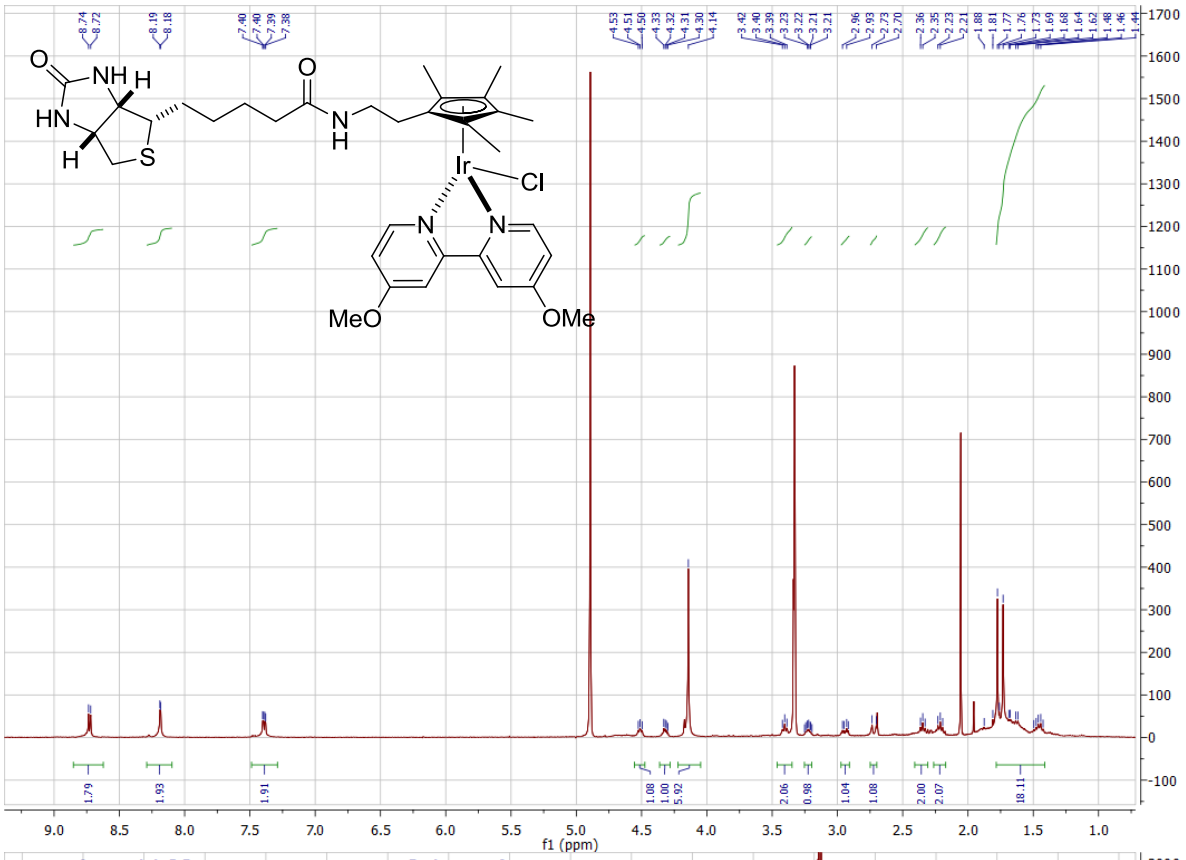
O
NH
H
HN
H
S
O
N
H
Ir
Cl
N
N
MeO
OMe
f1 (ppm)

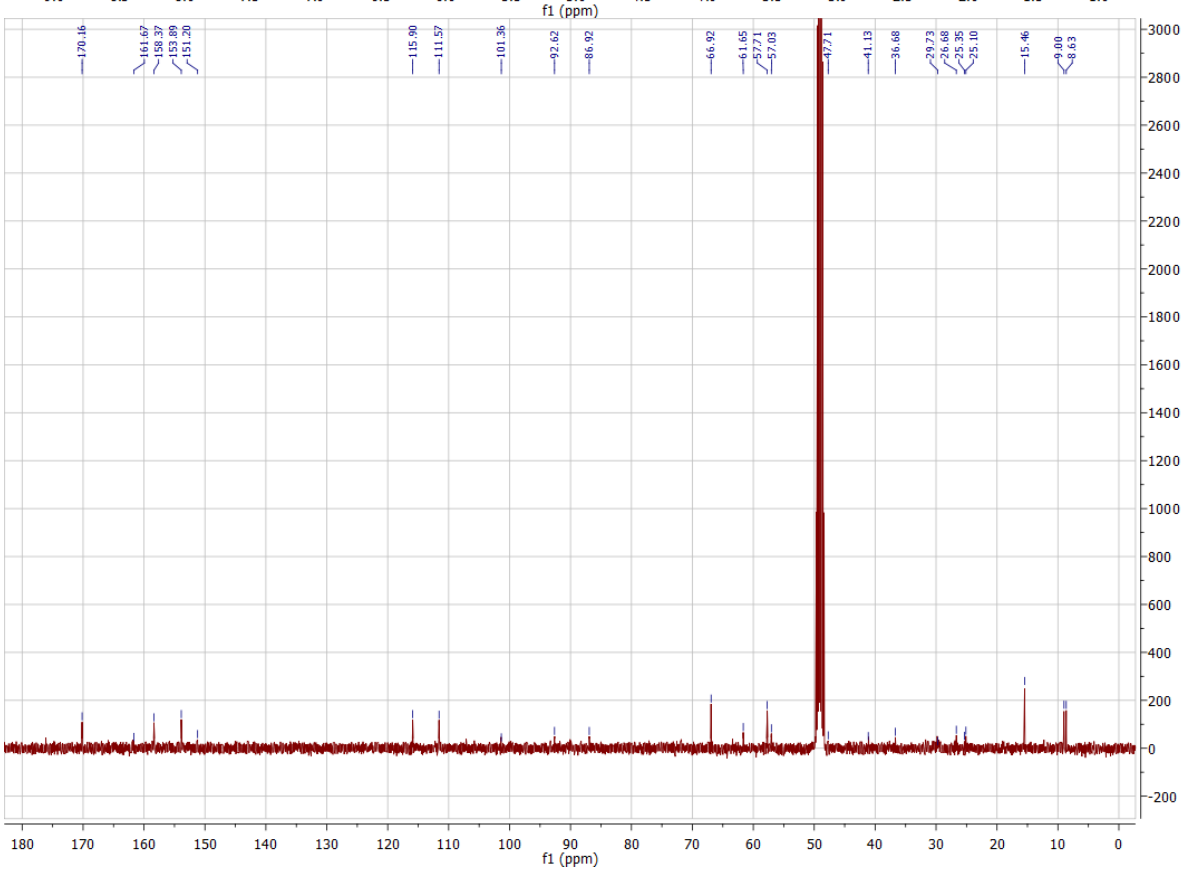
f1 (ppm)

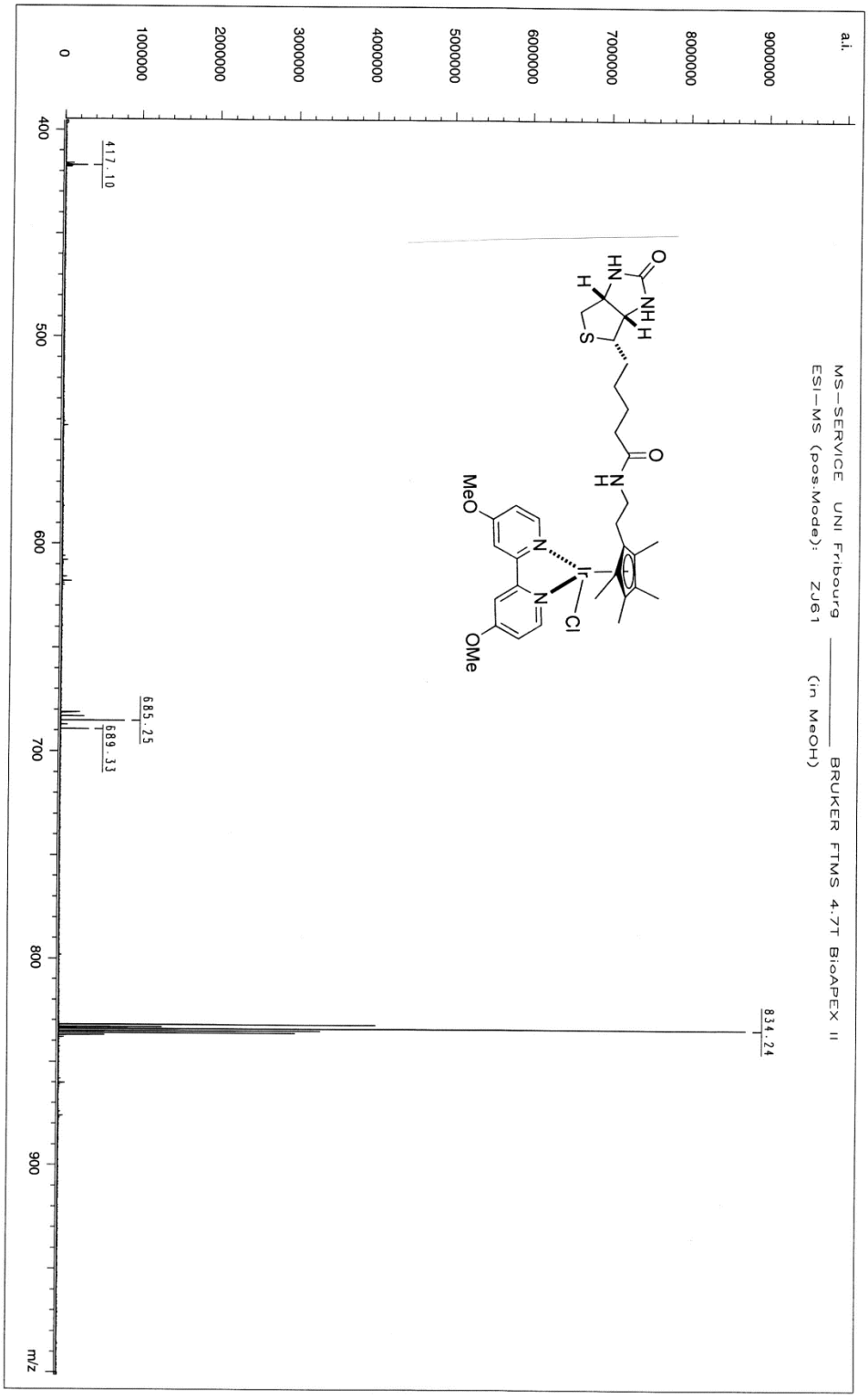
a.i.
MS-SERVICE UNI Fribourg BRUKER FTMS 4.7T BioAPEX II
ESI-MS (pos.Mode): ZJ61 (in MeOH)
9000000
8000000
7000000
6000000
5000000
4000000
3000000
2000000
1000000
0
400
500
600
700
800
900
m/z
417.10
685.25
689.33
834.24
MeO
OMe
Cl
Ir
/Data/UNI_BS/ZIMB6208_ESI/1/pdata/1 FTMS USER Wed Dec 7 15:07:08 2011

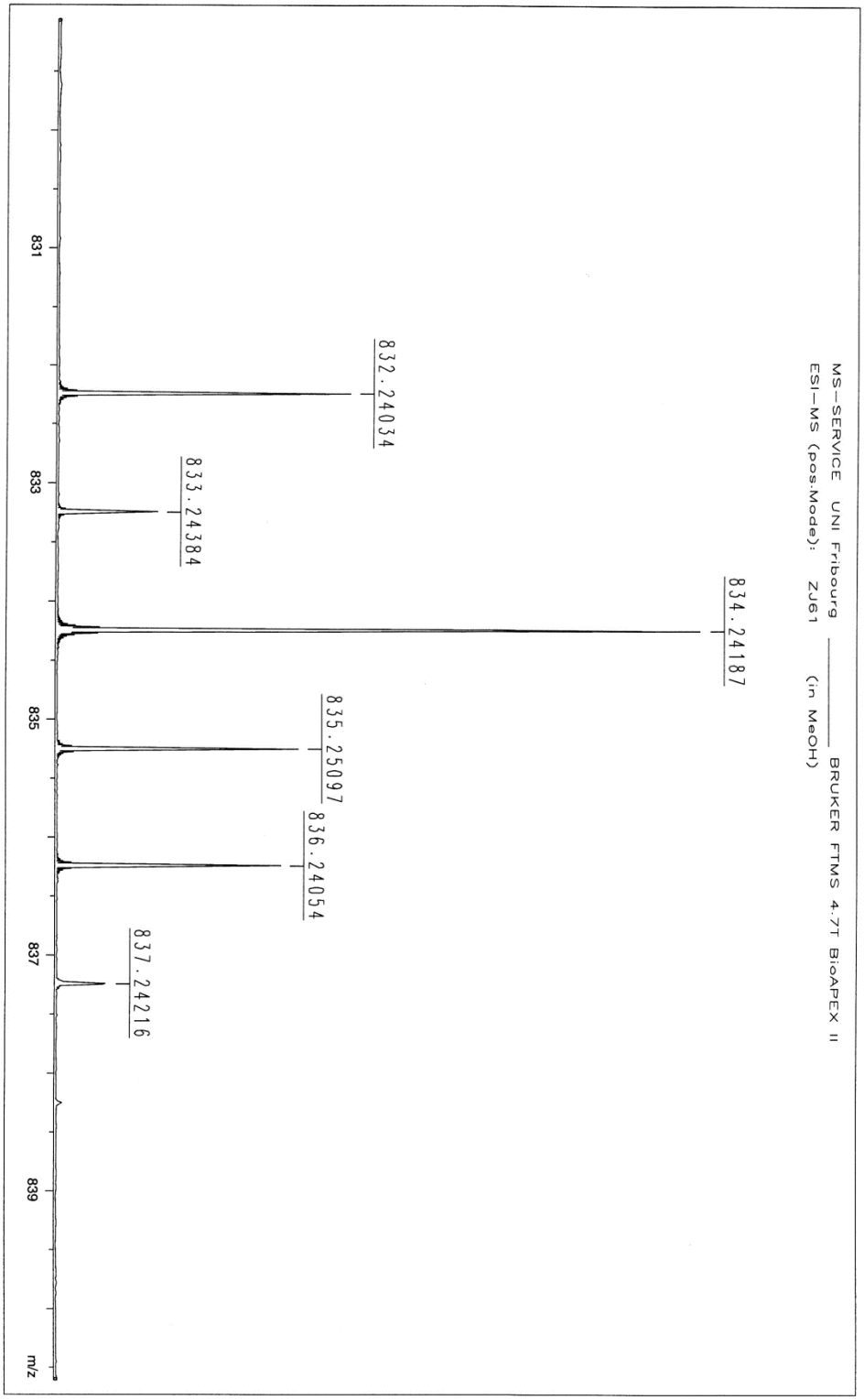
MS-SERVICE UNI Fribourg BRUKER FTMS 4.7T BioAPEX II
ESI-MS (pos.Mode): ZJ61 (in MeOH)
832.24034
833.24384
834.24187
835.25097
836.24054
837.24216
831
833
835
837
839
m/z
/Data/UNI_BS/ZIMB6208_ESI/3/pdata/1 FTMS USER Wed Dec 7 15:06:18 2011

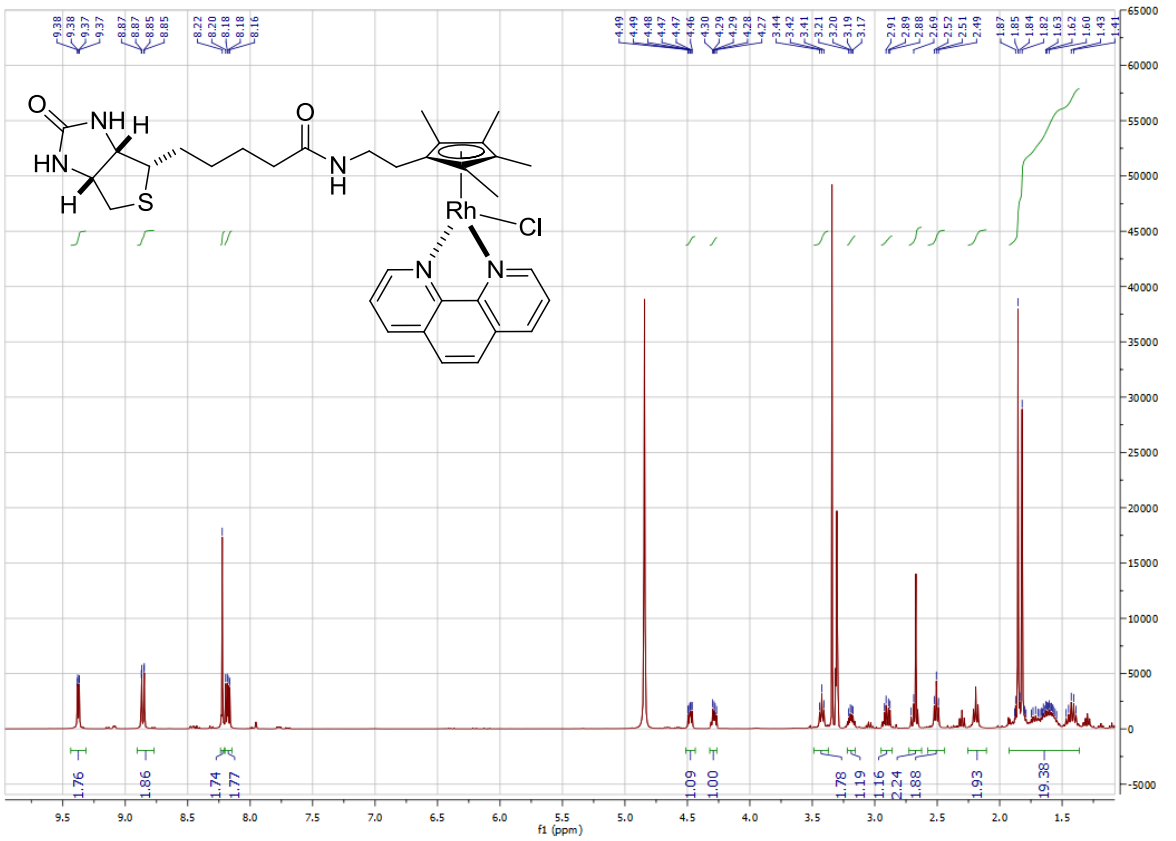
O
NH H
HN
H
S
O
N
H
Rh
Cl
N
N
f1 (ppm)

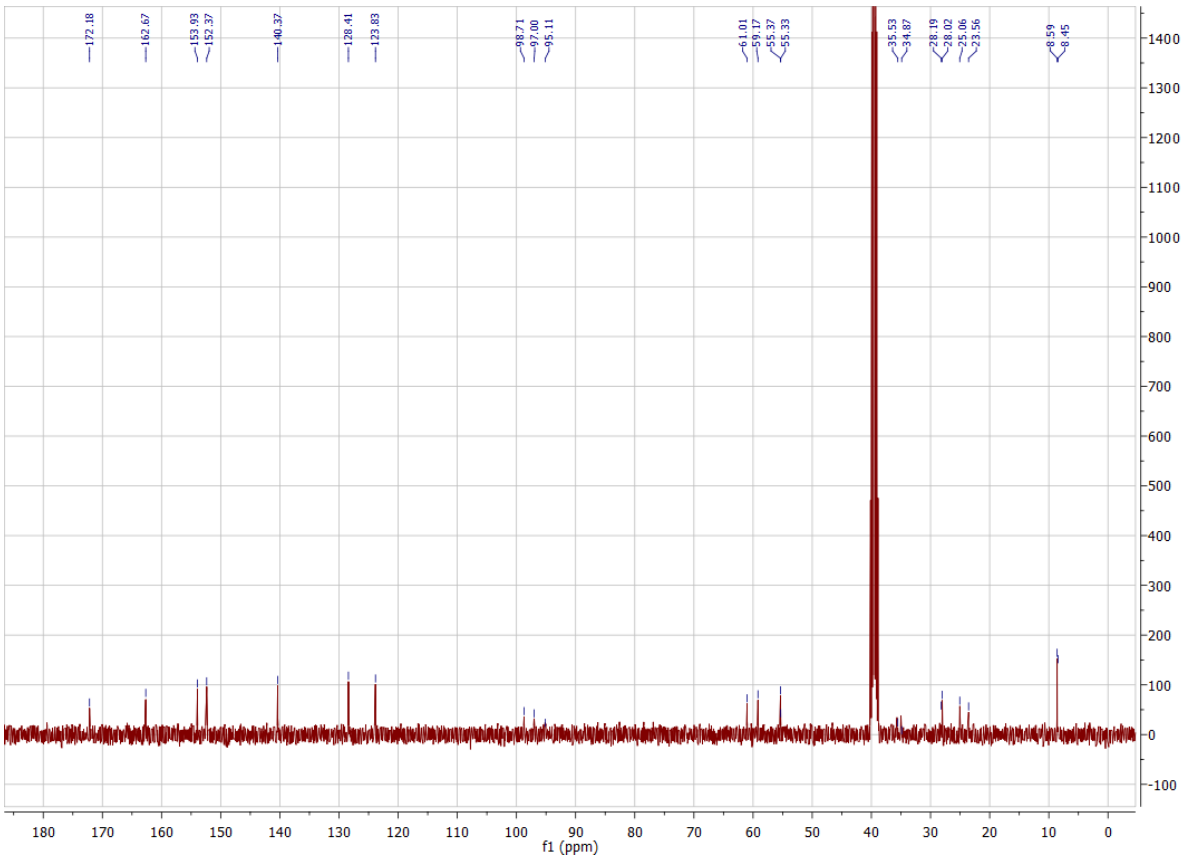
f1 (ppm)

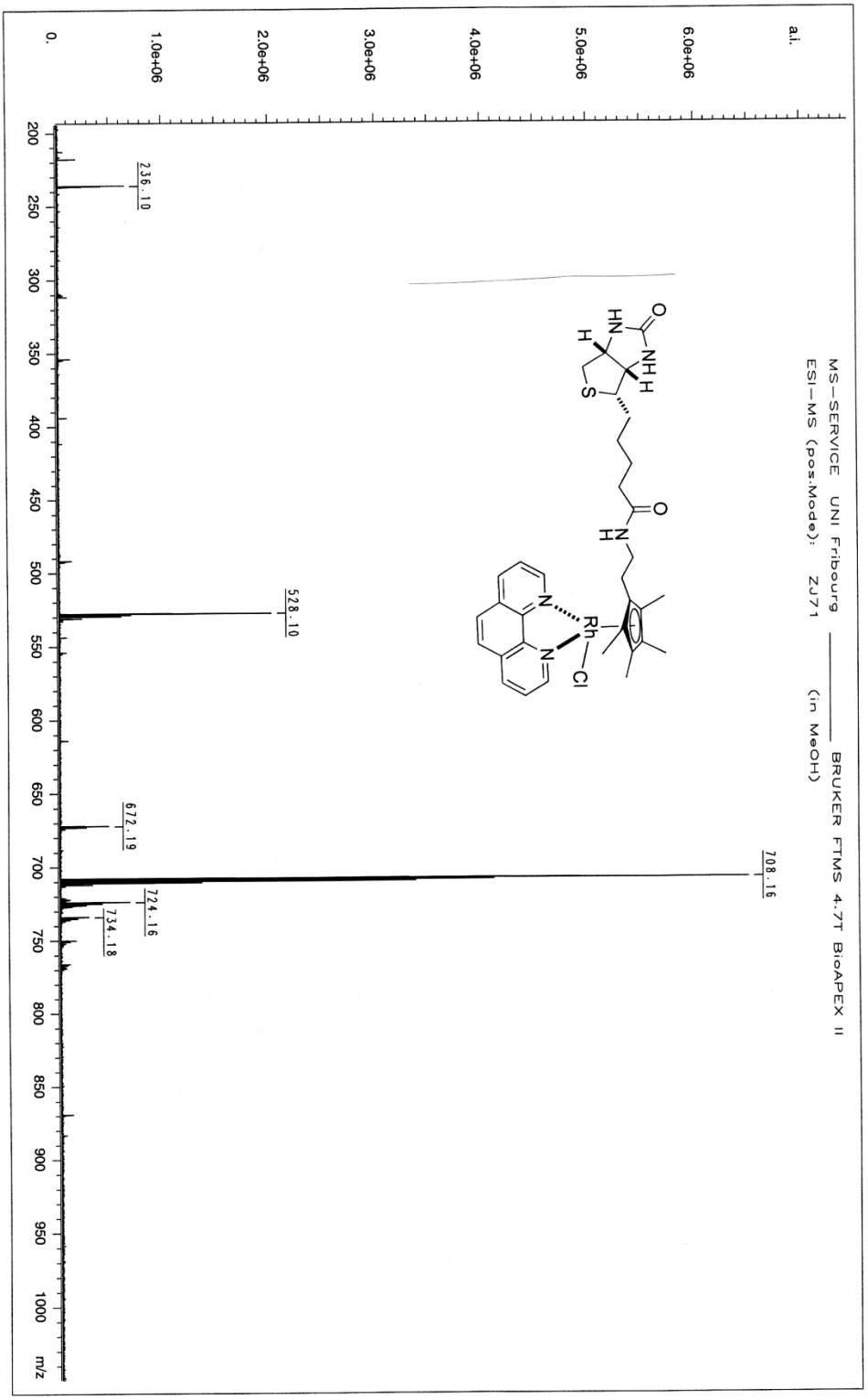
MS-SERVICE UNI Fribourg BRUKER FTMS 4.7T BioAPEX II
ESI-MS (pos.Mode): ZJ71 (in MeOH)
a.i.
6.0e+06
5.0e+06
4.0e+06
3.0e+06
2.0e+06
1.0e+06
0.
236.10
528.10
672.19
708.16
724.16
734.18
m/z
/Data/UNI_BS/ZIMB5205_ESI/1/pdata/1 FTMS USER Fri Nov 19 15:15:28 2010

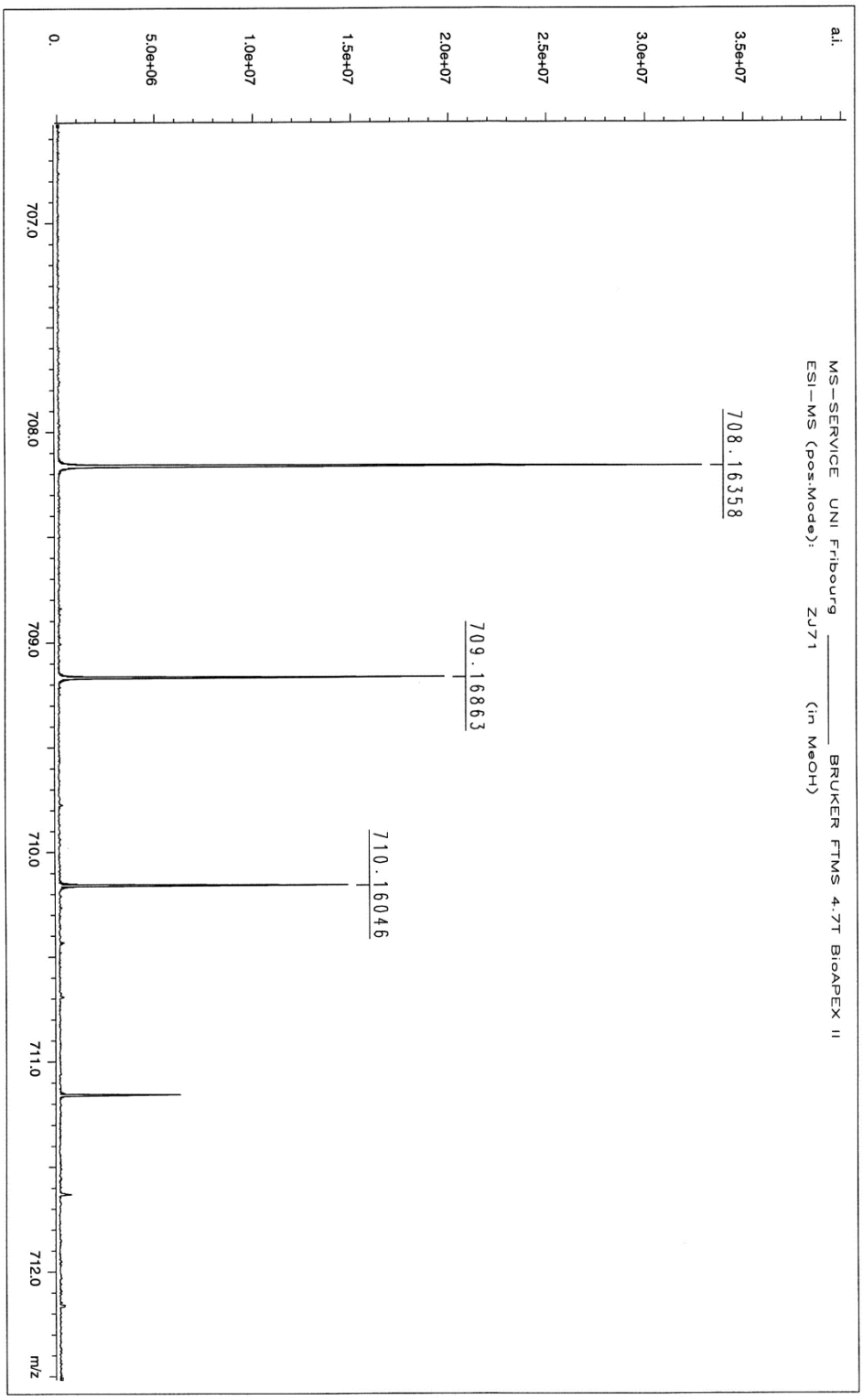
a.i.
MS-SERVICE UNI Fribourg BRUKER FTMS 4.7T BioAPEX II
ESI-MS (pos:Mode): ZJ71 (in MeOH)
708.16358
709.16863
710.16046
3.5e+07
3.0e+07
2.5e+07
2.0e+07
1.5e+07
1.0e+07
5.0e+06
0.
707.0
708.0
709.0
710.0
711.0
712.0
m/z
/Data/UNI_BS/ZIMB5205_ESI/10/pdata/1 FTMS USER Fri Nov 19 15:25:36 2010

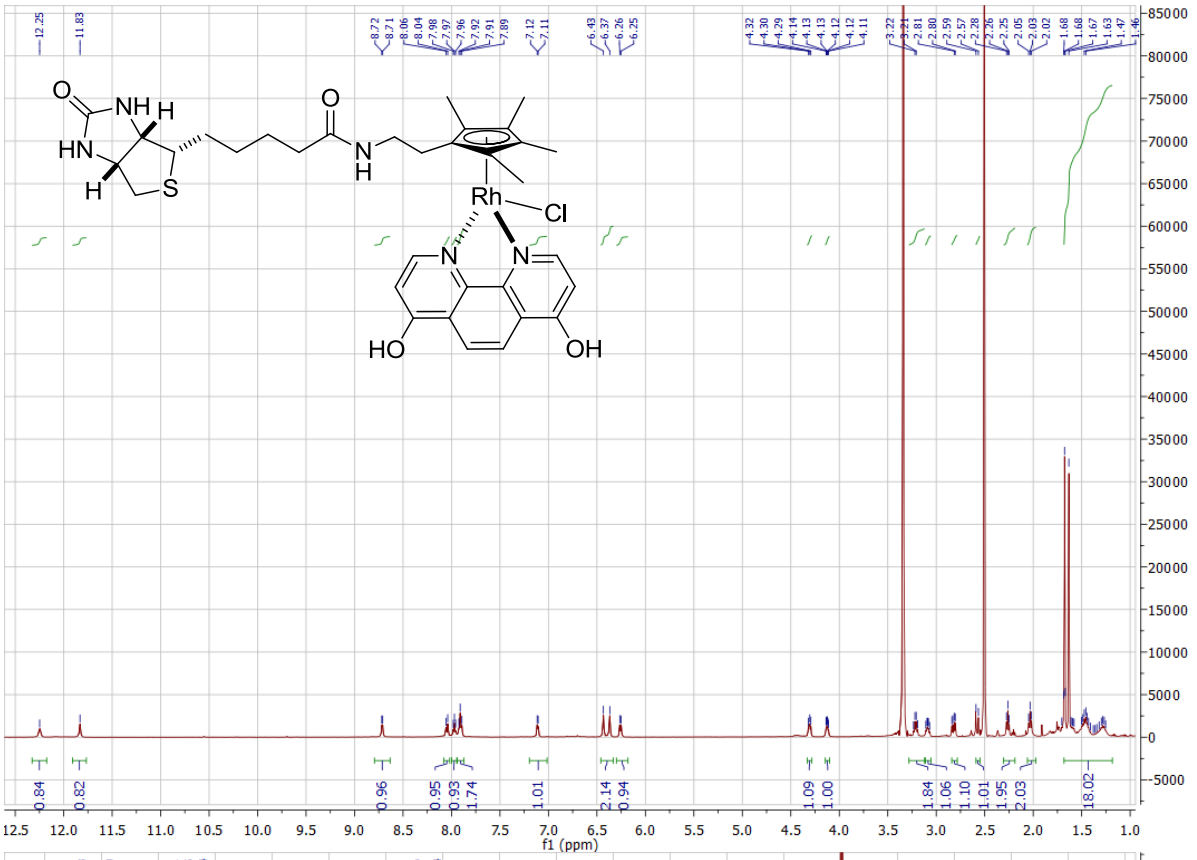
O
NH H
HN
H
S
O
N
H
Rh
Cl
N
N
HO
OH
f1 (ppm)

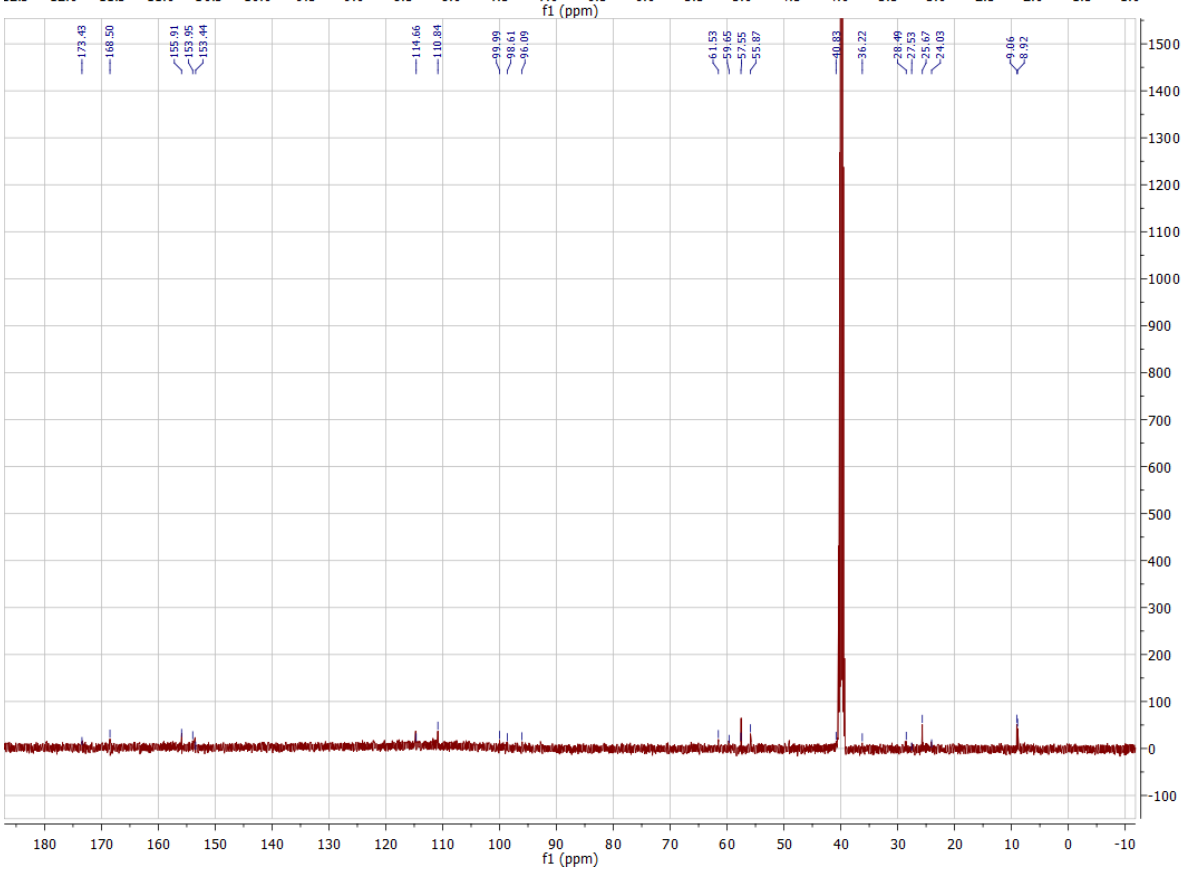
f1 (ppm)

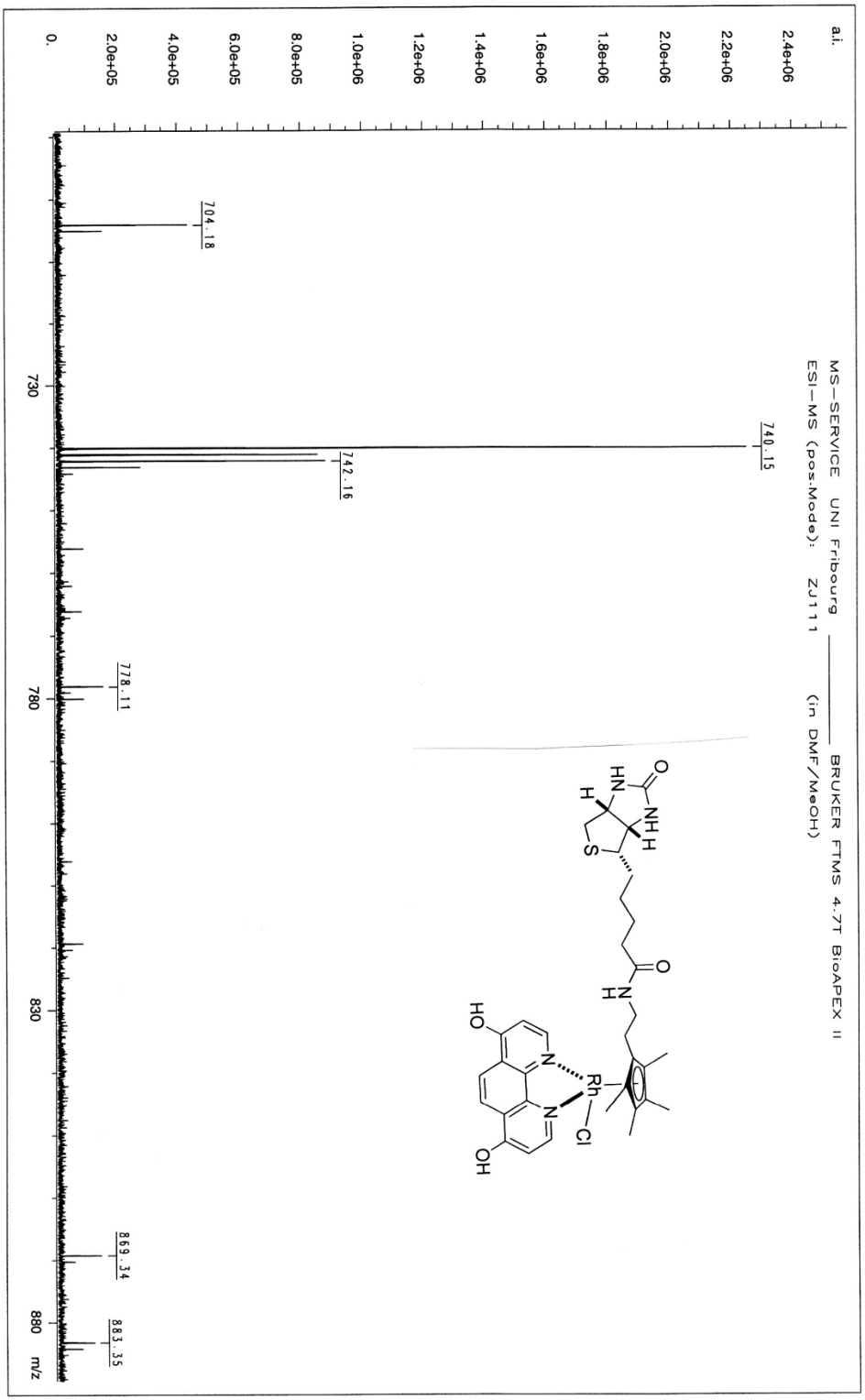
a.i.
MS-SERVICE UNI Fribourg BRUKER FTMS 4.7T BioAPEX II
ESI-MS (pos.Mode): ZJ111 (in DMF/MeOH)
740.15
742.16
704.18
778.11
869.34
883.35
m/z
/Data/UNI_BS/ZIMB5204_ESI/1/pdata/1 FTMS USER Fri Nov 19 15:13:56 2010

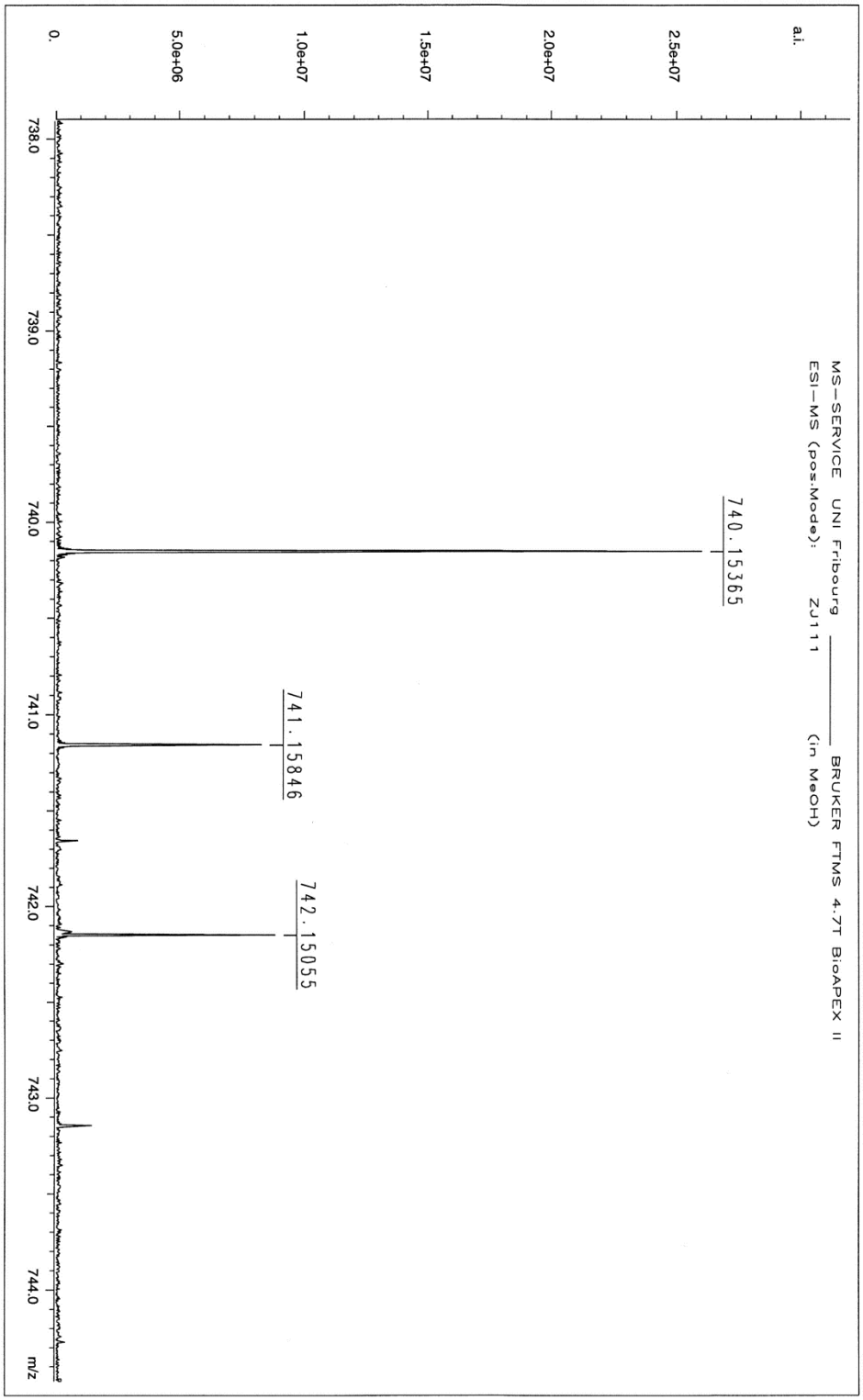
MS-SERVICE UNI Fribourg BRUKER FTMS 4.7T BioAPEX II
ESI-MS (pos:Mode): ZJ111 (in MeOH)
a.i.
2.5e+07
2.0e+07
1.5e+07
1.0e+07
5.0e+06
0.
740.15365
741.15846
742.15055
738.0
739.0
740.0
741.0
742.0
743.0
744.0
m/z
/Data/UNI_BS/ZIMB5204_ESI/10/pdata/1 FTMS USER Fri Nov 19 15:32:51 2010

CV

Professional Experience

PhD thesis in Chemistry, University of Basel (CH) *2007 – 2012*
Artificial Metalloenzymes Laboratory (AMEL)

Objective: Engineering artificial metalloenzymes based on biotin-streptavidin technology for DNA recognition and Asymmetric Transfer Hydrogenation catalysis.
Supervisor: Prof T. R. Ward
Summary: I synthesized various biotinylated metal complexes for incorporation into a host protein (Streptavidin) to create artificial metalloenzymes able to perform specific DNA targeting *in vitro* and enantioselective catalysis in water.

Master thesis in Novartis Pharma, Basel (CH) *February/August 2007*
Department of Chemical and Analytical Development

Objective: Development of a robust and practical process for the Darzens condensation and α,β-epoxide rearrangement: Scope and limitations of the methodology.
Supervisor: Dr. F. Gallou
Summary: I developed a practical and robust process for a fast oxazole and thiazoles synthesis. I studied the electronic effects of the Darzens condensation and subsequent rearrangement. The process developed is both amenable to large scale and parallel synthesis.

Training course in organic synthesis, Montpellier (F) *March/August 2006*
Co-operative Laboratory Servier CNRS UM-Center of Structural
Biochemistry CNRS UMR 5048-UM1-INSERM UMR 554.

Objective: Synthesis and biological evaluation of new inhibitors of human Cyclophilin A.
Supervisor: Pr. J. F Guichou and Pr. A. Chavanieu
Summary: I synthesized various organic compounds related to Medicinal Chemistry and I tested them using enzymatic assays followed by UV spectroscopy.

Education

MSc in Professional Chemistry, University Montpellier 2 (F) *2007*
Specialized in Organic Chemistry, Biomolecules, Conception, Separation and Screening.

BSc in Chemical Engineering, University Montpellier 2 (F) *2005*

Publications

«Development of a robust and practical process for the Darzens condensation and α,β-epoxide rearrangement: scope and limitations of the methodology», J. M. Zimbron, M.Seeger-Weibel, H. Hirt, F. Gallou, *Synthesis* **2008**, *8*, 1221 - 1226.

«Chemo-genetic optimization of DNA recognition by metallodrugs using a presenter protein strategy» J. M. Zimbron, A. Sardo, T. Heinisch, T. Wohlschlager, J. Gradinaru, C. Massa, T. Schirmer, M. Creus, T. R.Ward, *Chem. Eur. J.* **2010,** *16*, 12883 - 12889.

« Artificial Transfer Hydrogenases for the Enantioselective Reduction of Cyclic Imines» M. Dürrenberger, T. Heinisch, T. Rossel, A. Mutschler, K. Kersten, J. M. Zimbron, J. Pierron, T. Schirmer and T. R. *Angew. Chem. Int. Ed. Engl.* **2011**, *50*, 3026 - 3029 and selected as “hot paper”.

«A dual anchoring strategy for the localization and activation of artificial metalloenzymes based on the biotin-streptavidin technology» In preparation

Award

Poster prize in the 29th REGIO-Symposium, Rheinfelden (D) *2009*
Topic: Organic and Bioorganic Chemistry
Poster: «Chemo-genetic optimization of DNA recognition by metallodrugs using a presenter protein strategy»

Conferences

Invited speaker

5th International Symposium on Bioorganometallic Chemistry, Bochum (D) *July 2010*

Oral presentation: «Chemo-genetic optimization of DNA recognition by metallodrugs using a presenter protein strategy»

Poster presentation

31th REGIO-Symposium on Bioorganic Chemistry, Mittelwhir (F) *2009, 2010, 2011*

Swiss Chemical Society Fall meeting, Lausanne (CH) *September 2009*

Biotrans, Bern (CH) *July 2009*

Technical skills

Synthesis: multi-step synthesis, work under controlled atmosphere (Schlenk techniques)

Catalysis: asymmetric homogeneous organometallic catalysis, parallel catalyst screening using a multireactor

Purifications: flash chromatography, preparative HPLC, Kugelrohr distillation

Characterisation: NMR, MS, UV-Vis, HPLC and GC

Biology: Protein production and characterisation, EMSA gels

Instruments: Responsible for the measurements using 500Hz NMR, ESI, MALDI and Isothermal Titration Calorimetry.

Skills

Courses attended

“Chemistry and Biology of Natural products” by the Prof. Dr. Karl Gademann

Languages:

French: mother tongue

Spanish: native language

English: fluent

German: basics

Teaching:

Supervisor of an undergraduate student during 4 weeks

Supervisor of two Master students during 6 months

Teaching Assistant (3 years) – Analytical Chemistry for 1st year students in Biology and Pharmacy

Informatics:

Scientific software: Scifinder, Reaxys, Chemdraw, Isisdraw, VMD, MestReNova, Inventory

Office software: Word, Excel, Powerpoint, EndNote

Activities and interests

President of the Chemistry Student Union I.U.P for two years *2003/2005*

Captain of the SOC football team (F)

I like to visit different cultures and learn about their local history